

Topics in Heterocyclic Chemistry 44

Series Editors: Bert Maes · Janine Cossy · Slovenko Polanc

Zdenko Časar *Editor*

# Synthesis of Heterocycles in Contemporary Medicinal Chemistry



Springer

**44**

## **Topics in Heterocyclic Chemistry**

### **Series Editors:**

Bert Maes, Antwerp, Belgium  
Janine Cossy, Paris, France  
Slovenko Polanc, Ljubljana, Slovenia

### **Editorial Board:**

D. Enders, Aachen, Germany  
S.V. Ley, Cambridge, UK  
G. Mehta, Bangalore, India  
R. Noyori, Hirosawa, Japan  
L.E. Overmann, Irvine, CA, USA  
A. Padwa, Atlanta, GA, USA

## **Aims and Scope**

The series Topics in Heterocyclic Chemistry presents critical reviews on present and future trends in the research of heterocyclic compounds. Overall the scope is to cover topics dealing with all areas within heterocyclic chemistry, both experimental and theoretical, of interest to the general heterocyclic chemistry community.

The series consists of topic related volumes edited by renowned editors with contributions of experts in the field.

More information about this series at <http://www.springer.com/series/7081>

Zdenko Časar

Editor

# Synthesis of Heterocycles in Contemporary Medicinal Chemistry

With contributions by

R. Barth · A. Bauer · Z. Časar · F. Gallou · S. Lemaire ·  
S. Nerdinger · F. Richter · C.A. Rose · D. Schils ·  
O. Schöne · E. Schreiner · Y.S. Tsantrizos

 Springer

*Editor*

Zdenko Časar

Sandoz Development Center Slovenia, Lek Pharmaceuticals d.d.

Ljubljana

Slovenia

Global Portfolio Management, Sandoz GmbH

Kundl

Austria

Faculty of Pharmacy

University of Ljubljana

Ljubljana

Slovenia

ISSN 1861-9282

ISSN 1861-9290 (electronic)

Topics in Heterocyclic Chemistry

ISBN 978-3-319-39915-7

ISBN 978-3-319-39917-1 (eBook)

DOI 10.1007/978-3-319-39917-1

Library of Congress Control Number: 2016944466

© Springer International Publishing Switzerland 2016

This work is subject to copyright. All rights are reserved by the Publisher, whether the whole or part of the material is concerned, specifically the rights of translation, reprinting, reuse of illustrations, recitation, broadcasting, reproduction on microfilms or in any other physical way, and transmission or information storage and retrieval, electronic adaptation, computer software, or by similar or dissimilar methodology now known or hereafter developed.

The use of general descriptive names, registered names, trademarks, service marks, etc. in this publication does not imply, even in the absence of a specific statement, that such names are exempt from the relevant protective laws and regulations and therefore free for general use.

The publisher, the authors and the editors are safe to assume that the advice and information in this book are believed to be true and accurate at the date of publication. Neither the publisher nor the authors or the editors give a warranty, express or implied, with respect to the material contained herein or for any errors or omissions that may have been made.

Printed on acid-free paper

This Springer imprint is published by Springer Nature

The registered company is Springer International Publishing AG Switzerland

# Preface

Heterocyclic compounds have had a central role in medicinal chemistry, and they have made notable contributions to the quality of life for humanity. It is difficult to imagine the progress in public health and the increased life expectancy that we have witnessed in the last 70 years without drugs such as  $\beta$ -lactam antibiotics, ACE inhibitors, calcium channel blockers, and others. Over the last decade, some particular compounds, like the statins, have established their position as important drugs, while many new therapeutic classes of compounds have emerged that have provided important advances in the area of modern medicinal chemistry. Indeed, statins, and in particular their heterocyclic derivatives that are frequently called the super-statins, have markedly improved the management of hypercholesterolemia, which has led to reduced risk of atherosclerosis and cardiovascular disease. Nowadays, these drugs are facing a patent cliff, which will allow the market entry of generic versions of these drugs and thus increase their access to patients worldwide. Then, early in this decade, a major breakthrough was achieved in the treatment of hepatitis C virus (HCV) infections. Several compound classes have emerged that can now provide significantly improved rates of sustained virological response in a few months of oral therapy, thus avoiding the use of less efficient and more difficult to tolerate ribavirin/pegylated interferon therapies. Among these compounds, sofosbuvir (NS5B HCV polymerase/protease inhibitor) and simeprevir (NS3/4A HCV protease inhibitors) and its analogs have a central role in the battle against hepatitis C. The treatment of type 2 diabetes has also moved to inhibition of glucose reabsorption in the kidney, which leads to reduced blood sugar levels. This has been achieved with a new class of compounds that inhibit sodium-glucose transport protein 2 (SGLT2), which are now referred to as the “gliflozin” drugs. Over the past 5 years, several gliflozin family members have been put on the market: canagliflozin, dapagliflozin, empagliflozin, ipragliflozin, and tofogliflozin. These arose from the fascinating new arsenal of synthetic chemistry that was constructed for their efficient preparation. HIV treatment has also witnessed notable progress in the last decade, and one recently approved drug that might change the landscape of anti-HIV therapies is the second-generation HIV integrase strand transfer inhibitor dolutegravir, with its impressive efficacy and good patient tolerability. Anticancer

drugs have also made significant progress in the last decade. Among these, the so-called tinibs and the tyrosine kinase inhibitors have had a pivotal role. At the same time, astonishing results have been achieved in the area of natural product derivatives, where eribulin was introduced into clinical practice recently for the treatment of metastatic breast cancer and inoperable liposarcoma. Based on its complex polyether macrolide structure with 19 stereocenters, the total synthesis for eribulin production requires more than 60 steps. This is an outstanding achievement in industrial synthesis, and it represents the longest commercial drug synthesis to date.

Therefore, all of these achievements have provided impetus for the assembly of this volume of *Topics in Heterocyclic Chemistry*, entitled *Synthesis of Heterocycles in Contemporary Medicinal Chemistry*, which highlights in detail the abovementioned achievements. This volume is special in several aspects. First, it was composed by industrial medicinal and process chemists with decades of industrial experience. Secondly, it is dedicated to the heterocyclic drug compounds that have particularly marked the area of medicinal chemistry over the last decade. As this volume contains a good blend of synthetic organic, medicinal, and process chemistry, it should be appealing to a broad area of chemistry professionals and graduate students. I hope that it will inspire current and future process and medicinal chemists to design new drugs in efficient and sustainable manners.

Gallou provides a chapter on the development of a manufacturing process for the formation of a hepatitis C drug candidate with immense tutorial value from the process chemistry perspective. Lemaire and Schils describe the synthetic and process chemistry aspects of SGLT2 inhibitors for the treatment of type 2 diabetes. Schöne et al. give a detailed overview of synthetic routes to sofosbuvir, one of the best selling drugs of this decade. Prof. Tsantrizos discusses the discovery, early synthetic chemistry, and process chemistry of macrocyclic HCV NS3/NS4A protease inhibitors for the case of ciluprevir (BILN-2061), which brought olefin metathesis to the industrial scale and paved the way for the assembly of the marketed analogs simeprevir, paritaprevir, and vaniprevir. The chapter that I have contributed reviews the recent progress in super-statin chemistry. Schreiner et al. provide an overview and detailed analysis of the synthetic routes to dolutegravir. Bauer summarizes the discovery and the initial synthetic routes toward eribulin and its analogs and describes the recent synthetic advances in the area.

To finish, I would like to thank the series editor, Prof. Slovenko Polanc, for giving me an outstanding opportunity to compile this volume of *Topics in Heterocyclic Chemistry*. I am also grateful to Prof. Janez Košmrlj for his support in this matter. I must also express my gratitude to the entire editorial and support staff at Springer for their prompt support and guidance during the preparation of this work. I would like to express my appreciation to all of the authors of this volume, for their hard work and outstanding contributions. I extend my sincere gratitude to Sandoz/Lek management for providing an inspiring scientific environment and, in particular, to Dr. Josef Egerbacher, Dr. Susanne Raehs, Mr. Matjaž Tršek, Dr. Bojan Mitrović, and Mr. Pavel Drnovšek, who have been supportive in all my scientific endeavors. I would also like to acknowledge Prof. Stanislav Gobec for his support

in my academic work. Finally, I would like to thank my family and especially my wife, Renata, and my daughter, Neža, for their patience and understanding during the time I spent writing my own chapter for this book, as well as during the time needed for the compilation of the whole volume.

Ljubljana, Slovenia  
March 2016

Zdenko Časar



# Contents

<b>Development of a Manufacturing Process for the Formation of a Nucleoside Drug Candidate . . . . .</b>	<b>1</b>
Fabrice Gallou	
<b>Development of Efficient Routes to Access C-Glycosides as SGLT-2 Inhibitors for the Treatment of Type 2 Diabetes . . . . .</b>	<b>29</b>
Sébastien Lemaire and Didier Schils	
<b>Synthetic Routes to Sofosbuvir . . . . .</b>	<b>51</b>
Roland Barth, Christopher A. Rose, and Olga Schöne	
<b>Synthetic Challenges in the Assembly of Macrocyclic HCV NS3/NS4A Protease Inhibitors: The Case of BILN 2061 and Its Analogs . . . . .</b>	<b>89</b>
Youla S. Tsantrizos	
<b>Recent Progress in the Synthesis of Super-Statins . . . . .</b>	<b>113</b>
Zdenko Časar	
<b>Development of Synthetic Routes to Dolutegravir . . . . .</b>	<b>187</b>
Erwin Schreiner, Frank Richter, and Sven Nerdinger	
<b>Story of Eribulin Mesylate: Development of the Longest Drug Synthesis . . . . .</b>	<b>209</b>
Armin Bauer	
<b>Index . . . . .</b>	<b>271</b>

# Development of a Manufacturing Process for the Formation of a Nucleoside Drug Candidate

Fabrice Gallou

**Abstract** The original synthesis of our oral prodrug of isatoribine, a nucleoside analogue potentially useful for the treatment of patients with chronic hepatitis C and other viral infections, suffered from various limitations. Herein we would like to report a practical and robust process identified for the synthesis of an isatoribine prodrug therefore in the course of our process R&D activities. Our efforts relied on the practical manufacture of the base in a straightforward sequence in a streamlined glycosylation process, followed by an effective and regioselective enzymatic hydrolysis, both with a much improved environmental impact. The catalytic activity of the immobilized lipase was demonstrated to be very robust as the enzyme displayed an excellent behavior as catalyst with high levels of activity, selectivity, and excellent operational stability. This process was further developed in a semi-continuous mode and demonstrated to proceed in an even more efficient manner from a throughput standpoint.

**Keywords** Glycosylation • Heterocycle • Immobilized lipase

## Contents

1	Introduction .....	2
2	The Impact of Process Research on the Route Selection .....	3
2.1	Cost vs. Speed .....	5
2.2	Robustness, Reproducibility, and Environment .....	5
2.3	Process Understanding .....	6
3	The Original Route .....	7
3.1	Process Research and Alternative Routes to Heterocyclic Base .....	9
3.2	Process Development: Understanding and Optimization of the Ultimate Process ...	11
4	Conclusions .....	26
	References .....	26

---

F. Gallou (✉)  
Chemical and Analytical Development, Novartis Pharma AG, 4002 Basel, Switzerland  
e-mail: [fabrice.gallou@novartis.com](mailto:fabrice.gallou@novartis.com)

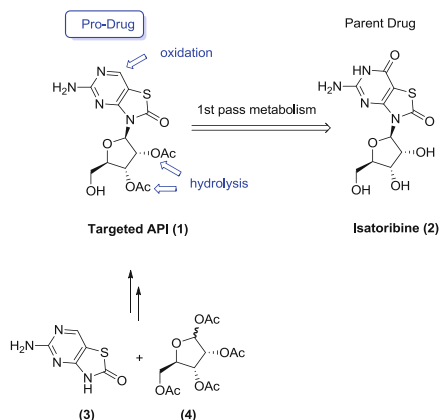
## Abbreviations

2-MeTHF	2-Methyltetrahydrofuran
Ac	Acetyl
API	Active pharmaceutical ingredient
BSA	Bis-silylacetamide
DMAP	Dimethyl aminopyridine
DMF	Dimethylformamide
GMP	Good manufacturing practice
h	Hour(s)
HMDS	Hexamethyldisilazane
HSE	Health safety, environment
kin	Kinetic
Me	Methyl
MTBE	Methyl- <i>tert</i> -butyl ether
PAT	Process analytical technology
rt	Room temperature
SM	Starting material
Tf	Triflate
Therm	Thermodynamic
THF	Tetrahydrofuran
TMS	Trimethylsilyl

## 1 Introduction

A variety of D- and L-purine nucleosides have been explored for use as immunomodulators [1]. In the course of one of our development projects, we became interested in a specific thiazolo[4,5-*d*]pyrimidine nucleoside [2]. Our candidate (**1**) is an oral prodrug of isatoribine (**2**), a nucleoside analogue potentially useful for viral infections (see Fig. 1). The prodrug (**1**) results in isatoribine (**2**) after full hydrolysis of the esters and oxidation of the deoxyribose moiety in vivo [3]. It is a specific toll-like receptor agonist that induces the production of such cytokines as alpha interferon.

The original synthesis of (**1**), suffered from various limitations. Preparation of the base moiety 5-aminothiazolo[4,5-*d*]pyrimidine-2,7-(3*H*,6*H*)-dione (**3**) lacked robustness and displayed high variability in quality; the assembly relied on a key glycosylation with the peracetylated sugar 1,2,3,5-tetra-*O*-acetyl- $\beta$ -D-ribofuranose (**4**) that required numerous and cumbersome operations. Besides, the physical properties and specifically the hygroscopicity and poor solubility of the base led to a tedious, low-yielding, and unreliable process in the glycosylation step. An ultimate hydrolysis of the primary alcohol under enzymatic conditions had proven very challenging on-scale, displaying very low throughput, poor productivity and yield, as well as high cost due to a high catalyst loading. All these challenges

**Fig. 1** Targeted API (1)

contributed to a very low overall performance of the initial process and a resulting high drug substance cost.

Herein we would like to report our journey to a practical and robust process that resulted in our final manufacturing process.

## 2 The Impact of Process Research on the Route Selection

Chemical development organizations in big pharmaceutical companies classically have the dual mission of creating synthetic routes and processes suitable for the long term of the targeted drug substances and to supply programs with the necessary high-quality drug substances for toxicological and clinical studies.

These activities are routinely supported in complex cross-functional teams with a key emphasis on the technical expertise of chemistry, analytics, and engineering (Fig. 2).

This expertise is there to guarantee that a drug substance is made in a robust and well-controlled manner to deliver consistently high-quality active pharmaceutical ingredient (API) required to formulate the drug substance into a drug product adequate to patients.

The ideal synthesis and process should fulfill such criteria as being efficient, scalable, cost-efficient, safe (both from operational and material standpoint), and ideally free of intellectual property constraint, versatile (i.e., simple to perform in standard equipment and multipurpose plant), environmentally sound (using chemicals as innocuous as possible, avoiding or minimizing waste), and very importantly robust with respect to deviations from ideal reaction parameters (Fig. 3).

**Fig. 2** The critical disciplines for the chemical process research and development

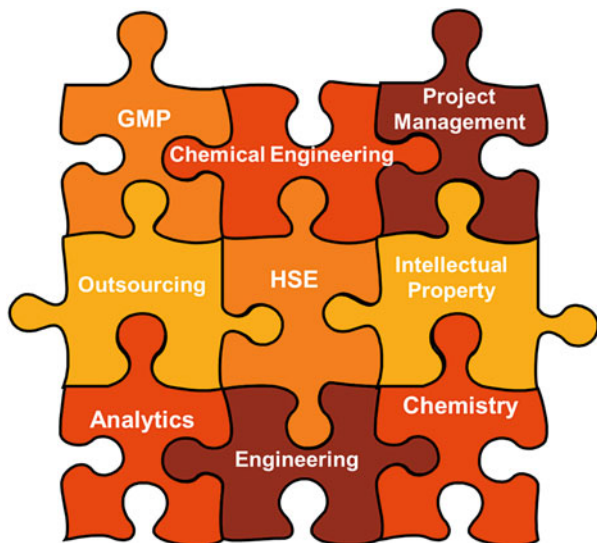
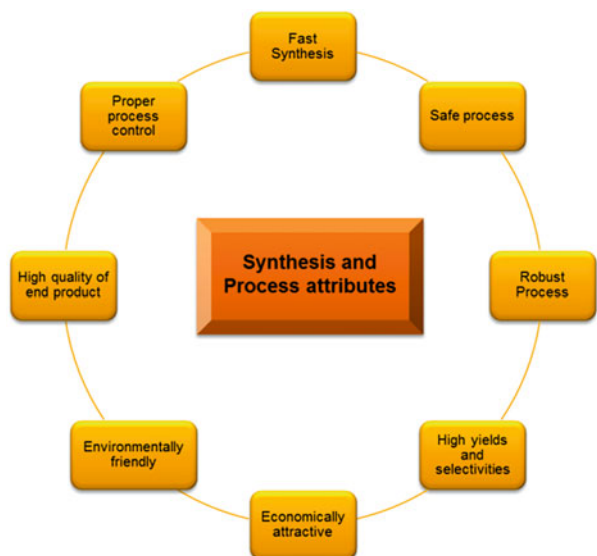


**Fig. 3** Synthesis and process attributes



Much has been written on the role of process chemists to achieve these goals and can be found in the authoritative compilation of best practices by Dr. Neal Anderson [4].

## ***2.1 Cost vs. Speed***

Depending on the nature of a project, indication, sales forecast, development timelines, and clinical plans, the focus of development activities can greatly vary. For a standard scenario project, a preliminary process research phase typically consists in the identification of the route that exhibits all the attributes of the final manufacturing routes in terms of quality, safety, cost-effectiveness, robustness, and environmental soundness. In contrast, for a forecasted low-volume product, the emphasis is generally shifted to the speed, safety, and robustness of the route. In both cases, it is well understood that any route should result in material of high quality. The quality will be controlled via a sound purification strategy ideally set at well-identified control points. These control points are typically set at crystalline intermediates. More generally, a process can be made less expensive via either reduction of the number of synthetic steps, usually done by selecting the shortest route or from a process by streamlining operations. Care should be taken in the control strategy when streamlining and shortcuts are taken, as they usually imply perfect understanding of the process and of critical parameters. Improvement of the reaction yields is typically accomplished by optimizing reaction conditions individually, by using DoE, for example. Reduction of the cost of raw materials and reagents can be done by changing the synthetic strategy or by finding a less expensive source, for example, with the help of the sourcing department.

Design of a proper and expedient strategy is undoubtedly the most effective of these three ways. For this reason, long syntheses are made economical best by finding a shorter synthesis rather than by improving each individual step. A standard preliminary task will therefore consist in identifying the proper synthetic strategy without major focus on the optimization, the pitfall being to lock an unsuitable route that will never have the potential to achieve the ultimate economic target. These strategies may be used not only to lower the cost of production but also to gain time during the development phases, to improve the logistics, and to lower capital investment. Practically for a given route, this could translate into minimization of the isolation operations or telescoping of multiple steps.

## ***2.2 Robustness, Reproducibility, and Environment***

Robustness and reproducibility are key attributes of good processes. They are best evaluated upon repetition of the reaction and upon scale-up. This aspect is often a deciding factor for accelerated projects. The reproducibility is particularly difficult to fully guarantee because of the difficulties to exactly simulate plant conditions with all identical physical parameters or the impact of diverse source of raw materials, for example, a standard root cause for challenges.

To design such a process and a system in a responsible and sustainable way, scientists must follow certain “green” principles considering impact on

environment, economy, safety, and society. Designing a sustainable synthesis is essential to our long-term success and requires the conscious use of relevant principles and methodologies. The 12 principles of green chemistry [5] widely adopted by the chemical and pharmaceutical community provide guidance on designing a chemical process to reduce or to eliminate the use and generation of hazardous substances. These principles outline fundamental approaches to achieve the green chemistry goals of benign products and processes. Although subtleties can exist from one company culture to another, meeting these principles for a given synthetic route or process is widely recognized and constitutes the chemist ultimate goals. In addition, ACS GCI recommends the 12 principles of green engineering [6], which focus on the development and commercialization of industrial processes that are economically feasible and can reduce the risk to human health and the environment.

A variety of metrics, often developed or tailor-made internally and fulfilling proprietary and internal requirements, has been introduced to measure the impact of a given route and process which essentially express quantitatively a combination of these different aspects and different weighing factors depending on the culture and strategy of the individual organizations [7].

### ***2.3 Process Understanding***

Once identified, the synthesis selected as the one to be used for manufacturing can be further and deeper evaluated to gain full understanding of critical process parameters, be further streamlined, and optimized. Additional regulatory-driven activities can then be ensued.

However, the evolution of drug development has made it rare to follow to such a scenario. Accelerating the development of a drug candidate often puts the whole process research and development activities under the critical path and requires compression of the activities. It is then more common now to assign higher priority to only non-negotiable attributes to avoid putting the supply of a drug substance on the critical path. Quality is of course non-negotiable that will never be put at risk. For example, given a low-volume project, organizations will often assign higher priority to a well-controlled and robust route that delivers the drug substance diligently, at the expense of the economics of the manufacture. This way, a project can more ideally go through the development phases without delaying the program, to ultimately to ultimately make the drug product accessible to patients as early as possible and enter the market (Fig. 4).

Such a compromise around the key requirements of a synthesis or a process is necessary in the bigger overall scheme and mission of the pharmaceutical industry.

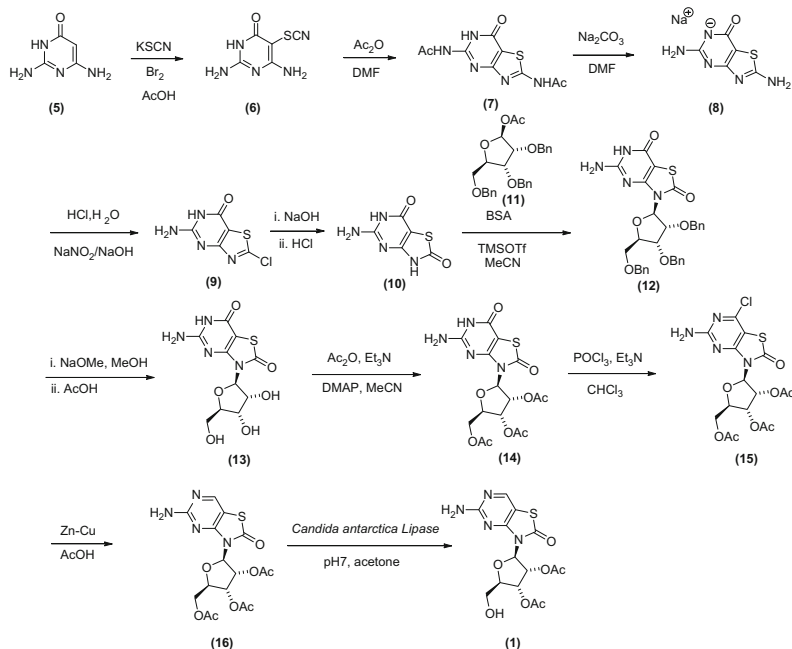
Fig. 4 Balancing speed and economics



### 3 The Original Route

With the above considerations in mind, in our currently described specific case, the objective was to develop a robust, expedient, and safe route delivering high-quality drug substance to be produced in multipurpose environment. The costs needed to be relatively moderate but without exaggerated pressure, the former attributes having more importance. This implied the chemistry needed to be readily established or ready in a minimal amount of time. From an availability of starting materials and reagents standpoint, there was also little flexibility as aggressive timelines did not allow for long lead times. With these boundaries of the projects in place, the original 11-step synthesis was first evaluated.

In this approach, 5-aminothiazolo[4,5-*d*]pyrimidine-2,7-(3*H*,6*H*)-dione (**10**) was prepared through a straightforward but rather long 5-step sequence. It was then coupled to 1-*O*-acetyl-2,3,5-tri-*O*-benzoyl- $\beta$ -D-ribofuranose (**11**) via a modified Vorbrüggen protocol [8] to result in 5-amino-3-(2',3',5'-tri-*O*-benzoyl- $\beta$ -D-ribofuranosyl)-3*H*-thiazolo[4,5-*d*]pyrimidin-2,7-dione (**12**) in high yield. A cumbersome manipulation of protecting and functional groups then was carried out to fully peracetylate the sugar moiety and reduce the pyrimidinone functionality into a pyrimidine. This lengthy sequence of a fully elaborated scaffold was clearly a weakness, displaying low overall yield (23% over four steps), complex operations, formation of a series of side-products difficult to remove, and ultimately an expensive process. The last step consisted in a powerful selective enzymatic catalytic hydrolysis of the primary alcohol, in the presence of the two other secondary alcohol of the ribofuranose. It performed rather well (87% yield) at that stage of development and could constitute a suitable end game (Scheme 1).



**Scheme 1** Original research synthesis from 2,6-diaminopyrimidin-4(3H)-one (5)

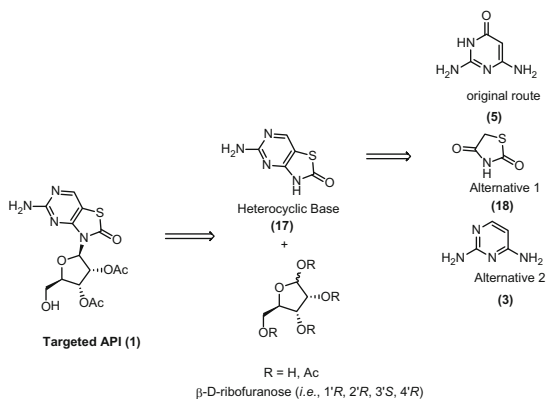


**Fig. 5** Proposed raw materials for targeted API (1)

The overall yield for the whole process was very low (<5%). Very long processing times were required which resulted into an extremely costly process. It was clearly unsuitable for future stages of development and made our attention rapidly turn to alternatives.

This first experience had demonstrated the relevance and adequacy of a glycosidation and the power of a final enzymatic selective hydrolysis for a

minimum number of steps from the glycosylation onwards. This would mean starting the synthesis from the desired base and a  $\beta$ -D-ribofuranose, peracetylated or not. The base could come from various precursors, thiazolidinone or pyrimidine based (alternatives 1 and 2, respectively) (Fig. 5).

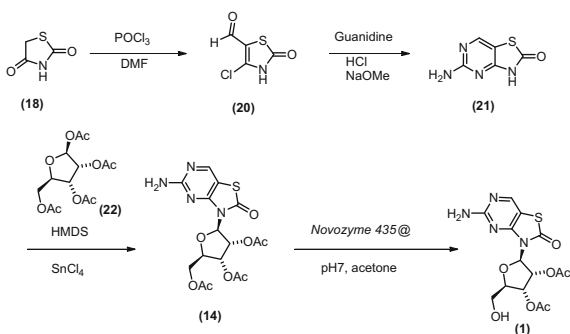
### 3.1 Process Research and Alternative Routes to Heterocyclic Base

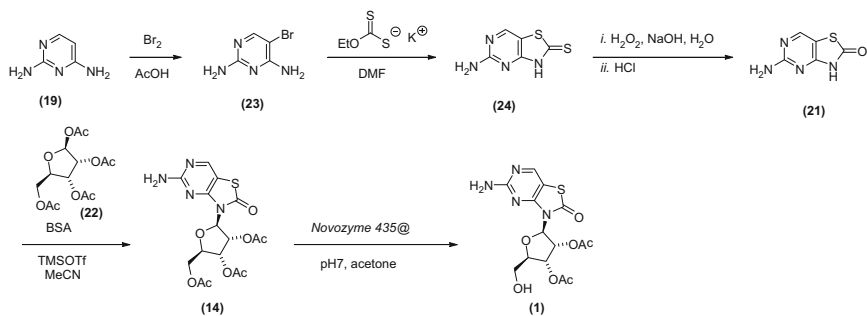
Our first alternative relied on the expedient construction of the heterocyclic base from the readily available thiazolidine-2,4-dione (**18**). The readily available commercial precursor was first hydroformylated with the Vilsmeier-Haack reagent [9]. This well-precedented functionalization turned to be very challenging and resulted in low yields, mostly due to decomposition of the starting material and product, and the lack of selectivity of the process (a low ca. 35% was obtained at best). The pyrimidine was then formed after condensation with guanidine, again in low yield (ca. 30%). The base (**21**) and the desired peracetylated ribofuranoside (**22**) could then be assembled using the previously described Vorbrüggen conditions [8] or via an alternative tin-tetrachloride-mediated process, for example [10] (Scheme 2).

This route had been demonstrated to be expedient and scalable; however, it still suffered from lack of robustness. The likelihood of success in the optimization was difficult to assess, but our early efforts clearly indicated the need for significant efforts.

The second alternative was evaluated in parallel whereby the readily available pyrimidine-2,4-diamine (**19**) was halogenated with bromine, condensed with a xanthate to result into the 5-amino-3*H*-thiazolo[4,5-*d*]pyrimidin-2-thione (**24**) that would then be oxidized into 5-amino-3*H*-thiazolo[4,5-*d*]pyrimidin-2-one (**21**). This sequence could proceed in ca. 35% overall yield, in a very simple and practical set of operations. The end game was by now frozen as a modified Vorbrüggen protocol and enzymatic hydrolysis (Scheme 3).

**Scheme 2** Alternative route: thiazolidine-2,4-dione precursor (**18**)





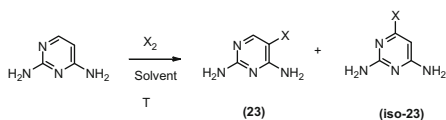
**Scheme 3** Alternative route: pyrimidine-2,4-diamine precursor (19)

Overall, we then had two alternative routes demonstrated, and we needed to decide which one to use for our scenario of rapid development. While most requirements were rather comparable, the determining factors relied on two aspects. First, the ease of purification of the base appeared critical. The poor solubility of the heterocyclic base in all solvents evaluated indeed prompted us to identify a method generating a penultimate heterocyclic base (21) of high purity. This way, we would minimize the risks for a need for a time-consuming and expensive and sophisticated means of purification. Second, the overall development timelines imposed on us that the chemistry and process were ready in very short time, thus leaving us limited opportunity to play around. It was judged it would take longer to understand and optimize the rather unselective and complex formylation of thiazolidine-2,4-dione (18) compared to the sequence starting from pyrimidine-2,4-diamine (19). This requirement is not unusual and should remind everyone of the ultimate goal of a project in pharma, namely, to deliver an innovative product to patients as soon as possible. This implies at times that innovative routes or chemistry needs to be developed when timelines allow for it or that the program needs to be supported as rapidly and reliably as possible. Alternatively, it can mean that the best demonstrated route needs to be developed, even if not ideal, if speed is of paramount importance. Process chemists should then be skilled at understanding the current scenario and maneuvering through the requirements to deliver what is expected for a given project. Such business mindset is key to the success of complex portfolio of projects that lead to increased chances of advancing an innovative drug for patients, but can be a challenge to pure scientists' mind at times.

It was therefore decided to focus our efforts of the second phase of process development onto the alternative 2, using pyrimidine-2,4-diamine (19) as the key raw material for the heterocyclic base (21) (Table 1).

**Table 1** Overview of options

	Original route from 2,6-diaminopyrimidin-4-(3 <i>H</i> )-one ( <b>5</b> )	Alternative 1 from thiazolidine-2,4-dione ( <b>18</b> )	Alternative 2 from pyrimidine-2,4-diamine ( <b>19</b> )
Scalability	No	Yes	Yes
Robustness	Difficult	Manageable	Manageable
Quality	Requires significant efforts	Manageable but challenging if too unselective	Manageable
Cost	Very high	High	Acceptable
Practicality	Low	Acceptable	Acceptable
Expediency	Long	Fast	Fast
Safety	Acceptable	Acceptable	Acceptable
Environment	Poor performance	Manageable	Manageable
Overall potential and potential time for developability	Low potential	High potential in reasonable amount of time	High potential in short amount of time
			Preferred route

**Table 2** Overview of the 2-halogenation of pyrimidine-2,4-diamine (**19**)

Conditions	Outcome
Cl <sub>2</sub> , various solvents	Mixture of regioisomers
Other chlorinating agents, various solvents	Mixture of regioisomers
Br <sub>2</sub> , H <sub>2</sub> O	High yield, medium selectivity
Pyridine – HBr <sub>3</sub> , H <sub>2</sub> O	High yield, high selectivity
Pyridine – HBr <sub>3</sub> , THF	High yield, high selectivity
Br <sub>2</sub> , AcOH	High yield, high selectivity

### 3.2 Process Development: Understanding and Optimization of the Ultimate Process

#### 2-Halogenation of Pyrimidine-2,4-diamine (**19**) to 5-Bromopyrimidine-2,4-diamine (**23**)

To build the desired heterocyclic base, selective functionalization of the corresponding regioisomer of pyrimidine-2,4-diamine (**19**) was required. While both chlorinating and brominating agent displayed good reactivity, all chlorinated agents tried resulted in mixtures of regioisomers. Out of the brominated agents tried, an equimolar amount of bromine in acetic acid at 0°C worked the best and resulted in 2 h into the corresponding salt HBr salt [11] (Table 2).

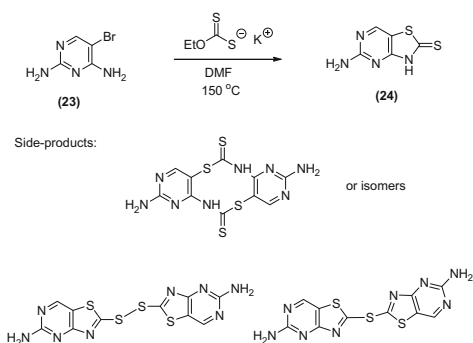
We rapidly focused our attention to these conditions and came up with the very productive process where a solution of bromine in acetic acid was added to a solution of pyrimidine-2,4-diamine at a rate such to maintain an internal temperature around 0°C (15 equivalent volume of DMF). The reaction mixture was then warmed up to room temperature to allow for rapid completion. The product crystallized in 1 h as a hydrobromic acid salt in the process was removed by filtration and used as such. It was resuspended into water; the pH was adjusted to neutral by addition of a dilute solution of sodium hydroxide. Formation of the highly pure crystalline 5-bromo-pyrimidine-2,4-diamine (**23**) ensued, which was removed by filtration, washed once with water, and dried to afford a white crystalline solid in 90% yield and high purity (>99%). The high crystallinity of the intermediates isolated and their desirable big particle size allowed for very fast filtration and drying, an additional benefit of the process.

### Condensation of 5-Bromopyrimidine-2,4-diamine (**23**) and Potassium Xanthogenate to the 5-Aminothiazolo[4,5-*d*]pyrimidine-2(3*H*)-thione (**24**)

Once again, we were fortunate to be close to a good process from the start and only had to conduct a short optimization on solvents, temperature, and stoichiometry. The optimization exercise concluded that an excess of 2.0–2.2 equivalent of potassium xanthogenate in such a polar aprotic solvent as DMF (10 equivalent volume) worked best at 140–160°C. The very limited solubility of the product was a major reason for such drastic conditions. Nonetheless good selectivity and efficiency were observed as demonstrated by isolated yields in the low 90%. As predicted, the formed side-products here tended to remain with the main product, due to the very limited solubility of the product and its related side-products, presumably the dimer(s)-like depicted below resulting from either standard dimerization or oxidation of the xanthogenate. We fortunately could limit their formation to no more than ca. 5% in total (Scheme 4).

The exact nature of the dimer-like side-products was not identified at that stage.

**Scheme 4** Condensation of 5-bromo-pyrimidine-2,4-diamine (**23**) and potassium xanthogenate to the 5-aminothiazolo[4,5-*d*]pyrimidine-2(3*H*)-thione (**24**) and related side-products

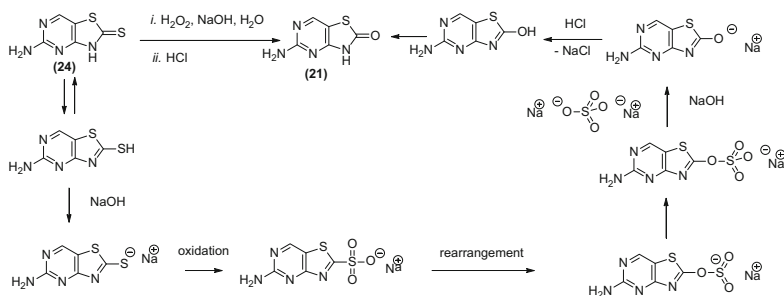


Ultimately, the process consisted in heating up a suspension of 5-bromo-pyrimidine-2,4-diamine (**23**) and potassium xanthogenate in 10 equivalent volume of DMF at ca. 150°C (careful calorimetric evaluation had showed this process to be manageable despite the elevated temperature). Within a few hours, the condensation was complete, at which point water (1.5 equivalent volume) was added, the temperature lowered to room temperature, and the pH adjusted to 5 with dilute sulfuric acid. Formation of an off-white solid was observed, which was removed by filtration. The solid was fine at the outcome of the precipitation, which required isolation with a centrifuge to minimize the bottleneck associated with a time-consuming filtration. The solid could then be used as such in the subsequent step.

### **Oxidation of the 5-Amino-3*H*-thiazolo[4,5-*d*]pyrimidin-2-thione (**24**) to the 5-Amino-3*H*-thiazolo[4,5-*d*]pyrimidin-2-one (**21**)**

The required net transformation here consists in a selective oxidation of the more basic sulfide onto its corresponding sulfinate salt that will further rearrange to the corresponding isomer. The latter is then hydrolyzed to the pyrimidinone after adjustment to acidic pH, thus releasing sodium sulfate in the process [12]. Several oxidizing agents were assessed and proven successful. We focused on the more desirable basic hydrogen peroxide. A standard optimization on solvent, temperature, stoichiometry of the various components of the system allowed us to determine that an equimolar excess of hydrogen peroxide and sodium hydroxide (4 equivalents) in water added to a suspension of 5-amino-3*H*-thiazolo[4,5-*d*]pyrimidin-2-thione (**24**) in water (10 equivalent volume) at 50–60°C allowed for the reaction to proceed to completion in ca. 1 h. Hydrochloric acid was demonstrated to be the optimal acid reagent that allowed for the purest overall transformation, with a minimum amount of overoxidation side-products and simplest process. None of these overoxidized side-products could actually be observed. The process resulted in material of good overall purity (96–98% by weight) isolated although in modest 75% yields. The earlier impurities formed would be carried over at that stage, due to the sparse solubility of this family of compounds. The process was eventually completed by adjusting the pH to below 1 at 0°C with dilute hydrochloric acid, filtering off the inorganic salts using celite as filtering aid, adjustment of the pH back to ca. 5, and isolation of the desired 5-amino-3*H*-thiazolo[4,5-*d*]pyrimidin-2-one (**21**) on a standard filter. Although in limited amount, most other side-products were not removed during the crystallization. They were however easily depleted in the subsequent step as will be depicted in the next section. Besides, we knew we could further improve in the near future by controlling the conversion even tighter and identifying a less dissociable and non-nucleophilic solvent as an alternative to DMF (Scheme 5) (Fig. 6).

The more problematic issue was the high hygroscopicity of the heterocyclic base (**21**). Indeed, while the base could be dried under standard conditions, it would dramatically and rapidly incorporate water under almost any conditions. While in the laboratory we could manage to carry out such inert and anhydrous conditions



**Scheme 5** Proposed pathway to the 5-amino-3*H*-thiazolo[4,5-*d*]pyrimidin-2-one (**21**)

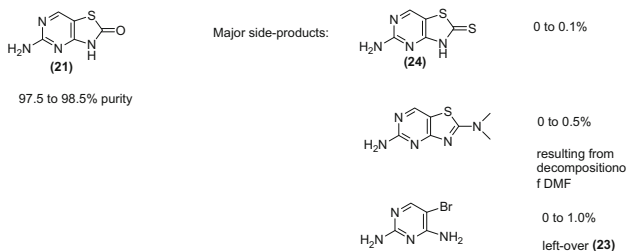


**Fig. 6** Typically observed purity profile of 5-amino-3*H*-thiazolo[4,5-*d*]pyrimidin-2-one (**21**)

during the drying and handling operations, it would turn to be impossible in a production environment, thus leaving us this practical issue to solve. Two strategies were evaluated to solve the issue: identification of a more stable nonhygroscopic form and designing a subsequent glycosylation process that could accommodate for the limitation.

For the former, all attempts failed. At no point, we could ever manage to crystallize the solid or even just to equilibrate its form into a more stable and nonhygroscopic one. An unsuccessful screening of even exotic solvents made us deprioritize this approach. While we knew we could achieve the task *in situ* prior to the glycosylation, we were uncertain this could be achieved in an efficient and productive process.

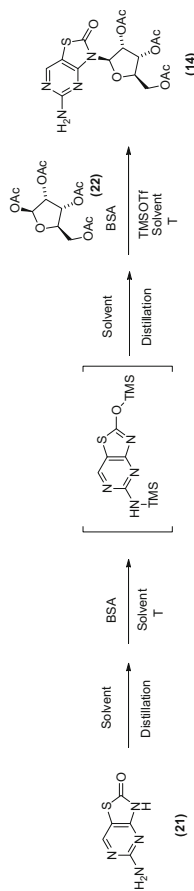
## The End Game: Glycosidation and Selective Enzymatic Hydrolysis to the API

The abovementioned hygroscopicity of the deoxyribose was our first major practical challenge. In the course of our preliminary route scouting, we were already able to recognize a Vorbrüggen protocol as being the most promising [8]. The next challenge consisted in the control of the various stages of the process (persilylation and then glycosidation). We indeed wanted to make sure the persilylation would proceed to completion, prior to the glycosylation step itself. Unfortunately, the

persilylated intermediate was too unstable for the standard in-process control. We therefore turned our attention to a nonintrusive technique such as in situ IR. In the meantime, we tried to find an alternative to the commonly used chlorinated solvents or acetonitrile for persilylation. Bis-silyl acetamide, one of the strongest silylating agents readily available, had been demonstrated to be required to guarantee complete persilylation, but its combination with acetonitrile clearly showed limitations with the formation of significant amount of side-products coming from the Ritter manifold. Initial monitoring of this persilylation step via in situ IR revealed that the double silylation occurred quite readily in a variety of polar aprotic solvents and could be easily monitored using this technique. Water content was however demonstrated to be critical (the presence of 0.5% water could severely impede the silylation). Bis-silyl acetamide itself could not be used as a solvent as it would lead not only to extensive decomposition of the product of the glycosidation (hydrolysis of acetates) but also to an increase of the overall process cost. Acetonitrile allowed for sufficient solubility but raised the challenges mentioned above (side-products resulting from Ritter manifold). Dichloromethane and dichloroethane were also known solvents for such transformation but were clear undesirable options for environmental reasons. We therefore turned our attention to the less often used aromatic solvents. Toluene has been reported to allow efficient glycosidation in certain cases [13] but did not allow solubilization of our specific deoxyribose, resulting in almost no reactivity. To our delight, the more polar aromatic and higher boiling point solvents were xylene, cymene, and anisole [14]. Xylene already displayed sufficient desirable solubilization properties and reactivity to allow for complete persilylation in a few minutes at 60°C (see Table 3 and 4). Although the mixture was heterogeneous at the beginning of the reaction, xylene offered the opportunity to reduce the water content from the hygroscopic heterocyclic base prior to the persilylation thanks to a very efficient azeotropic drying, thus limiting the need for excess BSA. In addition, at the outcome of the persilylation, the excess bis-silyl acetamide (BSA) and its resulting side-products could be removed by distillation. This allowed minimizing the decomposition of the product and the bis-sugar side-products. It also allowed for maintaining the overall throughput attractive as the volume would remain constant despite the successive addition of the various components. The final benefit resulting from our findings was the opportunity to recycle easily xylene as well as silyl acetamide after treatment with HMDS.

This finding had allowed us to solve not only the issue of controlling the preliminary persilylation step but also to address that of hygroscopicity of the deoxyribose. We indeed now had a practical solution. The glycosidation event itself was then extensively evaluated. In the absence of silyl acetamide side-products, a smaller amount of decomposition was observed (no more than 5–8% di- or monoacetates observed). However, the presence of regioisomer and bis-sugars was still observed and needed to be minimized. Trimethylsilyl triflate had appeared as the optimal acid catalyst from the various Lewis acids evaluated ( $\text{SnCl}_4$ ,  $\text{ZnCl}_2$ ,  $\text{TiCl}_4$ ,  $\text{BF}_3\text{-OEt}_2$ ,  $\text{AlCl}_3$ ). Careful monitoring of the reaction profile gave us a good understanding of the equilibration process between the kinetic and

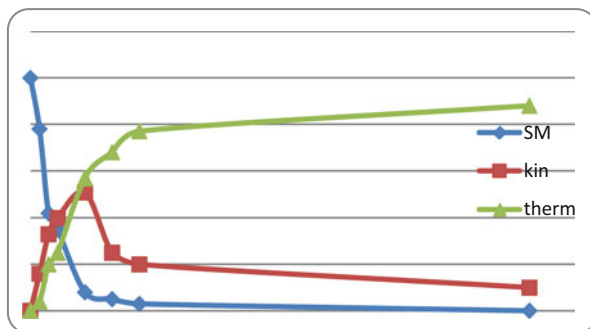
**Table 3** Selected experiments for the optimization of the glycosidation step



Entry	Solvent	Temperature (°C)	Sugar addition	Rate of addition	Yield of <b>14</b>
1	CH <sub>3</sub> CN	40	Solid	1 h	80% assay
2	Toluene	40	Solid	1 h	45% assay
3	Xylene	40	Solid	1 h	ca. 85% assay
4	Cymene	40	Solid	1 h	ca. 85% assay
5	Anisole	40	Solid	1 h	ca. 85% assay

**Table 4** Temperature effect in the glycosidation to (14)

Entry	Solvent	Temperature (°C)	Sugar addition	Yield of 14
1	Xylene	20	Solid	51% assay
2	Xylene	40	Solid	ca. 85% assay
3	Xylene	60	Solid	85% assay (16 h reaction time)
4	Xylene	80	Solid	85% assay (3 h reaction time)

**Fig. 7** Influence of temperature on kinetic and thermodynamic products**Table 5** Addition effect in the glycosidation to (14)

Entry	Solvent	Temperature (°C)	Sugar addition	Yield of 14
1	Xylene	60	Solution added in 1 h	85% assay yield
				65% isolated yield
				Purity >99% after crystallization
2	Xylene	60	Slurry added in 1 h	85% assay yield
				67% isolated yield
				Purity >99%
3	Xylene	60	Solid added in 1 h	65% isolated yield, ca. 20% loss in ML
				Purity >99%
4	Xylene	60	Solid added in 1 portion	77% assay yield
				57% isolated yield
				Purity >99%
5	Xylene	60	Solid added in 1 h portionwise	85% assay yield
				65% isolated yield
				Purity >99%
6	Xylene	60	Solid added in 4 h portionwise	85% assay yield
				65% isolated yield
				Purity >99%

thermodynamic products. Under our conditions, the two isomers were observed to form at similar rate for the first ca. 3 h, and the kinetic one then isomerized into the desired thermodynamic one (see Fig. 7).

The peracetylated ribofuranoside (**22**) also displayed limited stability under the reaction conditions (ca. 50% decomposition after 24 h at 80°C) as well as the product (**14**) itself (ca. 20% decomposition after 24 h at 80°C). Addition of the sugar in solution, as a slurry or as a solid, had no impact on the outcome of the reaction. The solid addition was therefore preferred in order to minimize the overall volume of the reaction. The rate of the sugar addition was also found to be critical. Best results were obtained with controlled addition of the sugar as a solid in at least 1 h (Table 5).

The preferred process eventually consisted in the single charging of the reaction vessel with the heterocyclic base, without precaution to prevent water adsorption, suspension in xylene, and distillation to a constant residual water content. The Lewis acid activator TMSOTf was charged and ribofuranoside (**22**) was added portionwise in 1 h. The resulting reaction mixture was stirred at 60°C for ca. 12 h until completion. Typically a 85% chemical yield is observed at that stage. The mixture is then cooled to ca. 30°C to go into the work-up part so as to allow for an optimal throughput. For the isolation and purification, our preliminary solvent screening had showed that a combination of aromatic solvent and an ester could result in crystalline material of very high purity. Therefore, we just had to proceed with an aqueous work-up followed by distillation to a ca. 20% mixture in xylene, resuspension in isopropyl acetate, demonstrated to be the optimal ester for purification and throughput reasons, and slow cooling to 0°C. This process robustly resulted in highly crystalline material that could be isolated by simple filtration and drying to result in an overall 65% yield of product from the heterocyclic base in a purity >99% (Figs. 8 and 9).

This process was repeated with various grades of heterocyclic base and turned extremely robust, both in terms of chemical yield and isolated purity, which was one of our major concerns to be able to produce on time. We had besides demonstrated a more than fourfold improvement in our throughput, based on the development of a heterogeneous process, and the recycling of the various components of the reaction which can be further illustrated by our overall performance in Process Mass Intensity [14], reduced by a similar five-fold ratio [2].

This practical process to glycosidate a sugar with a poorly soluble base was later demonstrated to be quite general. Its operational simplicity and high practicality that can accommodate numerous variations without significant deviation of both the yield and the purity made us investigate its scope. It is of particular interest for highly hygroscopic and poorly soluble bases as we demonstrated in the robust glycosidation of otherwise difficult to obtain nucleosides (D. Lupp and F. Gallou, unpublished result). In all cases, yields ranging between 75% and 85% were observed, along with high purity (Fig. 10).

Overall, the process proved highly reproducible and robust, but as it is sometimes the case, we encountered a technical challenge when we went to our final equipment. Marginal differences were indeed observed during the quench and in

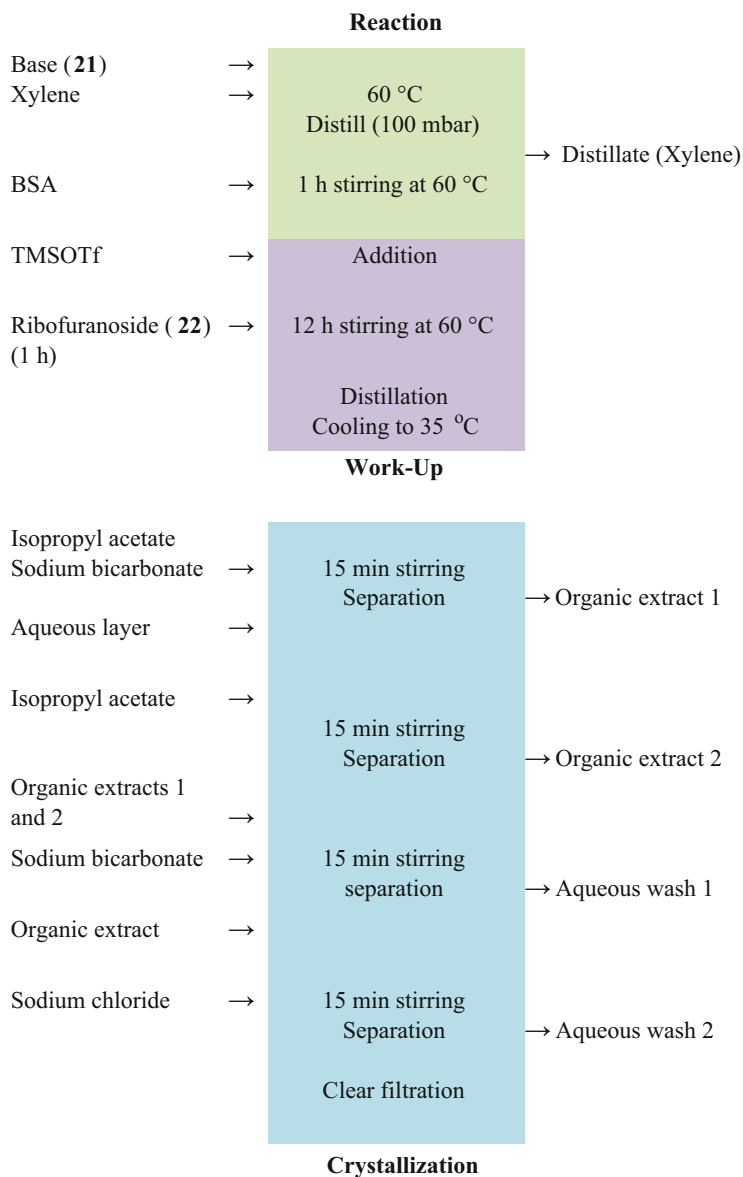
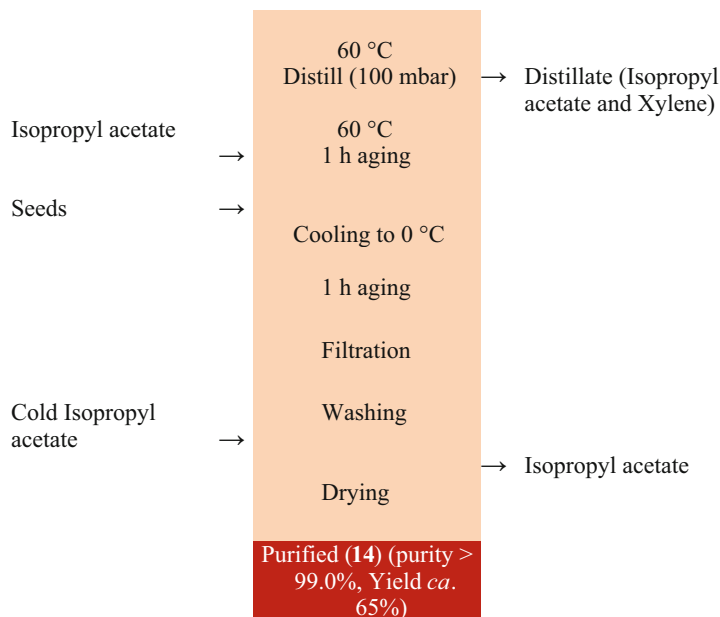
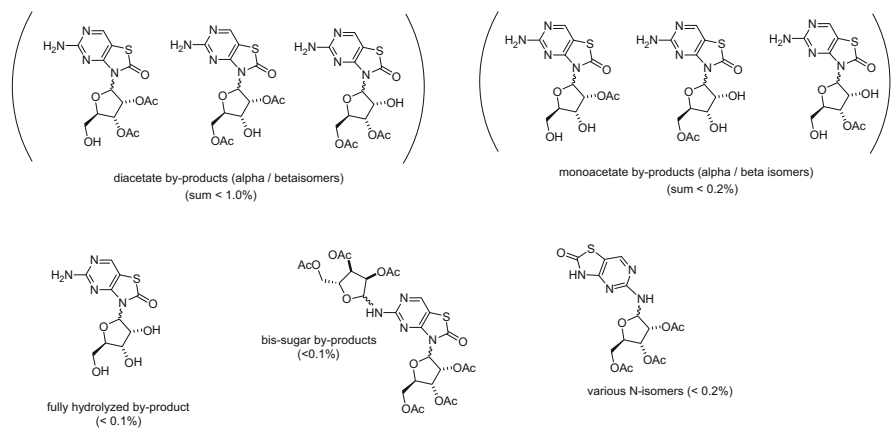


Fig. 8 (continued)



**Fig. 8** Block flow diagram of final process to (14)



**Fig. 9** Main side-products of (14)

the aqueous extracts with formation of oily residue. No impact on the quality was observed, but the discrepancy in physical aspect led to a 5–10% lowered isolated yield. We investigated this deviation carefully and recognized the underemphasized criticality of stirring in our process. Stirring had indeed been identified as critical at the persilylation stage (heterogeneous reaction at the beginning) and for the work-up (to avoid gumming of the product) during our laboratory investigations. We

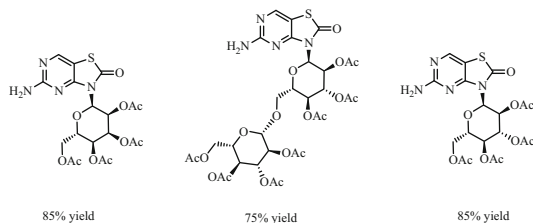


**Fig. 10** Scope of newly developed glycosidation protocol

believed we had addressed this sufficiently as demonstrated by our successful preliminary pilot trials. However, the final vessel equipped with an anchor stirrer did not allow rates greater than 40 rpm and turned to be insufficient on our scale. This led to the formation of a triphasic system after quench with a thick oil containing mostly product at the bottom of the reactor. In order to solve this technical challenge, we went back to the laboratory and repeated the glycosidation with an anchor stirrer and very slow rotation.

Similar observations to the ones from the plant were made. An important loss was observed in the first aqueous extract at a level significantly higher than usual (5–6% instead of 1–2%). Rapid stirring was sufficient to recover the more conventional aqueous and organic biphasic system. Ultimately, it appeared that reduction of the xylene content by distillation and simple control to a limit of no more than 15% volume followed by the addition of isopropyl acetate prior to the aqueous work-up solved our original challenge in the simplest and reliable manner. Additionally, a second organic extraction that would allow us to minimize the loss or better stirring was implemented.

The final step consisted in the regioselective hydrolysis of the acetate of the primary alcohol. We were now in the fortunate position to enter this last chemical transformation with a high-quality starting material (purity > 98% by weight). This allowed us to really optimize the transformation and to focus on the productivity of the process.

Enzymes have long been demonstrated to be the best option in cases where such selectivity is expected from a transformation and in the presence of sensitive functional groups. Immobilized lipases are generally used to perform biotransformations of most interesting industrial applications that quite often take place in nonaqueous media [15]. The process was originally conducted with the polymer immobilized *Candida Antarctica* Lipase Novozyme435@ (repetition (CAL-B, Novozym435@, 7300PLU/g). For typical uses of this lipase, see, for example, [16]) in acetone or *tert*-butanol, under phosphate buffer conditions to allow for the hydrolysis and avoid further decomposition of the product. The transformation was nevertheless long (completion was generally observed after up to 2 days) and lacked selectivity (substantial amounts of mono- and diacetates side-products were observed, typically in the range of 8–12%). Our goal was therefore to improve the productivity and selectivity while minimizing the loading of the costly enzyme. The robustness and simplicity of the process were also of paramount importance as

our preliminary experience had been mediocre with high variability and complex downstream process especially. We first looked into the optimal enzyme to achieve the transformation in a productive fashion. It was clear from our earlier experience and state-of-the-art methodologies that immobilized enzymes would be required, if we wanted to minimize the loading and recycle it. A variety of options were then available and assessed. The readily available IMB-111 [17] and Novozym435@ were proven superior to most other enzymes tried. We extended our investigations with these two enzymes and needed to rapidly decide which one we would select based on technical and economic considerations. Results showed that under non-denaturing conditions (used in the aqueous-based tributyrin/tricaprylin medium), Novozym435@ was slightly less active than IMB-111 but displayed marginally better selectivity. Besides, Novozym435@ displayed a narrower window of operation on terms of temperature, both in terms of lowered kinetic profile and side-products formed at increased temperature. Ultimately, IMB-111 was able to convert > 99% of starting material in 22 h at 22°C for starting material at 6%

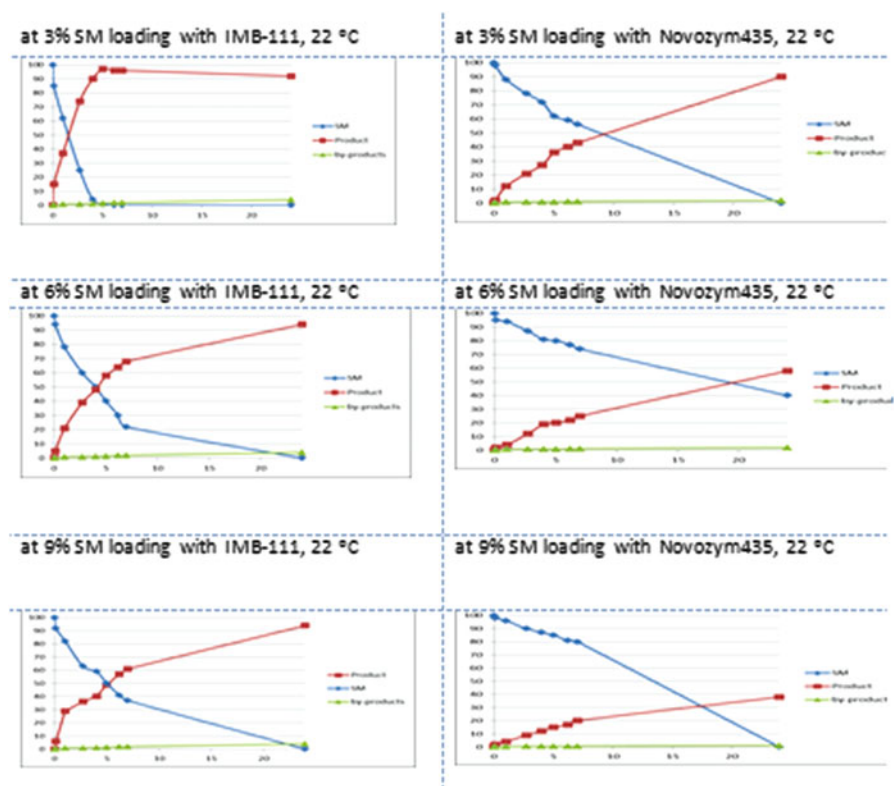


**Fig. 11** Kinetic profile of the enzymatic hydrolysis of (14) to (1) as a function of loading in (14) and enzyme

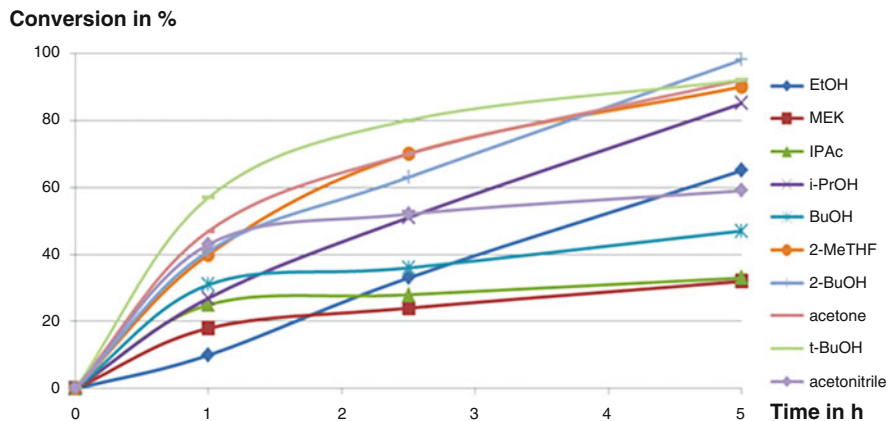


**Fig. 12** Solvent screening for the enzymatic hydrolysis to (1)

concentration, while Novozym435@ would achieve the same under the same conditions but at 3% starting material concentration (Fig. 11).

While IMB111 had proven slightly superior in terms of potential throughput especially, there was no real obvious benefit when it came to robustness. Ultimately, the main deciding factor was the readily availability of the enzyme. There was indeed a lesser likelihood that we would encounter issues in our supply chain with the more readily available Novozyme435@. We therefore concluded that it would be the lipase of choice to enter the more intense optimization phase.

We first screened a variety of mono- and biphasic solvent systems. Solvent selection is known to be critical factor for biocatalysis [18, 19], as organic solvents are known to influence the enzyme activity and selectivity [20–23]. Solvents are indeed reported to impact an enzyme conformation by interacting with the hydration layer essential for catalysis and by altering hydrophobic or H-bonding in the core of the protein as well as protein solvation sites.

Our screening confirmed that *tert*-butanol and acetone were some of the optimal solvents from a reactivity standpoint. However, alternatives were identified such as isopropanol, 2-butanol, and 2-MeTHF (Fig. 12).

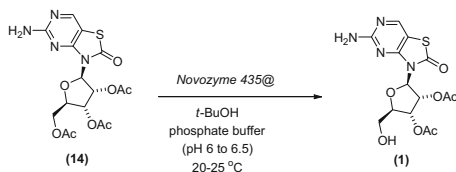
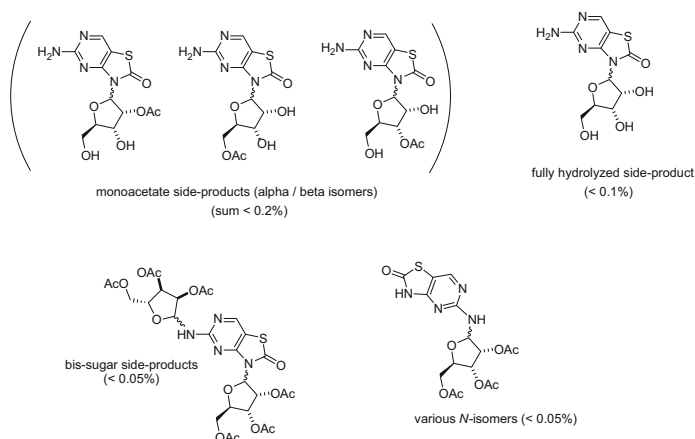
The latter especially attracted our attention as solubility studies had revealed the product to be more than 50 times more soluble in 2-MeTHF than in MTBE, the extraction solvent used originally. Put together, this meant a dramatic reduction of the solvent requirements for the work-up in particular as no additional water immiscible solvent was required. This resulted in an immediate improvement in the volume efficiency by ca. 30%.

We continued our optimization of the volume efficiency and demonstrated that the enzyme was actually very robust in this solvent system. No deactivation was observed even with relatively high concentration of starting material (see Table 6).

The main side-products observed then would be for the main part over-hydrolyzed-related compounds (1.7–1.9%) and the related carry-over of the dimers (<0.4%). Based on all of these improvements, a first-generation batch process was

**Table 6** Optimization on throughput

Entry <sup>a</sup>	Concentration in wt%	Yield	HPLC purity <sup>b</sup>	Reaction volume efficiency (overall volume/kg product ( <b>1</b> ))
1	3.8%	85%	94.3%	26
2	4.7%		94.6%	21
3	5.7%		95.3%	17
4	7.3%		94.5%	13

<sup>a</sup>16 h reaction time<sup>b</sup>HPLC purity by area % at 230 nm**Scheme 6** Selective batch process for the enzymatic hydrolysis to the API (**1**)**Fig. 13** Side-products from hydrolysis step (**1**)

implemented that consisted in running the enzymatic hydrolysis in *tert*-butanol at 20°C at ca. 7% weight of (**14**) and 10% weight of Novozym435@ over 16 h, while maintaining the pH constantly between 6.0 and 6.5 with a 0.5 M Na<sub>2</sub>HPO<sub>4</sub> solution. At completion, the crude reaction mixture was filtered to remove the immobilized enzyme, extracted with 2-MeTHF, and washed with water to provide the crude product (**1**) (Scheme 6).

The crude product could be readily crystallized as a free base from the 2-MeTHF solution using MTBE as an anti-solvent. It resulted into material of very high purity, typically > 99.50%, with over-hydrolyzed compounds as the major side-products (Fig. 13).

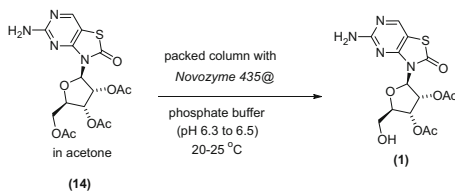
The consecutive nature of the main side-products coming from over-hydrolysis of the desired product prompted us to consider a semicontinuous process as an alternative. A potential benefit would come from an accelerated hydrolysis that could minimize the reaction time and avoid further hydrolysis of the diacetate product to the mono and fully hydrolyzed side-products, thus enabling a continuous or semicontinuous process that could allow for recycling of the immobilized enzyme. We had observed such a phenomenon when we screened a series of additives, such as various Lewis acids ( $\text{FeCl}_3$ ), for example, inorganic salts  $\text{NaCl}$  [24],  $\text{LiCl}$  [25], or other additives such as PEG [26]. An interesting but moderate effect with  $\text{LiCl}$  and PEG was observed (5–10% acceleration) so that the added benefit did not appear significant enough to justify such a change.

Fortunately, the high stability of the enzyme provided an even simpler handle for acceleration, while maintaining the desired selectivity. A ca. 20% maximum reaction acceleration was indeed observed when increasing the temperature to  $35^\circ\text{C}$  but unfortunately only in acetone, thus requiring a second immiscible solvent for the isolation, 2-MeTHF as previously identified. Put together, these findings provided the basis for an improved process for the regioselective enzymatic hydrolysis which overcomes many of the shortcomings of previously used regioselective enzymatic hydrolysis process.

With these considerations, a system was designed using a column packed with Novozym435@ and swollen with acetone. At that stage, a feed of the starting material in acetone at a concentration of 1.6 mol/L and  $35^\circ\text{C}$  was circulated at various flow rates in a loop mode until full conversion was observed as indicated by the plateau observed during the in situ pH measurement. The pH was constantly adjusted to 6.3–6.5 with a phosphate buffer. It was rapidly discovered that the reaction could be >98% complete within a couple of hours by recirculating the reaction mixture in a loop with this simple set-up, with ca. 1.0% over-hydrolysis side-product and a steady yield of 97.0% [27]. This was achieved at this stage with a relatively high enzyme loading of 3 equivalent weight ratio of enzyme to substrate and a 6.4 mL/L flow rate. By comparison, a batch mode hydrolysis would result in same conversion within 16 h and would display 3–5% over-hydrolysis, with the same catalyst loading.

Under these conditions, the reaction could run for days without significant loss of activity for an overall increase of productivity by a factor close to 3 compared to our optimal batch data. Besides, this second-generation semicontinuous process was easy to implement with minimal capital investment for the column system and the PAT infrastructure to be used to control the progress of the reaction. Ultimately, the crude drug substance (**1**) was extracted as previously described in the batch

**Scheme 7** Semicontinuous process to (**1**)



process and crystallized from MeTHF/MTBE to result in highly pure material (>99.5% purity), in >90% yield overall (Scheme 7).

This process has several advantages over the batch process previously described, such as improved yield, faster reaction, continuous process possible for work-up, no more filtration, enzyme loading, increased throughput, reduced waste, and, importantly, improved selectivity and minimized hydrolysis to the undesired monoacetate and tris-hydroxy compounds. All these factors contributed to a greatly improved economic impact for this last step of the synthesis.

## 4 Conclusions

The process research and development activities to the final route and process for (1) an oral prodrug of isatoribine (2) have been highlighted in the subsections above. Of particular importance was the development of a robust and readily available process which directed our manufacture of the base in a straightforward sequence and the development of a highly practical and streamlined glycosylation process, followed by an effective and regioselective enzymatic hydrolysis via the readily available Novozm435@ *Candida Antractica* lipase, both with a much improved environmental impact.

## References

1. Xiang AX, Webber SE, Kerr BM, Rueden EJ, Lennox JR, Haley GJ, Wang T, Ng JS, Herbert MR, Clark DL, Banh VN, Li W, Fletcher SP, Steffy KR, Bartkowski DM, Kirkovsky LI, Bauman LA, Averett DR (2007) Discovery of ANA975: an oral prodrug of the TLR-7 agonist isatoribine. *Nucleosides Nucleotides Nucleic Acids* 26:635–640
2. Gallou F, Seeger-Weibel M, Chassagne P (2013) Development of a robust and sustainable process for nucleoside formation. *Org Process Res Dev* 17:390–396
3. Fletcher S, Steffy K, Averett D (2006) Masked oral prodrugs of toll-like receptor 7 agonists: a new approach for the treatment of infectious disease. *Curr Opin Investig Drugs* 7(8):702–708
4. Anderson NG (2012) Practical process research and development – a guide for organic chemists, 2nd edn. Academic, Amsterdam
5. Anastas PT, Warner JC (1998) Green chemistry: theory and practice. Oxford University Press, New York
6. Anastas PT, Zimmerman JB (2003) Through the 12 principles of green engineering. *Environ Sci Technol* 37(5):94A–101A
7. Roschangar F, Sheldon RA, Senanayake CH (2015) Overcoming barriers to green chemistry in the pharmaceutical industry – the Green Aspiration Level™ concept. *Green Chem* 17:752–768
8. Vorbrueggen H (1995) Adventures in silicon-organic chemistry. *Acc Chem Res* 28(12): 509–520
9. Jutz C (1976) Iminium salts in organic chemistry. Wiley, New York
10. Hanessian S, Banoub J (1977) Chemistry of the glycosidic linkage. *Carbohydr Res* 59: C13–C16
11. English JP, Clark H, Clapp JW, Seeger D, Ebel RH (1946) *J Am Chem Soc* 68:453

12. D'Amico JJ, Bollinger FG, Freeman JJ (1988) Synthesis of 2-oxo and 2-thioxo-3(2*H*)-benzothiazoleethanimic acid anhydride with acetic acid and related products. *J Heterocycl Chem* 25(5):1503–1509
13. Li N-S, Piccirilli JA (2006) Efficient synthesis of 2'-C- $\beta$ -methylguanosine. *J Org Chem* 71(10):4018–4020
14. Jimenez-Gonzalez C, Ponder CS, Broxterman QB, Manley JB (2011) Using the right green yardstick: why process mass intensity is used in the pharmaceutical industry to drive more sustainable processes. *Org Process Res Dev* 15(4):912
15. Palomo JM, Filice M, Fernandez-Lafuente R, Terreni M, Guisana JM (2007) Regioselective hydrolysis of different peracetylated  $\beta$ -monosaccharides by immobilized lipases from different sources. Key role of the immobilization. *Adv Synth Catal* 349(11):1969–1976
16. Orrenius C, Norin T, Hult K, Carrea G (1995) The *Candida antarctica* lipase B catalysed kinetic resolution of seudenol in non-aqueous media of controlled water activity. *Tetrahedron Asymmetry* 6(12):3023–3030
17. Dicosimo R, Payne MS, Croud VB, Gavagan JE, Wagner LW, Hann EC (2007) US 20070042924
18. Kinoshita M, Ohno A (1996) Factors influencing enantioselectivity of lipase-catalyzed hydrolysis. *Tetrahedron* 52(15):5397–5406
19. Kitamoto Y, Kuruma Y, Suzuki K, Hattori T (2015) Effect of solvent polarity on enantioselectivity in *Candida antarctica* lipase B catalyzed kinetic resolution of primary and secondary alcohols. *J Org Chem* 80(1):521–527
20. Burke PA, Griffin RG, Klivanov AM (1993) Solid-state nuclear magnetic resonance investigation of solvent dependence of tyrosyl ring motion in an enzyme. *Biotechnol Bioeng* 42(1):87–94
21. Margolin AL, Tai DF, Klivanov AM (1987) Incorporation of D-amino acids into peptides via enzymic condensation in organic solvents. *J Am Chem Soc* 109(25):7885–7887
22. Sakurai T, Margolin AL, Russell AJ, Klivanov AM (1988) Control of enzyme enantioselectivity by the reaction medium. *J Am Chem Soc* 110(21):7236–7237
23. Dordick JS (1992) Designing enzymes for use in organic solvents. *Biotechnol Prog* 8(4):259–267
24. Takahashi K, Tamaura Y, Kodera Y, Mihama T, Saito Y, Inada Y (1987) Magnetic lipase active in organic solvents. *Biochem Biophys Res Commun* 142(2):291–296
25. Talukder MM, Rahman B, Ko LM, Song OP, Pu S, Wu J, Chuan W, Jae C, Chow Y (2008) Improved method for efficient production of biodiesel from palm oil. *Energy Fuels* 22(1):141–144
26. Secundo F, Carrea G (2002) Lipase activity and conformation in neat organic solvents. *J Mol Catal B: Enzym* 19:93–102
27. Gallou F, Beney P US 20110091943

# Development of Efficient Routes to Access C-Glycosides as SGLT-2 Inhibitors for the Treatment of Type 2 Diabetes

Sébastien Lemaire and Didier Schils

**Abstract** C-Glycosides represent an attractive class of compounds for the medicinal chemist because they are more resistant to enzymatic hydrolysis than O-glycosides and therefore are considered as potential drug candidates. The potential was confirmed by the emergence of a new family of C-glycosides known as the SGLT-2 inhibitors leading to the development of new drugs for the treatment of type 2 diabetes. In this chapter, chemical processes to access new active pharmaceutical ingredients (API) will be described focusing on the key C-glycosylation step.

**Keywords** C-glycosylation · Canagliflozin · Dapagliflozin · Ertugliflozin · Ipragliflozin · Luseogliflozin · Sotagliflozin · Tofogliflozin

## Contents

1	Introduction .....	31
2	C-Glycoside Synthesis <i>via</i> Nucleophilic Addition to Carbonyl Derivatives .....	32
2.1	Addition on Lactone Derivatives .....	32
2.2	Addition to Amide Derivatives .....	39
3	Direct C-Glycosylation .....	42
3.1	Introduction to Direct C-Glycosylation .....	42
3.2	Direct C-Glycosylation in the Presence of Diarylzinc and Its Application to Canagliflozin and Dapagliflozin .....	43
3.3	Direct C-Glycosylation in the Presence of Arylalanines and Its Application to Canagliflozin and Dapagliflozin .....	46
4	Conclusion .....	48
	References .....	49

---

S. Lemaire (✉)

API Small Molecule Development, Janssen Research and Development, Turnhoutseweg 30,  
2340 Beerse, Belgium  
e-mail: [slemaire@its.jnj.com](mailto:slemaire@its.jnj.com)

D. Schils

Galapagos NV, CMC Development, Gen. De Wittelaan L11 A3, 2800 Mechelen, Belgium

## Abbreviations

Ac	Acetyl
acac	Acetylacetonate
API	Active pharmaceutical ingredient
Ar	Aryl
Bn	Benzyl
Bz	Benzoyl
d	Day(s)
DBE	Di- <i>n</i> -butyl ether
DIBAL-H	Diisobutylaluminum hydride
DMAP	4-(Dimethylamino)pyridine
DMP	Dess–Martin periodinane
DMSO	Dimethyl sulfoxide
equiv	Equivalent(s)
Et	Ethyl
Et <sub>3</sub> SiH	Triethylsilane
h	Hour(s)
<i>i</i> -Pr	Isopropyl
LG	Leaving group
L-PGA	L-Pyroglutamic acid
Me	Methyl
MSA	Methanesulfonic acid
MTBE	Methyl <i>tert</i> -butyl ether
<i>n</i> -Bu	Butyl
<i>n</i> -Hex	<i>n</i> -Hexane
Nu	Nucleophile
PG	Protecting group
Ph	Phenyl
Piv	Pivaloyl
PMB	4-Methoxyphenyl
PNB	4-Nitrobenzoyl
py	Pyridine
R	Alkyl
rt	Room temperature
<i>s</i> -Bu	<i>sec</i> -Butyl
TBAF	Tetrabutylammonium fluoride
TBDPS	<i>tert</i> -Butyldiphenylsilyl
<i>t</i> -Bu	<i>tert</i> -Butyl
TEA	Triethylamine
TFA	Trifluoroacetic acid

THF	Tetrahydrofuran
TMEDA	<i>N,N,N',N'</i> -Tetramethyl-1,2-ethylenediamine
TMS	Trimethylsilyl
Tol	Toluene, 4-methylphenyl

## 1 Introduction

C-Glycosides are ubiquitous natural products of high medicinal significance [1]. In addition to naturally occurring C-glycosides, synthetic C-glycosides are also of interest. Recently, a new type of therapeutic agents belonging to the class of sodium-coupled glucose cotransporter 2 (SGLT-2) inhibitors has received much interest. These new drugs block the body's capacity to reabsorb glucose *via* the kidney leading to glucose elimination in the urine and a reduction in blood glucose levels [2]. It represents a new treatment for people suffering from type 2 diabetes (90% of all cases of diabetes). According to the World Health Organization, more than 346 million people have diabetes of which an estimated 3.4 million patients have passed away from the disease [3]. The importance of this new class of drug is emphasized by the marketing approval by the FDA of four SGLT-2 inhibitors since 2012 (Fig. 1): canagliflozin **1a**, dapagliflozin **1b**, ipragliflozin **1c**, and empagliflozin **1d**.

Other SGLT-2 inhibitors, which are currently in late phase development, include ertugliflozin **2**, tofogliflozin **3**, luseogliflozin **4** and sotagliflozin **5** (Fig. 2).

There are basically two strategies to construct the C-aryl glycosides that are depicted in Figs. 1 and 2. The first strategy involves the addition of an organometallic species to a carbonyl derivative followed by a reduction to afford the desired C-glycoside with the correct oxidation state at the anomeric carbon (two-step sequence, classical approach). The second strategy avoids the reduction step and involves a one-step direct substitution reaction at the anomeric carbon by an appropriate nucleophile (new approach).

In this chapter both strategies are discussed and exemplified by the synthesis of these SGLT-2 inhibitors. The most salient features of the process research work

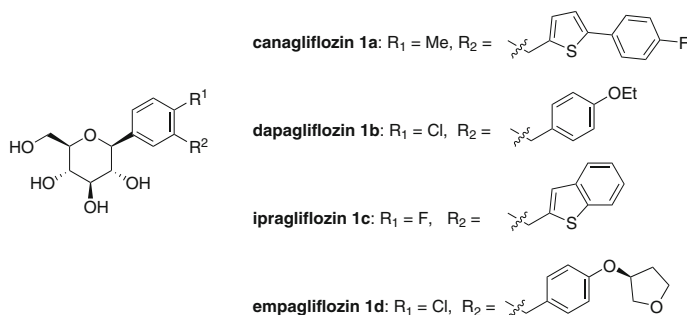


Fig. 1 SGLT-2 inhibitors that gained marketing authorization

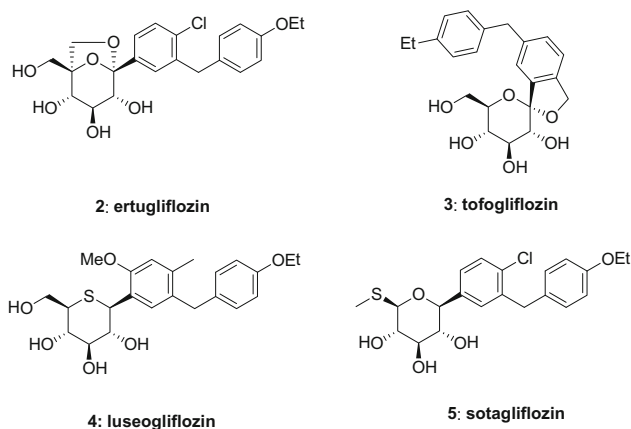


Fig. 2 SGLT-2 inhibitors in late phase development

leading to optimized processes will also be highlighted. After an introduction on the traditional approach to access *C*-glycoside starting from the gluconolactone, the medicinal chemistry approaches will be described followed by the efforts and achievements allowing transfer to production plant. In a final section, recent reports describing direct *C*-glycosylation *via* arylzinc and arylalane derivatives will be presented.

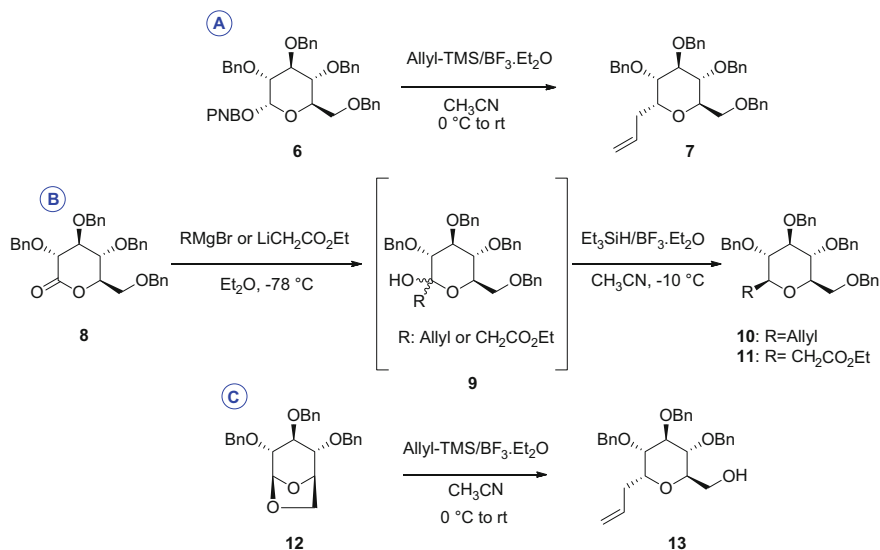
## 2 *C*-Glycoside Synthesis *via* Nucleophilic Addition to Carbonyl Derivatives

### 2.1 Addition on Lactone Derivatives

#### 2.1.1 *C*-Glycoside Stereoselective Synthesis

Although several stereoselective syntheses of  $\beta$ -D-glucopyranosides were developed in the seventies, the first efficient syntheses with high stereoselectivity were reported by Kishi's group in 1982 ([4], and references cited therein). Three strategies are described in the article (Scheme 1):

- A. Substitution of the *p*-methoxybenzoyl group in position 6 of (**6**) by allyl (trimethyl)silane in the presence of boron trifluoride gives exclusively the  $\alpha$ -product (**7**) in high yield (80%) and diastereoselectivity (10:1). The stereochemical control is realized by the addition of the nucleophile to the oxonium ion derived from the protected pyranose derivative. The oxonium ion is preferentially attacked on the  $\alpha$ -face by nucleophiles.



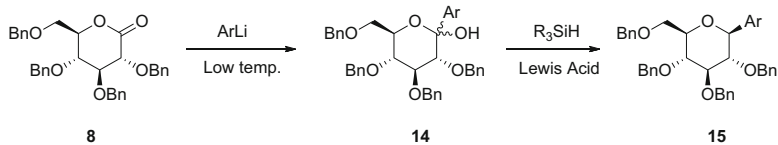
**Scheme 1** Kishi's procedures to substitute glucose derivatives with high diastereoselectivity

- B. Addition of allyl Grignard or lithium enolate at low temperature on the perbenzylated gluconolactone **8** gives the opposite anomer in 85%. The intermediate lactol **9** is not isolated but directly reduced to the desired product using triethylsilane and boron trifluoride. The diastereoselectivity is also 10:1 in favour of the  $\beta$ -anomer **10** for the Grignard addition. For the lithium enolate, only the  $\beta$ -anomer **11** is observed.
- C. Addition of allyl(trimethyl)silane in the presence of boron trifluoride on the benzyl-protected 1,6-anhydroglucose **12** under the same reaction conditions as described for *p*-methoxybenzoyl gives in this case the  $\alpha$ -anomer **13** in 60% yield and diastereoselectivity >10:1.

The good yields and high diastereoselectivities observed render these strategies very attractive for the synthesis of C-glycosides.

### 2.1.2 Aryl Addition on Gluconolactone Derivatives

The use of gluconolactone derivatives for the introduction of aryl moieties was demonstrated by Kraus and Molina in 1988 [5] followed by Czernecki and Ville in 1989 [6]. These groups have shown that a variety of aryllithium derivatives are added at low temperature with high selectivities to protected gluconolactone **8**. Subsequent reduction of the lactol product **14** with a silane in the presence of a Lewis acid allowed the isolation of  $\beta$ -D-aryl glycosides **15** in high yield (>80%)



**Scheme 2** Kraus–Molina and Czernecki–Ville approach for the synthesis of aryl glycosides

with very high diastereoisomeric purity. The preferred protecting group is the benzyl since it is compatible with aryllithiums reagents and is easy to remove afterwards. The general approach is depicted in Scheme 2.

Both research groups concluded that only the  $\beta$ -isomer was formed in the reaction.

### 2.1.3 Use in Discovery (Medicinal Chemistry)

The addition of aryllithiums or Grignard derivatives on protected gluconolactone derivatives was extensively used in medicinal chemistry for hit-to-lead optimization since it allows the introduction of a wide variety of aryl moieties on sugar derivatives in a simple way from readily available starting material.

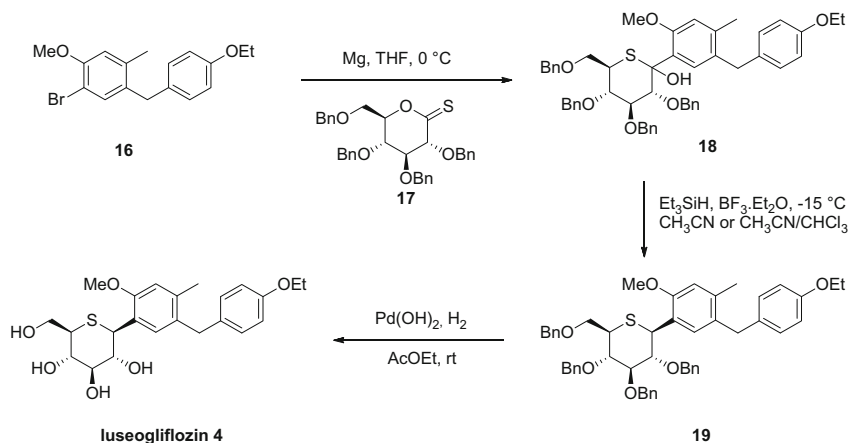
Medicinal chemists employed the TMS-protected D-gluconolactone for the synthesis of dapagliflozin [7], canagliflozin [8], ertugliflozin [9] and empagliflozin [10].

The benzyl-protected D-gluconolactone was used for the synthesis of ipragliflozin [11] and tofogliflozin [12, 13] and can be extended to the thiogluconolactone **17** as in the case of luseogliflozin **4** (Scheme 3) [14].

The method is very general but it suffers from several drawbacks that need to be addressed for commercial processes:

- Expensive starting material (for benzyl-protected gluconolactone and thiogluconolactone).
- Lack of crystalline intermediates at the lactol stage.
- The intermediate lactol does not always give high diastereoselectivity in the reduction step.
- The debenzilation can be problematic and not always compatible with the functional groups present on the aryl moiety.

In the next sections we will describe the development work done by the process research groups that led to commercial processes for several marketed SGLT-2 inhibitors while highlighting the most important features.



Scheme 3 Luseogliflozin synthesis

### 2.1.4 Diastereoselectivity Improvement

A significant contribution to improve the selectivity of the lactol reduction was reported by the process research group of Deshpande et al. at Bristol–Myers Squibb when developing the manufacturing route for dapagliflozin. They have demonstrated that the reduction of perbenzylated lactol intermediate **20** was not as selective as it was previously reported by Czerniecky and Ville [6]. Actually, the reduction of the perbenzylated lactol with triethylsilane in the presence of trifluoroboron etherate affords a 4:1  $\beta$ : $\alpha$  isomeric mixture [15]. When the mixture is subjected to atmospheric hydrogenation over Pd/C and subsequently acylated using the Czerniecky conditions, only the  $\beta$ -isomer **23** is obtained. But a careful analysis revealed that the minor component was preferentially lost in the mother liquor during the hydrogenolysis step misleading to completely stereoselective ketal reduction (Scheme 4).

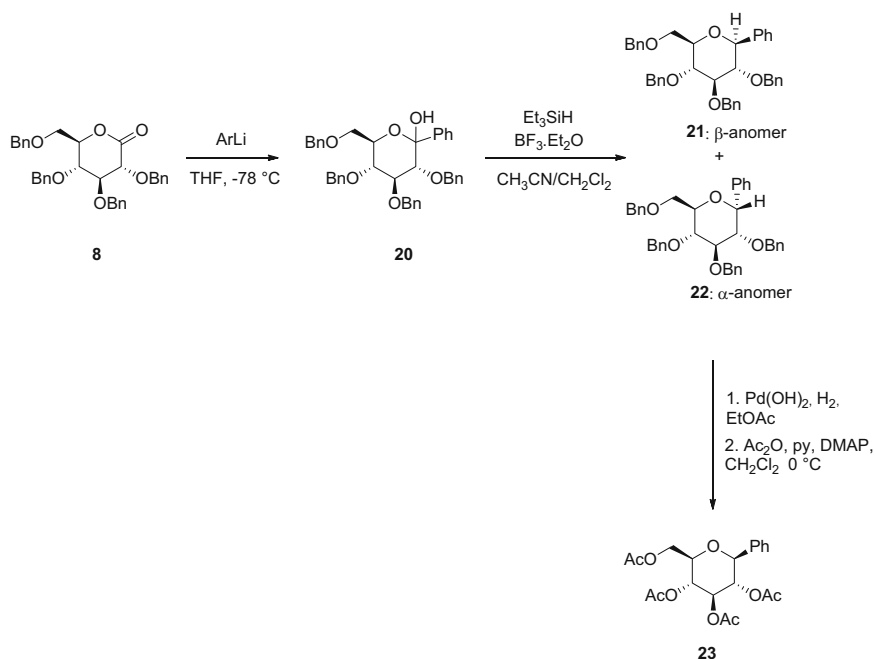
The selectivity of the reduction is influenced by the steric bulk of the silane, and the use of the triisopropylsilane as reducing agent gives the best  $\beta$ : $\alpha$  ratio (>35:1).

### 2.1.5 Commercial Processes

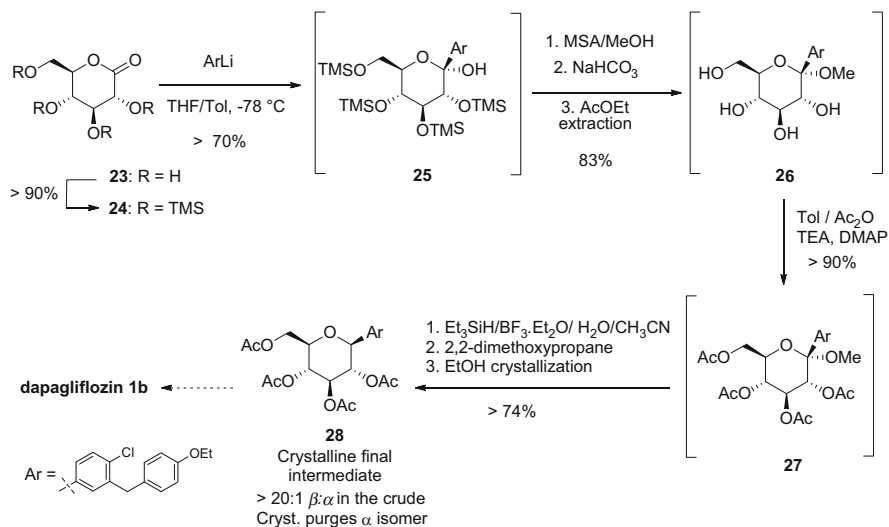
#### Dapagliflozin

Further process research work was performed at Bristol–Myers Squibb for the development of the commercial manufacturing route of dapagliflozin. The final process incorporates the following improvements [16, 17] (Scheme 5):

- The use of less polar solvent to perform the aryllithium addition (THF/toluene or THF/heptanes) instead of pure THF leads to higher yield.



**Scheme 4** Stereoselectivity observed for the reduction of perbenzylated lactol adduct



**Scheme 5** Telescope sequence in the dapagliflozin synthesis leading to the enantiopure crystalline tetra-acetate intermediate

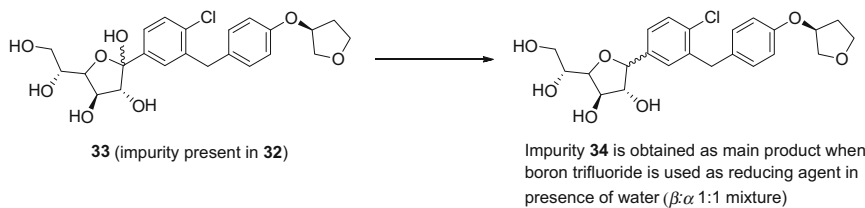
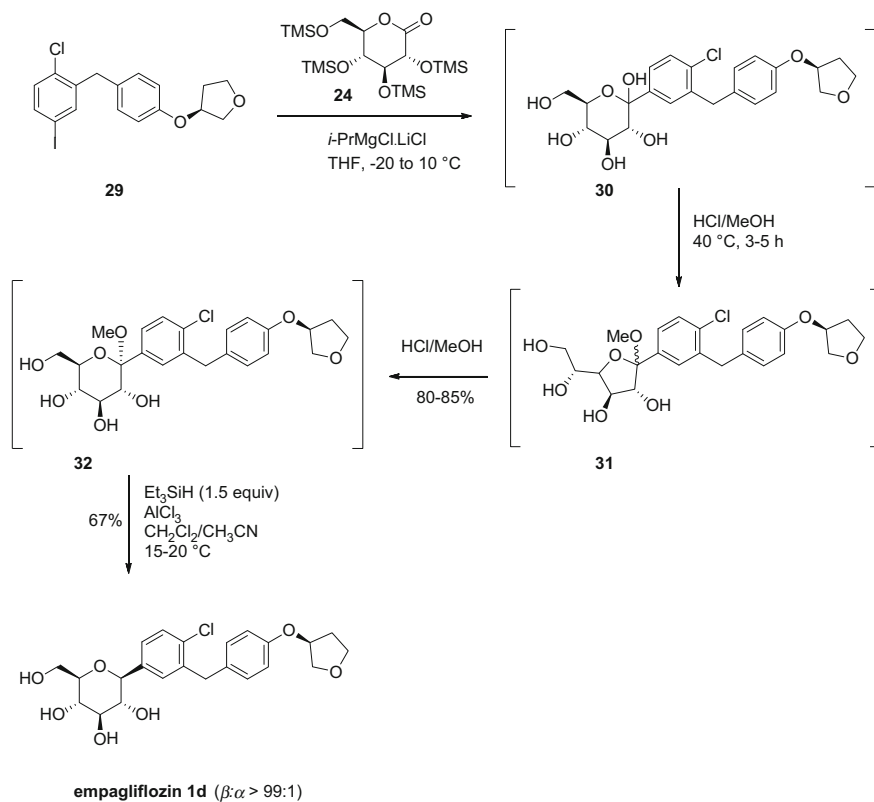
- The use of TMS protecting groups on the gluconolactone to perform the aryllithium addition followed by acidic quench with methanol and isolation of the tetra-acetylated ketal **27** (stable and crystalline compound) in a one-pot process.
- High diastereoselectivity is achieved with triethylsilane/boron trifluoride etherate when acetate is the protecting group. This was not the case when benzyl was the protecting group (sterically hindered and costly silanes were necessary). The acetate group does not stabilize the carbocation, and the delivery of the hydride is made via the  $\alpha$ -face to give the  $\beta$ -1-C-aryl glycoside **28**.
- Water is a critical additive for the reduction step of the ketal most probably by forming a stronger Lewis acid with the boron trifluoride. On plant scale 1 mol of water and  $>2$  equiv. of boron trifluoride are required to drive the reduction to completion.

It is worth noting that the Bristol–Myers Squibb strategy relies on the use of two different protecting groups to better control the selectivity of the aryllithium addition and the selective reduction step. This protecting–deprotecting–reprotecting strategy was made financially possible by telescoping the sequence and never isolating any of the intermediates. Moreover, it allows isolating an enantiopure crystalline intermediate at the penultimate stage of the synthesis and achieving an overall yield around 50% starting from the inexpensive and readily available D-gluconolactone. The last step of the synthesis is the deprotection of the acetyl groups followed by the isolation of the dapagliflozin.

### Empagliflozin

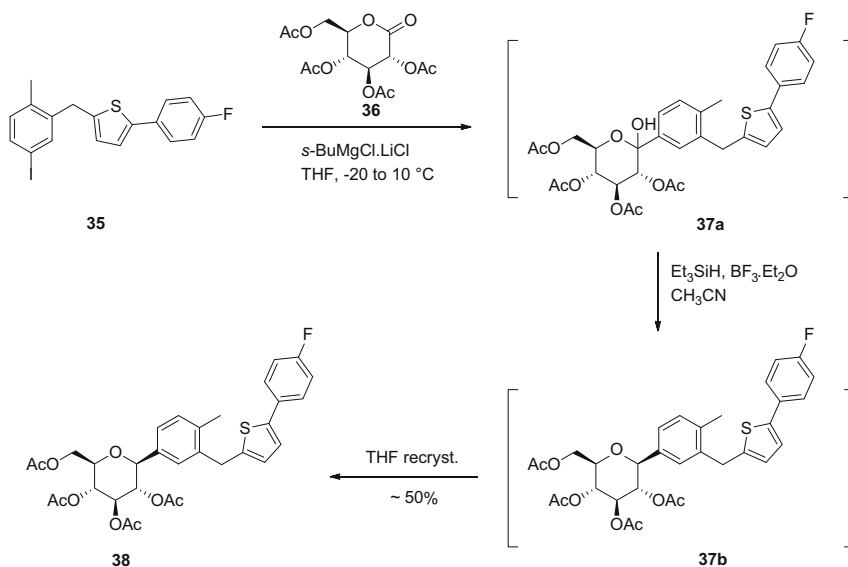
The optimized process developed at Boehringer Ingelheim followed a similar synthetic strategy but contains several different and interesting features [18]:

- The aromatic iodo moiety **29** was preferred to the cheaper aryl bromo derivative because the aryl addition to the lactone can be done at higher temperature ( $-20^{\circ}\text{C}$  to  $10^{\circ}\text{C}$ ) and does not require deep cooling.
- After addition on the TMS-gluconolactone derivative, the in situ produced lactol **30** is converted in a mixture of  $\alpha/\beta$ -furanoketals **31**, which is finally transformed into the  $\beta$ -pyranoketal **32** after pH adjustment (Scheme 6).
- No protecting group is needed for the reduction of the  $\beta$ -glucopyranoside, but the presence of water is detrimental as it generates an undesired furanose impurity **33** leading to compound **34** upon reduction conditions. This problem was circumvented by the use of  $\text{AlCl}_3$  instead of  $\text{BF}_3 \cdot \text{Et}_2\text{O}$  in combination with an azeotropic distillation prior to starting the reduction.



**Scheme 6** Process for empagliflozin synthesis (addition on the gluconolactone)

After reduction and a solvent switch to *i*-PrOAc, the final API is crystallized in 60–70% yield. Empagliflozin is obtained in about 50% overall yield from D-gluconolactone derivative **24**. This process was implemented at ton scale and used for the launch of commercial supplies.



**Scheme 7** Canagliflozin synthesis (addition of tetra-acetate D-gluconolactone)

### Canagliflozin (First-Generation Process)

The commercial process for the production of canagliflozin is also based on the addition of an aryl-Grignard derivative on protected D-gluconolactone **36**. The Grignard is generated from the iodo aryl **35** using Knochel's methodology. The interesting point is that the protecting groups used are acetate because it allows isolating a crystalline tetra-acetate intermediate **38** that showed very good purifying capabilities [19] (Scheme 7).

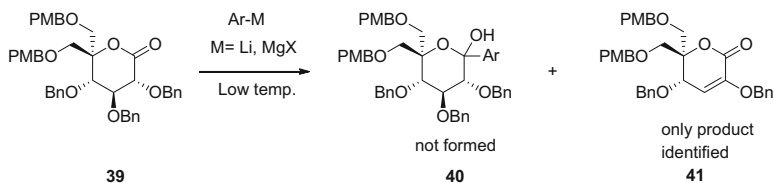
The acetate protecting groups are removed under basic conditions using a solution of sodium methoxide in methanol, and the crude API is recrystallized in *i*-PrOAc/water to deliver the canagliflozin API.

The overall yield of the synthesis is around 40% from D-gluconolactone. The process is used at ton scale to supply the market demand for canagliflozin.

## 2.2 Addition to Amide Derivatives

### 2.2.1 Ertugliflozin

The deliveries of ertugliflozin to support the early clinical phases were based on the classical approach (lactone addition). But it rapidly appears that an alternative synthesis will be required for commercial process: the steric hindrance on C5



**Scheme 8** Lactone C5 disubstitution prevents addition on the carbonyl

which is disubstituted in the case of ertugliflozin derivative **39** leads to elimination product **41** instead of the desired lactol **40** (Scheme 8).

A nice alternative approach developed by the Pfizer process research group is based on the addition of the aryl moiety to an open chain amide. The pyranose ring is reformed in the late stage of the synthetic sequence [20]. The key steps of the synthesis are:

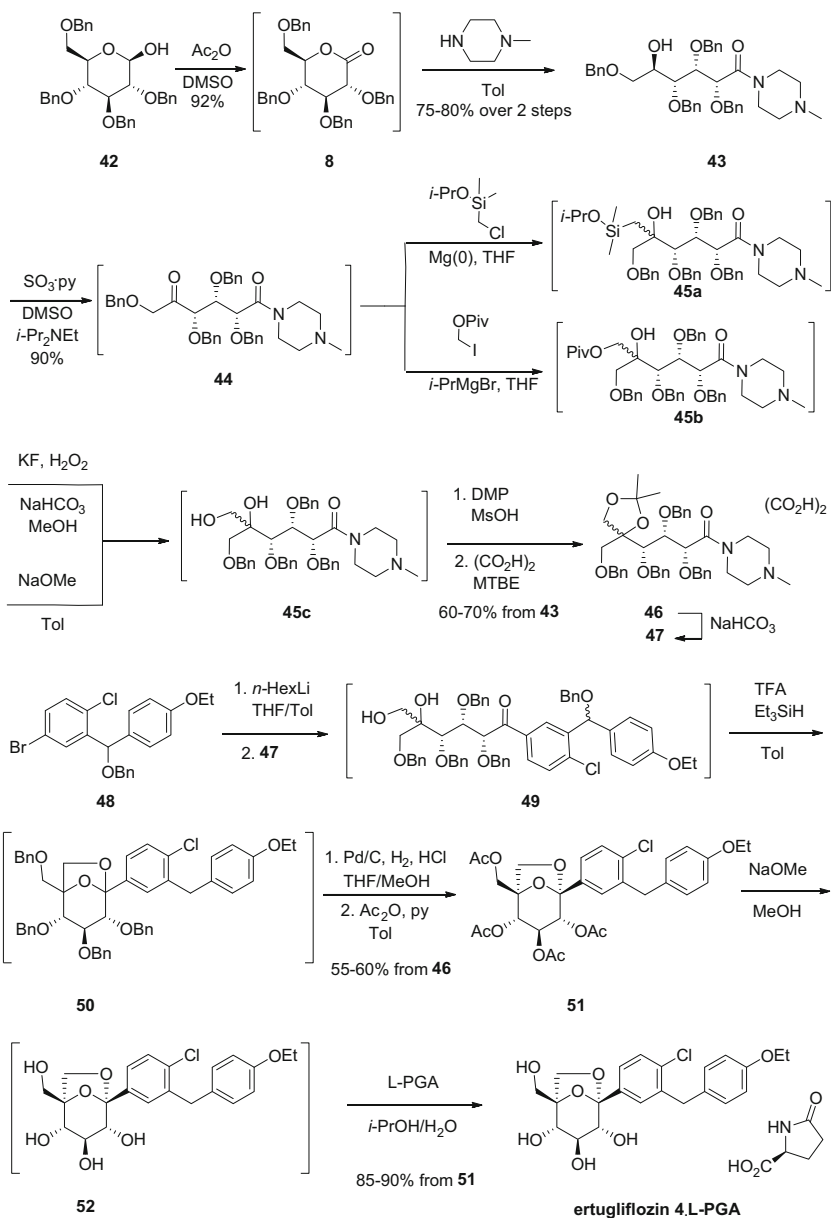
- Nucleophilic hydroxymethylation of a ketogluconamide intermediate **44**
- Introduction of the aglycone moiety *via* aryl anion addition on a methylpiperazine amide **47**

Based on this methodology, an efficient 12-step synthesis was developed for ertugliflozin starting from tetra-benzyl-D-glucose and including only three isolated intermediates (**43**, **46**, **51**). The overall yield of the synthesis is a respectable 30% (Scheme 9).

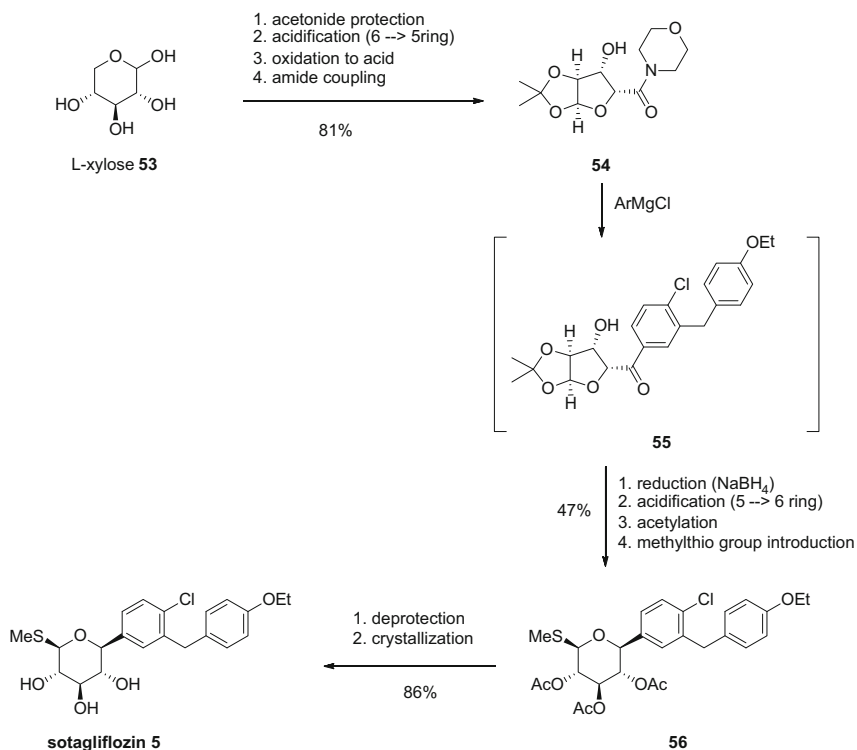
### 2.2.2 Sotagliflozin

Sotagliflozin is a dual SGLT-1/SGLT-2 inhibitor which is currently under development by Lexicon Pharmaceuticals (phase III). It follows a similar strategy to ertugliflozin, i.e. aryl addition on an acyclic precursor. The synthesis starts from L-xylose **53**, and the aryl moiety (same aryl moiety as for dapagliflozin) is introduced on an amide derivative (morpholine amide **54**) *via* Grignard addition. A subsequent transformation leads to the sotagliflozin (Scheme 10) [21].

The overall yield of the synthesis is around 30%.



**Scheme 9** Synthesis of ertugliflozin “adapted with permission from [20]. Copyright (2014) American Chemical Society”

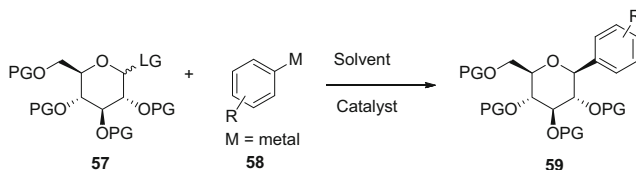


Scheme 10 Sotagliflozin synthesis (following [21])

### 3 Direct C-Glycosylation

#### 3.1 Introduction to Direct C-Glycosylation

In the previous section, we have presented the traditional methodology employed to access C-glycosides in a 2-step sequence by 1,2-addition of an organometallic species to a  $\text{C}_{\text{sp}^2}$  carbonyl function. Even if this approach is an adequate tool for the medicinal chemist, it is suffering from limitations for the scale-up such as low temperature reactions and sensitive reduction steps. With the growing demand for type 2 diabetes treatment with those new aryl glycosides, a demand for new synthetic methodologies, avoiding oxidation/reduction sequence, is generating an enormous interest. In this approach, the presence of an appropriate leaving group (LG) at the anomeric position of the glycoside moiety **57** should react with an organometallic nucleophile **58**. Choice of the protecting groups, solvent composition as well as the presence or not of catalyst should be precisely selected to generate high yield and excellent selectivity (Scheme 11).



**Scheme 11** General approach for direct C-glycosylation

In this respect, Gagné has described a transition metal approach allowing Ni-catalysed coupling of organozinc reagents with glycosyl bromides to obtain with good stereoselectivity the aryl derivative (PG=Ac, R=H,  $\beta/\alpha$  ratio of 12:1) [22–24]. Cossy has also demonstrated efficient C-glycosylation with Co(acac)<sub>3</sub>/TMEDA in the presence of Grignard reagents [25, 26]. However, the high transition metal catalyst loading (e.g. up to 10 mol% for Ni) and the high toxicity of residual salts hamper potential industrial applications of this coupling reaction.

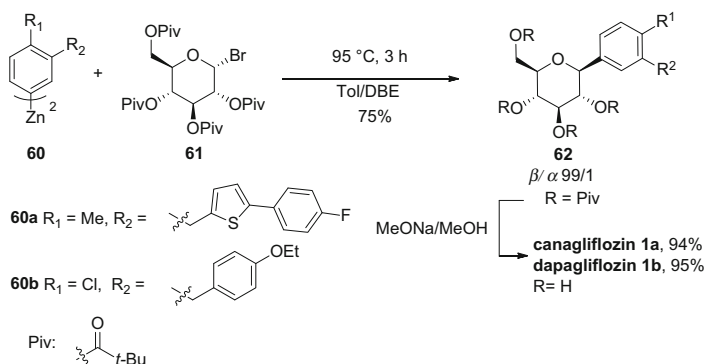
Alternatively to the transition metal-catalysed approach, ionic pathways have been recently developed and applied to access canagliflozin and dapagliflozin.

### 3.2 Direct C-Glycosylation in the Presence of Diarylzinc and Its Application to Canagliflozin and Dapagliflozin

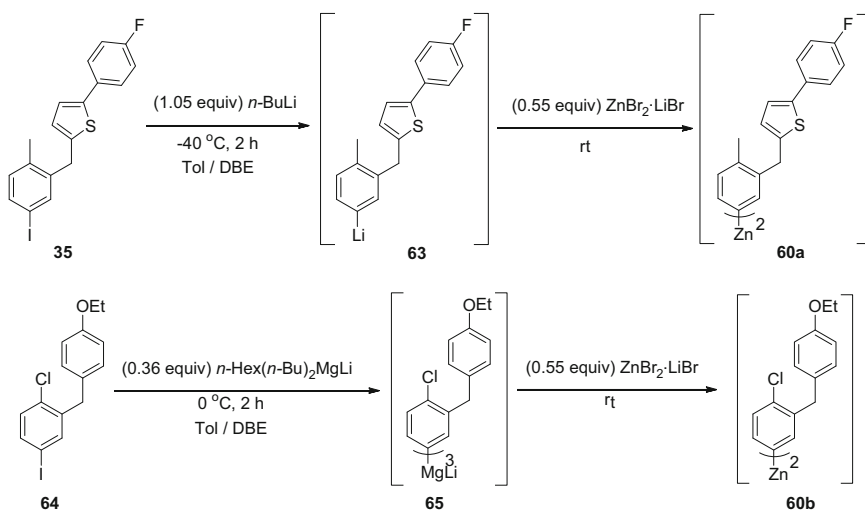
Lemaire et al. have reported high stereoselective access to C-aryl glycosides **62** in transition-metal-free conditions by treatment of a per-*O*-pivaloyl-protected glucosyl bromide **61** substrate with diarylzinc **60** [27] and its application to the preparation of canagliflozin and dapagliflozin (Scheme 12).

The coupling step is conducted at 95°C for 3 hours affording the desired C-aryl glycoside derivative **62** in 75% yield with excellent  $\beta$  selectivity ( $\beta/\alpha$  99/1). Further treatment with sodium methoxide allows removal of the pivaloyl protecting group in almost quantitative yield providing canagliflozin as well as dapagliflozin.

A judicious choice of the solvent mixture of toluene/di-*n*-butyl ether (DBE) allows a successful coupling step under the needed thermal conditions. In the presence of THF (or similar ethereal solvents), the Zn(II) salts initiate ring opening of the THF and formation of side products by reaction with the bromo glucoside **61**. To circumvent this reaction, a combination of toluene with a nonreactive ether like cyclopentyl methyl ether or di-*n*-butyl ether allows a successful coupling. Nevertheless, in the absence of THF, direct insertion of metallic zinc was more cumbersome for the formation of the diarylzinc species. Therefore, the metalation reaction was carried out using *n*-BuLi or lithium tri-*n*-butyl magnesate followed by transmetalation with ZnBr<sub>2</sub>·LiBr complex in di-*n*-butyl ether. The use of ZnBr<sub>2</sub>·LiBr complex in di-*n*-butyl ether solution allows fast transmetalation step (Scheme 13).



**Scheme 12** Direct C-glycosylation in presence of diarylzinc

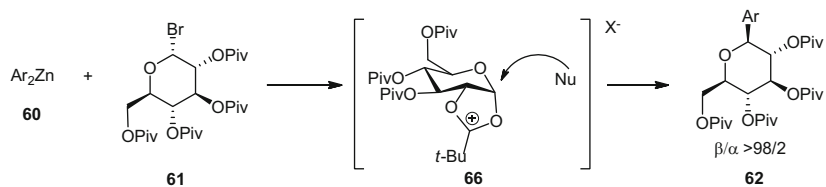


**Scheme 13** Formation of the diarylzinc species

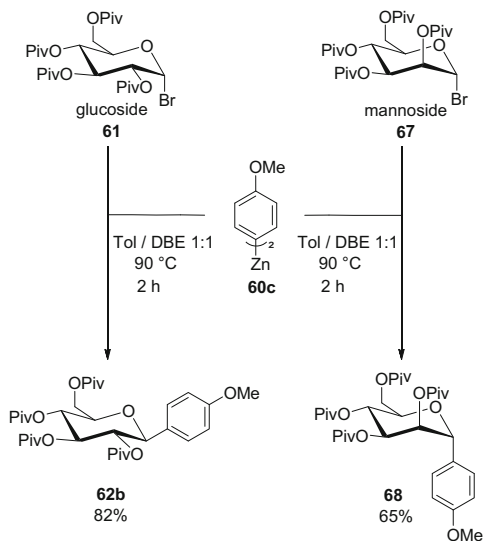
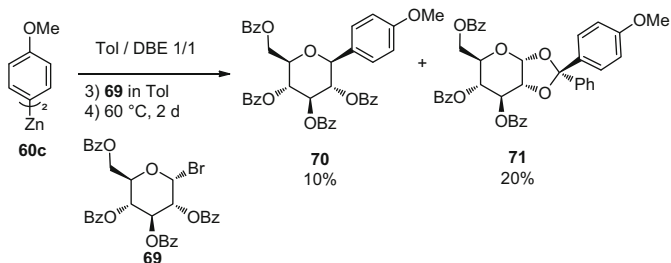
The high diastereoselectivity for this direct C-glycosylation is based on a “substrate control” approach via anomeric oxonium ion participation. The presence of the pivaloyl group under the Lewis acid conditions participates in the formation of the anomeric oxonium ion intermediate **66** (Scheme 14) limiting the access of the nucleophile through the  $\alpha$ -face. The aryl adds thereafter from the top face affording the  $\beta$ -C-arylglycoside **62**.

To support this proposed mechanism, a series of confirmation experiments was performed (Scheme 15 and 16):

- Replacement of the glucose derivative **61** by mannose analogue **67** (C2 epimer) delivers the  $\alpha$ -C-glycoside **68** corresponding to the addition anti to the pivaloyl group.



Scheme 14 Proposed mechanism

Scheme 15 Mechanistic experiments with mannoside **67**

Scheme 16 Mechanistic experiment with benzoylated protected glycoside

- If the pivaloyl protecting group is replaced by a benzoyl group (starting material **69**), product **71** from the direct addition to the carboxium intermediate is obtained in low yield.

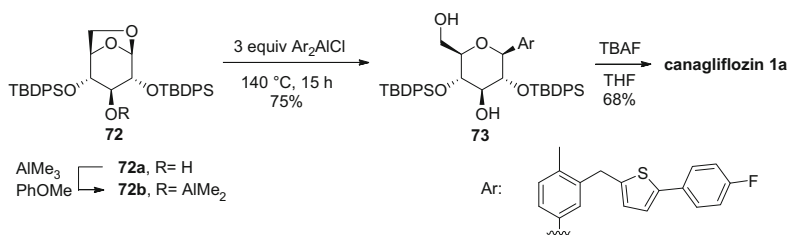
### 3.3 Direct C-Glycosylation in the Presence of Arylalanes and Its Application to Canagliflozin and Dapagliflozin

In the scope of preparation of SGLT-2 inhibitors, Henschke et al. have developed a direct C-glycosylation by stereoselective arylation of hydroxyl-protected 1,6-anhydro- $\beta$ -D-glucose **72** with arylalanes under thermal conditions to access canagliflozin in 51% overall yield (Scheme 17) [28].

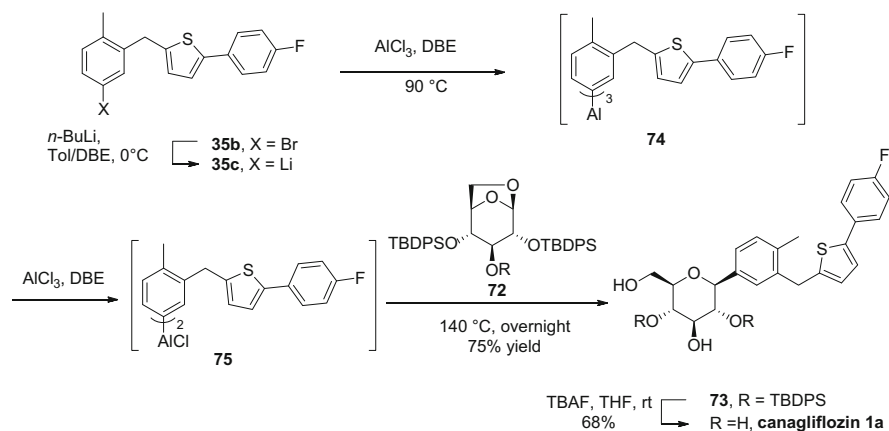
Deprotonation of the hydroxyl-protected 1,6-anhydro- $\beta$ -D-glucose **72a** by treatment with  $\text{AlMe}_3$  allows the formation of the alkoxydimethylalanes **72b**. This intermediate is later arylated in 75% yield using 3 equivalents of diarylalanane chloride at  $140^\circ\text{C}$  for 15 h. The opening of the anhydroglucose **72** is completely stereoselective for the  $\beta$ -isomer **73**, and no trace of the  $\alpha$ -derivative is detected. A large excess of the diarylalanane chloride is needed because the reaction is sensitive to the steric hindrance of the nucleophile. Reducing the amount of alane derivative to 1.5 equivalents provides only a 16% yield with 80% of unreactive species. After purification by chromatography, canagliflozin **1a** is isolated 68% yield after the removal of the *tert*-butyldiphenylsilyl protection group with fluoride source.

The coupling step is successful in solvents such as toluene, anisole, chlorobenzene, and di-*n*-butyl ether. In the presence of ethereal solvent, such as THF, the reaction does not work because the arylalane derivative complexes better to the oxygen lone pair of the solvent compared to anhydroglucose derivative.

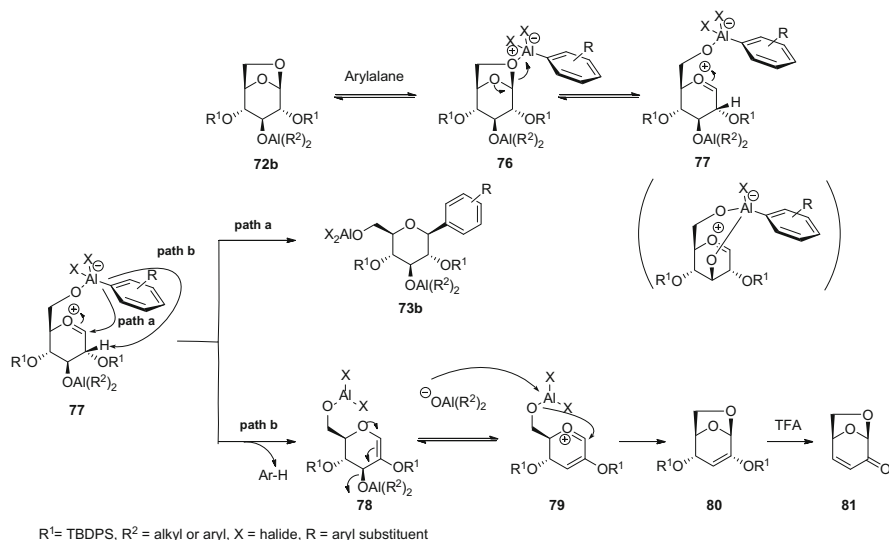
The formation of the diarylalanane chloride **75** for the preparation of canagliflozin **1a** was also costly. The aryl bromide **35b** was lithiated in a mixture of toluene/diisopropyl ether with *n*-BuLi at  $0^\circ\text{C}$  and transmetalated with  $\text{AlCl}_3$  in di-*n*-butyl ether at  $90^\circ\text{C}$  to afford the trisarylalanane species **74** as a milky suspension. After dilution in toluene, the diisopropyl ether was removed by evaporation, and the solution was filtered to remove the lithium chloride (LiCl) and was concentrated further. Extensive examination of the effect of the metal halides has highlighted the



**Scheme 17** Arylation of 1,6-anhydroglucose using arylalanes



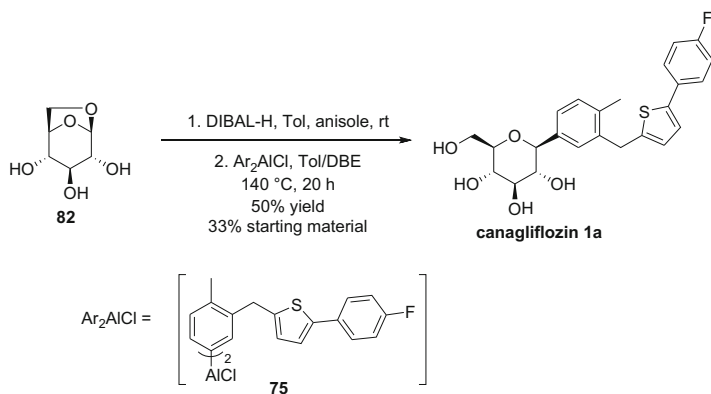
**Scheme 18** Preparation of canagliflozin by reaction of bis-aryllane chloride



**Scheme 19** Proposed mechanism “adapted with permission from [28]. Copyright (2015) American Chemical Society”

negative effect of the chloride anions to inhibit the arylation step. When filtration of the LiCl is omitted, the arylation fails to reach completion. Finally the trisaryllane **74** species was treated with  $\text{AlCl}_3$  in  $n\text{-Bu}_2\text{O}$  to generate in situ the active species diaryllane chloride **75** suitable for the coupling with the 1,6-anhydroglucose **72** deprotonated by  $\text{Me}_3\text{Al}$  (Scheme 18).

The proposed mechanism to support the high stereoselectivity is depicted in Scheme 19.



**Scheme 20** Synthesis of canagliflozin by arylation of 1,6-anhydroglucose **82**

In parallel to the formation of the desired product, the presence of the enol ether side product **81** was consistently observed. Although the relative ratios of the two differed under different reaction conditions, the relative rates of their formation implied a common intermediate. Therefore, the proposed mechanism is suggested: After complexation of the arylalane species with the C6-O ether linkage (complex **76**), the ring is opened to afford the oxonium intermediate **77**. This intermediate undergoes either an aryl shift (path a) to furnish the desired C-glycoside **73b** via ipso substitution or a deprotonation intramolecularly at the C2 position to afford the glycal intermediate **78** (path b). Further elimination of the dialkylaluminum oxide forms the oxonium **79** followed by ring closing to form back the 1,6-anhydro moiety **80** [28].

In extension to this direct approach, Henschke has developed a modified version starting directly from unprotected 1,6-anhydroglucose **82** and thus avoiding the protection step with the TBDPS (Scheme 20).

The treatment of 1,6-anhydroglucose **82** with 3 equiv. of DIBAL-H allows after addition of the  $\text{Ar}_2\text{AlCl}$  **75** the direct formation of canagliflozin **1a** in 50% under thermal conditions [29]. Unfortunately, conversion was not complete even with prolonged reaction times.

## 4 Conclusion

With the growing demand for the treatment of the type 2 diabetes, the aryl C-glycoside derivatives are rapidly becoming the choice treatment. As developed above, the main approach to access this extremely efficacious medicinal agent remains the nucleophilic addition of an organometallic species to per-protected gluconolactone derivatives followed by selective reduction. This path allows the medicinal chemists to access diversity that process chemists further developed even

to commercial plant. Nevertheless, more straightforward approaches have been recently reported by direct formation of the key C–C bond either by treatment with organozinc or organoalane reagents. In the particular case of canagliflozin, the direct C-glycosylation in the presence of diarylzinc species has been transferred to commercial plant.

## References

1. Štambaský J, Hocek M, Kočovský P (2009) C-Nucleosides: Synthetic strategies and biological applications. *Chem Rev* 129:6729–6764
2. Isaji M (2007) Sodium-glucose cotransporter inhibitors for diabetes. *Curr Opin Invest Drugs* 8:285–292
3. World Health Organization (2011) Diabetes: Facts Sheet N0. 312. Geneva. <http://www.who.int/mediacenter/factsheets/fs312/en>
4. Lewis M, Cha J, Kishi Y (1982) Highly stereoselective approaches to  $\alpha$ - and  $\beta$ -C-glycopyranosides. *J Am Chem Soc* 104:4976–4978
5. Kraus G, Molina M (1988) A direct synthesis of C-glycosyl compounds. *J Org Chem* 53:752–753
6. Czerniecki S, Ville G (1989) C-Glycosides. 7. stereospecific C-glycosylation of aromatic and heterocyclic rings. *J Org Chem* 54:610–612
7. Meng W, Ellsworth B, Nirschl A, McCann P, Patel M, Girotra R, Wu G, Sher P, Morrison E, Biller S, Zahler R, Deshpande P, Pullockaran A, Hagan D, Morgan N, Taylor J, Obermeier M, Humphreys W, Khanna A, Discenza L, Robertson J, Wang A, Han S, Wetterau J, Janovitz E, Flint O, Whaley J, Washburn W (2008) Discovery of dapagliflozin: a potent, selective renal sodium-dependent glucose cotransporter 2 (SGLT2) inhibitor for the treatment of type 2 diabetes. *J Med Chem* 51:1145–1149
8. Nomura S, Sakamaki S, Hongu M, Kawanishi E, Koga Y, Sakamoto T, Yamamoto Y, Ueta K, Kimata H, Nakayama K, Tsuda-Tsukimoto M (2010) Discovery of canagliflozin, a novel C-glucoside with thiophene ring, as sodium-dependent glucose cotransporter 2 inhibitor for the treatment of type 2 diabetes mellitus. *J Med Chem* 53:6355–6360
9. Bernhardson D, Brandt T, Hulford C, Lehner R, Preston B, Price K, Sagal J, St. Pierre M, Thompson P, Thuma B (2014) Development of an early-phase bulk enabling route to sodium-dependent glucose cotransporter 2 inhibitor ertugliflozin. *Org Process Res Dev* 18:57–65
10. Eckhardt M, Himmelsbach F, Wang X, Sun X, Zhang L, Tang W, Krishnamurthy D, Senanayake C, Han Z (2006) Processes for preparing of glucopyranosyl-substituted benzylbenzene derivatives and intermediates therein. *WO Pat. Appl.* 2006120,208, 7 Sept 2007
11. Imamura M, Nakanishi K, Suzuki T, Ikegai K, Shiraki R, Ogiyama T, Murakami T, Kurosaki E, Noda A, Kobayashi Y, Yokota M, Koide T, Kosakai K, Ohkura Y, Takeuchi M, Tomiyama H, Ohta M (2012) Discovery of ipragliflozin (ASP1941): a novel C-glucoside with benzothiophene structure as a potent and selective sodium glucose co-transporter 2 (SGLT2) inhibitor for the treatment of type 2 diabetes mellitus. *Bioorg Med Chem* 20:3263–3279
12. Ohtake Y, Sato T, Kobayashi T, Nishimoto M, Taka N, Takano K, Yamamoto K, Ohmori M, Yamaguchi M, Takami K, Yeu S, Ahn K, Matsuoka H, Morikawa K, Suzuki M, Hagita H, Ozawa K, Yamaguchi K, Kato M, Ikeda S (2012) Discovery of tofogliflozin, a novel C-arylglucoside with an O-spiroketal ring system, as a highly selective sodium glucose cotransporter 2 (SGLT2) inhibitor for the treatment of type 2 diabetes. *J Med Chem* 55:7828–7840
13. Liu Y, Fu T, Ou C, Fan W, Peng G (2013) Improved preparation of (1S,3'R,4'S,5'S,6'R)-5-chloro-6-[(4-(ethylphenyl)methyl)-3',4',5',6'-tetrahydro-6'-(hydroxymethyl)-spiro [isobenzofuran-1(3H),2'-[2H]pyran-3',4',5'-triole]. *Chin Chem Lett* 24:131–133

14. Kakinuma H, Oi T, Hashimoto-Tsuchiya Y, Arai M, Kawakita Y, Fukasawa Y, Iida I, Hagima N, Takeuchi H, Chino Y, Asami J, Okumura-Kitajima L, Io F, Yamamoto D, Miyata N, Takahashi T, Uchida S, Yamamoto K (2010) (1S)-1,5-Anhydro-1-[5-(4-ethoxybenzyl)-2-methoxy-4-methylphenyl]1-thio-D-glucitol (TS-071) is a potent, selective sodium-dependent glucose cotransporter 2 (SGLT2) inhibitor for type 2 diabetes treatment. *J Med Chem* 53:3247–3261
15. Ellsworth B, Doyle A, Patel M, Caceres-Cortes J, Mend W, Deshpande P, Pullockaran A, Washburn W (2003) C-Arylglucoside synthesis: triisopropyl silane as a selective reagent for the reduction of an anomeric C-phenyl ketal. *Tetrahedron Asymmetry* 14:3243–3247
16. Deshpande P, Ellsworth B, Buono F, Pullockaran A, Singh J, Kissick T, Huan M-H, Lobinger H, Denzel T, Mueller R (2007) Remarkable  $\beta$ -selectivity in the synthesis of  $\beta$ -1-C-arylglucosides: stereoselective reduction of acetyl-protected methyl 1-C-arylglucosides without acetoxy-group participation. *J Org Chem* 72:9746–9749
17. Ellsworth B, Washburn W, Sher P, Wu G, Meng W (2002) C-Aryl glucoside SGLT2 inhibitors and method. *US Pat. Appl.* 6,414,126, 2 July 2002
18. Wang X-J, Zhang L, Byrne D, Nummy L, Weber D, Krishnamurthy D, Yee N, Senanayake C (2014) Efficient synthesis of empagliflozin, an inhibitor of SGLT-2, utilizing an  $\text{AlCl}_3$ -promoted silane reduction of a  $\beta$ -glycopyranoside. *Org Lett* 16:4090–4093
19. Filliers W, Broeckx R, Nieste P, Hatsuda M, Yoshinaga M, Yada M (2010) Process for the preparation of compounds useful as inhibitor of SGLT. *WO Pat. Appl.* 2010043,682, 22 Apr 2010
20. Bowles P, Brenek J, Caron S, Do N, Drexler M, Duan S, Dubé P, Hansen E, Jones B, Jones K, Ljubicic T, Makowski T, Mustakis J, Nelson J, Olivier M, Peng Z, Perfect H, Place D, Ragan J, Salisbury J, Stanchina C, Vanderplas B, Webster M, Weekly R (2014) Commercial route research and development for SGLT2 inhibitor candidate ertugliflozin. *Org Process Res Dev* 18:66–81
21. De Paul S, Perlberg A, Zhao M (2010) Solid forms of (2S,3R,4R,5S,6R)-2-(4-chloro-3-(4-ethoxybenzyl)phenyl)-6-(methylthio)tetrahydro-2H-pyran-3,4,5-triol and methods of their use. *WO Pat. Appl.* 2010009,197, 21 Jan 2010
22. Gong H, Andrews RS, Zuccarello JL, Lee SJ, Gagné MR (2009) Sn-Free Ni-catalyzed reductive coupling of glycosyl bromides with activated alkenes. *Org Lett* 11:879–882
23. Gong H, Gagné MR (2008) Diastereoselective Ni-catalyzed Negishi cross-coupling approach to saturated, fully oxygenated C-alkyl and C-aryl glycosides. *J Am Chem Soc* 130:12177–12183
24. Gong H, Sinisi R, Gagné MR (2007) A room temperature Negishi cross-coupling approach to C-alkyl glycosides. *J Am Chem Soc* 129:1908–1909
25. Nicholas L, Angibaud P, Stansfield I, Bonnet P, Meerpoel L, Reymond S, Cossy J (2012) Diastereoselective metal-catalyzed synthesis of C-aryl and C-vinyl glycosides. *Angew Chem Int Ed* 51:11101–11104
26. Nicolas L, Izquierdo E, Angibaud P, Stansfield I, Meerpoel L, Reymond S, Cossy J (2013) Cobalt-catalyzed diastereoselective synthesis of C-furanosides. total synthesis of (–)-isoalthalactone. *J Org Chem* 78:11807–11814
27. Lemaire S, Houpius IN, Xiao T, Li J, Digard E, Gozlan C, Liu R, Gavryushin A, Diene C, Wang Y, Farina V, Knochel P (2012) Stereoselective C-glycosylation reactions with arylzinc reagents. *Org Lett* 14:1480–1483
28. Henschke JP, Wu P-Y, Lin C-W, Chen S-F, Chiang P-C, Hsiao C-N (2105)  $\beta$ -Selective C-arylation of silyl protected 1,6-anhydroglucose with arylalanes: the synthesis of SGLT2 inhibitors. *J Org Chem* 80:2295–2309
29. Henschke JP, Lin C-W, Wu P-Y, Tsao W-S, Liao J-H, Chiang P-H (2015)  $\beta$ -Selective C-arylation of diisobutylaluminum hydride modified 1,6-anhydroglucose: synthesis of canagliflozin without recourse to conventional protecting groups. *J Org Chem* (80):5189–5195

# Synthetic Routes to Sofosbuvir

Roland Barth, Christopher A. Rose, and Olga Schöne

**Abstract** Due to its global pervasiveness and chronicity, the hepatitis C virus (HCV) is a major health problem that claims around half a million lives annually. In recent years, the pharmaceutical industry has witnessed a surge in the development of new therapies for the treatment of hepatitis C. One such drug, sofosbuvir, marketed by Gilead Sciences, was recently approved for clinical use in several countries. In combination with other antiviral agents, sofosbuvir has shown remarkable efficacy for a broad range of viral genotypes, along with high tolerability. The clinical success of sofosbuvir demands efficient approaches for the synthesis of this pharmaceutical. Marketed as a single isomer, sofosbuvir presents several interesting synthetic challenges, including fluorination chemistry, nucleotide synthesis, and regio- and stereoselective phosphoramidation. This review provides a brief pharmacological background of sofosbuvir including its mode of action, followed by an in-depth analysis of the current synthetic approaches to sofosbuvir and its close analogues.

**Keywords** Fluorination · Hepatitis C virus · Nucleoside synthesis · Phosphoramidate synthesis · Sofosbuvir

## Contents

1	Introduction .....	54
2	An Overview of the Biology and Pharmacology of Sofosbuvir .....	55
3	Synthetic Approaches to Sofosbuvir .....	58

---

R. Barth and O. Schöne (✉)  
Sandoz Development Center Austria, Sandoz GmbH, Biochemiestr. 10, 6336 Langkampfen,  
Austria  
e-mail: [olga.schoene@sandoz.com](mailto:olga.schoene@sandoz.com)

C.A. Rose  
Sandoz Development Center Austria, Sandoz GmbH, Biochemiestr. 10, 6250 Kundl, Austria

3.1	The Nucleoside Core: Early-Stage Fluorination Approaches .....	59
3.2	The Nucleoside Core: Late-Stage Fluorination Approaches .....	65
3.3	Phosphoramidation of the Nucleoside Core .....	74
4	Conclusions .....	84
	References .....	85

## Abbreviations

Ac	Acetyl
AcOH	Acetic acid
API	Active pharmaceutical ingredient
aq	Aqueous
Ar	Aryl
Bn	Benzyl
Boc	<i>tert</i> -Butoxycarbonyl
bp	Boiling point
Bu	Butyl
Bz	Benzoyl
Bz <sub>2</sub> O	Benzoic anhydride
CALB	<i>Candida antarctica</i> lipase B
cat	Catalyst, catalytic
Cbz	Benzyloxycarbonyl
conc	Concentrated
Cyt	Cytosine
Cyt <sup>Bz</sup>	<i>N</i> <sup>4</sup> -benzoylcytosine
DAA	Direct-acting antiviral
DABCO	1,4-Diazabicyclo[2.2.2]octane
DAST	(Diethylamino)sulfur trifluoride
DBU	1,8-Diazabicyclo [5.4.0]undec-7-ene
de	Diastereomer excess
DIBALH	<i>Diisobutylaluminum</i> hydride
DIPEA	<i>N,N</i> - <i>Diisopropylethylamine</i>
DMAP	4-(Dimethylamino)pyridine
DMF	Dimethylformamide
DMP	Dess–Martin periodinane
DMSO	Dimethyl sulfoxide
dr	Diastereomer ratio
equiv	Equivalent(s)
Et	Ethyl
EWG	Electron withdrawing group
FDA	Food and Drug Administration (U.S.A.)
GC	Gas chromatography
h	Hour(s)

HATU	1-[Bis(dimethylamino)methylene]-1 <i>H</i> -1,2,3-triazolo[4,5- <i>b</i> ]pyridinium 3-oxid hexafluorophosphate
HCV	Hepatitis C virus
HMDS	1,1,1,3,3,3-Hexamethyldisilazane
HPLC	High-performance (pressure) liquid chromatography
IPC	In-process control
<i>i</i> -Pr	<i>isopropyl</i>
LC	Liquid chromatography
LDA	Lithium <i>diisopropylamide</i>
LG	Leaving group
M	Molar
<i>m</i> -CPBA	<i>m</i> -Chloroperoxybenzoic acid
Me	Methyl
mol	Mole(s)
MOM	Methoxymethyl
MS	Mass spectrometry
Ms	Methanesulfonyl ( <i>mesyl</i> )
NCS	<i>N</i> -chlorosuccinimide
NMI	<i>N</i> -methylimidazole
NMP	<i>N</i> -methyl-2-pyrrolidone
Nph	Naphthyl
Nu	Nucleophile
Nuc	Nucleoside
PCC	Pyridinium chlorochromate
PDC	Pyridinium dichromate
PEG-INF	Pegylated interferon $\alpha$
Ph	Phenyl
Piv	Pivaloyl
PLG	Potential leaving group
PMB	4-Methoxyphenyl
PPA	Poly(phosphoric acid)
PPTS	Pyridinium <i>p</i> -toluenesulfonate
Pr	Propyl
py	Pyridine
quant	Quantitative
rac	Racemic
RBV	Ribavirin
RdRp	RNA-dependent RNA polymerase
Red-Al	Sodium bis(2-methoxyethoxy)aluminumhydride
RNA	Ribonucleic acid
RP	Reverse phase
rt	Room temperature
SFC	Supercritical fluid chromatography
TASF	Tris(dimethylamino)sulfonium difluorotrimethylsilicate

TBAF	Tetrabutylammonium fluoride
TBDMS, TBS	<i>tert</i> -Butyldimethylsilyl
TBDMSCl	<i>tert</i> -Butyldimethylsilyl chloride
TBDPS	<i>tert</i> -Butyldiphenylsilyl
TBDPSCI	<i>tert</i> -Butyl(chloro)diphenylsilane
TBSOTf	<i>tert</i> -Butyldimethylsilyl trifluoromethanesulfonate
TCA	Trichloroacetyl
<i>t</i> -Bu	<i>tert</i> -Butyl
TEA	Triethylamine
TEMPO	(2,2,6,6-Tetramethylpiperidin-1-yl)oxyl, free radical
Tf	Trifluoromethanesulfonyl (triflyl)
TFA	Trifluoroacetic acid
TFAA	Trifluoroacetic anhydride
THF	Tetrahydrofuran
THP	Tetrahydropyran-2-yl
TIPDS	1,1,3,3-Tetra <i>is</i> opropylidisiloxane- 1,3-diyl
TIPDSCl <sub>2</sub>	1,3-Dichloro-tetra <i>is</i> opropylidisiloxane
TMP	2,2,6,6-Tetramethylpiperidine
TMS	Trimethylsilyl
Tol	4-Methylphenyl
XTalFluor E	(Diethylamino) difluorosulfonium tetrafluoroborate

## 1 Introduction

Since their discovery in the 1950s, synthetic nucleoside analogues have rapidly become indispensable clinical agents in the treatment of cancers and viral infections. In 1970, a systematic search for antiviral and antitumor molecules by ICN Pharmaceuticals, Inc., yielded ribavirin – a nucleoside mimic exhibiting broad spectrum antiviral properties [1]. Although it took almost 30 years since its initial synthesis, ribavirin (RBV) eventually established itself in the first effective therapy of previously incurable hepatitis C. Since 1998, the combination of oral RBV and injections of pegylated interferon- $\alpha$  (PEG-INF) has constituted the standard of care for all six common genotypes of the hepatitis C virus (HCV). Nevertheless, sustained virologic response for the most widespread HCV genotypes 1–4 achieved with the RBV/PEG-INF combination is rather modest at 40–75% and even lower in certain subpopulations [2, 3]. The added burden of severe side effects, which often leads to treatment discontinuation, has spurred an intensive search for new HCV therapies. In 2011, first-generation HCV protease inhibitors were approved for clinical use, which gave an improved sustained virologic response for HCV genotype 1 when administered as a triple combination with RBV and PEG-INF.

The success of these protease inhibitors proved to be limited, however, due to rapid emergence of viral resistance [4] combined with increased side effects and more complicated dosing.

In December 2013, the FDA approved a new antiviral agent for HCV, which was named sofosbuvir by its developers at Pharmasset and Gilead. Sofosbuvir is a nucleotide mimic which acts as an antimetabolite in viral replication. Unlike ribavirin, whose mechanism is ultimately not fully understood, sofosbuvir was specifically designed to target the NS5B polymerase in the HCV replication machinery. In combination with RBV and other antiviral agents, up to 100% sustained virologic response has been achieved for HCV genotypes 1–4 at shorter treatment times and in a variety of patient populations [5], thus representing a significant breakthrough in the HCV therapy. In addition, interferon-free regimens which combine sofosbuvir with other antivirals in all oral formulations present greater ease of administration and considerably fewer side effects.

Today, hepatitis C virus is still estimated to affect 160–180 million people worldwide and claim around half a million lives annually [5]. Together with chronic hepatitis B, the disease is the leading cause for liver cirrhosis and hepatocellular carcinoma and the most common reason for liver transplants. Efficient large-scale manufacture of sofosbuvir will thus represent an enormously important goal in eradicating hepatitis C across the globe.

This chapter aims to provide an overview of the synthetic approaches to sofosbuvir and, whenever appropriate, its close analogues and synthetic intermediates. The surveyed literature covers scientific publications primarily disclosed during the drug discovery and the clinical phases of development, as well as major patent applications up to May 2015. It is important to note that patent regulations in most countries allow inventions to be disclosed to the public only 18 months or longer after the filing; thus relevant discoveries made prior to or during the writing of this review could be expected to appear in the near future. The first section of this chapter presents a brief overview of the pharmacological properties of sofosbuvir including its mode of action. This is followed by a discussion of the current synthetic approaches to sofosbuvir, including present challenges, improvements, and new strategies toward the drug and its individual structural motifs. The reader is also encouraged to refer to the excellent review recently published by Schinazi and colleagues, which focuses on the phosphorylation strategies for nucleoside prodrugs, including sofosbuvir [6].

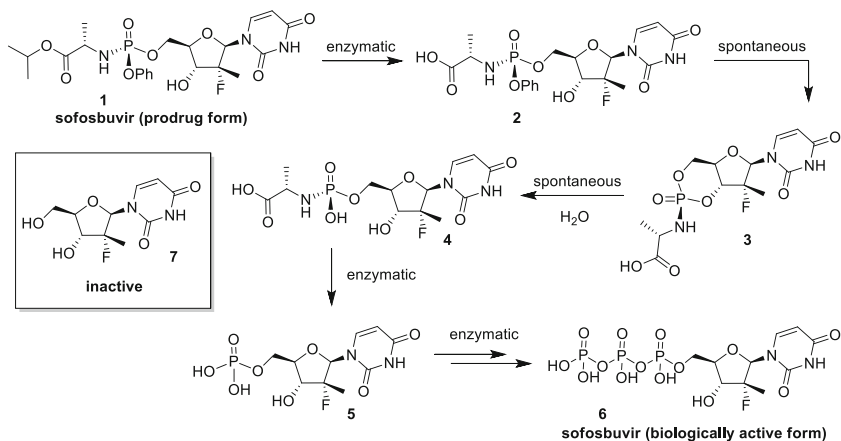
## **2 An Overview of the Biology and Pharmacology of Sofosbuvir**

Until 2011, the standard of care for HCV infections has been a combination of ribavirin and pegylated interferon- $\alpha$  (RBV/PEG-INF), which primarily works by stimulating the patient's own immune response against the virus. Although the

treatment can achieve a sustained virologic response, the success rate of 40–75% is rather low and depends on both the viral genotype and the patient's genetic polymorphism [2, 3]. Furthermore, the complex and not fully understood series of biological pathways by which the RBV/PEG-INFs operate make drug optimization difficult. Using small molecules to selectively inhibit specific structural elements of the virus' replication machinery represents a more effective strategy – which has long existed for other major viral pathogens including HIV and hepatitis B virus [7]. Although efforts to develop such direct-acting antivirals (DAAs) for HCV have been ongoing for decades, it was not until 2003 that the first in-human data on a DAA, a protease inhibitor, was reported in the literature [8]. The following decade has witnessed an explosion in DAA therapies for HCV, with several FDA new drug approvals since 2011.

Recently, the nonstructural HCV protein NS5B has been identified as a good molecular target for inhibition. This 66 kDa protein is as an RNA-dependent RNA polymerase (RdRp), an essential and uniquely viral enzyme responsible for the transcription of complementary-strand RNA from an RNA template. Three-dimensionally, the enzyme has a typical palm–finger–thumb structure, with the palm domain containing the active site in which ribonucleoside triphosphates are added to the 3'-end of the growing viral RNA chain [9]. In addition to several sites in the thumb and palm domains suitable for allosteric inhibition [10], the active site of NS5B makes an excellent target for inhibition with a substrate (nucleotide) mimic. In this strategy, selective binding of the inhibitor to the RdRp active site results in incorporation of this molecule into the nascent RNA and subsequent chain termination. Importantly, the NS5B active site is highly conserved across all HCV genotypes, offering the possibility of pan-genotypic treatments and ensuring a high barrier to drug resistance, since any amino acid mutations in this region are likely to compromise the virus' ability to replicate.

Apart from high cellular selectivity to minimize toxicity to the host, an essential prerequisite of RdRp inhibitors is the ability to reach and enter infected cells. As nucleotide mimics, polymerase inhibitors must bear a 5'-triphosphate moiety to be pharmacologically active; the negatively charged triphosphate group, however, is neither stable nor able to easily cross biological membranes. For this reason, early HCV RdRp inhibitors were ribonucleoside analogues, which relied on *in vivo* phosphorylation after entering the target cell [3]. However, the metabolism of converting a nucleoside to its 5'-triphosphate derivative involves three separate kinases, with the first one being most substrate-selective. Ineffective or nonproductive phosphorylation, especially in the first step, has thus impeded the early development of nucleoside inhibitors of HCV RdRp which often appeared ineffective simply because they never reached their pharmacologically active form. Indeed, reexamination of some nucleoside inhibitors which were inactive or poorly active in whole-cell replicon systems revealed them to be highly potent when their 5'-triphosphate derivatives were tested in biochemical assays [11]. A major advance in the development of effective HCV RdRp inhibitors came with the use of the so-called nucleotide prodrug approach [6]. In this method, nucleoside inhibitors bear a specially designed 5'-phosph(on)ate group which renders the



**Scheme 1** Mechanism of phosphoramidate cleavage in sofosbuvir to reveal the pharmacologically active 2'-F,2'-C-methyluridine triphosphate **6**

resulting molecule metabolically stable and membrane permeable. Once the prodrug enters the target cell, the 5'-phosph(on)ate group is unmasked by cellular enzymes to reveal a 5'-phosphate group. This effectively bypasses the first critical kinase-assisted phosphorylation and can thus dramatically improve the pharmacokinetic properties of the drug.

Sofosbuvir (**1**, Scheme 1) was the first HCV RdRp inhibitor to combine a promising nucleoside core with a nucleotide prodrug strategy. This combination proved to be extremely effective in producing a selective, potent, and orally bioavailable drug, which was approved in the USA in late 2013 and in other countries shortly thereafter. The uridine nucleoside core **7** is inactive in whole-cell replicon systems but has a high potency and intracellular half-life as its 5'-triphosphate **6** [12–14]. The phosphoramidate moiety of sofosbuvir is metabolized to a phosphate group in vivo through a series of chemical and enzymatic reactions [3, 15]. As shown in Scheme 1, first-pass metabolism by liver enzymes hydrolyzes the terminal isopropyl ester to a free carboxylic acid (compound **2**). This is followed by a spontaneous reaction in which the 3'-hydroxyl group displaces the phenol moiety forming a cyclic phosphoramidate intermediate **3**, which is then hydrolyzed to an open-chain form **4** under physiological conditions. Finally, a phosphoramidase or histidine triad nucleotide-binding protein 1 cleaves the amino acid to reveal a phosphate group (product **5**). Notably, the absolute stereochemistry at phosphorus has a significant impact on the potency and pharmacokinetic properties of the drug [16]. Once 5'-triphosphorylated, the biologically active form of sofosbuvir acts as a nonobligate chain terminator during the RNA synthesis by NS5B RdRp.

In accordance with expectations, sofosbuvir proved to have high clinical efficacy against all six HCV genotypes in a variety of patient populations [17]. Combinations of sofosbuvir with ribavirin, second-generation protease inhibitors, and other

antivirals now offer the possibility of highly effective all oral treatments. Interferon-free regimens are also feasible in many cases, eliminating severe side effects associated with this agent.

### 3 Synthetic Approaches to Sofosbuvir

Since sofosbuvir is a uridine analogue, the atom numbering used throughout this review corresponds to the conventional numbering of nucleosides, with C1'–C5' referring to the carbohydrate portion of the molecule and C1–C6 referring to the uracil nucleobase (Fig. 1). The phosphoramidate moiety is subsequently numbered C7–C14, as shown. To differentiate between the carbon and phosphorus stereocenters of sofosbuvir, the phosphorus stereogenic descriptor is always denoted as  $S_P$  or  $R_P$  in this work.

As a prodrug, sofosbuvir consists of two principal building blocks – the bioactive uridine analogue **7** and the phosphoramidate **8**, which imparts the molecule its bioavailability and cell membrane permeability (Scheme 2). Although both fragments require multistep synthesis, considerably more routes have been disclosed toward the nucleoside core **7**, both in the context of drug discovery and as a result of the synthetic challenges the molecule poses. Subsequently, the first two sections of this review are devoted to the construction of **7**, whereas the last section covers both the synthesis of **8** and the coupling of the two building blocks.

While **7** is structurally very similar to the natural nucleoside uridine, the presence of a tertiary fluorinated stereocenter at C-2' significantly increases the molecule's complexity. Indeed, the logic behind the various synthetic approaches to **7** appears to mainly rely on the timing and nature of the fluorination step. For this reason, the synthetic routes to **7** were divided into two sections, which we have termed “early-stage fluorination” and “late-stage fluorination” (Scheme 3).

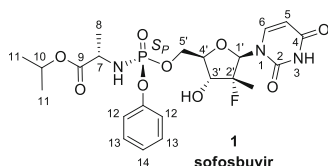
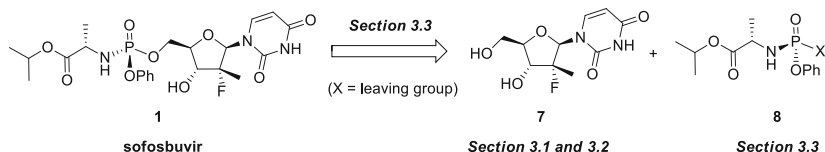
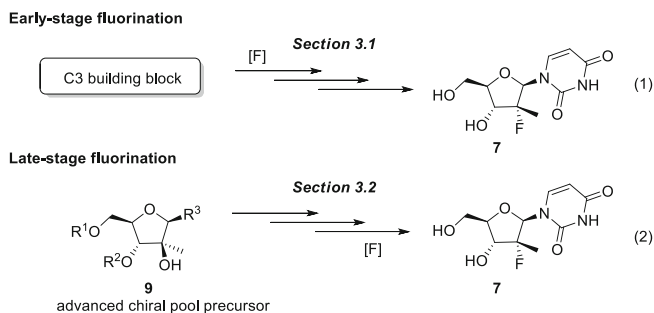


**Fig. 1** Structure of sofosbuvir and the atom numbering adopted in this review



**Scheme 2** Retrosynthetic disconnection of sofosbuvir



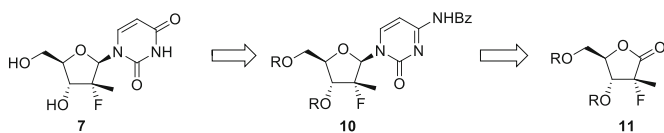
**Scheme 3** Systematization of synthetic approaches to **7**

In particular, the early-fluorination approaches start from simple building blocks which contain up to three carbons expressed in the final product and either already incorporate a fluorine atom or are fluorinated early in the synthetic sequence (Scheme 3, Eq. 1). In contrast, the late-stage fluorination approaches are semisynthetic in nature and start from advanced chiral pool precursors which are fluorinated as one of the last steps (Scheme 3, Eq. 2). Although this division provides a useful way of systematizing the various synthetic routes toward **7**, some conceptual overlap in Sects. 3.1 and 3.2 could not be avoided.

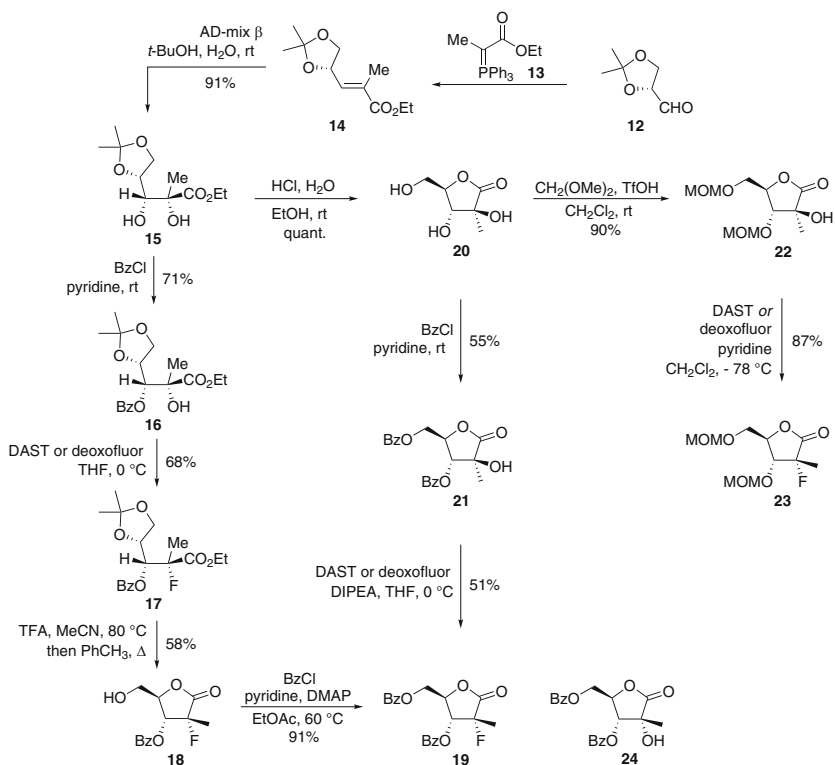
### 3.1 The Nucleoside Core: Early-Stage Fluorination Approaches

All of the disclosed early-stage fluorination approaches to the nucleoside core of sofosbuvir **7** can be traced back to the globally protected cytidine derivative **10** which can in turn be disconnected at the glycosidic bond to give the precursor D-ribo- $\gamma$ -lactone derivative **11** (Scheme 4). Several different routes of synthesis have been reported for these building blocks during the last years, providing various solutions for the stereoselective introduction of the tertiary fluorine atom at the C-2' position.

During the early stages of sofosbuvir development, chemists at Pharmasset reported a strategy toward the 3,5-di-*O*-protected D-ribo- $\gamma$ -lactone **19** starting with enantiomerically pure glyceraldehyde acetonide **12** (Scheme 5) [18]. In their route, Wittig olefination of **12** followed by Sharpless dihydroxylation with AD-mix  $\beta$  furnished enantiomerically enriched diol **15**. Different protecting group strategies were followed starting from this intermediate, either employing the open-chain form of diol **15** or its lactone equivalent **20**, prepared by deprotection of the acetonide group. In the former approach, **15** was selectively benzoyl-protected at the less substituted alcohol and treated with DAST or deoxofluor to smoothly effect stereoselective deoxyfluorination. Subsequent ring closure to ribonolactone derivative **18** was achieved with TFA, followed by treatment with benzoyl chloride to



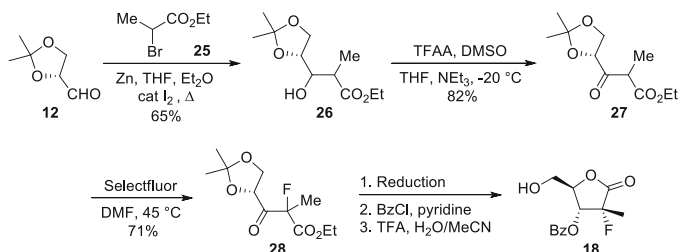
**Scheme 4** Retrosynthetic disconnection of **7** in early-fluorination approaches



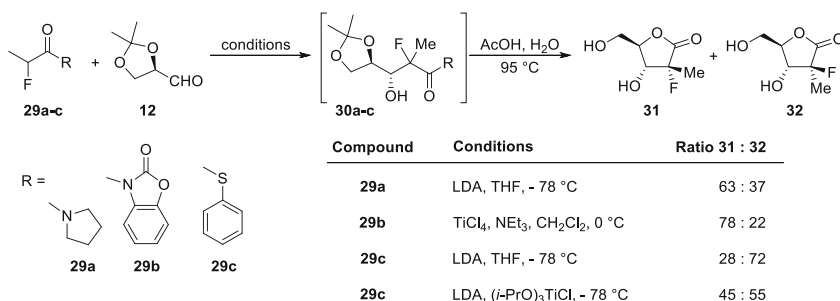
**Scheme 5** First-generation approach to **19** using nucleophilic fluorination

give the 3',5'-bis-benzoylated building block **19**. Alternatively, the deoxyfluorination could be carried out with  $\gamma$ -lactone **21**, which was protected at the 3'- and 5'-positions with benzoyl groups, to give the product **19**. In contrast to substrate **16**, fluorination of **21** required the presence of a tertiary amine base (DIPEA) in excess to avoid the formation of undesired compound **24**. A higher yield (87%) for the nucleophilic fluorination could also be achieved by using the MOM-protected derivative **22**.

A complementary electrophilic fluorination strategy from the Pharmasset team is outlined in Scheme 6 [18]. Using enantiopure glycerinaldehyde acetonide **12**, the authors carried out a Reformatsky reaction with  $\alpha$ -bromopropionate **25** to obtain  $\beta$ -hydroxy ester **26**. Omura–Sharma–Swern oxidation of this compound gave



**Scheme 6** An electrophilic fluorination approach to **18** via a Reformatsky reaction

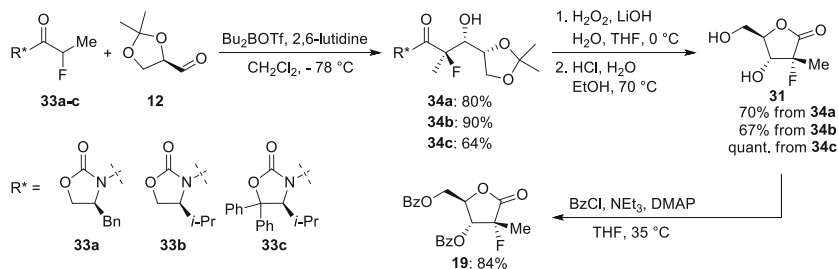


**Scheme 7** Initial aldol approach to unprotected lactone **31**

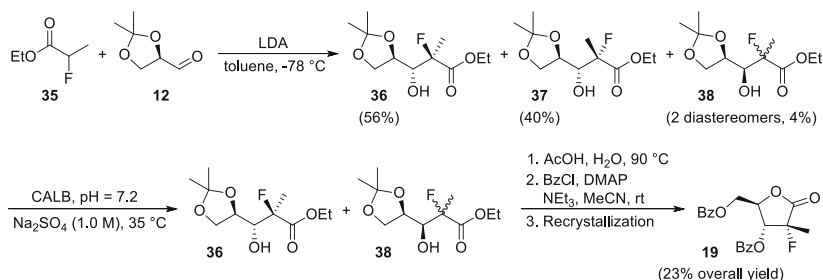
ketone **27** as a mixture of diastereomers. The mixture was treated with Selectfluor in DMF to give tertiary fluoride **28** in good yield as a 1:1 mixture at the C-2 stereocenter. Although no experimental proof for the conversion of fluoride **28** into  $\gamma$ -lactone **18** was provided in the patent application, the remaining steps are described to involve a selective reduction of the ketone, followed by benzoylation of the resulting alcohol and acidic acetonide deprotection/lactonization with TFA.

Scientists from Hoffmann–La Roche have disclosed an alternative strategy for the preparation of 2-fluoro-2-*C*-methyl-*D*-ribo- $\gamma$ -lactone (**31**) in a patent application (Scheme 7) [19]. The method is based on an aldol reaction between a prochiral enolate of  $\alpha$ -fluoropropionates **29a–c** and enantiomerically pure glycerinaldehyde acetonide **12**. Directly quenching the reaction with acetic acid was found to accomplish acetonide deprotection and cyclization to the diastereomeric lactone products **31** and **32**. Although several chelating groups R and Lewis acid/base combinations were explored, only moderate facial selectivities (up to 78:22 dr) could be achieved (data on overall yields were not provided).

An improved aldol approach was subsequently published by researchers at Hoffman–La Roche, which utilized chiral auxiliaries on the fluoropropionate coupling partner to enhance the diastereoselectivity (Scheme 8) [20]. Compounds **33a–c** were prepared from 2-fluoropropionic chloride and the corresponding chiral oxazolidinones. The reaction between the boron enolates of compounds **33a–c** and glycerinaldehyde acetonide **12** gave the corresponding aldol products **34a–c** in good yield (diastereoselectivity was not provided). The aldol products could be



**Scheme 8** A stereoselective aldol approach to protected lactone **19**



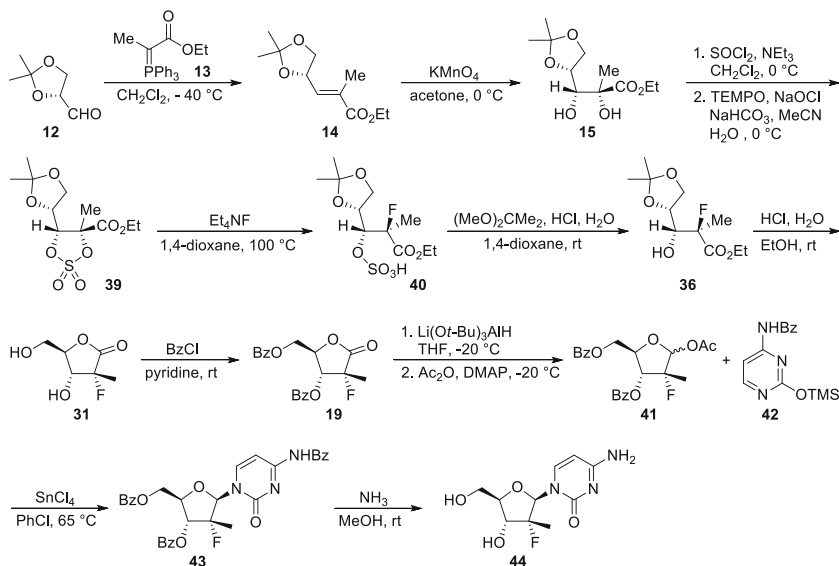
**Scheme 9** A scalable aldol/bioenzymatic approach to protected lactone **19**

converted into the fluorinated lactone **19** upon oxidative cleavage of the auxiliary, acid-catalyzed cyclization and benzoyl protection.

A scalable aldol reaction process between the prochiral enolate of  $\alpha$ -fluoropropionate **35** and glycerinaldehyde derivative **12** was also reported by the same team, and is outlined in Scheme 9 [21]. The initial LDA-mediated aldol reaction was found to give a 56:40:4 mixture of four stereoisomers **36–38** as determined by GC analysis. This mixture was treated with a hydrolase (CALB) which exclusively hydrolyzed isomer **37** to its corresponding carboxylic acid. Subsequent aqueous extraction removed the carboxylic acid component, and the remaining diastereoisomers **36** and **38** were cyclized in the presence of acetic acid. Final recrystallization of the benzoate **19** gave the desired product in 23% overall yield.

On a quest for a suitable large-scale preparation of fluorinated  $\gamma$ -lactone **19** and nucleoside **44**, scientists at Pharmasset reevaluated the initial dihydroxylation/nucleophilic substitution route. To achieve an industrially compatible process for the preparation of compound **44**, the authors sought to minimize the number of chromatographic purification steps by isolating solid intermediates and ideally avoid problematic reagents such as DAST. The result was a scalable route of synthesis outlined in Scheme 10 [22–24].

The reaction sequence begins with the conversion of glycerinaldehyde acetone **12** to *syn*-diol **15** by a sequence of Wittig olefination ( $E/Z = 97:3$ ) and  $\text{KMnO}_4$ -mediated dihydroxylation, which proceeded with a 12:1 diastereoselectivity.

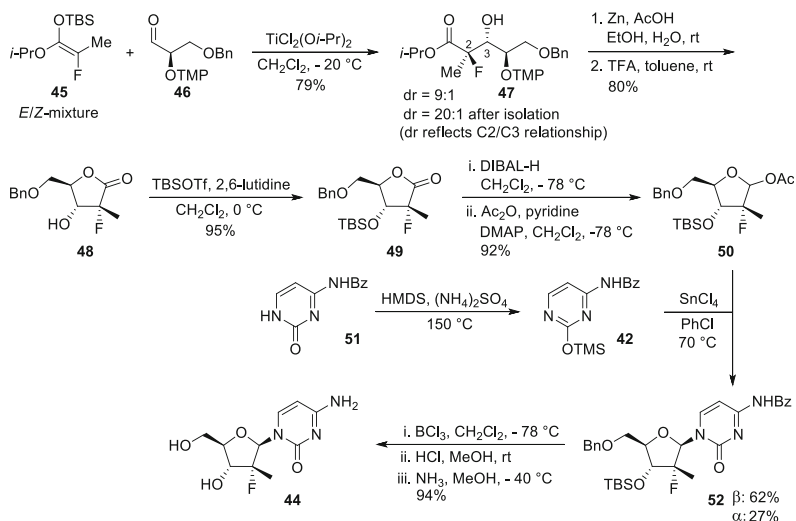


**Scheme 10** An approach to **44** based on scalable dihydroxylation of **14**

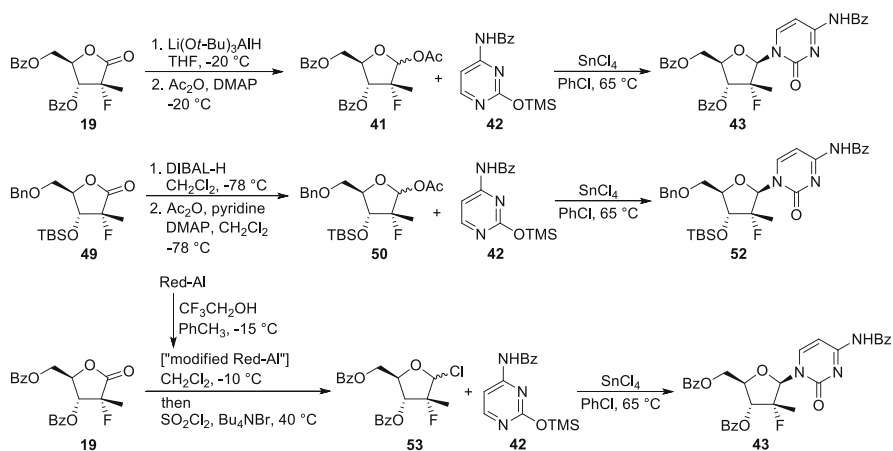
In order to avoid DAST, the diol was converted in two steps to the cyclic sulfate **39** and treated with tetraethylammonium fluoride [25] in acetonitrile or 1,4-dioxane to give product **40**. It should be noted that this nucleophilic substitution with fluoride proceeded in a completely regioselective manner. The hydrolysis of the sulfate and the acetonide groups in compound **40** was performed in two separate steps to ensure complete conversion of the starting material and minimize the formation of side products. Lactone **31** was obtained directly from the reaction mixture upon acetonide deprotection. Finally, compound **31** was converted to the dibenzoate **19** followed by a reduction/acetylation sequence to provide compound **41** for the final  $\text{SnCl}_4$ -catalyzed Vorbrüggen glycosidation. Overall, the route of synthesis allowed the preparation of **44** in 6.4% overall yield from **12** on a multikilogram scale.

Recently, an improvement to the aldol approach was reported by the group of MacMillan (Scheme 11) [26]. This reaction sequence is based on a highly selective Mukaiyama aldol reaction between silyl ketene acetal **45** (*E/Z* ratio not given) and glyceraldehyde **46** to furnish diastereomerically enriched aldol product **47**. Cleavage of the TMP group was achieved with  $\text{Zn}/\text{AcOH}$ , followed by a TFA-mediated lactonization to give **48**. The sequence was completed with TBS protection of the 3'-hydroxyl group, lactone reduction, acetylation, and a Vorbrüggen glycosidation with protected cytosine **42**. Overall, the sequence combines the advantages of an effective early-stage fluorination together with good diastereoselectivity for the aldol reaction.

Approaches for the conversion of D-ribo- $\gamma$ -lactone derivatives **19** and **49** to the nucleosides **43** and **52** are summarized in Scheme 12 [24]. The sequence starts with the reduction of **19** and **49** to the corresponding lactols which are then activated as



**Scheme 11** An approach to **44** based on a diastereoselective Mukaiyama aldol reaction



**Scheme 12** Glycosidation approaches for the synthesis of protected nucleosides **43** and **52**

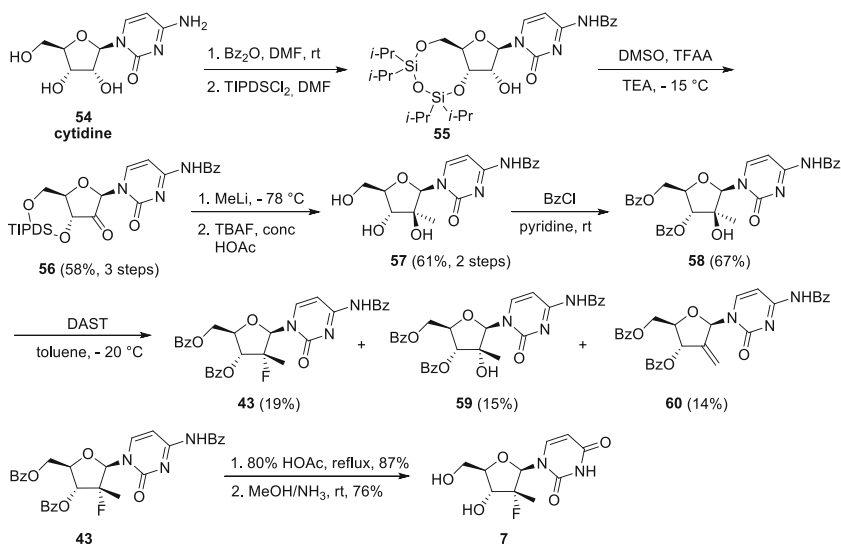
glycosyl donors by acylation or halogenation. The resulting compounds are then coupled with the protected cytosine **42** in the presence of  $\text{SnCl}_4$  according to the Vorbrüggen protocol to obtain the nucleosides **43** and **52**. Cytosine hydrolysis and hydroxyl group deprotection ultimately afford the uridine core of sofosbuvir **7**.

### 3.2 The Nucleoside Core: Late-Stage Fluorination Approaches

In addition to the total synthesis approaches described in Sect. 3.1, the nucleoside core of sofosbuvir (**7**) can be constructed by complementary semisynthetic methods. These rely on the modification of naturally occurring chiral pool precursors, such as the nucleosides cytidine and uridine, followed by a late-stage fluorination. Due to the availability of inexpensive ribose nucleosides and the existence of well-established methods for their 2'-functionalization, the semisynthetic approaches have been widely exploited in the development of sofosbuvir and its analogues. However, compared to the generally unproblematic early-stage fluorination, introduction of the fluorine atom into complex advanced intermediates is often capricious, low yielding, and expensive. Thus, most of the late-stage fluorination routes remain industrially unapplicable and limited to medicinal chemistry applications.

In their development of HCV RNA polymerase inhibitors, chemists at Pharmasset used a late-stage fluorination approach to access protected 2'-deoxy-2'-fluoro-2'-C-methylcytidine **43**, which serves as a direct synthetic precursor to the uridine core of sofosbuvir [27–30] (Scheme 13).

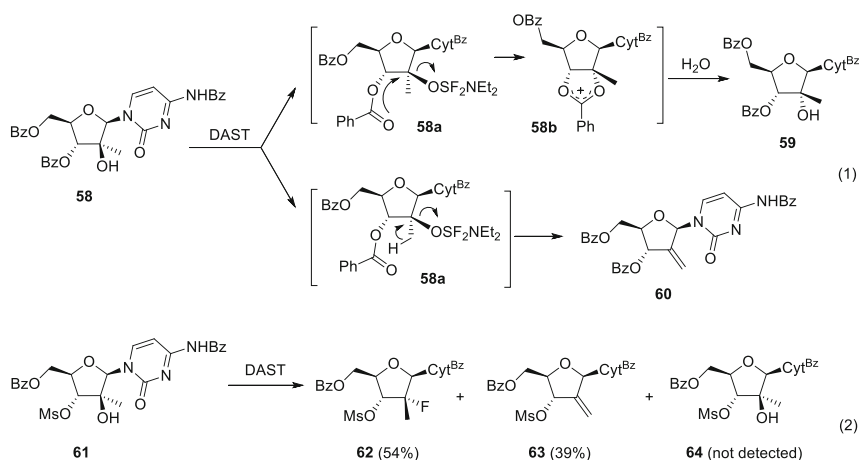
Starting with cytidine (**54**), the nucleoside was first selectively *N*-benzoylated with benzoic anhydride in DMF [31] and then treated with TIPDSCl<sub>2</sub> to simultaneously protect the 3'- and 5'-hydroxyl groups as the kinetically preferred 8-membered cyclic disiloxane [32]. The remaining secondary alcohol was oxidized under Omura–Sharma–Swern conditions (TFAA, DMSO), [33] and the resulting



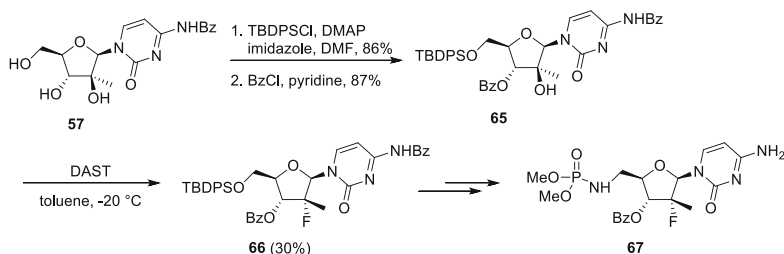
**Scheme 13** Pharmasset approach to **7** by linear functionalization of cytidine

ketone treated with methyl lithium to give **57** as the exclusive product of an  $\alpha$ -face attack after deprotection [34]. To introduce the fluorine atom at the 2'-position, the authors chose direct deoxyfluorination with DAST, hoping for a clean inversion of configuration. Although DAST fluorination has been carried out in the presence of a TIPDS group with carbocyclic nucleosides [35, 36], the authors opted to exchange this silicon-based protecting group for more robust benzoyl groups by a deprotection/protection sequence. Upon treatment of **58** with DAST, a mixture of three products was obtained, which could be separated in about 20% yield each, and unambiguously characterized after deprotection. The desired product **43** was obtained as a single diastereomer showing stereospecific inversion of the configuration at C-2'. The two side products were identified as the 2'-epimerized starting material **59** and an exocyclic elimination product **60**. To obtain the uridine core of sofosbuvir, selective debenzoylation and deamination of the cytosine moiety were performed by refluxing **43** in 80% acetic acid. Finally, aminolysis with  $\text{NH}_3$  in methanol afforded the deprotected building block **7**, setting the stage for the phosphoramidation (Sect. 3.3).

In their corresponding patent disclosure [18], the authors reported interesting mechanistic insight into the DAST fluorination of **58** and in particular the origin of the two side products **59** and **60**. In accordance with earlier literature [37], formation of the epimerized starting material **59** was attributed to the neighboring-group participation of the 3'-benzoyl ester substituent, which forms a stable 1,2-cyclic benzoxonium ion **58b** from the activated sulfane species **58a** as a competing process to fluorination (Scheme 14). Upon exposure to water, this intermediate collapses back to 2'-epimer **59**. The elimination product **60** was reasoned to form from the sulfane species **58a** by loss of a methyl proton. Based on this mechanism, the authors proposed that the use of nonparticipating groups such as acetal, alkyl, benzyl, mesyl, tosyl, trifluoroacetyl, and trichloroacetyl groups should effectively prevent the formation of **59**-type products. Although no experimental details are



**Scheme 14** The role of 3'-hydroxyl protecting group in DAST fluorination



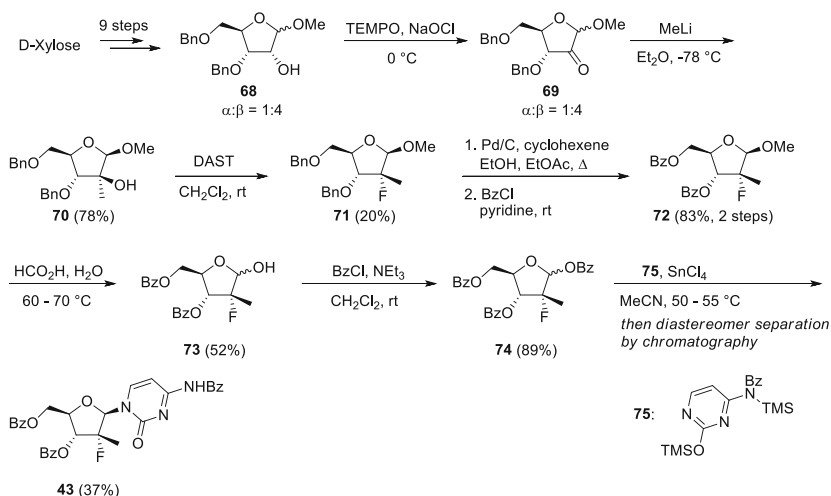
**Scheme 15** Late-stage fluorination of cytidine derivative **65**

given, the fluorination of compound **61** protected at 3'-hydroxyl group with a nonparticipating mesyl group is indeed reported to give an improved yield of 54% for the desired fluorinated compound **62**, along with 39% of the elimination product **63** and no detectable epimer **64**. With protecting groups showing no/poor leaving group ability such as acetals, the fluorination is claimed to proceed even more effectively [18].

Chemists at Enanta Pharmaceuticals employed a similar late-stage fluorination route for the preparation of the fluorinated cytidine derivative **66**, a building block used to construct nucleoside phosphoramidates of type **67** [38] (Scheme 15). Starting with the intermediate **57**, prepared as above, the authors first protected the more accessible 5'-hydroxyl group as a TBDPS ether, followed by the secondary 3'-hydroxyl group as a benzoyl ester. Treatment of the resulting compound **65** with DAST afforded the desired product **66** in a moderate yield of 30% after chromatography, presumably due to formation of side products similar to **59** and **60** (Scheme 13).

Seeking a convergent approach to different base-modified nucleoside analogues for structure–activity relationship studies, researchers at Pharmasset also developed a route to **43** that does not rely on a linear functionalization of cytidine [28, 39]. Instead, the authors prepared a fluorinated ribofuranoside **74**, which could then be coupled with protected cytosine (or, in principle, any other nucleobase) by a Vorbrüggen condensation (Scheme 16).

In this approach, a slightly modified procedure of Ritzmann et al. [40] was used to convert D-xylose to the benzyl-protected furanoside **68** in nine steps as an inseparable 1:4  $\alpha/\beta$  mixture of anomers. Catalytic TEMPO oxidation [41] furnished ketone **69** which was alkylated with methyl lithium to give **70** as the major diastereomer in 78% isolated yield. Similarly to the deoxyfluorination of nucleosides, treatment of the ribofuranoside **70** with DAST gave a complex mixture of products, from which the desired compound **71** was isolated in 20% yield. A transfer hydrogenation/acylation sequence was used to exchange the benzyl protecting groups on the 3'- and 5'-hydroxyl groups for benzoyl esters (product **72**). Hydrolytic cleavage of the glycoside bond and 1'-hydroxyl group benzylation completed the synthesis of the carbohydrate building block **74** as an anomeric mixture (dr not given). Finally, Vorbrüggen condensation with silylated



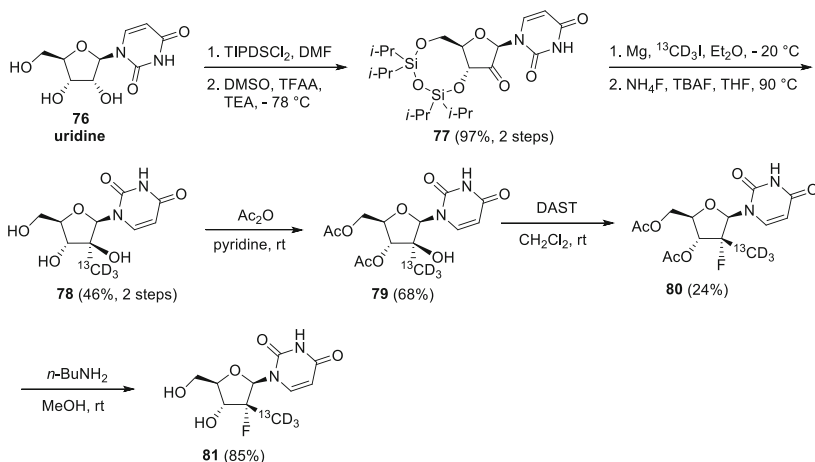
**Scheme 16** Convergent synthesis of **43** from fluorinated ribofuranose **74** and protected cytosine

*N*-benzoylcytosine **75** in the presence of  $\text{SnCl}_4$  [42, 43] gave the product as a 1:1 anomeric mixture, from which the desired  $\beta$ -anomer **43** was isolated in 37% yield.

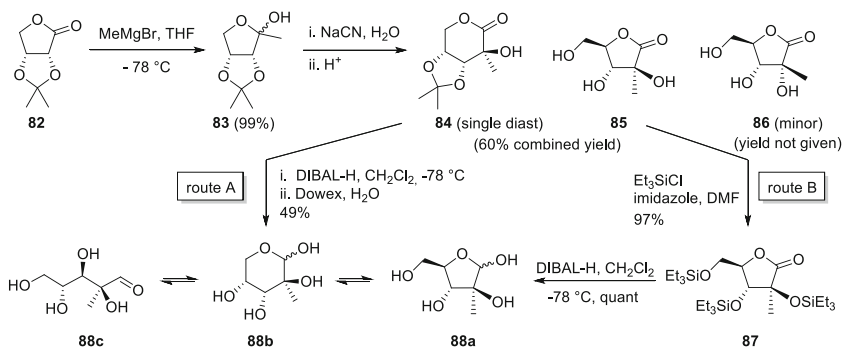
During the clinical development of sofosbuvir at Pharmasset, it was necessary to prepare stable isotope-labeled analogues of the compound for quantitative bioanalytical LC-MS analysis of plasma samples [44, 45]. Toward this end, the  $^{13}\text{CD}_3$ -derivative **81** was identified as the compound that satisfied all physicochemical characteristics. For the synthesis of **81**, the original Pharmasset “cytidine route” (Scheme 13) was slightly modified, not only to allow the introduction of an isotope-labeled methyl group but also to obviate unnecessary nucleobase manipulations. Indeed, early work of Moffatt, Matsuda, and Miyasada has shown that nucleosides containing an unprotected uracil can be cleanly 2'-oxidized [32, 46] and 2'-methylated [47]. Guided by this precedent, the Pharmasset chemists commenced the synthesis of **81** directly with uridine, which was selectively protected at the 3'- and 5'-hydroxyl groups as the bulky cyclic disiloxane (Scheme 17).

Oxidation of the resulting compound under Omura–Sharma–Swern conditions smoothly afforded the corresponding ketone **77** which was methylated with an excess (5 equiv) of a freshly prepared Grignard reagent  $^{13}\text{CD}_3\text{MgI}$ . As in the cytidine route, the siloxane protecting group was exchanged for ester groups prior to fluorination; this time however, the authors chose acetyl instead of benzoyl groups. Treatment with DAST gave the fluorinated product **80** with the typically modest yield of 24% after silica gel chromatography. Deprotection of the acetyl groups furnished the isotope-labeled uridine core of sofosbuvir, **81** used in the next step for 5'-hydroxyl group phosphoramidation (Sect. 3.3).

It is worth noting that the non-labeled uridine building block **78** (numbered **92** without any heavy isotopes) could also be assembled from 2-*C*-methyl arabinose via a Holý reaction [48, 49], rather than uridine functionalization [50]. Researchers



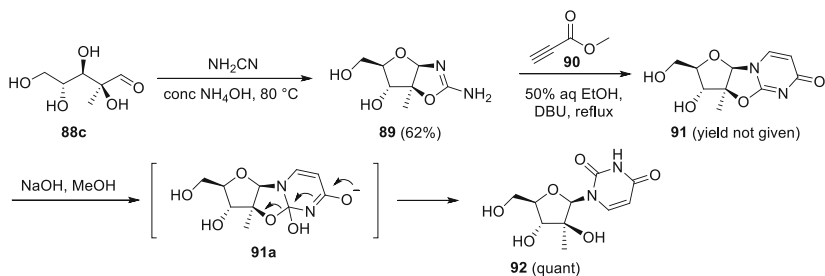
**Scheme 17** Synthesis of isotopically labeled **81** by linear functionalization of uridine



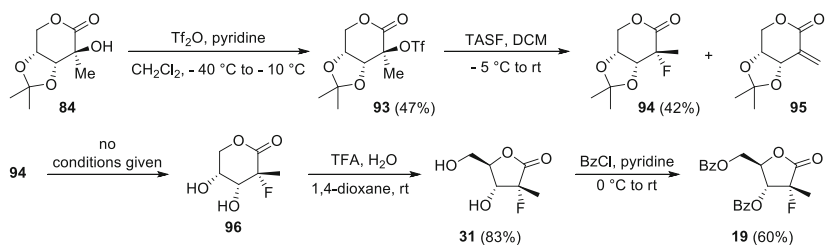
**Scheme 18** Synthesis of 2-*C*-methyl arabinose **88**

at the University of Oxford, Idenix Pharmaceuticals, and Novartis have developed this method in an effort to improve existing approaches to 2'-*C*-methyl  $\beta$ -nucleosides, which suffer from problems of anomeric control during glycosidation, or multiple protections and functional group manipulations involved in the linear functionalization of a nucleoside (as in Schemes 13 and 17). 2-*C*-Methyl arabinose (**88**) can be accessed from protected ribonolactone **82** in 4 steps (Scheme 18, route A), which involve Grignard methylation, Kiliani ascension [51], DIBALH reduction of the resulting arabinono-1,5-lactone **84**, and deprotection. The other major product of the Kiliani ascension, arabinono-1,4-lactone **85**, can give additional amounts of **88** by alcohol protection, lactone reduction, and deprotection (Scheme 18, route B).

Treating arabinose **88** under Holý conditions with cyanamide and aqueous ammonia furnished oxazoline **89** (Scheme 19). Subsequent reaction with methyl propiolate (**90**) gave 2'-*C*-methyl-anhydrouridine **91** which could be hydrolytically



**Scheme 19** Synthesis of the methylated uridine **92** via Holý reaction of **88**

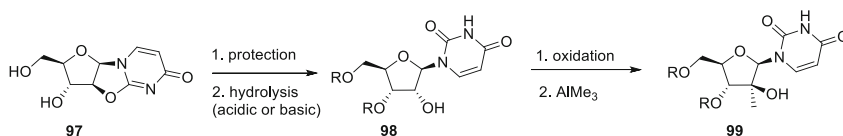


**Scheme 20** Synthesis of ribonolactone **19** via TASF fluorination

ring-opened to give **92**. Basic conditions of hydrolysis were crucial to achieve complete retention of configuration at C-2', presumably via the mechanism shown.

Researchers at Idenix Pharmaceuticals have furthermore demonstrated that the lactone intermediate **84** is suitable for fluorination at C-2' [52]. The authors exploited the activated nature of the tertiary alcohol, positioned  $\alpha$  to an electron-withdrawing carbonyl to obviate the use of DAST. Instead, the tertiary alcohol could be triflated and substituted using the nucleophilic fluoride source TASF (Scheme 20). Although exocyclic elimination also proved to be a competing reaction (giving product **95**), a slightly improved yield of 42% could be achieved after chromatographic purification compared to most DAST methods. The fluorinated product was ring-contracted to a ribonolactone **31** upon acetonide deprotection and benzoyl-protected at the 3'- and 5'-positions. As described in Sect. 3.1 (Scheme 12), the building block **19** can be further converted to the nucleoside core of sofosbuvir after reduction and glycosidic coupling.

Our development team at Sandoz was also attracted by the semisynthetic approaches to sofosbuvir's nucleoside core, given that almost all of the atoms and stereogenic centers of the molecule can be derived from an inexpensive pyrimidine nucleoside precursor. In our approach, commercially available 2,2'-anhydrouridine **97** was employed as the starting material for selective protection of the 3'- and 5'-positions with various functional groups [48], followed by hydrolytic ring-opening under either acidic or basic conditions to unmask the 2'-hydroxyl group (product **98**, Scheme 21). Depending on the protecting groups "R," oxidation of the 2'-hydroxyl group was carried out under Swern or Dess–Martin conditions.



**Scheme 21** Synthesis of variously protected 2'-C-methyluridine derivatives **99** from 2,2'-anhydrouridine **97**

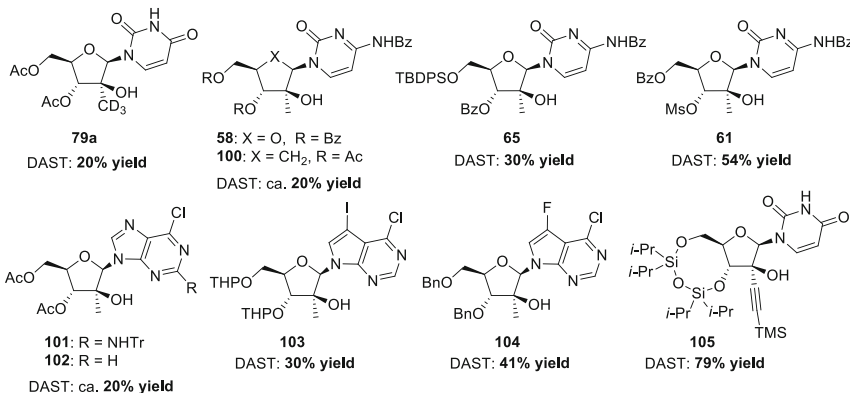


**Fig. 2** Literature known DAST deoxyfluorination of 2'-C-methyl *arabino*-pyrimidines and -purines [18, 27, 38, 44, 53–56]

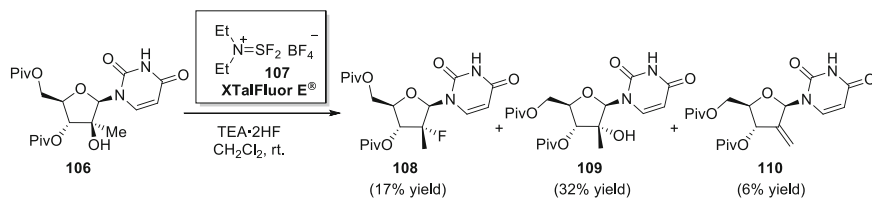
Subsequent ketone methylation with AlMe<sub>3</sub> proved to be compatible even in the presence of benzoyl protecting groups, obviating the need for additional protecting group manipulations.

With substrates **99** in hand, we focused on the development of an efficient and scalable reaction to introduce the fluorine atom. A foray into the literature on deoxyfluorination of 2'-C-methyl *arabino*-nucleosides indicated that only DAST has been employed in this type of reactions,<sup>1</sup> giving the product with a generally modest yield regardless of the nucleobase substituent but with a clear influence of the hydroxyl protecting groups as discussed before (for neighboring-group effect, see Scheme 14) [27, 38, 44, 53–56].

Whenever discussed, the low yield was attributed to the formation of side products rather than problems of reactivity. It is noteworthy that a DAST deoxyfluorination of the propargylic substrate **105** (Fig. 2) has been reported to proceed in 79% yield [57], suggesting that electronically activated tertiary alcohols do not suffer from the same problems.

We initially attempted to effect the deoxyfluorination of **99** bearing various protecting groups with inexpensive metal fluorides, HF–amine and HF–borane

<sup>1</sup> Although it has been stated in some patent literature that deoxofluor can serve as a suitable fluorinating agent, no experimental evidence could be found.



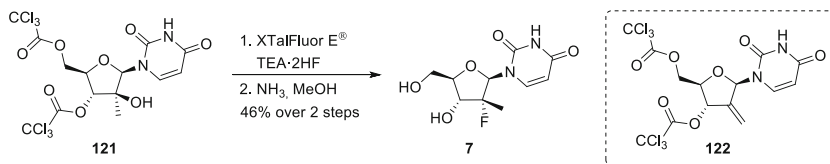
**Scheme 22** Fluorination of pivaloyl-protected 2'-C-methyl *arabino*-uridine **106** with XTalFluor E<sup>®</sup>

complexes. However, none of these agents proved reactive even under forcing conditions; additional activation of the tertiary alcohol as a leaving group by sulfonylation, deoxychlorination, and incorporation of the 2'-oxygen into a strained ring system [58–60] proved equally ineffective. In light of these setbacks, we were prompted to reconsider aminosulfur fluoride derivatives and turned to a recent variant, XTalFluor E<sup>®</sup> (**107**, Scheme 22) [61, 62]. Significantly less expensive than DAST, this stable, free-flowing solid is commercially available on multikilogram scale, does not spontaneously release HF, and features an industrially compatible thermal profile [61]. In addition, XTalFluor E<sup>®</sup>, which is an aminodifluoro sulfonium salt, has been shown to have greater selectivity with alcohols which are prone to elimination compared to DAST. Treatment of **106** with XTalFluor E<sup>®</sup> and a TEA·HF additive furnished the same three products as with DAST (compare to Scheme 13), albeit in a ratio that favored the epimerized starting material **109** over the elimination product **110** (Scheme 22).

To optimize this reaction, we opted for a systematic screen of common protecting groups at the 3'-position, given that they can significantly influence the nature and distribution of the side products [18]. For simplicity, the 5'-position was simultaneously protected with the same group. Our findings can be mechanistically summarized as shown in Scheme 23 [63]. The initial instantaneous reaction of the substrate **99** with XTalFluor E<sup>®</sup> forms an activated sulfane species **111** [61], which can then be displaced by a fluoride in a slower process to form the desired product **112**. Alternatively, **111** can undergo a competing elimination to form the olefinic product **115** or participate in a fast neighboring-group-specific side reaction. As with DAST, ester protecting groups (Ac, Piv, Bz), were found to engage in neighboring-group participation, forming a stable dioxolenium ion **116**. This intermediate appears not to be susceptible to fluorination, but is trapped by water upon aqueous workup to form orthoester **117** and decompose to side product **118** and occasionally its regioisomer **119**. Alternatively, in a relatively slow process, **116** can lose a proton, forming the olefinic product **115**. In contrast to DAST, electron-donating groups (Bn, PMB, silyloxy<sup>2</sup>) were found to engage in a different type of neighboring-group participation. Transient formation of a carbocation at the

<sup>2</sup> Acetal protecting groups were found to be unstable under the reaction conditions.





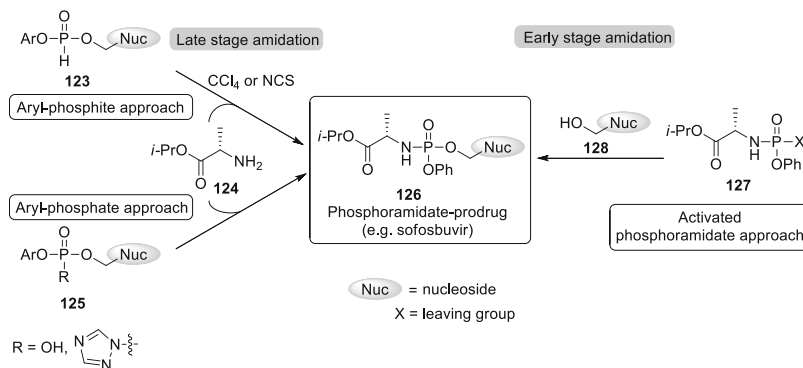
**Scheme 24** Fluorination of TCA-protected substrate **121** with XTalFluor E<sup>®</sup>

gram scale to afford the product in approximately 60% yield. Deprotection of the crude reaction mixture with methanolic ammonia furnished **7** in an overall yield of 46% (Scheme 24). It is noteworthy that the fluorinated product is significantly more reactive toward deprotection than the corresponding unsaturated side product **122** and becomes completely water soluble upon deprotection, enabling its purification by an appropriately designed aqueous workup [63].

### 3.3 Phosphoramidation of the Nucleoside Core

As described in Sect. 2, the nucleoside core of sofosbuvir is inactive in biological systems and relies on a 5'-phosphoramidate moiety to become pharmaceutically active in vivo. This structural unit consists of a central P (V) atom bearing the uridine analogue, a phenoxy residue, and an N-linked amino acid alkyl ester in a defined stereochemical configuration. As already mentioned, the absolute configuration at phosphorus has a significant impact on the pharmacological activity of sofosbuvir, with the different diastereomers showing a markedly different potency [16]. As a consequence, synthetic methodologies capable of generating stereochemically defined phosphoramidates are critical in the context of sofosbuvir synthesis. To date, solutions to this problem mainly consist of either separating diastereomeric mixtures by fractional crystallization or chromatography or diastereoselective approaches using stereochemically enriched phosphoramidation reagents.

The synthesis of aryloxyphosphoramidate nucleoside prodrugs (“pro-Tides”) has been recently summarized in Schinazi’s comprehensive review [6]. Briefly, the various methodologies can be classified based on the order of bond disconnection around the central phosphorus atom (Scheme 25). The “aryl phosphite approach” capitalizes on Atherton–Todd-type chemistry for the late-stage introduction of the amino acid building block. In this reaction, phosphite **123** is treated with  $\text{CCl}_4$  or NCS to generate the active electrophile (presumably a chlorophosphate) in situ [64], which is then intercepted by amino acid alkyl ester **124** to form the P–N bond. Late-stage amidation is also performed in the “aryl phosphate approach,” in which an activated phosphate **125** bearing a triazole or hydroxyl-based leaving group is reacted with the amino acid derivative. The third strategy relies on preforming an activated phosphoramidate building block **127** which is then reacted with the 5'-hydroxyl group of the nucleoside. In most



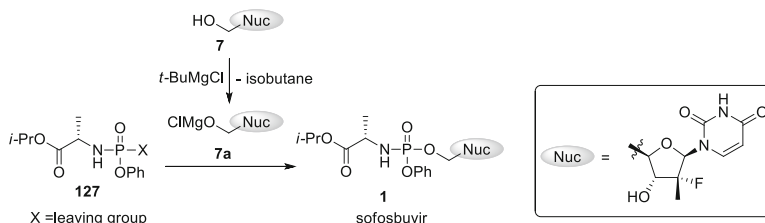
**Scheme 25** Classification of synthetic approaches to phosphoramidate prodrugs

instances, either chloride or a substituted phenolate acts as the leaving group in the phosphoramidate reagent. In general, all nucleophilic substitution reactions at the P (V) center proceed stereospecifically with an inversion of configuration.

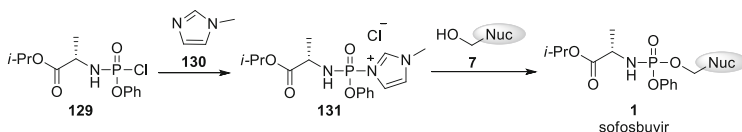
All syntheses of sofosbuvir reported to date rely on the “activated phosphoramidate approach” shown in Scheme 25. In order to facilitate the nucleophilic displacement of the leaving group “X” on phosphorus (compound 127), different strategies have been devised. Considering the underlying mode of reactivity, we have termed these synthetic approaches “acidic activation” and “basic activation.”

The majority of the reports dealing with the synthesis of sofosbuvir employ the “basic activation” strategy, with either the Lewis base *N*-methyl imidazole (NMI) or the Brønsted base *t*-BuMgCl acting as promoters of the 5'-hydroxyl group phosphorylation. Both of these reagents have been successfully applied in the synthesis of numerous other nucleoside prodrugs, whereby their suitability is substrate dependent and can be affected by the nature of the nucleobase and presence of competing hydroxyl groups [6]. The Grignard reagent *t*-BuMgCl acts as a strong base, activating the 5'-hydroxyl group of the nucleoside as its corresponding Mg-alkoxide, which subsequently attacks 127 to yield the phosphoramidate prodrug [65] (Scheme 26). Although *N*-phosphorylation of pyrimidine bases under these conditions has been detected in similar systems [65], this process is sufficiently slow and reversible not to present problems of chemoselectivity in the synthesis of sofosbuvir.

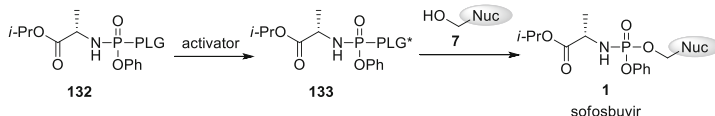
In contrast, the mechanism of NMI activation involves the formation of a phosphoryl imidazolium species 131 (Scheme 27) from the phosphoramido-chloridate reagent 129. The activated species 131 then undergoes a nucleophilic displacement by the 5'-hydroxyl group of the nucleoside 7 forming the stable P–O bond (Scheme 27). Originally pioneered by McGuigan et al. [66], the NMI approach was later optimized by Lehsten et al. and demonstrated to be applicable to multikilogram syntheses of a variety of phosphoramidates in high purity (>99%) [67]. Although the active form of this nucleophilic catalyst is theoretically



**Scheme 26** Nucleoside phosphoramidation: the *t*-BuMgCl – approach



**Scheme 27** Nucleoside phosphoramidation: the NMI approach



**Scheme 28** Nucleoside phosphoramidation: the acidic activation approach

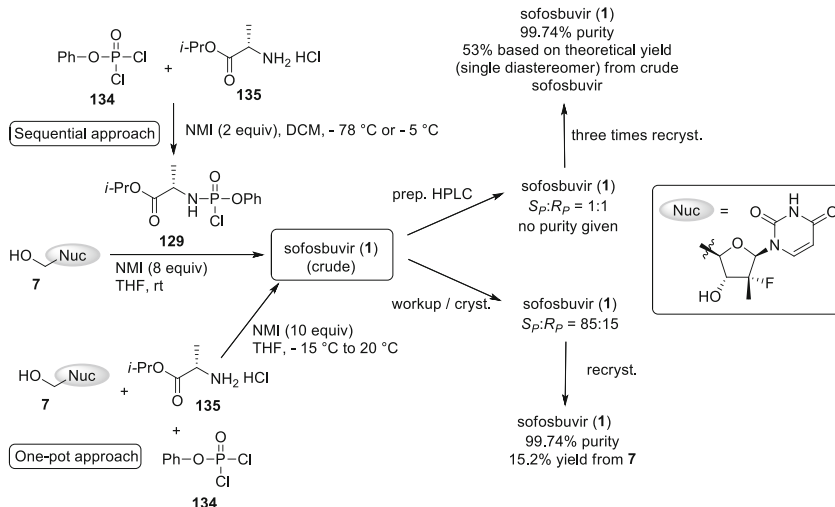
regenerated after each cycle, it is known that (super-)stoichiometric amounts of NMI are beneficial [67].

In the less explored “acidic activation” mode, Lewis or Brønsted acids are utilized to mediate the 5′-phosphorylation. The phosphoryl-transfer reagent **132** is equipped with a potential leaving group (PLG), which can be activated for nucleophilic displacement by **7** upon treatment with an acid (Scheme 28). Due to the scarcity of mechanistic studies on this type of activation in the literature,<sup>3</sup> only speculative discussions can be made about the mechanism of this transformation.

The general synthetic strategy toward various activated phosphoramidate reagents used in the synthesis of sofosbuvir is shown in Scheme 29. The approach consists of reacting phosphorodichloridate **134** with *L*-alanine isopropyl ester hydrochloride **135** under basic conditions to form the first P-N bond, followed by a non-diastereoselective introduction of a leaving group through the substitution of the second chloride. As already mentioned, the intermediate phosphorochloridate **129** can be used as a reagent without any further functionalization, in particular under NMI catalysis. However, as a moisture-sensitive oil, **129** poses difficulties in handling, purification, and diastereomer separation. For this reason, different

<sup>3</sup> Some mechanistic studies have been performed in the context of phosphate synthesis; see, for example, [68] Liu C-Y, Pawar VD, Kao J-Q, Chen C-T (2010) *Adv. Synth. Catal.* 352: 188–194, and references therein.





**Scheme 30** Phosphoramidation (NMI approach) and isolation of sofosbuvir

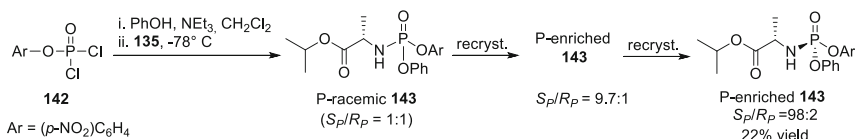
the authors also report a strategy to efficiently deplete impurities, in particular the 3'-phosphorylated derivative **137** (Scheme 31). End-stage silylation with TBDMSCl was found to be selective for the 5'-hydroxyl group of the undesired side product **137**, which can be subsequently separated by chromatography along with the doubly phosphorylated product **138** [70]. This protocol has been successfully applied on multikilogram scale, whereby the amount of the 3'-regioisomer could be depleted to <0.1% (previously 1–3%).<sup>4</sup>

The NMI protocol was also employed for the phosphoramidation of the isotopically labeled nucleoside building block **78**, used as a standard for quantitative LC-MS studies (Scheme 32) [44, 45]. The product **141** was isolated as a 1:1 mixture of P-diastereomers in 52% yield after flash chromatography (isotopic purity 99% as determined by MS).

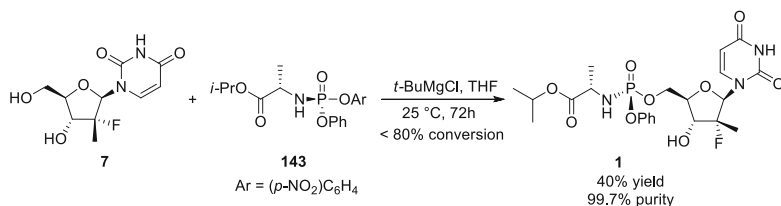
With respect to efficiency, scalability, and cost, the isolation-by-crystallization approach pursued during the discovery of sofosbuvir exhibits clear limitations. In an effort to develop a diastereoselective approach (ideally omitting multiple crystallization steps), chemists at Pharmasset devised a protocol utilizing crystalline *p*-nitrophenolate-substituted phosphoramidate **143** as a coupling partner [70, 71]. The activated phosphoramidate reagent was prepared according to Scheme 33: commercially available *p*-nitrophenyl phosphorodichloridate **142** was treated with phenol in the presence of triethylamine, followed by the addition of L-alanine

<sup>4</sup> Other methods for the separation of impurities disclosed by development chemists of Pharmasset include: a) oiling out from crude sofosbuvir (11.6% overall chemical yield, single diastereomer ( $S_P$ ), purity >99%) and b) silica loading of crude sofosbuvir followed by successive washes with increasingly polar eluents and two final recrystallizations (~12 % overall chemical yield, single diastereomer ( $S_P$ ), purity > 99%).

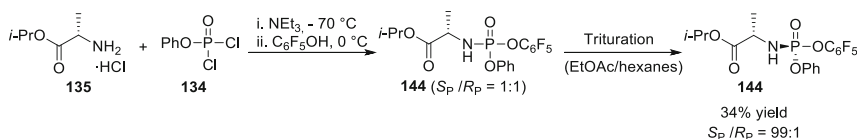




**Scheme 33** Synthesis of *p*-nitrophenolate-substituted phosphoramidate **143**



**Scheme 34** Diastereoselective synthesis of sofosbuvir with *p*-nitrophenolate reagents

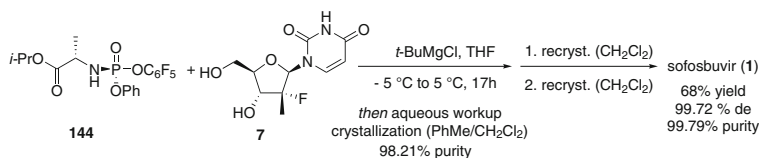


**Scheme 35** Synthesis of the pentafluorophenol-substituted phosphoramidate reagent **144**

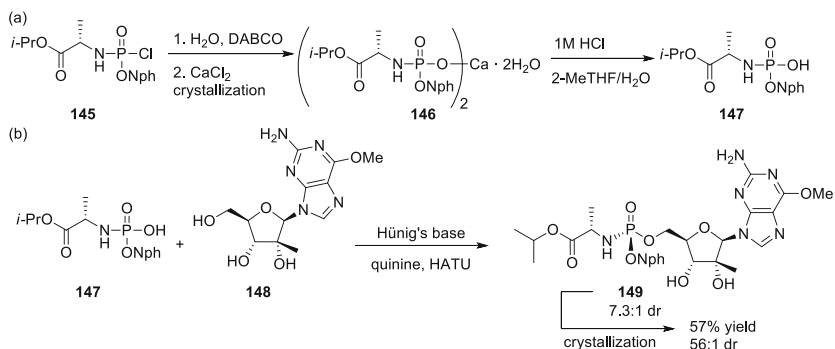
phosphorodichloridate as a starting material. Enrichment of the desired  $S_P$  diastereomer was accomplished via crystallization or chromatography [70]. Alternatively, a different order of addition was also found to be possible: L-alanine isopropyl ester hydrochloride **135** was reacted with phenyl phosphoramidate **134** in the presence of triethylamine at  $-70^\circ\text{C}$  (Scheme 35); subsequent treatment with pentafluorophenol gave rise to crude **144** as a 1:1 mixture of  $S_P/R_P$  diastereomers. A final trituration with EtOAc/hexanes yielded 34% of the desired  $S_P$  diastereomer with a 99:1 diastereomeric ratio [71].

Following a thorough optimization of reaction conditions including the reaction temperature and the order of addition, coupling of 2'-deoxy-2'-fluoro-*C*-methyluridine **7** and **144** led to the formation of sofosbuvir in 68% overall yield. After two successive recrystallization steps, the API was ultimately obtained in 99.79% purity and 99.72% diastereomeric excess (Scheme 36) [71].

In a patent application, researchers at Gilead Sciences also took advantage of the *p*-nitrophenolate-substituted phosphoramidate **143**, albeit under slightly different conditions compared those used at Pharmasset [74]. Their method comprised of reacting 2'-deoxy-2'-fluoro-*C*-methyluridine **7** and *t*-BuMgCl with **143** in a mixture of THF and anhydrous NMP (3:1 v/v). Instead of keeping the mixture at low temperatures, the reaction was performed at  $55^\circ\text{C}$  which led to an almost complete consumption of the starting materials. Ultimately, sofosbuvir (**1**) was isolated in



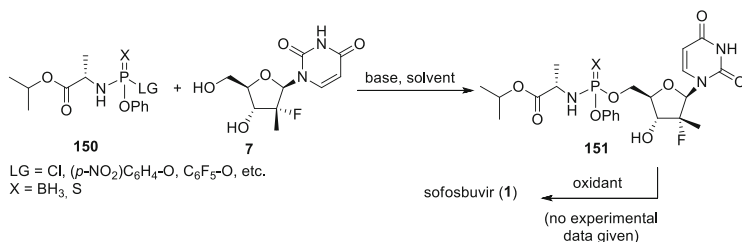
**Scheme 36** Diastereoselective synthesis of sofosbuvir with pentafluorophosphoramidate reagent **144**



**Scheme 37** A dynamic kinetic resolution approach to diastereoselective phosphoramidation

65% yield as a single diastereomer after successive preparative RP-HPLC and column chromatographic purification.

A somewhat different strategy which could be still classified as “basic activation” was devised by scientists at Bristol-Myers Squibb for the synthesis of a related phosphoramidate prodrug **149** (Scheme 37). The authors employed phosphoramidic acid **147** in the presence of a chiral base (quinine), a peptide coupling reagent, and a bulky Brønsted base for nucleoside phosphoramidation [75, 76]. The reagent **147**, an unstable oil, was prepared from the phosphorochloridate **145** by hydrolysis and formation of a DABCO phosphate salt, followed by a counterion switch to furnish a stable calcium salt hydrate **146**. The calcium salt could be conveniently purified by recrystallization and re-protonated to give organic-soluble **147**. In the example shown, **147** was coupled with nucleoside **148** in the presence of Hünig's base, HATU, and quinine. Mechanistic studies by the authors [76] revealed that the reaction of **147** with HATU in the presence of an amine base proceeded rapidly and non-diastereoselectively, giving a 1:1 mixture of P-chiral activated esters. Subsequent addition of quinine and the nucleoside **148** led to the formation of **149** diastereoselectively, whereby the 1:1 ratio of both P-chiral activated esters remained constant throughout the reaction. This observation suggested a dynamic kinetic resolution of the HATU-activated phosphoramidate esters promoted by quinine to give the  $S_P$ -enriched diastereomer of the coupled product. Although the exact details of quinine's involvement are not clear, structure–activity studies by the authors suggest that its association with the nucleoside or the phosphoramidate active ester through non-covalent interactions is likely. Under



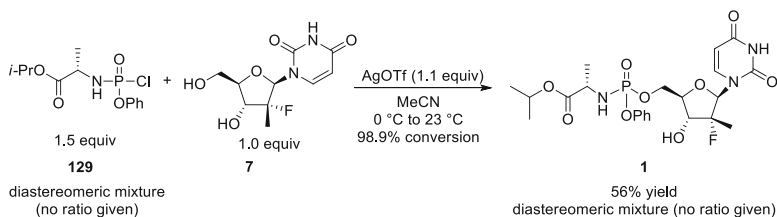
**Scheme 38** Synthesis of sofosbuvir with thiophosphoramidates or phosphoramidite–borane complexes as phosphoramidate surrogates

optimized conditions, a 7.1:1 dr at phosphorus was achieved for product **149** which could be further enriched to 56:1 dr by crystallization. Although the synthesis of sofosbuvir was not provided as an example, the procedure is claimed to be applicable in the patent disclosure.

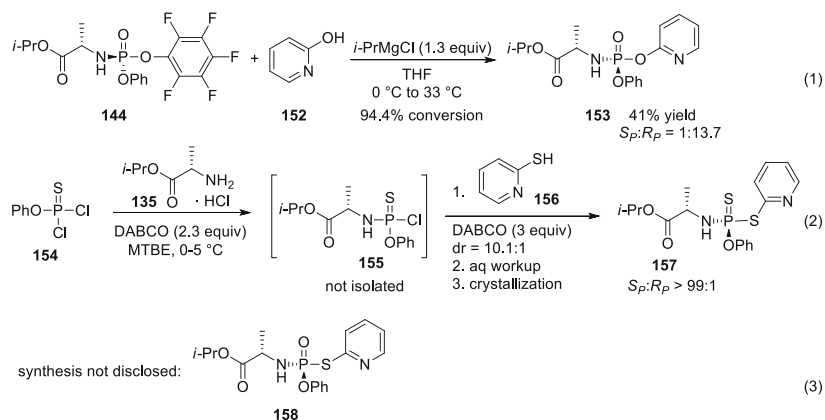
Recently, researchers at Bristol-Myers Squibb also disclosed an alternative strategy to synthesize sofosbuvir in a patent application [77]. Taking advantage of a basic activation mode, they exploited thiophosphoramidates or phosphoramidite–borane complexes **150** as surrogates for the phosphoramidate moiety (Scheme 38). Their approach comprises of reacting 2'-deoxy-2'-fluoro-*C*-methyluridine **7** with the coupling partner **150** in the presence of a base such as triethylamine or DBU, giving rise to “masked” pro-Tide compounds **151**. Conversion to the pharmacologically active phosphoramidate (such as sofosbuvir) is then accomplished by treatment with an oxidant (e.g., *m*-CPBA). No efforts were made to separate the phosphorus stereoisomers ( $S_P/R_P$ ). It has to be noted that although synthesis of sofosbuvir is claimed, the inventors do not give corresponding experimental information in the example section.

As mentioned earlier, the “acidic activation” mode has been applied much less frequently to the synthesis of sofosbuvir: at present, there is only one published patent application exploiting this chemistry. Considering the established coupling of the nucleoside 5'-hydroxyl group with the phosphoryl-transfer reagents used in the “basic activation” mode, scientists at Vertex Pharmaceuticals investigated whether the same building blocks could be coupled under the influence of a (Lewis) acid [69]. Indeed, they were able to isolate sofosbuvir in 56% yield as a diastereomeric mixture (no ratio given) upon reacting 2'-deoxy-2'-fluoro-*C*-methyluridine **7** with phosphorochloridate **129** in combination with a stoichiometric amount of silver (I) triflate (Scheme 39). The reaction was found to proceed to 98.9% conversion when stirred in acetonitrile for 3 h at 0°C followed by additional 2 h at 23°C. Although no mechanistic proposals are given, it can be hypothesized that one of the main drivers is the formation of solid silver (I) chloride.

In the same patent application, the inventors disclose various novel phosphoramidate reagents, bearing 2-hydroxypyridine and 2-mercaptopyridine substituents (Scheme 40).



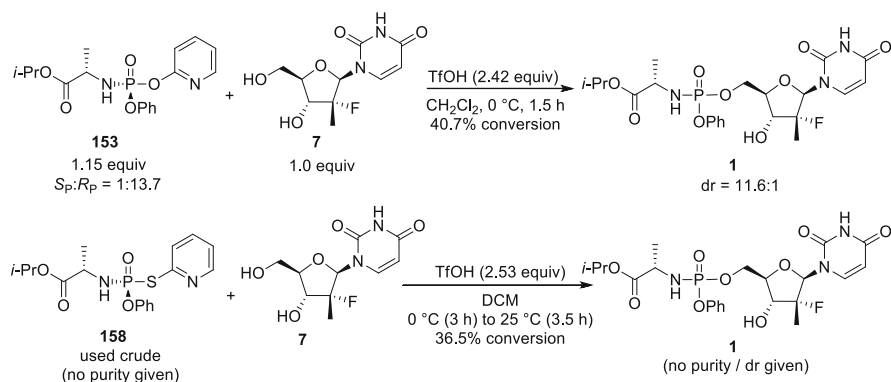
**Scheme 39** Phosphoramidation using phosphoramidochloridate **129** in combination with silver (I) triflate



**Scheme 40** Preparation of 2-hydroxypyridine and 2-mercaptopyridine phosphoramidate reagents

For the preparation of derivative **153**, 2-hydroxypyridine was deprotonated with *i*-PrMgCl, followed by addition to the pentafluoro derivative **144** (Eq. 1). By this means, the desired phosphoramidate reagent **153** could be isolated in 41% yield and a diastereomeric ratio of 1:13.7 ( $S_P/R_P$ ). The derivative **157** was prepared from phosphorodichloridothioate **154** by a stepwise P–N and P–S bond formation, followed by crystallization (Eq. 2). No experimental details were provided for the preparation of mercapto-derivative **158** (Eq. 3). The applicability of these novel phosphoryl-transfer reagents was demonstrated in the coupling of 2'-deoxy-2'-fluoro-*C*-methyluridine **7** with phosphoramidates **153**<sup>5</sup> and **158** (Scheme 41). In the presence of excess triflic acid, sofosbuvir (**1**) could be obtained with 40.7% conversion and 11.6:1 dr (absolute stereochemistry at phosphorus not explicitly provided). It should be noted that the diastereomeric ratio of the phosphoramidate reagent ( $S_P/R_P = 1:13.7$ ) does not completely translate into the product

<sup>5</sup> While the patent application (example 3B) shows a structure number which is inconsistent with compound **153** and a IUPAC name which is inconsistent with **1**, the experimental conditions (starting material dr and reaction scale) together with the scheme provided lead us to believe that **153** was employed to make **1** as drawn.



**Scheme 41** Phosphoramidation using 2-hydroxy- or 2-mercaptopyridine phosphoramidate reagents in combination with triflic acid [5]

(dr = 11.6:1) and that an  $S_N2$ -type inversion should give the undesired diastereomer of sofosbuvir. Under very similar reaction conditions, 36.5% conversion to **1** was achieved utilizing the 2-mercapto derivate **158**. However, in this case, crude phosphoryl-transfer reagent was used and no diastereomeric ratios are provided. Mechanistically, *N*-protonation of the 2-hydroxy- or 2-mercaptopyridine moiety to make it a good leaving group (i.e., producing a stable 2-pyridone/2-thiopyridone) is the likely driving force in the reaction.

Recently, Pertusati and McGuigan reported a copper-catalyzed, diastereoselective synthesis of P-chiral phosphoramidate prodrugs based on a dynamic kinetic resolution of P-racemic phosphorochloridates [78]. Although the yields are still moderate and sofosbuvir was not chosen as an example to demonstrate the scope, the catalytic methodology represents a novel and highly promising approach that could be broadly applicable.

## 4 Conclusions

The past several years have witnessed an exciting breakthrough in the treatment of hepatitis C. After over a decade of stalemate in the face of intense research efforts, the number of new HCV drugs or combinations that have been approved for clinical use is already approaching ten, with the pipeline showing no signs of dwindling. Among them is Gilead's HCV polymerase inhibitor sofosbuvir, which set a new standard for HCV therapy in 2013 as the first non-protease inhibitor DAA. Despite the surge of new therapies, sofosbuvir is unlikely to become overtaken by the newer approvals. Indeed, the remarkable efficacy, high tolerance, and drug resistance barrier of sofosbuvir, together with the many opportunities for combination regimens, predict a stable demand for this antiviral. Cost-efficient and innovative syntheses of sofosbuvir will thus continue to be an important goal for the

pharmaceutical industry. Valuable contributions can be expected from the academic community, as already attested by its early interest in sofosbuvir and similar nucleotide drugs [26, 78].

The synthetic approaches to sofosbuvir covered in this chapter demonstrate the interesting challenges inherent to the compound. Sofosbuvir's nucleoside core is distinguished by the presence of a tertiary fluorine-containing stereocenter, the introduction of which is generally difficult and inefficient when performed late in the route. This limitation has so far prohibited industrially applicable semisynthetic approaches to sofosbuvir, which rely on naturally occurring nucleosides as starting materials. Indeed, the benchmark industrial route is a 10-step total synthesis from protected glyceraldehyde, which features an early fluorination [22]. Better fluorination methodologies which could be used to functionalize readily available advanced precursors thus represent an important goal for the synthesis of sofosbuvir. Creative new solutions for stereoselective phosphoramidation are another synthetic aspect that could benefit not only the production of sofosbuvir but also other P-chiral nucleotide prodrugs. Currently, diastereomeric resolution of either the final product or the phosphorylation reagent is the most reliable method, though some progress in the use of dynamic kinetic resolution has been made [75, 76, 78].

Considering the variety of the chemistry described in this chapter, it is likely that more powerful and/or optimized processes for the synthesis of sofosbuvir will emerge in the near future. This is one of the requirements for ensuring a greater availability of this powerful pharmaceutical to the patients around the world.

## References

1. de Clercq E (2012) *Acta Pharm Sin* 2:535–548
2. Manns MP, Foster GR, Rockstroh JK, Zeuzem S, Zoulim F, Houghton M (2007) *Nat. Rev Drug Disc* 6:991–1000
3. Sophia MJ (2013) *Adv Pharmacol* 67:39–73
4. Rong L, Dahrai H, Ribiero RM, Perelson AS (2010) *Sci Transl Med* 2:30ra32
5. Hill A, Khoo S, Fortunak J, Simmons B, Ford N (2014) *Clin Infect Dis* 58:928–936
6. Pradere U, Garnier-Amblard EC, Coats SJ, Amblard F, Schinazi RF (2014) *Chem Rev* 114:9154–9218
7. Manns MP, von Hanh T (2013) *Nat Rev Drug Disc* 12:595–610
8. Lamarre D, Anderson P, Bailey M, Beaulieu P, Bolger G, Bonneau P, Bös M, Cameron D, Cartier M, Cordingley M, Faucher A, Goudreau N, Kawai S, Kukulj G, Lagacé L, LaPlante S, Narjes H, Poupart M, Rancourt J, Sentjens R, St George R, Simoneau B, Steinmann G, Thibeault D, Tsantrizos Y, Weldon S, Yong C, Llinàs-Brunet M (2003) *Nature* 426:186–189
9. Miller R, Purcell R (1990) *Proc Natl Acad Sci USA* 87:2057–2061
10. Patil VM, Gupta SP, Samanta S, Masand N (2011) *Curr Med Chem* 18:5564–5597
11. Sofia MJ (2011) *Antiv Chem Chemother* 22:23–49
12. Murakami E, Bao H, Ramesh M, McBrayer TR, Whitaker T, Micolochick Steuer HM, Schinazi RF, Stuyver LJ, Obikhod A, Otto MJ, Furman PA (2007) *Antimicrob Agents Chemother* 51:503–509

13. Ma H, Jiang W-R, Robledo N, Leveque V, Ali S, Lara-Jaime T, Masjedizadeh M, Smith DB, Cammack N, Klumpp K, Symons J (2007) *J Biol Chem* 282:29812–29820
14. Murakami E, Niu C, Bao H, Micolochick Steuer HM, T. W, Nachman T, Sofia MJ, Wang P, Otto MJ, Furman PA (2008) *Antimicrob Agents Chemother* 52:458–464
15. Mehellou Y, Balzarini J, McGuigan C (2009) *ChemMedChem* 4:1779–1791
16. Sofia MJ, Bao D, Chang W, Du J, Nagarathnam D, Rachakonda S, Reddy PG, Ross BS, Wang P, Zhang H-R, Bansal S, Espiritu C, Keilman M, Lam AM, Micolochick Steuer HM, Niu C, Otto MJ, Furman PA (2010) *J Med Chem* 53:7202–7218
17. Koff RS (2014) *Aliment Pharmacol Ther* 39:478–487
18. Wang P, Stec W, Clark J, Chun B-K, Shi J, Du J (2006) Preparation of alkyl-substituted 2-deoxy-2-fluoro-D-ribofuranosyl pyrimidines and purines and their derivatives. WO Pat Appl 2006012,440 A2
19. Cedilote M, Cleary TP, Zhang P (2008) Alternate process for preparing 3,5-di-omicron-acyl-2-fluoro-2-C-methyl-D-ribo- $\gamma$ -lactone. WO Pat Appl 2008090,046 A1
20. Chen R, Li Y, Zhao J, Zheng J, Zhu G (2014) Process for the preparation of a fluorolactone derivative. WO Pat Appl 2014108,525 A1
21. Zhang P, Iding H, Cedilote M, Brunner S, Williamson T, Cleary TP (2009) *Tetrahedron Asymmetry* 20:305–312
22. Wang P, Chun BK, Rachakonda S, Du J, Khan N, Shi J, Stec W, Cleary D, Ross B, Sofia M (2009) *J Org Chem* 74:6819–6824
23. Chun BK, Wang P (2006) Preparation of 2'-fluoro 2-alkyl-substituted or other optionally substituted ribofuranosyl pyrimidines and purines and their derivatives. WO Pat Appl 2006031,725 A2
24. Axt SD, Sarma K, Vitale J, Zhu J, Ross BS, Rachakonda S, Jin Q, Chun B-K (2008) Preparation of nucleosides ribofuranosyl pyrimidines. WO Pat Appl 2008045,419 A1
25. Gao Y, Sharpless KB (1988) *J Am Chem Soc* 110:7538–7539
26. Peifer M, Berger R, Shurtleff VW, Conrad JC, MacMillan DWC (2014) *J Am Chem Soc* 136:5900–5903
27. Clark JL, Hollecker L, Mason JC, Stuyver LJ, Tharnish PM, Lostia S, McBrayer TR, Schinazi RF, Watanabe KA, Otto MJ, Furman PA, Stec WJ, Patterson SE, Pankiewicz KW (2005) *J Med Chem* 48:5504–5508
28. Clark J (2005) Modified fluorinated nucleoside analogues. WO Pat Appl 2005003,147 A2
29. Sofia MJ, Du J, Wang P, Nagarathnam D (2008) Nucleoside phosphoramidate prodrugs. WO Pat Appl 2008121,634 A2
30. Delaney WE, Link JO, Mo H, Oldach DW, Ray AS, Watkins WJ, Yang CY, Zhong W (2013) Methods for treating HCV. US Pat Appl 0,273,005
31. Bhat V, Ugarkar BG, Sayeed VA, Grimm K, Kosora N, Domenico PA, Stocker E (1989) *Nucleos Nucleot* 8:179–183
32. Matsuda A, Takenuku K, Tanaka M, Sasaki T, Ueda T (1991) *J Med Chem* 34:812–819
33. Appell RB, Duguid RJ (2000) *Org Process Res Dev* 4:172–174
34. Matsuda A, Itoh H, Takenuki K, Sasaki T, Ueda T (1988) *Chem Pharm Bull* 36:945–953
35. Wójtowicz-Rajchel H (2012) *J Fluor Chem* 143:11–48
36. Biggadike K, Borthwick AD, Evans D, Exall AM, Kirk BE, Roberts SM, Stephenson L, Youds P (1988) *J Chem Soc Perkin Trans* 1:549–554
37. Sofiana ASM, Lee CK (2001) *J Carbohydr Chem* 20:431–440
38. Or YS, Ying L, Peng X, Wang C, Qui Y-L (2009) Nucleoside Phosphonate Derivatives. US Pat Appl 0,274,686
39. Clark JL, Mason JC, Hobbs AJ, Hollecker L, Schinazi RF (2006) *J Carbohydr Chem* 25:461–470
40. Ritzmann G, Klein RS, Hollenberg DH, Fox JJ (1975) *Carbohydr Res* 39:227–236
41. Nomura M, Sato T, Washinosu M, Tanaka M, Asao T, Shuto S, Matsuda A (2002) *Tetrahedron* 58:1279–1288
42. Wolfe MS, Harry-O'kuru RE (1995) *Tetrahedron Lett* 36:7611–7614

43. Harry-O'kuru RE, Smith JM, Wolfe MS (1997) *J Org Chem* 62:1754–1759
44. Chun B-K, Du J, Zhang H-R, Chang W, Ross BS, Jiang Y, Bao D, Espiritu CL, Keilman M, Micolochick-Steuer HM, Furman PA, Sofia MJ (2011) *Nucleos Nucleot Nucl* 30:886–896
45. Ross BS, Sofia MJ, Pamulapati GR, Rachakonda S, Zhang H-R, Chun B-K, Wang P (2010) N-[(2'R)-2'-deoxy-2'-fluoro-2'-methyl-P-phenyl-5'-uridylyl]-L-alanine 1-methylethyl ester and process for its production. WO Pat Appl 2010135,569 A1
46. Cook AF, Moffatt JG (1967) *J Am Chem Soc* 89:2697–2705
47. Hayakawa H, Tanaka H, Itoh N, Nakajima M, Miyasaka T, Yamaguchi K, Iitaka Y (1987) *Chem Pharm Bull* 35:2605–2608
48. Elgemeie GEH, Attia AME, Alkabei SS (2000) *Nucleos Nucleot Nucl* 19:723–733
49. Holý A (1973) *Tetrahedron Lett* 14:1147–1150
50. Jenkinson SF, Jones NA, Moussa A, Stewart AJ, Heinz T, Fleet GWJ (2007) *Tetrahedron Lett* 48:4441–4444
51. Hotchkiss DJ, Jenkinson SF, Storer R, Heinz T, Fleet GWJ (2006) *Tetrahedron Lett* 47:315–318
52. Mayes BA, Moussa A (2007) Process for preparing a synthetic intermediate for the preparation of branched nucleosides. WO Pat Appl 2007075,876 A2
53. Liu J, Du J, Wang P, Nagarathnam D, Espiritu CL, Bao H, Murakami E, Furman PA, Sofia MJ (2012) *Nucleos Nucleot Nucl* 31:277–285
54. Clark JL, Mason JC, Hollecker L, Stuyver LJ, Tharnish PM, McBrayer TR, Otto MJ, Furman PA, Schinazi RF, Watanabe KA (2006) *Bioorg Med Chem Lett* 16:1712–1715
55. Roberts CD, Griffith RC, Dyatkina NB, Prhvac M (2006) Nucleoside compounds for treating viral infections. US Pat Appl 0,241,064
56. Hu W, Yang Q, Wang S, Huang G, Zhang Y, Dong J, Kang J, Song C, Chang J (2013) *Nucleos Nucleot Nucl* 32:389–395
57. Wang G, Beigelman L (2013) Substituted phosphorothioate analogs. WO Pat Appl 2013096,680 A1
58. Shi J, Du J, Ma T, Pankiewicz KW, Patterson SE, Hassan AE, Tharnish PM, McBrayer TR, Lostia S, Stuyver LJ, Watanabe KA, Chu CK, Schinazi RF, Otto MJ (2005) *Nucleos Nucleot Nucl* 24:875–879
59. Liu LJ, Hong JH (2010) *Nucleos Nucleot Nucl* 29:216–227
60. Li H, Yoo JC, Baik YC, Lee W, Hong JH (2010) *Bull Korean Chem Soc* 31:2514–2518
61. L'Heureux A, Beaulieu F, Bennett C, Bill DR, Clayton S, LaFlamme F, Mirmehrabi M, Tadayon S, Tovell D, Couturier M (2010) *J Org Chem* 75:3401–3411
62. Beaulieu F, Beaugard L-P, Courchesne G, Couturier M, LaFlamme F, L'Heureux A (2009) *Org Lett* 11:5050–5053
63. Schöne O, Spitzenstätter H-P, Juen J (2014) Pat Appl, filed June 2014
64. Le Corre SS, Berchel M, Couthon-Gourves H, Haelters J-P, Jaffres P-A (2014) *Beilstein J Org Chem* 10:1166–1196
65. Uchiyama M, Aso Y, Noyori R, Hayakawa Y (1993) *J Org Chem* 58:373–379
66. McGuigan C, Pathirana RN, Mahmood N, Devine KG, Hay AJ (1992) *Antiviral Res* 17:311–321
67. Lehsten DM, Baehr DN, Lobl TJ, Vaino AR (2002) *Org Process Res Dev* 6:819–822
68. Liu C-Y, Pawar VD, Kao J-Q, Chen C-T (2010) *Adv Synth Catal* 352:188–194
69. Rose PJ, Jung YC, Blight CM, Ibrahim S, Anzalone L, Miller DB, Van Alsten J, Curran TT (2014) Methods of stereoselective synthesis of substituted nucleoside analogs. WO Pat Appl 2014164,533 A1
70. Ross BS, Sofia MJ, Pamulapati GR, Rachakonda S, Zhang H-R, Chun B-K, Wang P (2010) A process for the preparation and diastereomeric resolution of N-[(2'R)-2'-deoxy-2'-fluoro-2'-methyl-P-phenyl-5'-uridylyl]-L-alanine 1-methylethyl ester. WO Pat Appl 2010135,569 A1
71. Ross BS, Ganapati Reddy P, Zhang H-R, Rachakonda S, Sofia MJ (2011) *J Org Chem* 76:8311–8319
72. Howes PD, Slater MJ, Wareing K (2003) *Nucleos Nucleot Nucl* 22:687–689

73. Perrone P, Luoni GM, Kelleher MR, Daverio F, Angell A, Mulready S, Congiatu C, Rajyaguru S, Martin JA, Leveque V, Le Pogam S, Najera I, Klumpp K, Smith DB, McGuigan C (2007) *J Med Chem* 50:1840–1849
74. Cho A, Wolckenhauer SA (2012) Methods for the preparation of diastereomerically pure nucleoside phosphoramidate prodrugs as antiviral agents. WO Pat Appl 2012012,465 A1
75. Tran K, Eastgate MD, Janey J, Chen K, Rosso VW (2014) Process for preparing diastereomerically enriched nucleoside phosphoramidates for potential treatment of viral infections. WO Pat Appl 2014008,236 A1
76. Tran K, Beutner GL, Schmidt M, Janey J, Chen K, Rosso V, Eastgate MD (2015) *J Org Chem* 80:4994–5003
77. Schmidt M, Silverman S, Eastgate MD (2014) Process for preparing phosphoramidate derivatives of nucleoside compounds for treatment of viral infections. WO Pat Appl 2014047,117 A1
78. Pertusati F, McGuigan C (2015) *Chem Commun* 51:8070–8073

# Synthetic Challenges in the Assembly of Macrocyclic HCV NS3/NS4A Protease Inhibitors: The Case of BILN 2061 and Its Analogs

Youla S. Tsantrizos

**Abstract** The virally encoded serine protease NS3/NS4A is essential for the life cycle of the hepatitis C virus (HCV), an important human pathogen causing chronic hepatitis, cirrhosis of the liver, and hepatocellular carcinoma. The quest for the discovery of antiviral agents targeting the NS3/NS4A was initiated with a substrate-based hexapeptide as the lead structure. Evaluation of the conformational pre-organization of this ligand to the bioactive conformation led to the design of macrocyclic peptides, typified by the antiviral agents BILN 2061. Today, closely related analogs of BILN 2061 represent an important class of human therapeutics for the treatment of HCV infection. The critical steps in the synthesis of these compounds involves the cyclization of a tripeptide diene, containing a (1*R*,2*S*)-vinyl aminocyclopropylcarboxylate residue, via ring-closing metathesis (RCM). Conformational factors, ligand effects, and reaction conditions were evaluated, and a protocol was developed for the efficient production of these peptidomimetics in high yield and diastereomeric purity. The assembly of these challenging molecules and the key optimization studies are described.

**Keywords** Hepatitis C virus · Macrocyclic peptides · NS3/NS4A protease inhibitors

## Contents

1	Introduction .....	91
2	Structure-Based Design of Peptidomimetic Inhibitors of the NS3/NS4A Serine Protease .....	92

---

Y.S. Tsantrizos (✉)

Department of Chemistry, McGill University, 801 Sherbrooke Street West, Montreal, QC, Canada, H3A 0B8

e-mail: [youla.tsantrizos@mcgill.ca](mailto:youla.tsantrizos@mcgill.ca)

3	Efficient Large-Scale Synthesis of Macrocyclic Inhibitors of HCV NS3/NS4A	
	Protease .....	95
3.1	Synthesis of the P1 Fragment (Vinyl ACCA) .....	96
3.2	Synthesis of the P2 Fragment .....	98
3.3	Synthesis of the P3 Fragment, ( <i>S</i> )-2-Aminonon-8-enoic Acid .....	100
3.4	Challenges and Optimizations of the Ring-Closing Metathesis Reaction .....	101
4	Conclusion .....	107
	References .....	108

## Abbreviations

Ac	Acetyl
ACCA	1-Aminocyclopropanecarboxylic acid
API	Active pharmaceutical ingredient
aq	Aqueous
BI	Boehringer Ingelheim
Bn	Benzyl
Boc	<i>tert</i> -Butoxycarbonyl
cod	Cyclooctadiene
Cy	Cyclohexyl
DEAD	Diethyl azodicarboxylate
DIAD	Diisopropyl azodicarboxylate
DIPEA	<i>N,N</i> -Diisopropylethylamine
DMF	Dimethylformamide
( <i>S,S</i> )-Et-	1,2-Bis[(2 <i>S</i> ,5 <i>S</i> )-2,5-diethylphospholano]benzene
DUPHOS	
EC <sub>50</sub>	Half maximal effective concentration
equiv	Equivalent(s)
Et	Ethyl
FDA	Food and Drug Administration
h	Hour(s)
HCV	Hepatitis C virus
HPLC	High-performance liquid chromatography
HTS	High-throughput screening
<i>i</i> -Bu	Isobutyl
IC <sub>50</sub>	Half maximal inhibitory concentration
IFN- $\alpha$	Pegylated interferon alpha
KHMDS	Potassium hexamethyldisilazide, potassium bis(trimethylsilyl)amide
LC-MS	Liquid chromatography-mass spectrometry
LiHMDS	Lithium hexamethyldisilazide, lithium bis(trimethylsilyl)amide
Me	Methyl
mol	Mole(s)
MTBE	Methyl <i>tert</i> -butyl ether
<i>n</i> -Bu	Butyl

NMR	Nuclear magnetic resonance
NS3	Nonstructural protein 3
Ph	Phenyl
PNBA	<i>p</i> -Nitrobenzoic
ppm	Parts per million
RCM	Ring-closing metathesis
RNA	Ribonucleic acid
ROESY	Rotating-frame Overhauser effect spectroscopy
rt	Room temperature
SAR	Structure–activity relationships
S <sub>N</sub> 2	Substitution nucleophilic (bimolecular)
TBTU	<i>N,N,N',N'</i> -Tetramethyl- <i>O</i> -(benzotriazol-1-yl)uronium tetrafluoroborate
<i>t</i> -Bu	<i>tert</i> -Butyl
Tf	Trifluoromethanesulfonyl (triflyl)
THF	Tetrahydrofuran
TON	Turnover number
Vinyl ACCA	1-Amino-2-vinylcyclopropanecarboxylic acid

## 1 Introduction

In 1989, Chiron sequenced the genome of the hepatitis C virus (HCV) and identified HCV as the agent causing non-A, non-B hepatitis in humans [1]. Although HCV infections can remain asymptomatic for many years (~20 years), the majority of infected individuals (>80%) become chronically infected and usually progress to end-stage liver diseases that may eventually lead to hepatocellular carcinomas (~2–4%). Due to the significant HCV-related health burden worldwide (an estimated 170 million people chronically infected), numerous pharmaceutical industries invested heavily in the discovery of antiviral agent for treating this infection. Initially, progress was very slow, as understanding of the HCV biology proved to be an extremely challenging endeavor [2].

The first options for treating HCV were limited to pegylated interferons (IFN- $\alpha$ ) [3] in combination with the broad-spectrum/nonselective antiviral nucleoside ribavirin [4]. However, this treatment was associated with severe side effects, and sustained reduction in viral load was achieved in only half of patients infected with HCV genotype 1a/b, the most prevalent genotype (~70%) in industrialized nations. Therefore, there was an urgent need for more effective and specific anti-HCV drugs targeting specific virally encoded enzymes that are essential for viral replication.

The HCV genome (a positive single-stranded RNA of ~9,600 nucleotides) encodes a precursor polypeptide of approximately 3,000 amino acids. This polyprotein is processed both co- and posttranslationally to produce structural (C, E1, E2, p7) and nonstructural (NS2, NS3, NS4A, NS4B, NS5A, NS5B) proteins [2]. Key nonstructural proteins include the NS3 protease enzyme (the N-terminal

**Table 1** Compounds currently approved for the treatment of HCV infections

Compound	Approved	Lead companies	Target
Telaprevir <sup>a</sup>	2011	Vertex/J&J	NS3/NS4A
Boceprevir <sup>a</sup>	2011	Schering-Plough/Merck	
Simeprevir	2013	Medivir/J&J	
Paritaprevir	2014	Abbott(AbbVie)/Enanta	
Sofosbuvir	2013	Gilead	NS5B
Dasabuvir	2014	Abbott	NS5A
Daclatasvir	2014	Bristol-Myers Squibb	
Ledipasvir	2014	Gilead	
Ombitasvir	2014	AbbVie	

<sup>a</sup>These activated carbonyl derivatives act as reversible covalent inhibitors of the NS3/NS4A; they exhibit significantly lower potency and oral bioavailability compared to the macrocyclic inhibitors simeprevir and paritaprevir, and their use has been discontinued [7]

domain of the NS3 protein) and the RNA-dependent RNA polymerase enzyme (NS5B); in vitro and ex vivo studies have validated both as therapeutic targets. For example, abrogating the catalytic function of the NS3 protease results in HCV clones that have lost their infectivity. Between 1995 and 2014, an estimated 712 unique drug discovery programs were initiated worldwide. To date, only nine selective inhibitors targeting a virally encoded HCV protein have been approved in the major markets (Table 1) [5]. Most of these compounds target the NS3/NS4A serine protease (4A is a short peptide that serves as a cofactor of the NS3 protease) and the NS5B RNA-dependent RNA polymerase. Interestingly, although the NS5A protein lacks enzymatic activity and its role in viral replication remains unclear, compounds that bind to this protein can also efficiently block HCV replication [6].

This chapter focuses on the design and synthesis of the macrocyclic inhibitors of the HCV NS3/NS4A serine protease, typified by the first clinically validated analog BILN 2061 (7). This class of compounds provided clinical validation for HCV-specific small-molecule antiviral agent targeting the NS3/NS4A protease. Numerous structurally related analogs have been under investigation by pharmaceutical industries worldwide. Recently, simeprevir (13) and paritaprevir (14) received FDA approval for the treatment of HCV infections (Table 1).

## 2 Structure-Based Design of Peptidomimetic Inhibitors of the NS3/NS4A Serine Protease

The HCV NS3 serine protease is responsible for the proteolytic processing of four out of five junctions along the nonstructural region of the HCV polyprotein and plays an essential role in viral replication. It is a heterodimeric enzyme that requires a non-covalent association with the NS4A cofactor peptide for its optimal catalytic function. Furthermore, this enzyme silences the host's antiviral immune response,

blocking the host's natural defense against infections [8]. Therefore, it is not surprising that the NS3/NS4A has been a primary target for drug discovery for over 20 years.

In spite of major investments by many pharmaceutical industries [9], high-throughput screening (HTS) failed to identify small molecules capable of inhibiting the NS3/NS4A protease; this is likely due to the enzyme's very shallow and solvent-exposed active site cavity. Contrary to conventional wisdom advocating against peptidomimetics (on the basis of their well-known poor oral bioavailability and rapid excretion), in the early 1990s, Boehringer Ingelheim (BI) [10] and the Istituto di Ricerche di Biologia Molecolare [11] independently began to explore hexapeptide inhibitors of the NS3/NS4A. Compounds such as peptide **1**, mimicking the N-terminal cleavage products derived from the HCV polyprotein substrate, became the lead structures for medicinal chemists (Fig. 1) [reference from P1 (cleavage site) to P6 for the amino acid residues is based on the terminology used to indicate protease specificity] [12]. Additionally, hexapeptides **1** and **2** were used as molecular tools to explore the interactions between these ligands and the NS3 protease domain by NMR and molecular modeling [13–15]. Although the inherent conformational flexibility of linear hexapeptides magnified the challenges of drug discovery, potent tetrapeptide inhibitors of the NS3/NS4A (**3** and **4**) were eventually identified [16, 17]. However, in spite of their significant intrinsic potency (e.g.,

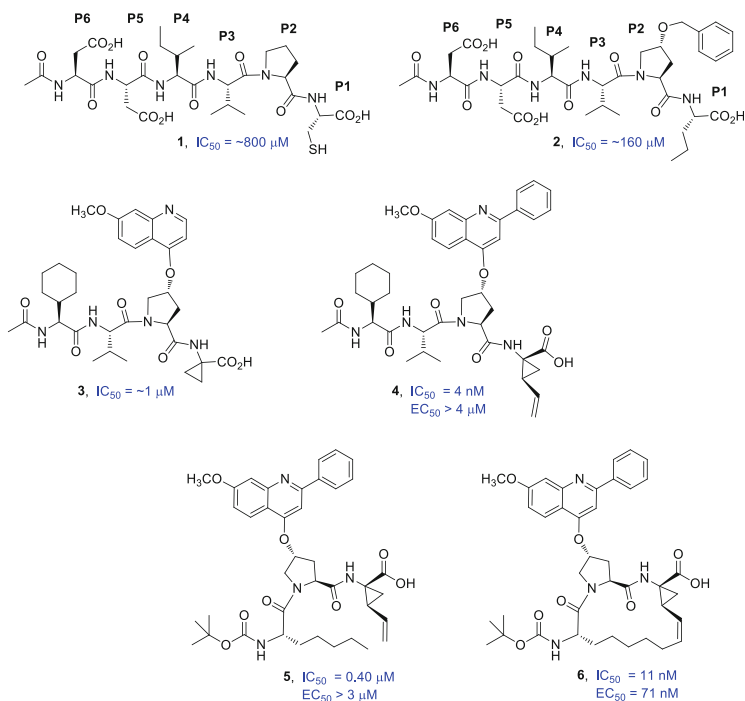


**Fig. 1** Progression of the early structure–activity relationship studies

compound **4** has an  $IC_{50}$  of 4 nM), these acyclic analogs did not exhibit any appreciable antiviral potency in the human hepatoma (Huh-7) sub-genomic HCV RNA replicon assay (the only validated tool for assessing antiviral efficacy at that time) [18].

In-depth investigation of the essential structural elements for favorable ligand–protein interactions led to the design of highly potent macrocyclic inhibitors of the NS3/NS4A [19]. For example, design of analog **6** (Fig. 1) was guided by the NMR data of the enzyme-bound hexapeptide **2**, indicating that the P3 side chain of **2** binds on the solvent-exposed surface of the protein and in close proximity to the P1 side chain, whereas the P5 and P6 residues did not interact with the protein [13]. The 15-membered ring tripeptide scaffold was designed to adopt in the *free state* the enzyme-bound secondary structure of hexapeptide **2**, forcing the P2–P3 amide bond to adopt exclusively the *trans* geometry preferred for binding [19]; this is in contrast to the linear proline-containing peptides that exist as mixtures of *cis*- and *trans*-rotamers. Furthermore, it was anticipated that the reduction in the conformational entropic penalty paid upon binding of the macrocyclic peptide to the enzyme could contribute in an overall favorable binding energy. Lastly, inspired by nature’s macrocyclic peptides (e.g., cyclosporine, vancomycin), the 15-membered ring inhibitors of HCV NS3/NS4A protease were expected to exhibit better biopharmaceutical properties than their corresponding linear analogs. Gratifyingly, we found that analog **6**, having the P1 vinyl moiety tethered to the P3 side chain via a hydrocarbon linker, exhibited low nanomolar potency in inhibiting the enzyme ( $IC_{50} = 11$  nM), as well as blocking replication of HCV sub-genomic RNA in the cell-based replicon assay ( $EC_{50} = 71$  nM) [19]. In contrast, its corresponding acyclic analog **5** was almost 40-fold less potent in the enzymatic assay and completely inactive in the cell-based replicon assay at the highest concentration that it could be tested (Fig. 1) [19, 20].

Further optimization of the prototype molecule **6** led to the first clinical candidate, BILN 2061 (**7**), targeting the HCV NS3/NS4A protease (Fig. 2) [21, 22]. Following the disclosure of these compounds by BI and the favorable Phase I clinical data of **7**, demonstrating its exceptional efficacy in reducing the viral load of HCV-infected patients, the macrocyclic scaffold was enthusiastically adopted in this field of HCV drug discovery (e.g., more than 60 patents on macrocyclic HCV NS3/NS4A inhibitors have been filed by many pharmaceutical companies). In the following years, numerous structurally related preclinical and clinical candidates were reported by pharmaceutical companies worldwide, including analogs **8–14** (Fig. 2). Two compounds, simeprevir (**13**) and paritaprevir (**14**), were recently approved as therapeutic agent in the treatment of hepatitis C infections in humans (Fig. 2).

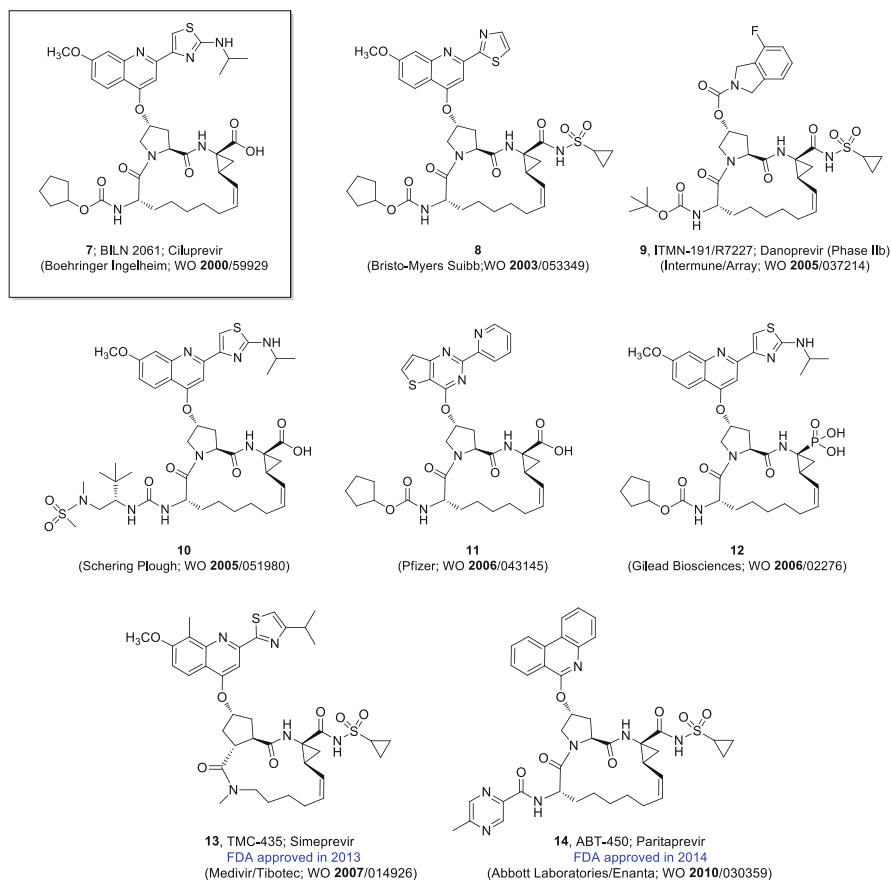


**Fig. 2** Macrocyclic inhibitors of the HCV NS3/NS4A protease; examples of exploratory, pre-clinical, clinically validated, and approved drugs

### 3 Efficient Large-Scale Synthesis of Macrocyclic Inhibitors of HCV NS3/NS4A Protease

Initially, the production of multi-kilogram quantities of a complex macrocyclic compound, such as BILN 2061 (7), presented enormous synthetic challenges, and failure to address these challenges would certainly prevent commercialization of this important class of human therapeutics. Retrosynthetic analysis of BILN 2061 (7) suggested that the macrocyclic backbone could be formed via ring-closing metathesis of an acyclic tripeptide diene (Fig. 3). Developing cost-efficient protocols for the preparation of each key building block (i.e., P1, P2, and P3), as well as assembling the macrocyclic tripeptide, was critical. After numerous modifications/optimizations of the synthetic methodologies implicated in Fig. 3, BILN 2061 (7) was synthesized in high efficiency and in multi-kilogram quantities.

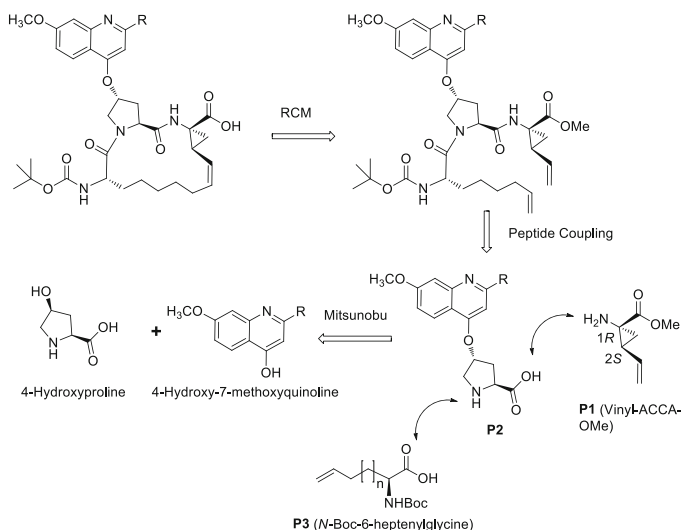


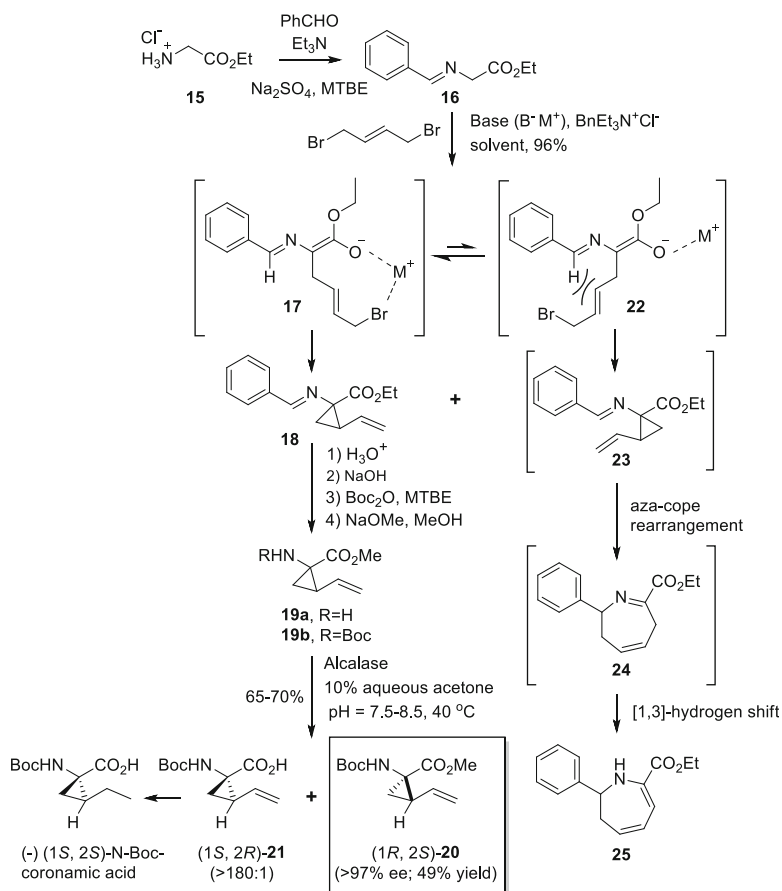
**Fig. 3** Retrosynthesis of macrocyclic inhibitors of the HCV NS3/NS4A protease

### 3.1 Synthesis of the P1 Fragment (Vinyl ACCA)

Following the initial discovery of 1-aminocyclopropanecarboxylic acid (ACCA) as a desirable substitute of the cysteine residue found in the substrate-based ligands (Fig. 1; P1; C-terminus residue of **1**) [16, 17], a number of substituted ACCA analogs were explored, leading to the identification of (1*R*,2*S*)-1-amino-2-vinylcyclopropanecarboxylic acid (Fig. 3; vinyl-ACCA methyl ester; P1) as the optimum P1 moiety [17]. Vinyl ACCA confers exceptional potency to both the linear and the macrocyclic inhibitor of this class and has become a common structural feature of most (*if not all*) second-generation HCV NS3/NS4A inhibitors (e.g., Table 1; Fig 2).

At the start of our investigations, the synthesis of vinyl ACCA had been reported in the literature [23]. Literature precedence for the asymmetric and phase transfer-catalyzed  $\alpha,\alpha$ -dialkylation of glycine imines was also known [24–26]. However, the published protocols usually required the use of expensive chiral complexes in order to achieve good levels of enantioselectivity and were not considered suitable for large-scale production of this unusual amino acid. Consequently, the BI team began to explore the development of a new methodology that was more suitable for large-scale production of vinyl ACCA, and after significant effort, the highly efficient preparation summarized in Scheme 1 was reported [27].

The sequential  $S_N2-S_N2'$  dialkylation of glycine with (*E*)-1,4-dibromobut-2-ene was pursued, and given the  $pK_a$  of  $\sim 19$  for imine **16** ( $H_\alpha$ ), formation of the  $C_\alpha$  anion was achieved under a variety of basic conditions [28]. The imine **16** was prepared in kilogram scales via condensation of benzaldehyde with the hydrochloride salt of ethyl glycinate (**15**) in the presence of a desiccant (Scheme 1). Following a simple



**Scheme 1** Pilot plant synthesis of (1R, 2S)-1-amino-2-vinylcyclopropylcarboxylic acid methyl ester [**20**; (1R, 2S)-vinyl-ACCA-OMe]

aqueous workup, Schiff base **16** was isolated in 96% yield and was then treated directly with *trans*-1,4-dibromo-2-butene, in the presence of base and catalytic amounts of the phase transfer catalyst. The formation of the racemic mixtures of the two diastereomeric products **18** and **23** was anticipated. Surprisingly, after an acid/base workup of the crude reaction mixture, the racemic vinyl-ACCA ethyl ester **19a** (R=H) was isolated as a single diastereomer in 45% yield. The  $^1\text{H}$  NMR data clearly indicated that the vinyl moiety was *cis* to the ester group (Scheme 1). Since this outcome was initially unexpected, the crude reaction mixture immediately after the cyclization step and before the acid/base workup (i.e., before cleaving the Schiff base) was analyzed by  $^1\text{H}$  NMR. This study revealed the presence of two products, compound **18** and a second minor component, presumed to be intermediate **23** (Scheme 1). Further analysis of the organic layer collected post-cyclization and during the acidic aqueous workup led to the isolation of the

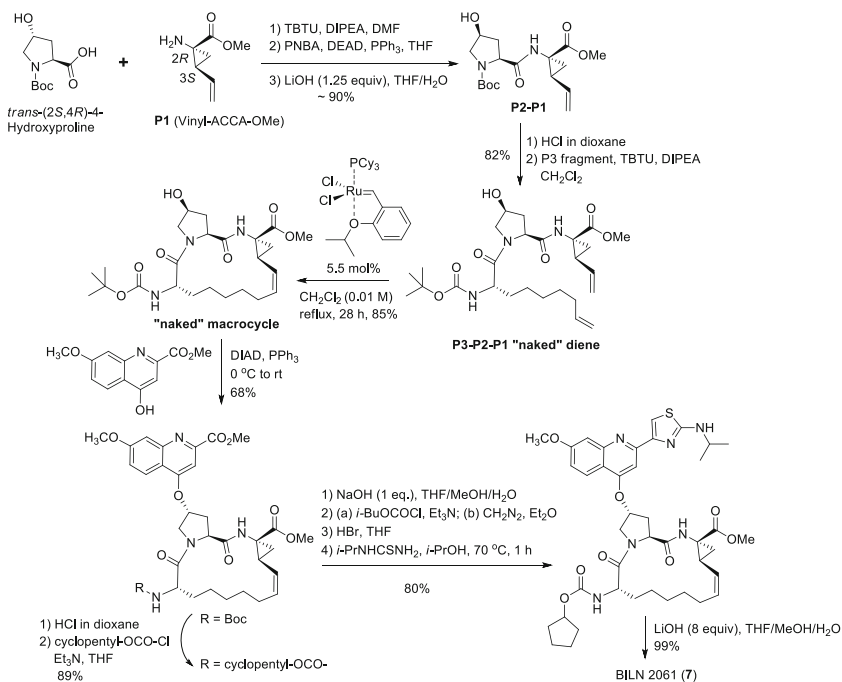
seven-membered ring side product **25**. Formation of compound **25** was rationalized to occur via the initial formation of the expected intermediate **23**, having the vinyl moiety *cis* to the imine. However, due to the geometry and functionality of this compound, a favorable and spontaneous aza-Cope rearrangement could occur to convert **23** to **24**, which upon [1,3]-hydride shift gave the final compound **25** (Scheme 1) [27].

In the initial reaction conditions for the sequential  $S_N2-S_N2'$  dialkylation of **16**, excess powdered KOH and catalytic amounts of  $BnEt_3N^+Cl^-$  (3%) as the phase transfer catalyst was used. The desired product **18** was formed, but with low diastereoselectivity (only a 3:1 ratio of the vinyl moiety *cis* to the ester versus *cis* to the imine was observed). Modifications of the imine **16**, which were previously reported to provide advantages in such reactions (e.g., replacing the benzaldehyde moiety with benzophenone) [29], were attempted without success and with a significant increase in the cost of raw materials. Similarly, replacement of the *trans*-1,4-dibromo-2-butene with other electrophiles did not provide any advantages. However, a systematic investigation of solvents, bases, and especially metal counterions that could stabilize the transition state enolate **17** proved to be extremely valuable. The reaction of **16** with *trans*-1,4-dibromo-2-butene in the presence of LiHMDS or *t*-BuOLi in a nonpolar solvent, such as toluene, led to the formation of the desired intermediate **18** in >40-fold higher yield as compared to **25** after 1 h. In contrast, more loosely coordinating metal ions (e.g., sodium or potassium), and/or the use of polar solvents (e.g., THF), led to the erosion of selectivity (**18:25** ratio of  $\sim 5 \pm 2:1$ ). These observations suggested that the strongly coordinated *s-trans* transition state enolate **17** is favored in nonpolar solvents (and in the presence of the strongly coordinating lithium ion) leading to the desired product **18**, whereas the disfavored and sterically hindered enolate **22** (favored more in polar solvents) leads to the formation of the side product **25** (Scheme 1) [27].

Finally, the enzymatic resolution of the Boc-protected racemic product **19b**, using the inexpensive and commercially available *subtilisin Carlsberg* (Alcalase), provided the key building block (1*R*, 2*S*)-vinyl-ACCA methyl ester **20** in greater than 97% enantiomeric purity, along with the hydrolyzed enantiomer **21**. Assignment of the absolute stereochemistry of **21** was confirmed after hydrogenation to the ethyl analog, which proved to be identical to authentic (+)-(1*S*,2*S*)-*N*-Boc coronamic acid (Scheme 1) [27, 30].

### 3.2 Synthesis of the P2 Fragment

The synthesis of the P2 building block was initiated from 4-hydroxy-7-methoxyquinolines, substituted at C-2 with various aromatic or heteroaromatic moieties, and 4-hydroxyproline (Fig. 3) [20]. It is noteworthy that although the C-2 substituent of the quinoline has minimal impact on the intrinsic potency of the macrocyclic inhibitors (IC<sub>50</sub>), this moiety modulates significantly the cell-based antiviral



**Scheme 2** Initial assembly of BILN 2061 (7)

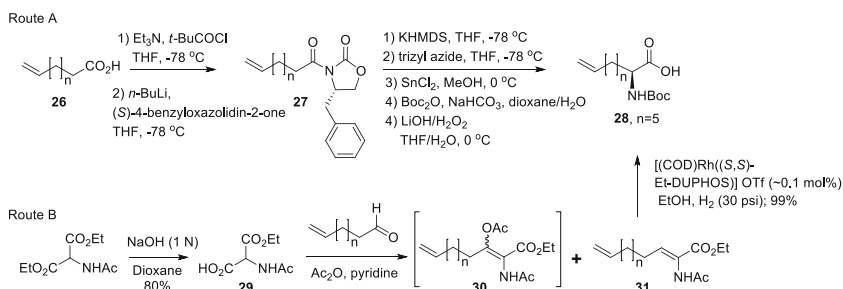
potency [31]. Therefore, a variety of quinolone moieties were coupled to the *cis*-4-hydroxyproline via the Mitsunobu reaction, proceeding with the expected inversion of stereochemistry at the C-4 of proline, to give the P2 fragment (Fig. 3) [16, 32, 33]. Alternatively, methyl 4-hydroxy-7-methoxyquinoline-2-carboxylate was coupled to the *cis*-4-hydroxyproline (via the Mitsunobu reaction), and the 2-carboxylate moiety was later modified to various heterocyclic analogs as part of our SAR studies, using various literature protocols.

However, the high cost of *cis*-4-hydroxyproline and its propensity to lactonize during the required peptide coupling reaction was a concern for the large-scale production of the P2 fragment. An alternative approach involved a double inversion of the stereochemistry at C-4 on the preformed macrocyclic scaffold (Scheme 2). Commercially available *trans*-(2*S*,4*R*)-Boc-hydroxyproline was first coupled with the methyl ester of the P1 fragment, (1*R*,2*S*)-vinyl-ACCA-OMe, using standard peptide coupling conditions. The resulting P1–P2 dipeptide was subsequently epimerized by first reacting the free C-4 hydroxyl of the proline with either *p*-nitrobenzoic acid or *p*-bromobenzenesulfonic acid via the Mitsunobu reaction, followed by regioselective hydrolysis of this moiety to afford the desired Boc-*cis*-(2*S*,4*S*)-4-hydroxyproline-(1*R*,2*S*)-vinyl-ACCA methyl ester [34]. The Boc group of the P1–P2 dipeptide was subsequently removed and coupled to the P3 amino acid to give the “naked” acyclic tripeptide diene (Scheme 2; P1–P2–P3 diene).

### 3.3 Synthesis of the P3 Fragment, (S)-2-Aminonon-8-enoic Acid

As part of our initial SAR studies, P3 fragments of various lengths and substitutions on the olefinic side chain were explored [20, 35]. A typical example of the synthetic methodology used for the P3 amino acid (2*S*)-*N*-Boc-6-heptenylglycine is shown in Scheme 3, Route A. The synthesis of the C-9 *N*-Boc-protected P3 (**28**;  $n = 5$ ) was initiated from the 8-nonenoic acid (**26**), previously obtained after a Grignard reaction of the commercially available 8-bromo-1-octene with CO<sub>2</sub> [20, 35]. After coupling **26** with the chiral auxiliary (*S*)-4-benzyloxazolidin-2-one, the enolate was formed in the presence of KHMDS and reacted with 2,4,6-triisopropylbenzenesulfonyl azide (trisyl azide) to achieve the asymmetric azidation at the C $\alpha$  position, as previously reported by Evans [36]. Reduction of the azide intermediate with SnCl<sub>2</sub> in methanol gave the corresponding free amine, which was protected as the *t*-butyl carbamates (Boc). Finally, the appropriately protected P3 fragment **28** was obtained in good yields after cleavage of the chiral auxiliary with LiOOH (Scheme 3, Route A). Although this synthetic approach (to the preparation of P3) was reasonable for our medicinal chemistry efforts, a methodology that was more atom economical and suitable for large-scale production of this fragment had to be developed in order to support the clinical development of BILN 2061 (**7**).

A sequence involving an enantioselective hydrogenation of the enamine **31** was pursued, as summarized in Scheme 3, Route B [33, 34]. Diethyl 2-acetamidomalonate was monohydrolyzed to intermediate **29**, and the latter was coupled to 6-heptenal under Perkin conditions to give selectively the *Z*-ethyl 2-acetamido-2,8-nonadienoate **31** (50% yield) along with a small amount of the side product **30**. At the same time, preparation of **31** via Horner–Wadsworth–Emmons olefination was also considered, but the so-called Perkin route was favored due to its simplicity. Intermediate **31** was subsequently enantioselectively hydrogenated using [(COD)Rh((*S,S*)-Et-DUPHOS)]OTf (catalyst load of ~0.1 mol %) to afford the ethyl (*S*)-2-acetamido-8-nonenoate in 99% enantiomeric excess and nearly quantitative yield [34]. The *N*-acetyl protecting group was replaced with

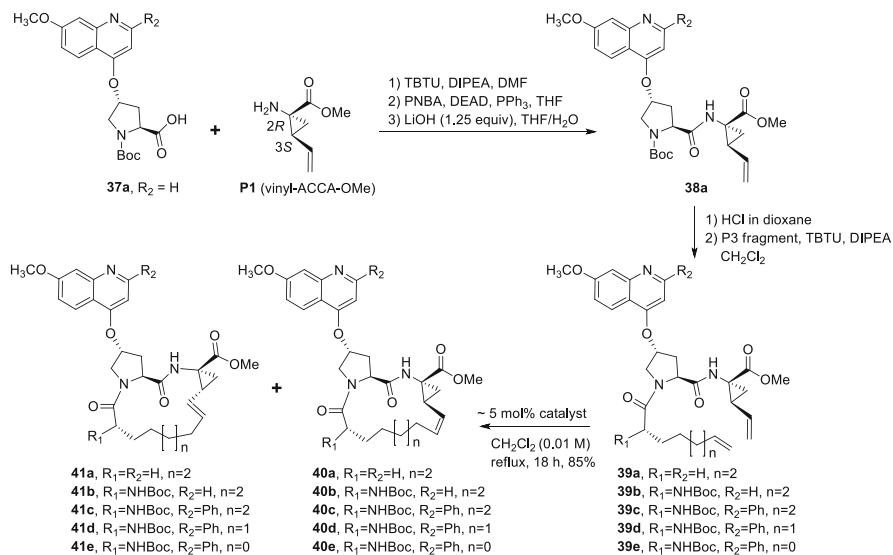


**Scheme 3** Synthesis of P3 fragment

the *t*-butyl carbamate, and the ethyl ester was saponified using standard conditions, to give the P3 building block **28** (Scheme 2, Route B).

### 3.4 Challenges and Optimizations of the Ring-Closing Metathesis Reaction

As mentioned previously, the assembly of the 15-membered ring was initiated by coupling the three key amino acids (P1, P2, and P3), via standard peptide coupling conditions, to give an acyclic tripeptide diene (Scheme 2). However, in an effort to address a number of issues with the subsequent ring-closing metathesis (RCM) of this diene, various forms of the P1–P2–P3 tripeptide were explored, including the “naked” tripeptide diene shown in Scheme 2, as well as dienes **39** having various preassembled quinolones attached to the C-4 of proline, shown in Scheme 4. At the start of the program, the RCM reaction was attempted using the ruthenium-based catalysts known at that time, which were the Grubbs first-generation catalyst **32** and the Hoveyda catalyst **33** (Fig. 4). The backbone conformation of the acyclic diene precursor **39a** (Scheme 4), and in particular the *cis*-/*trans*-rotamer ratio of the proline amide bond (P2–P3 amide), was found to be crucial for the RCM reaction, as well as the diastereomeric purity of the macrocyclic product(s) formed [35]. Furthermore, the length of the olefinic side chain of P3 (used to modulate the ring size) had a profound effect on the diastereomeric purity of the macrocyclic product. For example, in the absence of the bulky *N*-Boc protecting group on the P3 nitrogen, or



**Scheme 4** Initial observation of the formation of macrocyclic products via the ring-closing metathesis reaction

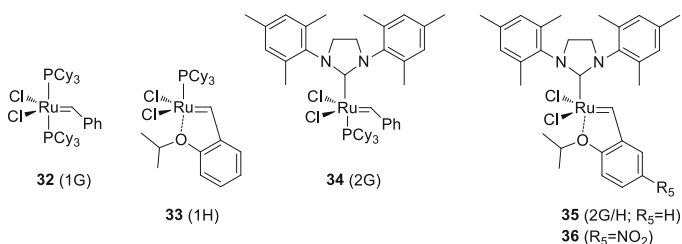


**Fig. 4** Ruthenium-based catalysts described in this study

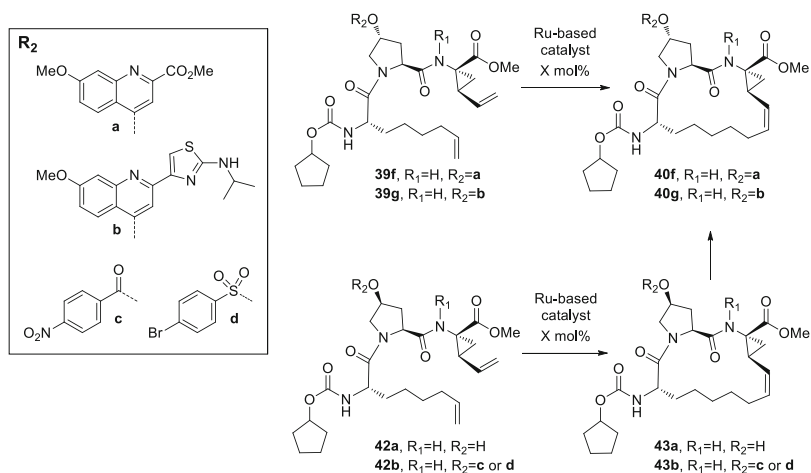
in the absence of substitution at the C $\alpha$  of the P3 fragment (e.g., Scheme 4; diene **39a**), the *cis*-/*trans*-rotamer ratio of the P2–P3 amide bond was approximately 1:1, and the outcome of the reaction was very poor, with only mixtures of product formed in <30% overall RCM conversion [35]. In contrast, the *cis*/*trans* ratio for diene **39b** (R<sub>1</sub>=NH*Boc*) was approximately 1:9, thus pre-organizing the peptidic backbone to the  $\beta$ -strand conformation and mimicking the backbone of the desired macrocyclic product; evidently, this conformational pre-organization facilitated the RCM reaction. The overall conversion of diene **39b** to the 15-membered ring product **40b** was achieved in 40% yield using 5 mol% of catalyst **32** in refluxing CH<sub>2</sub>Cl<sub>2</sub> (0.01 M solution) after approximately 2 h (~60% of total RCM conversion). Further improvement was observed using diene **39c**, which gave the desired diastereomer **40c** in 80% yield under the same RCM conditions (Scheme 4). These observations are analogous to those previously reported by Grubbs and coworkers on template-directed RCM reactions [37–39]. Remote control effects on the outcome of the RCM reaction were also reported in the synthesis of macrocyclic natural products, such as salicylihalamide [40, 41] and epothilones [42].

Interestingly, the RCM reaction of the acyclic dienes **39d** and **39e** proceeded almost exclusively via epimerization at the C $\beta$  of the cyclopropyl ring and the formation of the 14-membered (**41d**) and 13-membered ring (**41e**) products, respectively (Scheme 4) [35]. Stereomutation at the C $\beta$  of the vinyl cyclopropyl moiety of P1 (i.e., epimerization of the vinyl group from *cis* to *trans* with respect to the ester) was also detected in the RCM formation of the 15-membered ring (i.e., formation of **41b,c**), but only in very small amounts (<5% of the overall RCM product) [35].

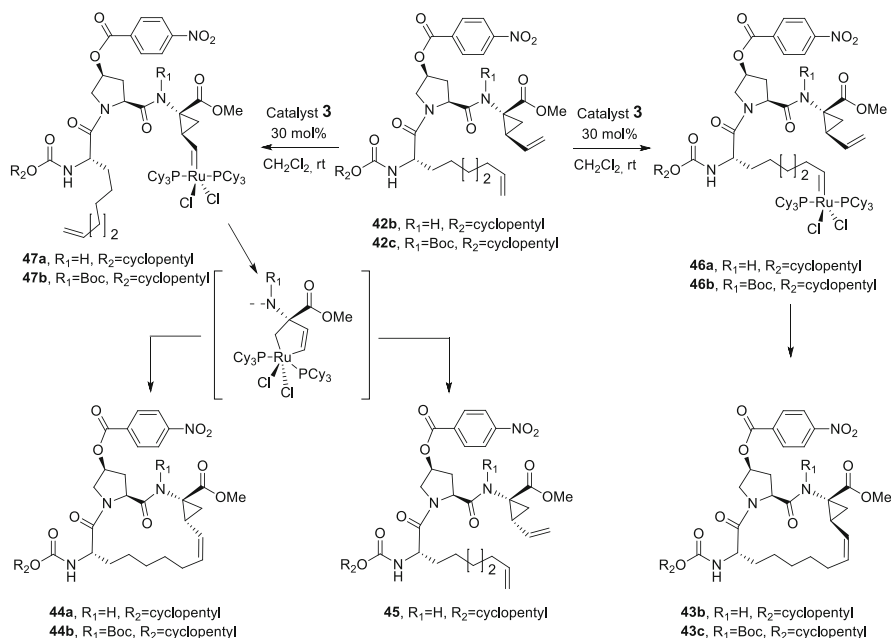
Faced with the challenge of having to produce multi-kilogram quantities of BILN 2061 (**7**) and related analogs for clinical development, the RCM reaction had to be optimized extensively. The chiral integrity of the (1*R*,2*S*)-vinyl ACCA moiety (P1) was crucial in the conformation of the macrocyclic scaffold and, consequently, the affinity of these inhibitors for their intended biological target. Therefore, maintaining absolute stereochemical fidelity during the RCM cyclization of the diene was critical to the development of this class of compounds (Fig. 2; analogs **7–14**). Our initial evaluation of the factors that modulate the outcome of the RCM reaction (Scheme 4) suggested a Ru-mediated side reaction (from here on referred to as the *epi*-RCM pathway) involving the vinyl ACCA moiety [35, 43, 44].

This *epi*-RCM pathway was unprecedented in the literature, in spite of the fact that RCM reactions involving vinylcyclopropanes had been previously reported without any evidence of stereomutation; examples include the synthesis of radicicol-type macrolides [45, 46], coronanes [47], and oligo-*gem*-difluorocyclopropanes [48].

This led us to examine several Ru-based catalysts, including the Hoveyda catalyst **33** [49], and the imidazolium-based catalysts **34** and **35**, as well as the Grell catalyst **36** (Fig. 4) [50]. These catalysts typically provide higher turnover number (TON) [51–54], and their use appeared to resolve the issue of epimerization, at least on small-scale reactions. However, loss for chiral integrity, in addition to formation of cyclic dimers, resurfaced as a major issue when the RCM reaction was attempted on large scale, in spite of tight quality control of all starting materials, solvent, and reagents. For example, prewashing the reaction solvent with acid, in order to eliminate traces of amines and/or phosphines, became part of our large-scale protocol [55], but did not eliminate the epimerization issue. Since formation of minor side products that could not be easily removed from the active pharmaceutical ingredient (API) on a large scale was a major challenge for development, detailed mechanistic studies of the RCM reaction of various dienes with general structure **39** and **42** were investigated (Schemes 4 and 5). Other related issues were also essential to address, including (a) the cost of the required catalyst (initially 5–10 mol%), (b) the need to bring the levels of residual Ru metal in the final API to less than 10 ppm, and (c) the high volumes of solvent (i.e., low substrate concentration; <0.01 M) typically required for RCM reactions in order to avoid dimerization/polymerization. Failing to overcome these synthetic challenges could prohibit the production of BILN 2061 (**7**) in a pilot plant and consequently prevent further development of this important clinical candidate.



**Scheme 5** Optimization of RCM reaction for the pilot plant synthesis of BILN 2061 (**7**)



**Scheme 6** Mechanistic pathway leading to the epimerization of vinyl ACCA and ways to block this pathway

Several complementary strategies for the assembly of substrate dienes **39** and **42** were carefully examined. This review cannot provide a complete and detailed account of all the studies undertaken during optimizations [43, 44, 55–57]. However, the critical effects of substitutions on the P1 nitrogen ( $R_1$ ) and, to a lesser extent, the C-4 of the P2 proline moiety ( $R_2$ ) in the outcome of the RCM reaction are summarized in Schemes 4, 5, and 6. Cyclization of dienes **39f** and **39g** (Scheme 5), already bearing the P2 quinoline construct and having the required stereochemistry at the C-4 of the proline, under RCM conditions gave very similar results to those observed previously with diene **39c** (Scheme 4). We also investigated the simpler dienes **42a,b**, having the C-4 hydroxyl of the P2 proline unprotected (**42a**) or temporarily protected as a benzoate or benzenesulfonate ester (**42b**), which can be activated post-cyclization for the introduction of the quinoline via  $S_N2$  inversion (i.e., Mitsunobu reaction).

The relative efficiency of each substrate diene was evaluated in the RCM reaction under a variety of catalytic conditions. For the development of a scale-up/pilot plant-relevant protocol, all substrate dienes were used as the crude products obtained after the assembly sequence of the tripeptide dienes (i.e., post-peptide coupling of the P1, P2, and P3). Peptide synthesis of these dienes was typically achieved in high purity (>95% w/w), and further purification appeared to only affect the catalytic TON obtained in the RCM reaction and not the course or outcome of the reaction. There was only one important exception to these

observations in that the presence of even small amounts (as little as 1%) of phosphines or amines led to a significant increase in the amounts of epimerized product formed (Scheme 4; compound **41**), as discussed later.

Diene **42a** was thought to be a very desirable starting material, because it eliminated the need for protection/deprotection of the C-4 hydroxy of proline. However, the subtle conformational differences between dienes **42a** and **42b** proved to be sufficient to modulate the amounts of side products formed during the RCM reaction. For example, in contrast to the RCM reaction with diene **42a**, cyclization of diene **42b** proceeded uneventfully in excellent yield (90%) with Hoveyda catalyst **33** (3.5–5 mol%) at concentration of substrate of 10 mM in toluene at 60°C in 20–24 h without the formation of cyclic dimers (confirmed by LC–MS). Nonetheless, even these conditions were considered by the BI development team to be inadequate for the large-scale synthesis of BILN 2061 (7).

Cyclization of various forms of our tripeptide dienes under RCM conditions catalyzed by the more active Ru-based catalysts **34** and **35** was also evaluated. Although a catalyst load of only 0.5–1 mol% was sufficient to completely cyclize diene **42b** within 1–4 h, the desired product **43b** was contaminated with various cyclic dimers (accounting for ~8–10% of the overall yield), as well as the epimerized side product **44a** (Scheme 6). In the past, formation of non-metathesis side products has been observed in RCM reactions; these are often attributed to the decomposition of the ruthenium-based catalyst. Examples include ring contraction [58]; addition of chloroform to alkenes [59]; isomerization of allylamines, amides, and ethers [60–68]; and hydrogenation of the olefin [69, 70]. In some cases, understanding the mechanism of these side reactions has been proven to be valuable in developing new synthetic methodologies. Examples include the tandem RCM–alkene isomerization process for glycol synthesis developed by Snapper [65], the metathesis/hydrogenation process developed by Grubbs [69], and the RCM–double-bond migration reaction developed by Schmidt [71]. At that time, the epimerization of a vinylcyclopropyl ring had not been previously observed in RCM reactions involving vinylcyclopropanes.

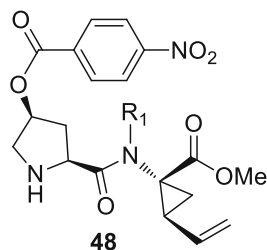
A Michael-type attack on the vinyl ACCA by the metal-dissociated PCy<sub>3</sub> ligand was ruled out, since epimerization was only observed at the C $\beta$  carbon, whereas the stereochemistry of the C $\alpha$  was unaffected under the RCM conditions. Furthermore, exposure of diene **39b** to PCy<sub>3</sub>, under strict anaerobic and anhydrous conditions in refluxing CH<sub>2</sub>Cl<sub>2</sub> over a period of 24 h, but in the absence of any Ru-based catalyst, failed to induce any epimerization of the vinyl ACCA (e.g., giving a product analogous to diene **45** in Scheme 6). It is noteworthy that all diastereomers of vinyl ACCA were previously isolated in high enantiomeric purity [27] and used independently in the synthesis of model tripeptide dienes. These compounds were independently used to study the epimerization phenomenon under RCM conditions, and the products formed were clearly distinguishable by their retention time on chiral HPLC, as well as their <sup>1</sup>H and ROESY NMR spectra. The results obtained from these model reactions confirmed that the mechanism of epimerization involved only the C $\beta$  of the cyclopropyl ring and did not affect the C $\alpha$  of the vinyl ACCA moiety.

A number of plausible mechanisms were considered that could involve a  $\pi$ -allyl-type shift of ruthenium hydride (formed as decomposition by-product of the catalyst) [72], an intermediate metal carbene or ruthenacyclopentene [35, 43] (formed via a metal-mediated expansion of the strained cyclopropyl ring) [73–77], or even an electron transfer oxidation mechanism [78]. Mindful of the ligands effects in modulating the reactivity and stereochemical outcome of the RCM/*epi*-RCM reactions, detailed kinetic studies and mechanistic investigations were undertaken. The tripeptide **42b** was subjected to RCM conditions with the first-generation Grubbs catalyst **32** (5 mol%) in toluene at 60°C, and the formation of **43b** and **44a** was observed in 1:1 ratio (Scheme 6). In addition, an isomer of the starting material, diene **45** was also observed [44]. However, when the Hoveyda catalyst **33** was used, under the same reaction conditions, the *epi*-RCM pathway was greatly suppressed giving less than 1% of the side products **44a** and **45**. Unfortunately, this initial observation turned out to be inconsistent from batch to batch, and occasionally product **44a** accounted for as much as 45% of the total RCM product. It was soon realized that competition between the RCM vs. the *epi*-RCM pathway was dependent on minor and variable impurities in the starting material.

A number of potential variables, including moisture, solvent, and substrate impurities, were analyzed by HPLC [44]. These studies revealed that small amounts of the free amine P1–P2 fragment **48** (as little as 1–2%) that escaped coupling with the P3 was in part responsible for catalyzing the *epi*-RCM pathway leading to the formation of **44a** and **45** (Scheme 6). To confirm this hypothesis, the RCM reaction was performed with highly pure diene **42b** in the presence of small amounts of **48** (Fig. 5) and independently with other basic amines (e.g., pyrrolidine and *N*-methylpyrrolidine) or an inorganic base (e.g., Cs<sub>2</sub>CO<sub>3</sub>). All amines tested promoted the epimerization reactions, whereas epimerization was not observed with the inorganic base. Similarly, various phosphines, such as PPh<sub>3</sub>, PCy<sub>3</sub>, and P(*n*-Bu)<sub>3</sub>, also promoted loss of chiral integrity, specifically at the C $\beta$  of vinyl ACCA [44, 56, 57].

To gain further insight into the RCM vs. *epi*-RCM mechanisms, the reaction was subsequently carried out using a high load of catalyst **32** (30 mol%) in a deuterated solvent (CD<sub>2</sub>Cl<sub>2</sub>) at room temperature, and the progress was monitored by <sup>1</sup>H NMR. Two transient intermediate species, **46a** and **47a**, were detected, where the latter (**47a**) was the major species (~96%). After the initial formation of

Fig. 5 Structure of compound **48**



intermediate **47a**, its epimer at the C $\beta$  of the cyclopropyl ring was also detected, and, simultaneously, the formation of products **44a** and **45** was observed. This surprising chemoselectivity for the more hindered olefin of diene **42b** could be driven by chelation of the Ru catalyst by the neighboring ester and amide bonds. It was presumed that substitution of the P1–P2 amide nitrogen with a bulky Boc group (Scheme 6; **42c**) might interrupt the coordination with the catalyst and redirect the Ru metal to the P3 side chain. This hypothesis was experimentally verified by <sup>1</sup>H NMR experiments, confirming that the cyclization of diene **42c** proceeded exclusively via intermediate **46b** leading to the desired product **43c**, without any evidence of intermediate **47b** in this reaction nor the formation of **44b**.

Further optimization of the RCM cyclization of diene **42c** and extensive catalyst screening (e.g., **34**, **35**, and **36**) led to the development of conditions that provide (a) higher yields, (b) lower reaction times, (c) much lower catalyst load, and (d) a dramatic improvement in the concentration required to achieve high yields of the desired product. For example, the formation of product **43b** decreased by 50% (from 85% to 35%) when the concentration of the precursor diene **42b** was increased by tenfold (from 0.01 to 0.10 M, respectively) if the RCM reaction was catalyzed by **36** (0.1 mol%). In contrast, cyclization of the *N*-Boc diene **42c** at 0.20 M concentration (at a 400 kg scale) using catalyst **36** (0.1 mol%) in toluene at 110 °C gave **43c** in 93% isolated yield (100% de; 100% conversion) after only 30 min. Furthermore, the superior robustness of catalyst **36** eliminated the need for oxygen sensors in the system, rendering the RCM reaction much easier to execute on a large scale. Additionally, although the epimerization reaction of the vinyl ACCA moiety can be avoided by acid-washing the solvents and using highly pure (>99%) dipeptide diene, by assuring that the reaction pathway proceed via intermediate **46b**, such precautions were no longer necessary for the RCM reaction. Finally, following the initial protocols for the preparation of BILN 2061 (**7**), the RCM reaction of 1 MT of the diene **42b** (e.g. Scheme 6) required as much as 150,000 L of solvent, whereas cyclization of the same amount of diene **42c** could be performed in only 7,500 L of solvent.

## 4 Conclusion

The stigma of poor drug-like properties associated with peptidomimetics, especially those that violate Lipinski's rules, is unlikely to be dispelled any time soon. Nonetheless, the 15-membered ring macrocyclic inhibitors of the HCV NS3/NS4A protease, which include the drugs simeprevir (**13**) and paritaprevir (**14**), are clearly an important class of antiviral agents for the treatment of HCV infection. From the perspective of modern medicinal chemistry, the *rational* design of these molecules was initially considered somewhat *irrational* by skeptics in the field of drug discovery (i.e., starting a discovery program from a hexapeptide lead with IC<sub>50</sub> of 800 μM). Perseverance by medicinal and process chemists, armed with insight gained from structural research on the factors influencing the pre-organization of

peptidic ligands to the bioactive conformation, led to the design of the  $\beta$ -strand macrocyclic core of the first clinically validated small molecule, BILN 2061 (7), that blocks HCV replication. However, the complex structure of BILN 2061, with three unnatural amino acids and five chiral centers, required considerable efforts in order to reach development status and enter clinical trials. This chapter provides a condensed summary of the most significant challenges and the key milestones in bringing this compound to clinical development. Collectively, overcoming the numerous obstacles in the design and synthesis of such a complex compound should be recognized as an important achievement not only in the development of BILN 2061 (7) but all the other analogs typified by the same 15-membered ring scaffold, having a vinyl ACCA moiety at P1. Evaluation/optimization of all the factors influencing the stereochemical integrity of the product during the key RCM macrocyclization step led to the first application of Ru-induced ring-closing metathesis in the pharmaceutical industry on multi-kilogram quantities.

## References

1. Choo QL, Kuo G, Weiner AJ, Overby LR, Bradley DW, Houghton M (1989) Isolation of a cDNA clone derived from a blood-borne non-A, non-B viral hepatitis genome. *Science* 244:359–362
2. Tellinghuisen TL, Evans MJ, von Hahn T, You S, Rice CM (2007) Studying Hepatitis C virus: making the best of a bad virus. *J Virol* 81:8853–8867
3. Hadziyannis SJ, Papatheodoridis GV (2003) Effects of host and virus related factors on interferon- $\alpha$ + ribavirin and pegylated-interferon+ribavirin treatment outcomes in chronic hepatitis C patients. *Expert Opin Pharmacother* 4:541–551
4. Chander G, Sulkowski MS, Jenckes MW, Torbenson MS, Herlong F, Bass EB, Gebo KA (2002) Treatment of chronic hepatitis C: a systematic review. *Hepatology* 36:S135–S144
5. Calcoen D, Elias L, Yu X (2015) What does it take to produce a breakthrough drug? *Nat Rev Drug Discovery* 14:161–162
6. Belema M, Lopez OD, Bender JA, Romine JL, St. Laurent DR, Langley DR, Lemm JA, O'Boyle II DR, Sun J-H, Wang C, Fridell RA, Meanwell NA (2014) Discovery and development of hepatitis C virus NS5A replication complex inhibitors. *J Med Chem* 57:1643–1672
7. Chen KX, Njoroge FG, Vibulbham B, Prongay A, Pichardo J, Madison V, Buevich A, Chan T-M (2005) Proline-based macrocyclic inhibitors of the hepatitis C virus: stereoselective synthesis and biological activity. *Angew Chem Int Ed* 44:7024–7028
8. Gale M Jr, Foy EM (2005) Evasion of intracellular host defence by hepatitis C virus. *Nature* 436:939–945
9. Chen KX, Njoroge FG (2009) A review of HCV protease inhibitors. *Curr Opin Invest Drugs* 10:821–837
10. Llinàs-Brunet M, Bailey M, Fazal G, Ghire E, Gorys V, Goulet S, Halmos T, Maurice R, Poirier M, Poupert M-A, Rancourt J, Thibeault D, Wernic D, Lamare D (2000) Highly potent and selective peptide-based inhibitors of the hepatitis C virus serine protease: towards smaller inhibitors. *Bioorg Med Chem Lett* 10:2267–2270
11. Ingallinella P, Altamura S, Bianchi E, Taliani M, Ingenito R, Cortese R, De Francesco R, Steinkühler C, Pessi A (1998) Potent peptide inhibitors of human hepatitis C virus NS3 protease are obtained by optimizing the cleavage products. *Biochemistry* 37:8906–8914
12. Schechter I, Berger A (1967) On the size of the active site in proteases. I. Papain. *Biochem Biophys Res Commun* 27:157–162

13. LaPlante SR, Cameron DR, Aubry N, Lefebvre S, Kukulj G, Maurice R, Thibeault D, Lamarre D, Llinàs-Brunet M (1999) Solution structure of substrate-based ligands when bound to hepatitis C virus NS3 protease domain. *J Biol Chem* 274:18618–18624
14. Cicero DO, Barbato G, Koch U, Ingallinella P, Bianchi E, Nardi MC, Steinkühler C, Cortese R, Matassa V, De Francesco R, Pessi A, Bazzo R (1999) Structural characterization of optimized product inhibitors with the N-terminal proteinase domain of the hepatitis C virus (HCV) NS3 protein by NMR and modelling studies. *J Mol Biol* 289:385–396
15. LaPlante SR, Aubry N, Bonneau PR, Kukulj G, Lamarre D, Lefebvre S, Li H, Llinàs-Brunet M, Plouffe C, Cameron DR (2000) NMR line-broadening and transferred NOESY as a medicinal chemistry tool for studying inhibitors of the hepatitis C virus NS3 protease domain. *Bioorg Med Chem Lett* 10:2271–2274
16. Poupart M-A, Cameron DR, Chabot C, Ghire E, Goudreau N, Goulet S, Poirier M, Tsantrizos YS (2001) Solid-phase synthesis of peptidomimetic inhibitors for the hepatitis C virus NS3 protease. *J Org Chem* 66:4743–4751
17. Rancourt J, Cameron DR, Gorys V, Lamarre D, Poirier M, Thibeault D, Llinàs-Brunet M (2004) Peptide-based inhibitors of the hepatitis C virus NS3 protease : structure-activity relationship at the C-terminal position. *J Med Chem* 47:2511–2522
18. Lohmann V, Körner F, Koch J-O, Herian U, Theilmann L, Bartenschlager R (1999) Replication of subgenomic hepatitis C virus RNAs in hepatoma cell lines. *Science* 285:110–113
19. Tsantrizos YS, Bolger G, Bonneau P, Cameron DR, Goudreau N, Kukulj G, LaPlante SR, Llinàs-Brunet M, Nar H, Lamarre D (2003) Macrocyclic inhibitors of the NS3 protease as potential therapeutic agents of hepatitis C virus infections. *Angew Chem Int Ed Engl* 42:1356–1360
20. Tsantrizos YS, Cameron DR, Faucher A-M, Ghire E, Goudreau N, Halmos T, Llinàs-Brunet M (2000) Macrocyclic peptides active against the hepatitis C virus. Boehringer Ingelheim (Canada) Ltd. WO Pat Appl 0,059,929A1
21. Lamarre D, Anderson PC, Bailey M, Beaulieu P, Bolger G, Bonneau P, Bös M, Cameron D, Cartier M, Cordingley MG, Faucher A-M, Goudreau N, Kawai SH, Kukulj G, Lagacé L, LaPlante SR, Narjes H, Poupart M-A, Rancourt J, Sentjens RE, St George R, Simoneau B, Steinmann G, Thibeault D, Tsantrizos YS, Weldon SM, Yong C-L, Llinàs-Brunet M (2003) An NS3 protease inhibitor with antiviral effects in humans infected with hepatitis C virus. *Nature* 426:186–189
22. Reiser M, Hinrichsen H, Benhamou Y, Reesink HW, Wedemeyer H, Avendano G, Riba N, Yong C-L, Nehmiz G, Steinmann GG (2005) Antiviral efficacy of NS3-serine protease inhibitor BILN-2061 in patients with chronic genotype 2 and 3 hepatitis C. *Hepatology* 41:832–835
23. Jiménez JM, Rifé J, Ortuño RM (1996) Enantioselective total syntheses of cyclopropane amino acids: natural products and protein methanologs. *Tetrahedron Asymmetry* 7:537–558
24. Ooi T, Takeuchi M, Kameda M, Maruoka K (2000) Practical catalytic enantioselective synthesis of  $\alpha$ ,  $\alpha$ -dialkyl- $\alpha$ -amino acids by chiral phase-transfer catalysis. *J Am Chem Soc* 122:5228–5229
25. Belokon YN, Kochetkov KA, Churkina TD, Ikonnikov NS, Chesnokov AA, Larionov OV, Singh I, Parmar VS, Vyskocil S, Henri B, Kagan HB (2000) Asymmetric PTC C-alkylation catalyzed by chiral derivatives of tartaric acid and aminophenols. Synthesis of (*R*)- and (*S*)- $\alpha$ -methyl amino acids. *J Org Chem* 65:7041–7048
26. Belokon YN, Bhave D, D'Addario D, Groaz E, Maleev V, North M, Petrosyan A (2003) Catalytic, asymmetric synthesis of  $\alpha$ ,  $\alpha$ -disubstituted amino acids. *Tetrahedron Lett* 44:2045–2048
27. Beaulieu PL, Gillard J, Bailey MD, Boucher C, Duceppe J-S, Simoneau B, Wang X-J, Zhang L, Grozinger K, Houpiis I, Farina V, Heimroth H, Krueger T, Schnaubelt J (2005) Synthesis of (1*R*,2*S*)-1-amino-2-vinylcyclopropanecarboxylic acid (Vinyl-ACCA) derivatives: key intermediates for the preparation of inhibitors of the hepatitis C virus NS3 protease. *J Org Chem* 70:5869–5879

28. O'Donnell MJ, Bennett WD, Bruder WA, Jacobsen WN, Knuth K, LeClef B, Polt RL, Bordwell FG, Mrozack SR, Cripe TA (1988) Acidities of glycine schiff bases and alkylation of their conjugate bases. *J Am Chem Soc* 110:8520–8525
29. O'Donnell MJ, Polt RL (1982) A mild and efficient route to schiff base derivatives of amino acids. *J Org Chem* 47:2663–2666
30. Charette AB, Côté B (1995) Stereoselective synthesis of all four isomers of coronamic acid: a general approach to 3-methanoamino acids. *J Am Chem Soc* 117:12721–12732
31. Llinàs-Brunet M, Bailey MD, Bolger G, Brochu C, Faucher A-M, Ferland JM, Garneau M, Ghiro E, Gorys V, Grand-Maitre C, Halmos T, Lapeyre-Paquette N, Liard F, Poirier M, Rhéaume M, Tsantrizos YS, Lamarre D (2004) Structure-activity study on a novel series of macrocyclic inhibitors of the hepatitis C virus NS3 protease leading to the discovery of BILN 2061. *J Med Chem* 47:1606–1608
32. Tsantrizos YS (2004) The design of a potent inhibitor of the hepatitis C virus NS3 protease: BILN2061—from the NMR tube to the clinic. *Biopolymers* 76:309–323
33. Goudreau N, Brochu C, Cameron DR, Duceppe J-S, Faucher A-M, Ferland J-M, Grand-Maitre C, Poirier M, Simoneau B, Tsantrizos YS (2004) Potent inhibitors of the hepatitis C virus NS3 protease: design and synthesis of macrocyclic substrate-based  $\beta$ -strand mimics. *J Org Chem* 69:6185–6201
34. Faucher A-M, Bailey M, Beaulieu P, Brochu C, Duceppe J-S, Ferland J-M, Ghiro E, Gorys V, Halmos T, Kawai SH, Poirier M, Simoneau B, Tsantrizos YS, Llinàs-Brunet M (2004) Synthesis of BILN 2061, an HCV NS3 protease inhibitor with proven antiviral effect in humans. *Org Lett* 6:2901–2904
35. Poirier M, Aubry N, Boucher C, Ferland J-M, LaPlante S, Tsantrizos YS (2005) RCM of tripeptide dienes containing a chiral vinylcyclopropane moiety: impact of different Ru-based catalysts on the stereochemical integrity of macrocyclic products. *J Org Chem* 70:10765–10773
36. Evans DA, Evrard DA, Rychnovsky SD, Früh T, Whittingham WG, DeVries KM (1992) A general approach to the asymmetric synthesis of vancomycin-related arylglycines by enolate azidation. *Tetrahedron Lett* 33:1189–1192
37. Weck M, Mohr B, Sauvage J-P, Grubbs RH (1999) Synthesis of catenane structures via ring-closing metathesis. *J Org Chem* 64:5463–5471
38. Mohr B, Weck M, Sauvage J-P, Grubbs RH (1997) High-yield synthesis of [2] catenanes by intramolecular ring-closing metathesis. *Angew Chem Int Ed Engl* 36:1308–1310
39. Marsella MJ, Maynard HD, Grubbs RH (1997) Template-directed ring-closing metathesis: synthesis and polymerization of unsaturated crown ether analogs. *Angew Chem Int Ed Engl* 36:1101–1103
40. Fürstner A, Dierkes T, Thiel OR, Blanda G (2001) Total synthesis of (–)-salicylilhalamide. *Chem Eur J* 7:5286–5298
41. Fürstner A, Thiel OR, Blanda G (2000) Asymmetric synthesis of the fully functional macrolide core of salicylilhalamide: remote control of olefin geometry during RCM. *Org Lett* 2:3731–3734
42. Meng D, Su D-S, Balog A, Bertinato P, Sorensen EJ, Danishefsky SJ, Zheng Y-H, Chou T-C, He L, Horwitz SB (1997) Remote effects in macrolide formation through ring-forming olefin metathesis: an application to the synthesis of fully active epothilone congeners. *J Am Chem Soc* 119:2733–2734
43. Tsantrizos YS, Ferland J-M, McClory A, Poirier M, Farina V, Yee NK, Wang X, Haddad N, Wei X, Xu J, Zhang L (2006) Olefin ring-closing metathesis as a powerful tool in drug discovery and development-potent macrocyclic inhibitors of hepatitis C virus NS3 protease. *J Organomet Chem* 691:5163–5171
44. Zeng X, Wei X, Farina V, Napolitano E, Xu Y, Zhang L, Haddad N, Yee NK, Grinberg N, Shen S, Senanayake CH (2006) Epimerization reaction of a substituted vinylcyclopropane catalyzed by ruthenium carbenes: mechanistic analysis. *J Org Chem* 71:8864–8875

45. Yang Z-Q, Geng X, Solit D, Pratilas CA, Rosen N, Danishefsky SJ (2004) New efficient synthesis of resorcinylic macrolides via ynolides: establishment of cycloproparadicol as synthetically feasible preclinical anticancer agent based on Hsp90 as the target. *J Am Chem Soc* 126:7881–7889
46. Yamamoto K, Biswas K, Gaul C, Danishefsky SJ (2003) Effects of temperature and concentration in some ring closing metathesis reactions. *Tetrahedron Lett* 44:3297–3299
47. Barrett AGM, Hamprecht D, James RA, Ohkubo M, Procopiou PA, Toledo MA, White AJP, Williams DJ (2001) Synthesis and characterization of coronanes: multicyclopropane-fused macrocyclic arrays. *J Org Chem* 66:2187–2196
48. Itoh T, Mitsukura K, Ishida N, Uneyama K (2000) Synthesis of bis- and oligo-*gem*-difluorocyclopropanes using the olefin metathesis reaction. *Org Lett* 2:1431–1434
49. Kingsbury JS, Harrity JPA, Bonitatebus PJ, Hoveyda AH (1999) A recyclable Ru-based metathesis catalyst. *J Am Chem Soc* 121:791–799
50. Michrowska A, Bujok R, Harutyunyan S, Sashuk V, Dolgonos G, Grela K (2004) Nitro-substituted Hoveyda-Grubbs ruthenium carbenes: enhancement of catalyst activity through electronic activation. *J Am Chem Soc* 126:9318–9325
51. Scholl M, Trnka TM, Morgan JP, Grubbs RH (1999) Increased ring closing metathesis activity of ruthenium-based olefin metathesis catalysts coordinated with imidazolin-2-ylidene ligands. *Tetrahedron Lett* 40:2247–2250
52. Weskamp T, Kohl FJ, Hieringer W, Gleich D, Herrmann WA (1999) Highly active ruthenium catalysts for olefin metathesis: the synergy of *N*-heterocyclic carbenes and coordinatively labile ligands. *Angew Chem Int Ed Engl* 38:2416–2419
53. Huang J, Stevens ED, Nolan SP, Petersen JL (1999) Olefin metathesis-active ruthenium complexes bearing a nucleophilic carbene ligand. *J Am Chem Soc* 121:2674–2678
54. Garber SB, Kingsbury JS, Gray BL, Hoveyda AH (2000) Efficient and recyclable monomeric and dendritic Ru-based metathesis catalysts. *J Am Chem Soc* 122:8168–8179
55. Nicola T, Brenner M, Donsbach K, Kreye P (2005) First scale-up to production scale of a ring closing metathesis reaction forming a 15-member macrocycle as a precursor of an active pharmaceutical ingredient. *Org Process Res Dev* 9:513–515
56. Yee NK, Farina V, Houpius I, Haddad N, Frutos RP, Gallou F, Wang X-J, Wei X, Simpson RD, Feng X, Fuchs V, Xu Y, Tan J, Zhang L, Xu J, Smith-Keenan LS, Vitous J, Ridges MD, Spinelli EM, Johnson M, Donsbach K, Nicola T, Brenner M, Winter E, Kreye P, Samstag W (2006) Efficient large-scale synthesis of BILN 2061, a potent HCV protease inhibitor, by a convergent approach based on ring-closing metathesis. *J Org Chem* 71:7133–7145
57. Shu C, Zeng X, Hao M-H, Wei X, Yee NK, Busacca CA, Han Z, Farina V, Senanayake CH (2008) RCM macrocyclization made practical: An efficient synthesis of HCV protease inhibitor BILN 2061. *Org Lett* 10:1303–1306
58. Fürstner A, Thiel OR, Ackermann L, Schanz H-J, Nolan SP (2000) Ruthenium carbene complexes with *N,N'*-bis(mesityl)imidazol-2-ylidene ligands: RCM catalysts of extended scope. *J Org Chem* 65:2204–2207
59. Tallarico JA, Malnick LM, Snapper ML (1999) New reactivity from  $(PCy_3)_2Cl_2Ru=CHPh$ : a Mild catalyst for Kharasch additions. *J Org Chem* 64:344–345
60. Hu Y-J, Dominique R, Das SK, Roy R (2000) A facile new procedure for the deprotection of allyl ethers under mild conditions. *Can J Chem* 78:838–846
61. Cadot C, Dalko PI, Cossy J (2002) Olefin isomerization by a ruthenium carbenoid complex. Cleavage of allyl and homoallyl groups. *Tetrahedron Lett* 43:1839–1841
62. Hoye TR, Zhao H (1999) Some allylic substituent effects in ring-closing metathesis reactions: allylic alcohol activation. *Org Lett* 1:1123–1125
63. Alcaide B, Almendros P, Alonso JM, Aly MF (2001) A novel use of Grubbs' carbene. Application to the catalytic deprotection of tertiary allylamines. *Org Lett* 3:3781–3784
64. Wipf P, Rector SR, Takahashi H (2002) Application in total synthesis of (-)-tuberostemonine. *J Am Chem Soc* 124:14848–14849

65. Sutton AE, Seigal BA, Finnegan DF, Snapper ML (2002) New tandem catalysis: preparation of cyclic enol ethers through a ruthenium-catalyzed ring-closing metathesis–olefin isomerization sequence. *J Am Chem Soc* 124:13390–13391
66. Arisawa M, Terada Y, Nakagawa M, Nishida A (2002) Selective isomerization of a terminal olefin catalyzed by a ruthenium complex: the synthesis of indoles through ring-closing metathesis. *Angew Chem Int Ed* 41:4732–4734
67. Braddock DC, Matsuno A (2002) In situ tandem allylic acetate isomerisation–ring closing metathesis: 1,3-dimesityl-4,5-dihydroimidazol-2-ylidene ruthenium benzylidenes and palladium(0)–phosphine combinations. *Tetrahedron Lett* 43:3305–3308
68. Braddock DC, Wildsmith AJ (2001) On the use of tandem allylic acetate isomerisation and ring-closing metathesis with palladium(0) phosphine complexes and ruthenium benzylidenes as orthogonal catalysts. *Tetrahedron Lett* 42:3239–3242
69. Bielawski CW, Louie J, Grubbs RH (2000) Tandem catalysis: three mechanistically distinct reactions from a single ruthenium complex. *J Am Chem Soc* 122:12872–12873
70. Watson MD, Wagener KB (2000) Tandem homogeneous metathesis/heterogeneous hydrogenation: preparing model ethylene/CO<sub>2</sub> and ethylene/CO copolymers. *Macromolecules* 33:3196–3201
71. Schmidt B (2004) Catalysis at the interface of ruthenium carbene and ruthenium hydride chemistry: organometallic aspects and applications to organic synthesis. *Eur J Org Chem* 2004:1865–1880
72. Ulman M, Grubbs RH (1999) Ruthenium carbene-based olefin metathesis initiators: catalyst decomposition and longevity. *J Org Chem* 64:7202–7207
73. Jordan RW, Khoury PR, Goddard JD, Tam W (2004) Ruthenium-catalyzed [2+2] cycloadditions between 7-substituted norbornadienes and alkynes: an experimental and theoretical study. *J Org Chem* 69:8467–8474
74. Echavarren AM, Nevado C (2004) Non-stabilized transition metal carbenes as intermediates in intramolecular reactions of alkynes with alkenes. *Chem Soc Rev* 33:431–436
75. Trost BM, Pinkerton AB, Toste FD, Sperrle M (2001) Synthesis of 1,1-disubstituted alkenes via a Ru-catalyzed addition. *J Am Chem Soc* 123:12504–12509
76. Wender PA, Husfeld CO, Langkopf E, Love JA (1998) First studies of the transition metal-catalyzed [5+2] cycloadditions of alkenes and vinylcyclopropanes: scope and stereochemistry. *J Am Chem Soc* 120:1940–1941
77. Wender PA, Takahashi H, Witulski B (1995) Transition metal catalyzed [5+2] cycloadditions of vinylcyclopropanes and alkynes: a homolog of the Diels–Alder reaction for the synthesis of seven-membered rings. *J Am Chem Soc* 117:4720–4721
78. Dinnocenzo JP, Schmittel M (1987) Cyclopropane stereomutation catalyzed by one-electron oxidants. *J Am Chem Soc* 109:1561–1562

# Recent Progress in the Synthesis of Super-Statins

Zdenko Časar

**Abstract** Super-statins now represent a mature class of marketed drugs that faces the patent cliff, as has already occurred for fluvastatin and atorvastatin and is approaching for rosuvastatin and pitavastatin. However, they continue to trigger huge scientific interest in terms of their efficient preparation. This is not surprising, as easier accessibility of super-statins will promote even bigger demand in the market and consequently the need for higher rates of the production and productivity. Therefore, the stimulus for the development of even more efficient synthetic approaches to the heterocyclic moieties of super-statins and their chiral lateral-chain precursors is at a peak, as also for the assembly of the these two parts into super-statins. The present report summarizes recent developments in the field of the synthesis of super-statins published from 2010 to 2015. Emphasis is given to the analysis of novel approaches to the formation of the chiral statin lateral chain, with detailed discussion of the development of new routes to respective heterocyclic cores and the assembly of these key units into the final super-statin structure.

**Keywords** Asymmetric synthesis • Catalysis • Heterocycles • Indole • Pyrimidine • Pyrrole • Quinoline • Statins

## Contents

1	Introduction .....	117
1.1	Discovery of Statins .....	117
1.2	Fully Synthetic Statins: Super-Statins .....	118

---

Z. Časar (✉)

Lek Pharmaceuticals d.d., Sandoz Development Centre Slovenia, Verovškova 57, 1526 Ljubljana, Slovenia

Faculty of Pharmacy, University of Ljubljana, Aškerčeva cesta 7, 1000 Ljubljana, Slovenia

Sandoz GmbH, Global Portfolio Management API, Biochemiestrasse 10, 6250 Kundl, Austria

e-mail: [zdenko.casar@sandoz.com](mailto:zdenko.casar@sandoz.com); [zdenko.casar@ffa.uni-lj.si](mailto:zdenko.casar@ffa.uni-lj.si)

1.3	Hepatosselective Super-Statins .....	119
1.4	Main Synthetic Strategies Towards Super-Statins .....	122
2	Synthesis of Chiral Super-Statins Lateral Chain Precursors .....	124
2.1	Structure of Advanced Super-Statins Lateral Chain Precursors .....	124
2.2	New Developments in the Area of Super-Statins Lateral-Chain Precursors .....	125
3	Fluvastatin .....	151
3.1	Synthesis of the Fluvastatin Indole Heterocyclic Core .....	151
3.2	Assembly of Fluvastatin .....	152
4	Atorvastatin .....	153
4.1	Synthesis of the Atorvastatin Pyrrole Heterocyclic Core .....	153
4.2	Assembly of Atorvastatin .....	156
5	Rosuvastatin .....	167
5.1	Synthesis of the Rosuvastatin Pyrimidine Heterocyclic Core .....	167
5.2	Assembly of Rosuvastatin .....	171
6	Pitavastatin .....	174
6.1	Synthesis of the Pitavastatin Quinoline Heterocyclic Core .....	175
6.2	Assembly of Pitavastatin .....	177
7	Conclusions .....	181
	References .....	181

## Abbreviations

Ac	Acetyl
acac	Acetylacetonate
All	Allyl
Ar	Aryl
Asn	Asparagine
atm	Atmosphere
AtNIT2	<i>Arabidopsis thaliana</i> nitrilase-2
BINOL	1,1'-bi-2-Naphthol
Bn	Benzyl
Cbz	Benzyloxycarbonyl
cod	Cyclooctadiene
CSA	Camphorsulfonic acid
Cy	Cyclohexyl
(R)-(+)-Cl-MeO-	(R)-(+)-5,5'-Dichloro-2,2'-bis(diphenylphosphino)-
BIPHEP	6,6'-dimethoxy-1,1'-biphenyl
d	Day(s)
dba	Dibenzylideneacetone
DBU	1,8-Diazabicyclo [5.4.0]undec-7-ene
DCE	1,2-Dichloroethane
de	Diastereomer excess
DEPC	Diethyl pyrocarbonate
DERA	Deoxyribose-5-phosphate aldolase
DMA	<i>N,N</i> -dimethylacetamide
DMAP	4-(Dimethylamino)pyridine

DMF	<i>N,N</i> -dimethylformamide
DmgH <sub>2</sub>	Dimethylglyoxime
DMP	Dess–Martin periodinane
DMPU	1,3-Dimethyl-3,4,5,6-tetrahydro-2(1 <i>H</i> )-pyrimidinone
DMSO	Dimethyl sulfoxide
dppb	1,4-bis(Diphenylphosphino)butane
<i>ee</i>	Enantiomeric excess
eosin Y	2-(2,4,5,7-Tetrabromo-6-oxido-3-oxo-3H-xanthen-9-yl)benzoate
equiv.	Equivalent(s)
<i>er</i>	Enantiomeric ratio
Et	Ethyl
g	Gram(s)
GC	Gas chromatography
GDH	Glucose dehydrogenase
G-H-II	Grubbs–Hoveyda second-generation catalyst
Glu	Glutamic acid
h	Hour(s)
Het	Heterocyclic core
HHDH	Halohydrin dehalogenase
His	Histidine
HMDS	Hexamethyldisilazane
HMG-CoA	3-Hydroxy-3-methylglutaryl-coenzyme A
HPLC	High-performance liquid chromatography
Hz	Hertz(s)
<i>hν</i>	Light energy
ImH	Imidazole
<i>i</i> -Pr	Isopropyl
KRED	Ketoreductase
L	Liter(s)
LDA	Lithium diisopropylamide
LED	Light-emitting diode
LiHMDS	Lithium hexamethyldisilazide, lithium bis(trimethylsilyl)amide
<i>m</i> -CPBA	Meta-chloroperoxybenzoic acid
Me	Methyl
min	Minute(s)
mol	Mole(s)
MS	Molecular sieve
MTBE	Methyl <i>tert</i> -butyl ether
MWCNTs	Multiwalled carbon nanotubes
NADH	Nicotinamide adenine dinucleotide
NADP	Nicotinamide adenine dinucleotide phosphate
NADPH	Reduced form of NADP
NaHMDS	Sodium hexamethyldisilazide, sodium bis(trimethylsilyl)amide

NBS	<i>N</i> -bromosuccinimide
<i>n</i> -Bu	Butyl (Bu)
NEt <sub>3</sub>	Triethylamine
NMR	Nuclear magnetic resonance
P	Protecting group
Ph	Phenyl
phen	Phenanthroline
( <i>S,S</i> )-Ph-BPE	(+)-1,2-bis(( <i>2S,5S</i> )-2,5-diphenylphospholano)ethane
Pin	Pinacolato
PPh <sub>3</sub>	Triphenylphosphine
( <i>R,R</i> )-Ph-BPE	(-)-1,2-bis(( <i>2R,5R</i> )-2,5-diphenylphospholano)ethane
PPQ	Pyroloquinoline quinone
<i>p</i> -TsOH	<i>p</i> -Toluenesulfonic acid
Pv	Pivaloyl
Py	Pyridine
PyBrOP	Bromo-tris-pyrrolidino phosphoniumhexafluorophosphate
R	Hydrocarbon side chain
rt	Room temperature
Ser	Serine
( <i>S</i> )-SunPhos	1,1'-[(4 <i>S</i> )-2,2,2',2'-tetramethyl[4,4'-bi-1,3-benzodioxole]-5,5'-diyl]bis[1,1-diphenyl-phosphine]
TBAB	Tetrabutylammonium bromide
TBAF	Tetrabutylammonium fluoride
TBDPS	<i>tert</i> -Butyldiphenylsilyl
TBHP	<i>tert</i> -Butyl hydroperoxide
TBS	<i>tert</i> -Butyldimethylsilyl
TBSOTf	<i>tert</i> -Butyldimethylsilyl trifluoromethanesulfonate
<i>t</i> -Bu	<i>tert</i> -Butyl
TCCA	Trichloroisocyanuric acid
TEMPO	2,2,6,6-Tetramethylpiperidinyloxy
Tf	Trifluoromethanesulfonyl (triflyl)
TfOH	Trifluoromethanesulfonic acid
THF	Tetrahydrofuran
TMS	Trimethylsilyl
Tr	Triphenylmethyl (trityl)
Tris	Tris(hydroxymethyl)aminomethane hydrochloride buffer
Ts	Tosyl, 4-toluenesulfonyl
W	Watt(s)

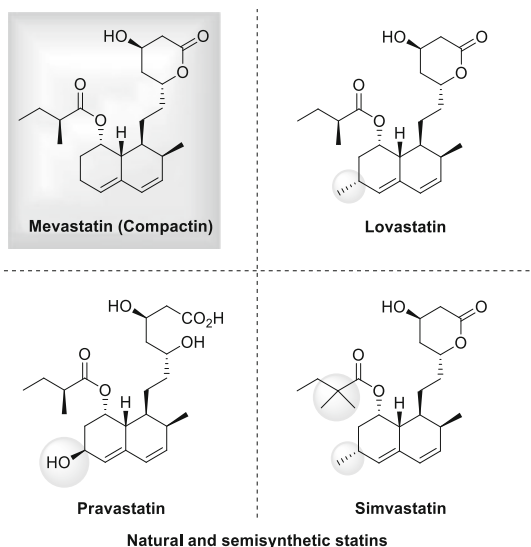
## 1 Introduction

### 1.1 Discovery of Statins

Since their discovery more than 40 years ago, statins have dramatically improved the quality of life of millions of patients worldwide who suffer from diseases related to increased levels of cholesterol (hypercholesterolemia), which increases the risk of atherosclerosis, the main cause of most cardiovascular diseases, and in particular of coronary heart disease. The story of statins is one of the most interesting in the field of modern medicinal chemistry and greatly resembles that of  $\beta$ -lactam antibiotics. Namely, statins were discovered in the early 1970s in a search for new antimicrobial agents in the fermentation broth of *Penicillium citrinum*. This breakthrough discovery was accomplished by Akira Endo at the Japanese pharmaceutical company Sankyo, who isolated a compound from *P. citrinum* P-51 broths that was given the code ML-236B, and which was later demonstrated to be compactin (also known as mevastatin) (Fig. 1). Compactin showed strong competitive inhibition of 3-hydroxy-3-methylglutaryl-coenzyme A (HMG-CoA) reductase, the rate-limiting enzyme in the biosynthetic pathway of cholesterol.

Although compactin underwent phase 2 clinical trials in 1980, and although it lowered low-density lipoprotein cholesterol (LDL-C) by about 30%, it did not reach the market, due to long-term toxicity concerns that appeared during tests on dogs. Nevertheless, compactin paved the way for the discovery of other similar compounds that obtained regulatory approval and reached patients worldwide. Indeed, in 1978, it became apparent that Merck had discovered a similar compound from *Aspergillus terreus*, known now as lovastatin. This statin differs only slightly

**Fig. 1** Structures of the natural and semisynthetic statins



compared to compactin, in that it has an addition methyl group on the decalin skeleton of the molecule (Fig. 1). Lovastatin successfully underwent clinical studies and regulatory reviews to become the first commercial statin on the US market after US Food and Drug Administration approval in 1987. Later on, Sankyo successfully developed a hydroxylated analog of compactin that contains an –OH group on the decalin ring. This compound was named as pravastatin (Fig. 1), and it entered the Japanese market in 1989; it was also licensed to Bristol Myers Squibb for the US market, where it was launched in 1991. Concurrent with the development of lovastatin, and in the search for even more potent HMG-CoA reductase inhibitors to be one step ahead of the competition, Merck developed a semisynthetic analog that was later named as simvastatin (Fig. 1). Simvastatin is a lovastatin analog where the (*S*)-2-methylbutanoic acid moiety on the decalin core is replaced with a 2,2-dimethylbutanoic acid moiety. Simvastatin obtained US regulatory approval in 1991 and entered the market some time later [1–7]. From the structural prospective, these natural and semisynthetic statins are chiral 3,5-dihydroxyheptanoic acids that bind at C-7 to the substituted chiral unsaturated decalin core. The 3,5-dihydroxyheptanoic acid structural motif has been shown to be responsible for the pharmacological activity of statins [8].

## 1.2 Fully Synthetic Statins: Super-Statins

The quest for more potent statins continued at the level of these natural and semisynthetic analogs. Indeed, the first generation of statins underwent significant structural modifications as a result of huge research efforts by many pharmaceutical companies. This led to the modification of the substituent at the C-7 terminus of the 3,5-dihydroxyheptanoic acid pharmacophore, and in some cases, the C=C double bond replaced the C-C bond on the C-6 to C-7 position of the C-7 acid moiety. These structural refinements resulted in the second generation of statins, which are also frequently referred to as super-statins, where the decalin core of the natural ancestors has been replaced by heterocyclic motifs.

As a result of these refinements, fluvastatin (1994), atorvastatin (1997), rosuvastatin (2003), and pitavastatin (2009) (Fig. 2) were developed and launched on the market as more efficient and potent statin alternatives [9–18]. In addition, cerivastatin (Fig. 2) also entered the market in 1998. However, it was withdrawn from use in 2001, as when used concomitant to gemfibrozil, its action was associated with severe rhabdomyolysis, which resulted in renal failure, thus causing several fatal events [19].

Although all of the marketed super-statins have a chiral C-7 diol lateral chain as a common essential structural element, along with additional common structural features like the *F-p*-Ph substituent, there are some distinct structural differences among these super-statins. Indeed, indole ring system containing fluvastatin is the only racemic compound among super-statins. The pyrrole-based atorvastatin is the only super-statin that has a fully saturated chiral C-7 diol lateral chain. The

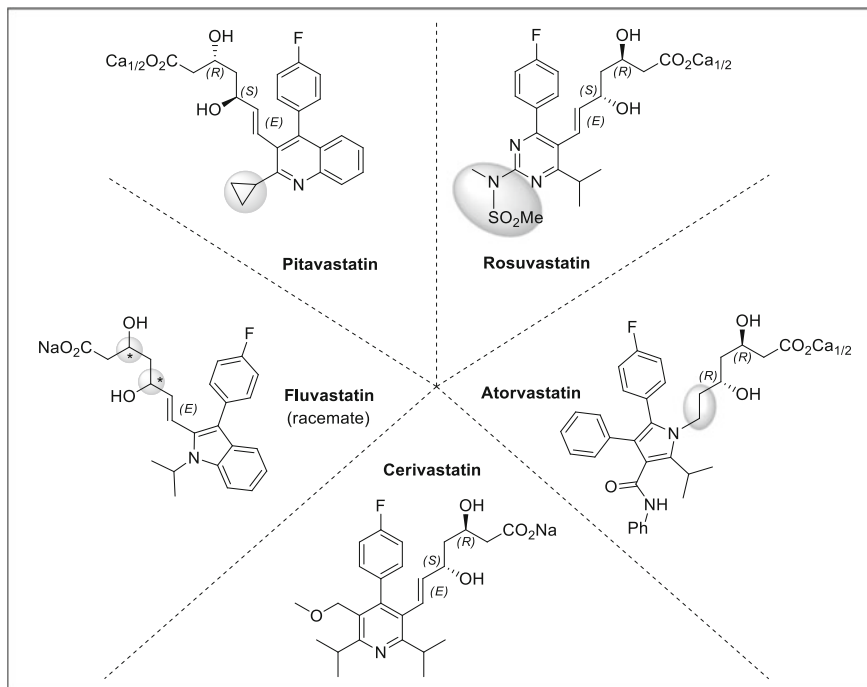


**Fig. 2** Structures of super-statins that have reached the market

pyrimidine motif comprising rosuvastatin is the only group member that contains the lipophilic sulfoneamide group, while the quinoline grounded pitavastatin is the only compound that contains *c*-Pr instead of the *i*-Pr substituent on the heterocyclic moiety. Therefore, as well as the synthetically challenging 3,5-dihydroxyheptenoic (heptanoic) acid scaffold, this rich pattern of substitutions on the heterocyclic cores for each of the marketed super-statins provides a diverse array of options for their construction. Consequently, the huge market potential and the structural diversity of the super-statins have created a rich area of synthetic heterocyclic chemistry [9–18].

### 1.3 Hepatoselective Super-Statins

In the years subsequent to the market entry of these super-statins, clinical practice for the patients with low to moderate risk of cardiovascular diseases has demonstrated that their current treatment regimens allow safe and effective lowering of LDL-C, the main risk factor for cardiovascular diseases and coronary heart disease, which has resulted in primary and secondary prevention of coronary heart disease.

Nevertheless, this approach has not addressed the unmet medical need of patients at high risk of coronary heart disease. Interestingly, several prevention clinical trials have indicated that more aggressive high-dose statin therapy in combination with other complementary agents (e.g., cholesterol absorption inhibitors, like ezetimib) can provide the desired lower LDL-C levels also for high-risk patients and might give additional primary and secondary coronary heart disease prevention overall. However, these important findings have come up against the limitations associated with adverse side effects of high-dose statin therapy. Here, sufficient clinical evidence has demonstrated that elevated doses of statins can induce mild to moderate muscle pain or weakness, known as myalgia. In rare cases, if myalgia is not recognized and the high-dose statin regimen is continued, this can result in life-threatening rhabdomyolysis and the consequent renal failure. Although the origin of this statin-induced myalgia is not fully understood, it is thought to relate to disrupted metabolic processes in non-hepatic tissues, like muscle. Therefore, considerable interest has emerged for the design of statins that are more selectively absorbed in hepatic tissues compared to non-hepatic tissues.

The existing clinical data related to the occurrence of myalgia and the statin lipophilicity data have suggested that the hepatoselectivity of statins correlates with their degree of lipophilicity. For example, rosuvastatin is the most potent and hydrophilic statin ( $\log D = -0.33$ ), and it has demonstrated higher affinity towards hepatocytes compared to more lipophilic statins (e.g., cerivastatin, simvastatin;  $\log D > 1.5$ ). The rationale for this behavior was based on the hypothesis that more hydrophilic statins are inherently less membrane permeable and thus tend to enter hepatocytes only via the active transport mechanisms based on anion-transporting polypeptides. In contrast, the hydrophobic statins can enter hepatocytes and myocytes nonselectively via a passive diffusion, which raises the peripheral tissue exposure. These concepts implied that hepatoselective statins can be obtained by lowering their lipophilicity [20, 21].

Over the last decade, these findings have triggered extensive research efforts by several pharmaceutical companies towards a new generation of super-statins (i.e., the third-generation super-statins) that show increased hepatoselectivity and potency. These studies have been focused on modifications to the heterocyclic cores of the known super-statins, while the 3,5-dihydroxyheptanoic/heptenoic acid moiety has generally remained unaltered [22–37]. Based on its overall favorable safety profile and efficiency in comparison to the other super-statins, a modification of the atorvastatin pyrrole heterocyclic core has been studied extensively in this context. As a consequence, several new hepatoselective analogs of atorvastatin were derived, such as **1** [22], **2** [22], **3** [23], **4** [27, 29], **5** [29], **6** [29], **7** [29], and **8** [35]. Similarly, more hepatoselective derivatives of rosuvastatin (e.g., derivative **9**) have been investigated [28, 30]. Quinoline derivatives analogous to pitavastatin (e.g., derivative **10**) have also been identified as interesting targets in this context [25, 32, 36]. In addition, drug candidates based on other heterocyclic motifs that had previously been less frequent in statin chemistry, such as pyrazole (e.g., derivatives **11**, **12**, **13**) [24, 26, 31, 34] and imidazole (e.g., derivatives **14**, **15**) [29, 33], have also been prepared and investigated within this framework (Fig. 3).

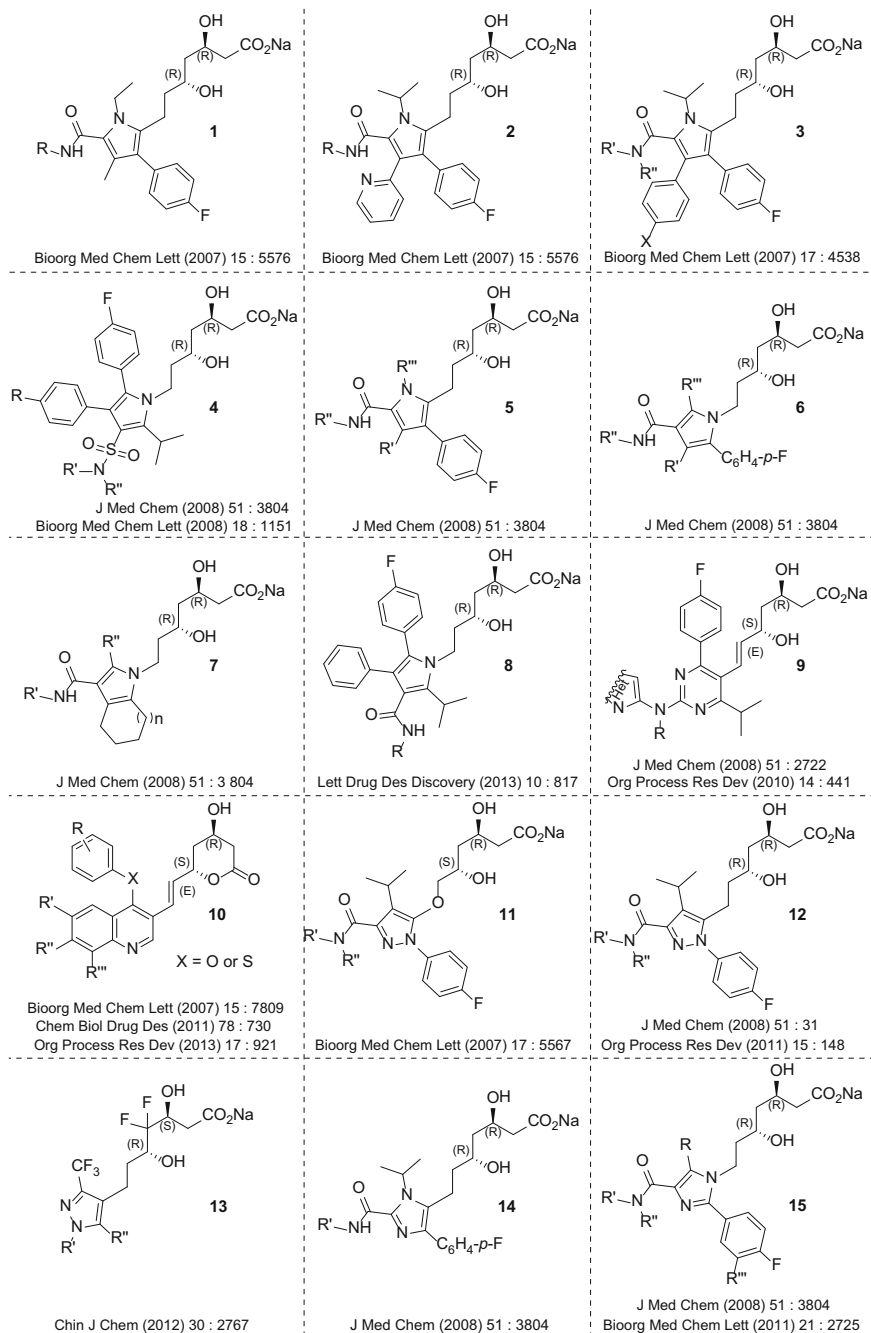
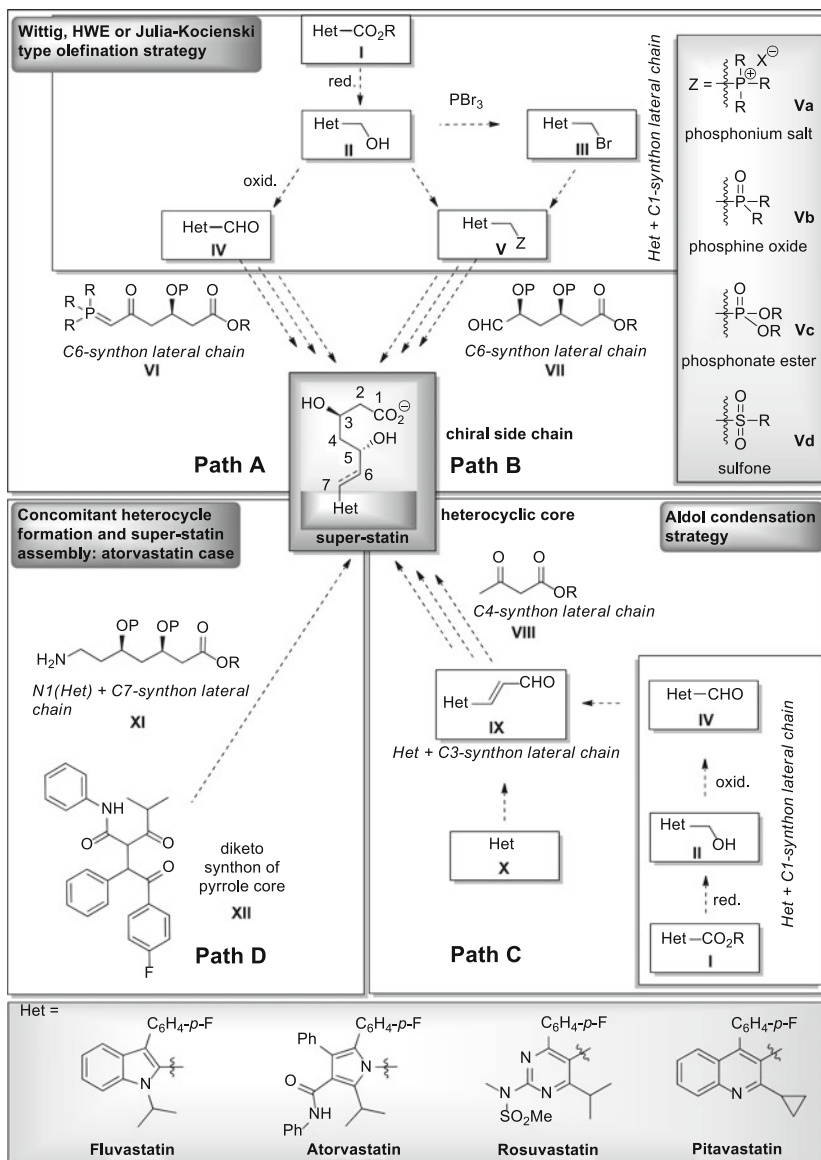


Fig. 3 Structures of the investigational super-statins

Interestingly, derivatives **13** are the only examples where the 3,5-dihydroxyheptenoic acid moiety modification has been investigated, through fluorination, in parallel with the introduction of a pyrazole core [34]. Some of these derivatives have already passed into clinical development, and viable processes for their efficient and practical preparation that would meet regulatory requirements have been reported [30, 31]. These reports represent masterpieces in heterocyclic process chemistry and are valuable additions to a general heterocyclic chemistry [30, 31].

#### 1.4 Main Synthetic Strategies Towards Super-Statins

Due to the structural diversity of the family of super-statin derivatives that has originated from these “highly decorated” heterocyclic scaffolds, the synthetic approaches needed constitute a rich plethora of methodologies [15]. Among these, a few distinct approaches have surfaced as the most commonly used strategies for the synthesis of these super-statins (Scheme 1). The most frequently used approaches to C=C bond containing super-statins involve the coupling of HetCHO (**IV**) with the C-6 phosphorane-type precursor (**VI**) of the lateral chain (Scheme 1, path A) or the coupling of various phosphorus-derivatized (**Va–c**) or sulfone-type (**Vd**) heterocyclic precursors with formyl-derivatized C-6 precursors (**VII**) of the lateral chain (Scheme 1, path B). Both types of the heterocyclic precursors (**IV**) and (**V**) can be accessed from the common starting ester derivative (**I**). Carboxylate (**I**) is initially reduced to an alcohol intermediate (**II**), which can be easily oxidized to an aldehyde derivative (**IV**). Moreover, the alcohol (**II**) can be transformed to phosphorous-containing derivatives (**V**) via alcohol activation, using an active ester approach followed by the reaction with phosphorous precursors. Alternatively, bromination of alcohol (**II**) with  $\text{PBr}_3$  results in the formation of the alkylbromide derivative (**III**) that gives (**V**) upon displacement of the bromine with various phosphorous precursors. Another interesting approach to the C=C bond containing super-statins is based on the Ti-species-catalyzed asymmetric aldol condensation of acetoacetate esters (**VIII**, C-4 units) with an “extended” aldehyde derivative (**IX**) that already contains three atoms of the future lateral chain and a C=C bond with the desired *E*-geometry (Scheme 1, path C). The advantage of this approach is the low content of the *Z*-isomer, which is not avoidable at considerable levels in various Wittig- or Horner–Wadsworth–Emmons-type olefinations, while the stereoselectivity of the Ti-catalyzed aldol condensation and the subsequent Prasad reduction is usually very high (>99%). The HetCH=CHCHO (**IX**) can be formed directly from the unfunctionalized Het (**X**) precursor or HetCHO (**IV**). The unique feature of atorvastatin is that the attachment of the lateral chain to the heterocyclic nucleus is through the endocyclic nitrogen atom of the pyrrole core and not through the endocyclic carbon atom, as in other super-statins. Consequently, different techniques have evolved for the assembly of atorvastatin compared to other super-statins. Therefore, the most convenient



Scheme 1 Key synthetic strategies for the super-statins

and industrially widely used approach for assembly of atorvastatin is based on pyrrole ring formation by condensation of the C-7 lateral-chain precursor (XI) already containing the amino moiety with diketone precursor (XII) under the Paal-Knorr conditions (Scheme 1, Path D).

Last but not least, many of other coupling/olefination approaches for the assembly of the heterocyclic core and the lateral-chain precursors into super-statins have also evolved (e.g., Heck, Sonogashira, Julia-Kocienski). However, to our knowledge, they have not been used in the industrial setting and commercialized, due to the high cost of the catalysts used or the commercially less frequently used unique precursors [15].

## 2 Synthesis of Chiral Super-Statins Lateral Chain Precursors

### 2.1 Structure of Advanced Super-Statins Lateral Chain Precursors

As the chiral 3,5-dihydroxyheptanoic acid derivatives represent the key pharmacophore in all of the super-statins [8], major efforts of the academic and industrial communities have been made for their efficient preparation [38–46]. In the course of time, biocatalysis [47–62] evolved as an important platform for greener and more efficient and stereoselective synthesis of 3,5-dihydroxyheptanoic (heptenoic) acid precursors [63–75]. Furthermore, due to the hydroxyl group that contains stereogenic centers in this fragment of super-statins, the corresponding precursors represent a great synthetic challenge in terms of the high stereochemical purity requirements imposed by regulatory requirements. Over the past decades, several precursors that are suitable for the construction of the statin chiral *syn*-1,3-diol C-7 acid moiety evolved. In general, these can be divided into the open side-chain derivatives **XIII–XIV** and the cyclic analogs **XV** (e.g., lactol and lactone derivatives). Synthetic practice has established monoprotected and diprotected open-chain derivatives as the most frequently used precursors for super-statin assembly. These precursors can be either phosphorus (**XVI**) or formyl (**XVII**) derivatives at their terminus, which allow for various Wittig- or Horner–Wadsworth–Emmons-type olefination approaches with the corresponding heterocyclic precursors. When the assembly of atorvastatin is considered, the C-7 precursors **XVIII** conveniently contain an amino-group terminus. Interestingly, the discovery of an efficient and highly stereoselective deoxyribose-5-phosphate aldolase (**DERA**)-catalyzed assembly of the chiral lactols from simple achiral materials like acetaldehyde and its analogs [76–80] has recently defined the lactone derivatives **XIX–XXI** as interesting precursor alternatives of the super-statin chiral lateral chain [81–84] (Fig. 4).

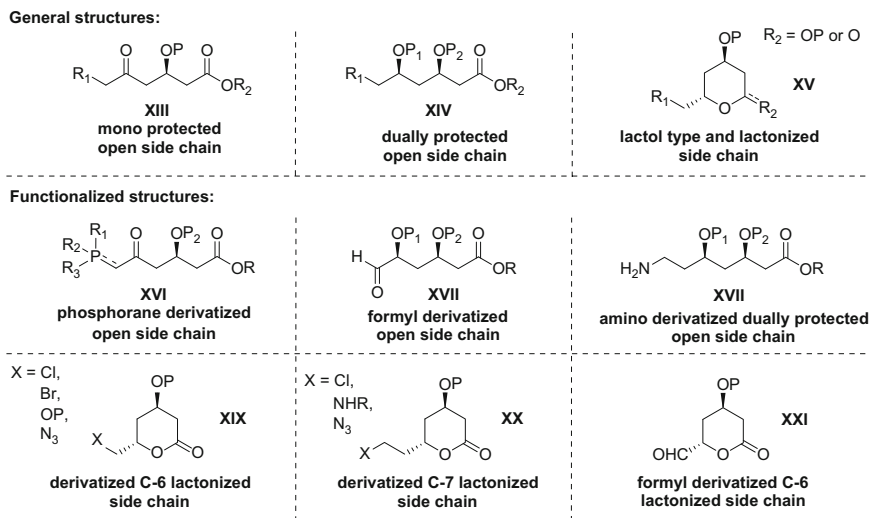
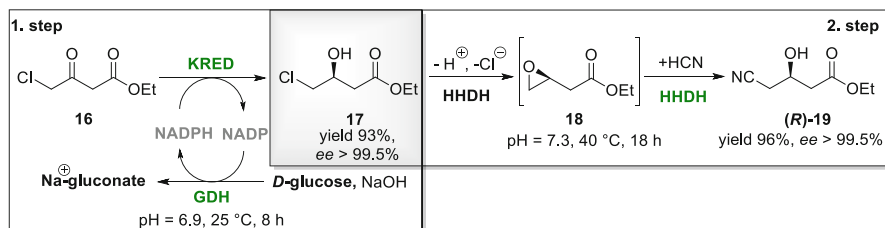


**Fig. 4** Structures of the most frequently used advanced C-6 and C-7 super-statin chiral lateral-chain precursors

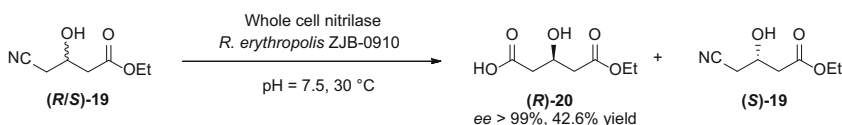
## 2.2 New Developments in the Area of Super-Statins Lateral-Chain Precursors

Ma et al. [85] developed an outstanding green-by-design biocatalytic process for the atorvastatin lateral-chain building block (*R*)-**19**. DNA shuffling technology enabled them to significantly improve the activity of the enzymes used in the proposed process (Scheme 2). In the first step, the reduction of ethyl-4-chloroacetate **16** using a mutant ketoreductase (**KRED**) in combination with glucose and an **NADP**-dependent glucose dehydrogenase (**GDH**) for the cofactor regeneration provided (*S*)-ethyl-4-chloro-3-hydroxybutyrate **17** at 96% isolated yield and with *ee* > 99.5% and 98% chemical purity at 160 g/L substrate loading. This reaction was complete in 8 h at 25°C in an aqueous buffer at pH 6.9 using 0.9 g/L biocatalyst. In the sequential step, halohydrin dehalogenase (**HHDH**) converted **17** to **18**, which was transformed in situ in the presence of NaCN to (*R*)-**19** at 40°C in 18 h, at 92% yield. This optimal outcome was obtained at pH 7.3 using 0.9 g/L of biocatalyst. The product (*R*)-**19** had a purity >99.5% and *ee* > 99.5%. Remarkably, the overall process allowed access to highly pure (*R*)-**19** with significantly improved productivity and multiple “green” features, which provided an E-factor of 5.8 (without counting the process water).

Dong et al. [86] described a convenient synthesis of (*R*)-ethyl-3-hydroxyglutarate (*R*)-**20** with high optical purity, via (*R*)-enantioselective hydrolysis of the racemic ethyl 4-cyano-3-hydroxybutyrate (*R/S*)-**19** using the nitrilase-containing whole cells of *Rhodococcus erythropolis* (Scheme 3). Indeed, a fast screening method that was based on a colorimetric complexation reaction between



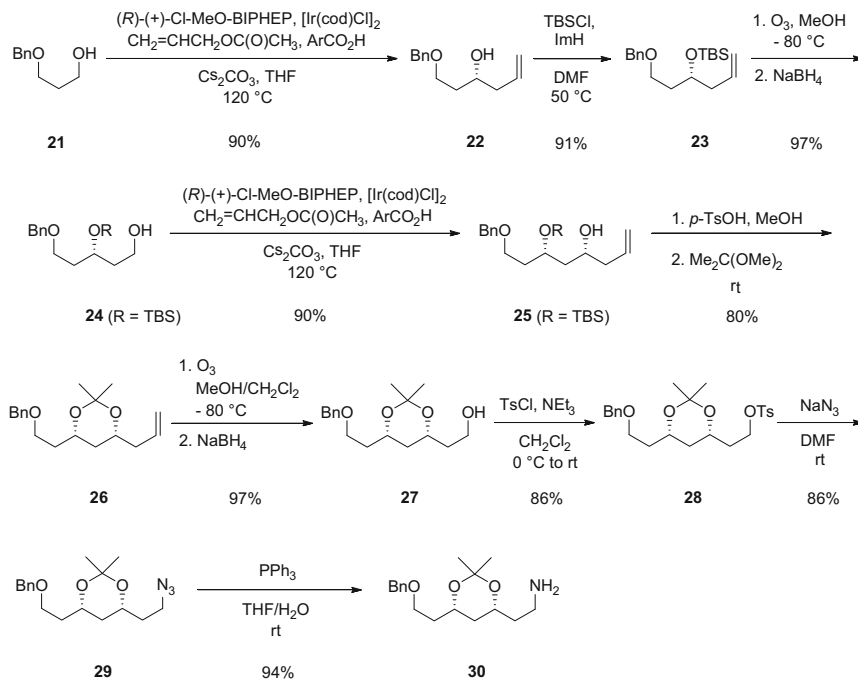
**Scheme 2** The Sheldon two-step, three-enzyme process to (*R*)-**19** from **16**



**Scheme 3** (*R*)-enantioselective hydrolysis of the racemic nitrile (*R/S*)-**19**

$\text{Co}^{2+}$  and ammonia (which is released upon hydrolysis of the cyano group) enabled Dong et al. [86] to identify the nitrilase-producing strain ZJB-0910, which provided (*R*)-enantioselective hydrolysis of (*R/S*)-**19** to (*R*)-**20** and (*S*)-**19** without concomitant hydrolysis of the ester bond. The optimized reaction conditions (pH 7.5, 30°C, 20 mM of substrate) enabled them to prepare (*R*)-**20** at 46.2% yield and  $ee > 99\%$ .

A new synthesis of a C-7 atorvastatin lateral-chain precursor was described by Sawant and Maier [87] (Scheme 4). The starting benzyloxy-propanol **21** was first subjected to the Krische asymmetric transfer hydrogenative carbonyl allylation using iridium *C,O*-benzoate generated in situ from  $[\text{Ir}(\text{cod})\text{Cl}]_2$ , (*R*)-(+)-Cl, MeO-BIPHEP, and 4-chloro-3-nitro-benzoic acid in the presence of  $\text{Cs}_2\text{CO}_3$  in tetrahydrofuran (THF) at 120°C, to provide **22**. The (3*R*)-1-(benzyloxy)hex-5-en-3-ol **22** was obtained at an excellent 90% yield and with high optical purity (er, 96:4). The subsequent hydroxyl group protection with *tert*-butyldimethylsilyl chloride (TBSCl) in the presence of imidazole provided the *O*-TBS protected alcohol **23** at 91% yield. In the next step, **23** was subjected to a low-temperature ozonolysis, followed by the reduction of the aldehyde formed with  $\text{NaBH}_4$ , which furnished the alcohol **24** at an excellent 97% yield. This alcohol **24** was submitted to another asymmetric transfer hydrogenative carbonyl allylation using the same conditions as in the first step here, to provide the *syn*-diol derivative **25** at 90% yield. Next, the *tert*-butyldimethylsilyl (TBS) moiety was removed in the presence of *p*-toluenesulfonic acid (*p*-TsOH) in MeOH, and the acetonide-protecting group was put onto the hydroxyl groups to provide the fully protected triol **26** at 80% yield. The use of an ozonolysis/reduction sequence for **26** resulted in the generation of the fourth hydroxyl group within the molecule and provided the polyol **27** at 97% yield. The free -OH group in **27** was reacted with TsCl in the presence of triethylamine ( $\text{NEt}_3$ ) in  $\text{CH}_2\text{Cl}_2$ , to provide the tosylate **28**, which was reacted with  $\text{NaN}_3$  in dimethylformamide (DMF) to provide the azide **29** (with each step at 86% yield). In

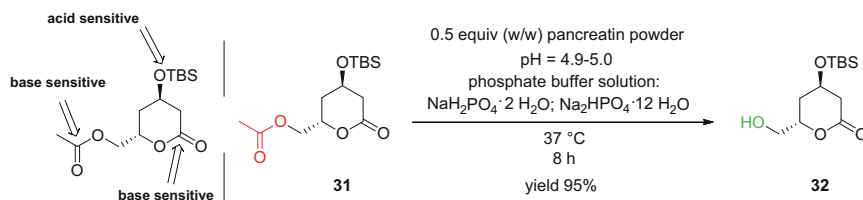


**Scheme 4** Synthesis of the C-7 lateral atorvastatin side-chain precursor **21**

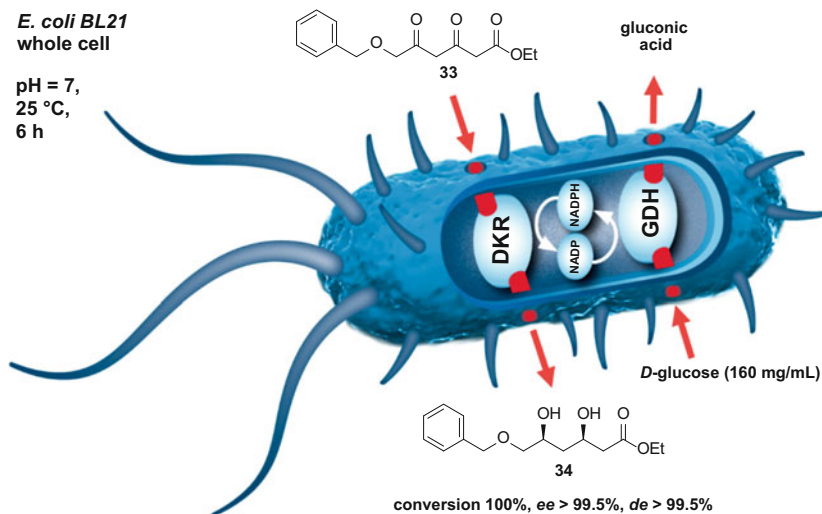
the last step, the amine **30** was isolated at 94% yield after the reduction of **29** with triphenylphosphine ( $\text{PPh}_3$ ) in  $\text{THF}/\text{H}_2\text{O}$  as a solvent.

We have recently reported a chemoselective pancreatin powder-catalyzed deacetylation reaction of ((2*S*,4*R*)-4-(*tert*-butyldimethylsilyloxy)-6-oxotetrahydro-2*H*-pyran-2-yl)methyl acetate **31**, which provides the corresponding (4*R*,6*S*)-4-(*tert*-butyldimethylsilyloxy)-6-(hydroxymethyl)-tetrahydro-2*H*-pyran-2-one **32** [88]. The lactone **32** has been recently established as a precursor of the superstatin lateral chain [83, 84]. The compound **31** has a relatively complex structure, as it contains both acid-sensitive (TBS protecting group) and base-sensitive (lactone ester bond, acetyl protecting group) groups, which makes the chemoselective removal of the acetyl group a challenging task. Indeed, screening of various reagents has demonstrated that only enzymatic reactions are sufficiently chemoselective to allow a preservation of the lactone ring. The optimized reaction conditions enables transformation of **31** to **32** at 95% isolated yield using a pure aqueous medium containing phosphate buffer to maintain the pH between 4.9 and 5.0, over 8 h at 37°C with 0.5 equiv. (w/w) of the cheap pancreatin powder catalyst (Scheme 5). The described method provides a greener and significantly more efficient approach to the production of **32** compared to the previous method based on the toxic tin catalysis [83].

An interesting report by Wu et al. [89] defined the activity and behavior of a dual enzyme system that consisted of diketoreductase (**DKR**) and **GDH** in a whole-cell



**Scheme 5** Chemoselective pancreatin-powder-catalyzed deacetylation of **31**

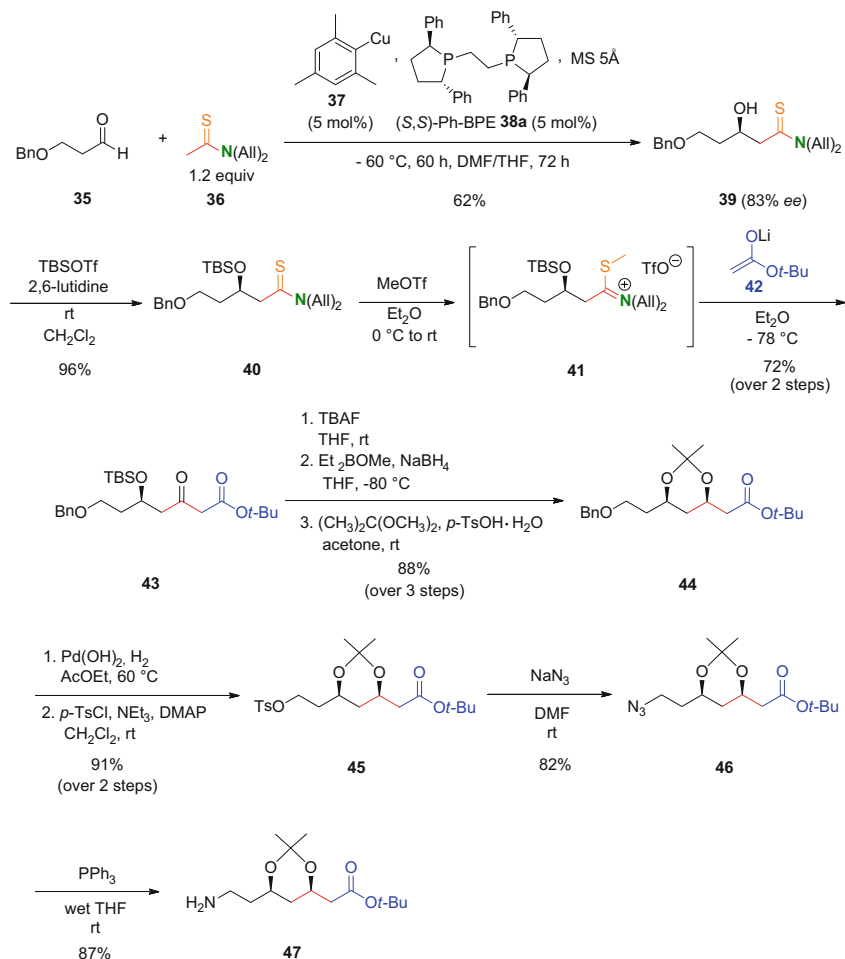


**Scheme 6** An efficient reduction of diketone **33** to *syn*-1,3-diol **34** using recombinant *E. coli* cells that co-express diketoreductase and glucose dehydrogenase

biocatalytic system for the reduction of ethyl 3,5-diketo-6-benzyloxy hexanoate **33** to ethyl 3*R*,5*S*-dihydroxy-6-benzyloxy hexanoate **34** (Scheme 6). The main challenge that was addressed in this study was the low substrate loads and the necessity for exogenous cofactors for the efficient reduction of **33** to **34** by **DKR** as described in previously reported approaches. Therefore, **DKR** and **GDH** from *Bacillus megaterium* were expressed in *Escherichia coli* cells, to take an advantage of the intracellular cofactors in the *E. coli* cells. It was established that the best enzymatic activity was obtained with *E. coli* cells harboring *pETDuet-gdh-dkr* after 14 h of incubation, which provided a complete conversion of **33** at 5 mg/mL of substrate. Surprisingly, it was discovered that even higher initial loads of **33** (8 mg/mL) can be completely converted to **34** if **33** is added to the fermentation broth containing the biocatalyst after 14 h of induction (14–20 h). This unexpected behavior was explored, and its origin was shown to be associated with a dynamic change in the intracellular cofactor concentration. After determination of the correlation between cofactor concentration and catalytic efficiency, the optimized reaction conditions were set at pH 7, 25°C, and 160 mg/mL glucose. Under these conditions, **33** was completely converted to **34** (*ee*, *de* >99.5%) in 6 h.

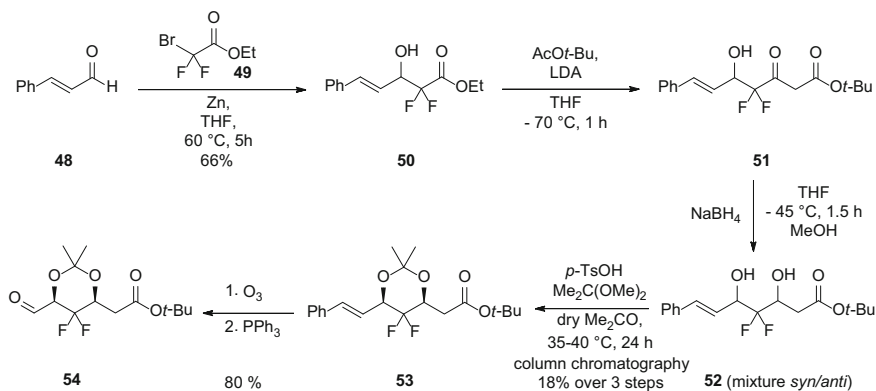
A novel route to the production of the C-7 atorvastatin lateral-chain precursor was described by Kawato et al. [90], who developed a novel aldol condensation methodology for this purpose. Indeed, the direct catalytic asymmetric aldol reaction of the 3-benzyloxypropanal **35** with the thioamide **36** was established with a newly developed second-generation catalytic system based on mesitylcopper **37**/*(S,S)*-Ph-BPE **38a**, which was shown to be superior to the previous system that was developed by the same authors. Indeed, when the 3-benzyloxypropanal **35** was reacted with **36** (1.2 equiv.) in the presence of the mesitylcopper **37** and *(S,S)*-Ph-BPE **38a** (both at 5 mol%) and molecular sieves (MS) 5 Å (1 g/mmol **35**) at  $-60^{\circ}\text{C}$  in DMF/THF for 72 h, the secondary alcohol **39** was obtained at 62% yield and *ee* 83%. In the next step, the secondary hydroxyl group was silyl protected using *tert*-butyldimethylsilyl trifluoromethanesulfonate (TBSOTf)/2,6-lutidine, to give the TBS-protected alcohol **40** at 96% yield. Activation of the thioamide group in **40** via an alkylation with methyl triflate at room temperature provided the thioimidate salt **41**, which was reacted in situ with the lithium enolate of *t*-butyl acetate **42** at  $-78^{\circ}\text{C}$ . This resulted in the formation of the  $\beta$ -hydroxyketone intermediate **43** at a high 72% yield over two steps. Subsequently, **43** was subjected to an efficient telescoped deprotection–reduction–protection sequence of tetrabutylammonium fluoride (TBAF)-mediated removal of the TBS protecting group, the Prasad diastereoselective 1,3-*syn* reduction of the keto moiety, and an installation of the acetonide-protecting group onto the derived *syn*-1,3-diol, to provide the ester **44** at a remarkable 88% yield over three steps. The subsequent one-pot deprotection–activation sequence that consisted of a benzyl ether deprotection with the Pd(OH)<sub>2</sub> catalyst at  $60^{\circ}\text{C}$  and 1 atm H<sub>2</sub> pressure followed by a tosylate ester formation with TsCl/4-(dimethylamino)pyridine (DMAP) provided the tosylate **45** at 91% yield over two steps. The ensuing azido-substitution reaction of the tosylate derivative **45** with NaN<sub>3</sub>/DMF at room temperature resulted in the formation of the azide **46** at 82% yield. Finally, the Staudinger reduction of **46** with PPh<sub>3</sub> in wet THF at room temperature provided the amino-derivatized C-7 atorvastatin lateral-chain precursor **47** at 87% yield (Scheme 7).

Recently, Wang et al. [91] reported the preparation of the *gem*-difluoromethylenated acetonide **53** at 15% to 20% overall yield. Their route started with the zinc-mediated Reformatsky reaction of cinnamyl aldehyde **48** and ethyl 2-bromo-2,2-difluoroacetate **49**, which provided the ester derivative **50** at 66% yield. In the next step, the Claisen condensation between **50** and lithium enolate of *t*-butyl acetate, which was derived in situ from *tert*-butyl acetate and lithium diisopropylamide (LDA), at  $-70^{\circ}\text{C}$  provided the  $\delta$ -hydroxy- $\beta$ -keto ester **51**. The reduction of **51** with NaBH<sub>4</sub> at  $-45^{\circ}\text{C}$  gave the mixture of *syn/anti*-1,3-diols **52**. Next, the acetonide-protected *syn*-1,3-diol **53** was obtained at 18% yield over three steps after treatment of **52** with 2,2-dimethoxypropane and *p*-toluenesulfonic acid in dry acetone, followed by purification on silica gel using column chromatography. Finally, the *gem*-difluoromethylenated aldehyde **54** was isolated at 80% yield when the olefin **53** was subjected to an ozonolytic cleavage (Scheme 8).



**Scheme 7** Synthesis of the C-7 atorvastatin lateral-chain precursor via a direct catalytic asymmetric aldol reaction of thioamides

An interesting methodology for the Ru-catalyzed asymmetric hydrogenation of  $\epsilon$ -substituted  $\delta$ -ketal- $\beta$ -keto esters **55** in the presence of catalytic amounts of  $\text{CaCO}_3$  was recently developed by Fan and coworkers [92] (Table 1). They envisioned that  $\epsilon$ -substituted  $\delta$ -ketal- $\beta$ -keto esters **55** can serve as convenient starting materials for the preparation of  $\epsilon$ -substituted  $\delta$ -ketal- $\beta$ -hydroxy esters **56**, which can easily be converted to phosphorous- or phosphorane-derivatized super-statin lateral-chain precursors that have one chiral center (Fig. 4) if the keto group within esters **55** can be efficiently enantioselectively reduced. Surprisingly, the initial experiments on **55a** using the  $[\text{RuCl}(\text{benzene})(S)\text{-SunPhos}]\text{Cl}$  catalyst (20 bar  $\text{H}_2$ ,  $55^\circ\text{C}$ , S/C 250, 10 h) demonstrated that product **56a** with the diethoxy ketal functionality had notable instability towards the acidic reaction conditions. Consequently, the

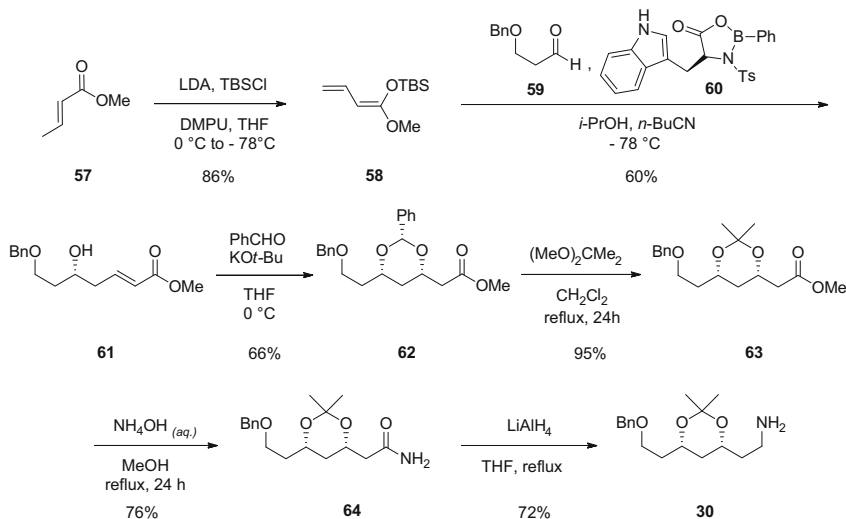


**Scheme 8** Synthesis of the fluorinated C-6 chiral super-statin lateral-chain precursor

**Table 1** Asymmetric hydrogenation of **55** using  $[\text{RuCl}(\text{benzene})(S)\text{-SunPhos}]\text{Cl}$  catalyst in the presence of  $\text{CaCO}_3$

Entry	$R''$	$R$	$R'$	<b>56</b>	$T$ (°C)	Solvent	Yield (%)	$ee$ (%)
1	Cl	Et	Me	<b>56a</b>	55	EtOH	97	99.2
2	Cl	Et	Et	<b>56b</b>	55	EtOH	95	99.4
3	Cl	Me	Me	<b>56c</b>	55	MeOH	91	99.2
4	BnO	$-(\text{CH}_2)_2$	Me	<b>56d</b>	65	EtOH	93	99.2
5	BnO	$-(\text{CH}_2)_2$	Et	<b>56e</b>	75	EtOH	91	99.2
6	BnO	$-(\text{CH}_2)_2$	<i>t</i> -Bu	<b>56f</b>	55	EtOH	95	99.6

deprotected 6-chloro-3-hydroxy-5-oxohexanoate derivative was formed and decomposed to multiple unidentifiable side products, which created an additional challenge from the practical prospective. The subsequent screening of basic additives on **55a** that should compensate for the acidity issue revealed that the product instability problems were addressed when a catalytic amount of  $\text{CaCO}_3$  was added to the reaction system. This established  $[\text{RuCl}(\text{benzene})(S)\text{-SunPhos}]\text{Cl}/\text{CaCO}_3$  as the ultimate catalytic system that performed the reduction of super-statin-relevant substrates **55a–f** with a remarkable enantioselectivity at 55–75 °C and 60 bar  $\text{H}_2$  with S/C of 250/1 in EtOH or MeOH. Under these conditions, the excellent isolated yields of products **56a–f** that ranged from 91% to 97% (entries 1–6) were obtained. Furthermore, the  $\epsilon$ -chloro-substituted  $\delta$ -ketal- $\beta$ -keto esters **55a–c** with an acyclic ketal moiety gave superb enantioselectivities that ranged from  $ee$  99.2% to 99.4% (entries 1–3). Moreover, the  $\epsilon$ -benzyloxy-substituted  $\delta$ -ketal- $\beta$ -keto esters **55d–f** (entries 4–6) that contained a cyclic ketal moiety gave equally outstanding

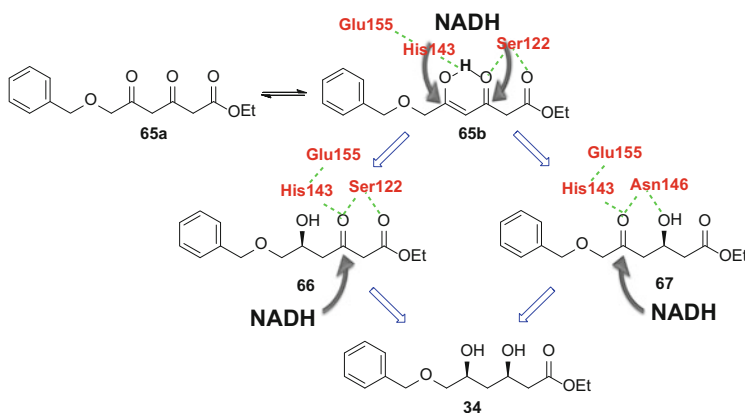


**Scheme 9** Synthesis of the C-7 amino-derivatized atorvastatin lateral-chain precursor via the Mukaiyama aldol reaction

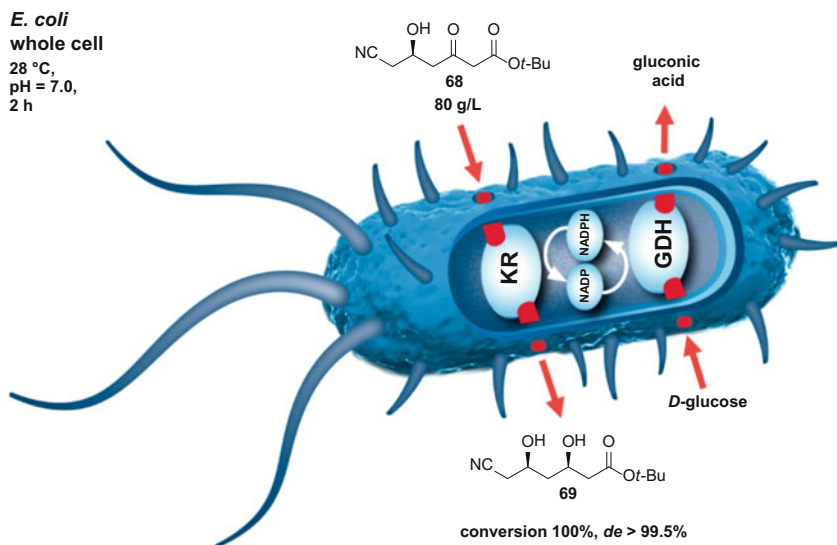
enantioselectivities that ranged from *ee* 99.2% to 99.6%, albeit at higher temperatures (65–75 °C) for derivatives **55d–e** (entries 4–5).

A concise simple (when compared to that of Scheme 4) six-step approach to obtain the C-7 amino-derivatized atorvastatin lateral-chain precursor **30** was also reported by Sawant and Maier [93] (Scheme 9). In the first step, the ketene acetal **58** was prepared at 88% yield by the treatment of methyl crotonate **57** in THF with LDA, followed by the addition of TMSCl, at low temperatures. In the second step, the first hydroxyl group with the chiral center and the C-7 skeleton of the superstatin lateral chain were assembled by an enantioselective vinylogous Mukaiyama aldol reaction, which involved vinylogous silyl ketene acetal **58** and benzyloxypropanal **59** in the presence of tryptophane-based *B*-phenyloxazaborolidinone Lewis acid **60**, at low temperature and in the presence of *i*-PrOH in *n*-BuCN. The desired 5-hydroxyheptenoate **61** was obtained at a reasonable 60% yield and *ee* of 88%, according to Mosher ester analysis. The protected *syn*-1,3-diol structure was constructed from **61** via the Evans diastereoselective base-catalyzed intramolecular conjugate addition of a hemiacetal-derived alkoxide, which was formed from the alcohol **61** and benzaldehyde, in the presence of KO*t*-Bu in THF at 0 °C. The expected benzylidene acetal **62** was obtained at 66% yield as a single stereoisomer. The subsequent cleavage of the benzylidene acetal-protecting group and installation of acetonide protection on the vicinal dihydroxyl groups provided the ester **63** in a single step at an excellent 95% yield, using *p*-TsOH and 2,2-dimethoxypropane in refluxing dichloromethane. Next, the ester **63** was converted to the amide derivative **64** at 76% yield, with aqueous NH<sub>3</sub> in methanol under reflux. The final reduction of the amide **64** with LiAlH<sub>4</sub> in THF under reflux provided the target amine **30** at 72% yield.

Recently, Lu and coworkers [94] explored the mechanistic background of the biocatalytic reduction of ethyl 6-(benzyloxy)-3,5-dioxohexanoate **65a** by **DKR**, a homodimeric protein of 283 amino acids. Although **DKR** was effective in dicarbonyl compound reductions, the mechanistic understanding of the **DKR** catalysis remained elusive. Thus, Lu and coworkers [94] solved the crystal structures of the apoenzyme and the binary complexes with NADH and NAD<sup>+</sup>. In addition, a molecular docking, a molecular dynamics simulation, and biochemical analyses were used to define the two-step dicarbonyl reduction of **65a** to the well-known super-statin precursor (3*R*,5*S*)-ethyl 6-(benzyloxy)-3,5-dihydroxyhexanoate **34**. Lu and coworkers [94] realized that diketone **65a** is in its enol tautomeric form **65b** at the catalytically relevant pH 6.0, where **DKR** is the most active. Therefore, the intramolecular hydrogen-bond-driven cyclic six-membered ring structure **65b** was used for further examination. Thus, to identify the catalytically relevant residues within **DKR** that are responsible for the dicarbonyl reduction, interactions between **65b** and **DKR** were probed using molecular docking and molecular dynamics simulations. The results of these studies revealed that the reduction of **65** is through two distinctive steps. In the first, **Ser122**, **His143**, and **Glu155** are clustered through a hydrogen-bonding network to form the catalytic triad that is responsible for the reduction of both the β-carbonyl and δ-carbonyl groups of substrate **65b**, which leads to the (*S*)-ethyl 6-(benzyloxy)-5-hydroxy-3-oxohexanoate **66** and (*R*)-ethyl 6-(benzyloxy)-3-hydroxy-5-oxohexanoate **67**. Finally, in the second step, the reduction of the remaining carbonyl groups in **66** and **67** proceeds via different catalytic pathways using different active sites within **DKR**. Interestingly, the same catalytic triad of **Ser122**, **His143**, and **Glu155** that is responsible for the reduction of the dicarbonyl compound **65b** in the first step is responsible for the reduction of the mono-carbonyl intermediate **66** to *syn*-1,3-diol **34**. On the other hand, the δ-carbonyl reduction of **67** proceeds via the assistance of a different catalytic cluster, where the key residue is **Asn146** (Scheme 10).



**Scheme 10** Pathways of diketoreductase-catalyzed bioreduction of 6-(benzyloxy)-3,5-dioxohexanoate **65a** to diol **34**



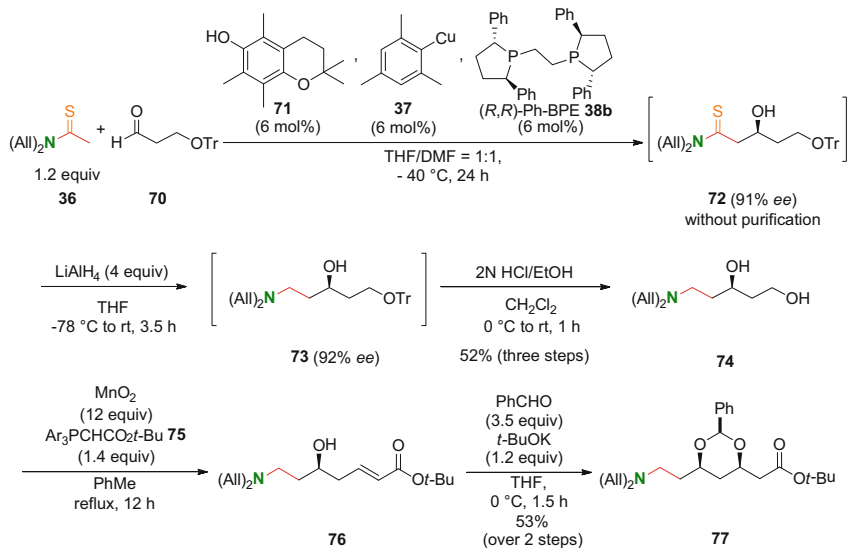
**Scheme 11** Biocatalyzed approach to the C-7 chiral atorvastatin lateral-chain precursor using *E. coli* cells expressing **KR** and **GDH** for a cofactor regeneration

A new recombinant 2-deoxyribose-5-phosphate aldolase (**DERA**) was synthesized by You et al. [95], who used *E. coli* BL21 (DE3) and the plasmid pET-28b for its expression. After this recombinant expression and the purification (2.3-fold at 56.3% yield) and characterization, the key biochemical attributes of this new **DERA** were evaluated. The optimal pH where the enzyme was stable was in a range of 4.0–7.0. The optimal activity of **DERA** was at 35°C, while the activity of the enzyme did not suffer any significant drop in the range from 20°C to 50°C. Also, the majority of metal ions, except Ni<sup>2+</sup>, Ba<sup>2+</sup>, and Fe<sup>2+</sup>, did not inhibit this **DERA**. All of this indicated that the newly prepared **DERA** can operate under mild conditions that are suitable for industrial applications. This new **DERA** was also efficient in the preparation of (3*R*,5*S*)-6-chloro-2,4,6-trideoxyhexose, a lactol-type precursor of the super-statin lateral chain (Fig. 4), through the reaction of chloroacetaldehyde and acetaldehyde. Indeed, the purified **DERA** provided almost a complete aldol condensation (94.4% conversion) of chloroacetaldehyde (80 mM) and acetaldehyde (160 mM) in 4 h at 35°C.

A whole-cell catalyst that used *E. coli* BL21 as a host for the co-expression of *R*-ketoreductase (**KR**) and **GDH** for cofactor regeneration was successfully constructed and used by Li and coworkers [96] for stereoselective reduction of *t*-butyl 6-cyano-(5*R*)-hydroxy-3-oxohexanoate **68** to *t*-butyl 6-cyano-(3*R*,5*R*)-dihydroxylhexanoate **69** (Scheme 11). The effects of multiple parameters on the progress of the asymmetric reduction were investigated to establish the optimal reaction conditions, including induction time, glucose, NADP<sup>+</sup> and substrate concentrations, temperature, and pH. This whole-cell biocatalyst performed optimally at 28°C and pH 7, with glucose to substrate ratio of 1:1 (w/w). Under these

conditions, 80.0 g/L loading of *t*-butyl 6-cyano-(5*R*)-hydroxy-3-oxohexanoate **68** was fully converted to *t*-butyl 6-cyano-(3*R*,5*R*)-dihydroxylhexanoate **69** in 2 h, with *de* > 99.5%.

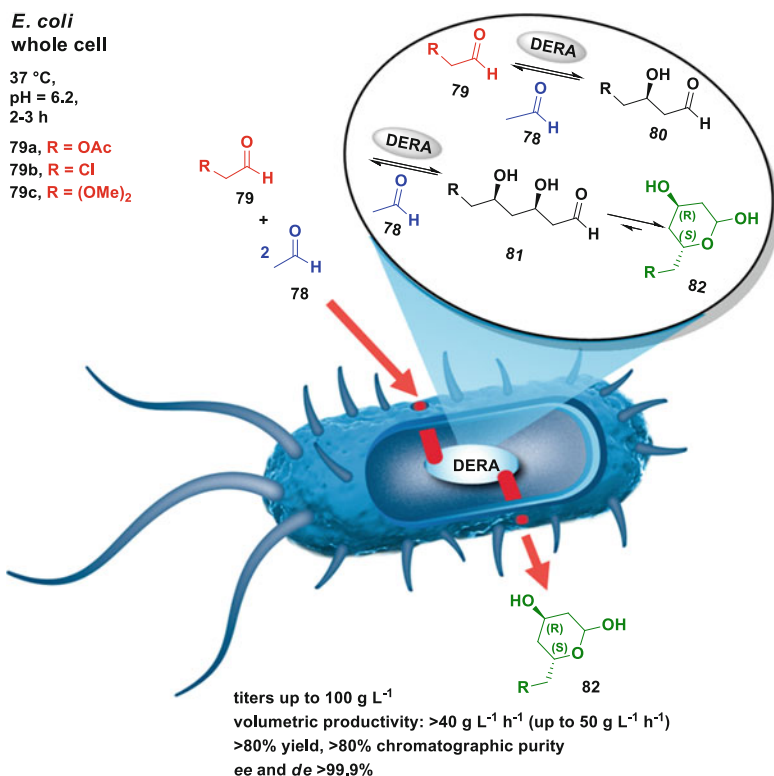
Kawato et al. [97] also upgraded their primary approach to the C-7 chiral atorvastatin lateral-chain precursor. Indeed, their previous route to the atorvastatin lateral-chain precursor **47** of 11 chemical steps (Scheme 7) [90] was streamlined to access the *N*-protected analog, with a different protective group on the 1,3-dihydroxyl moiety with only five chemical steps, which provided only two process steps as a result of telescoping (Scheme 12). The synthesis started similarly with the catalytic asymmetric aldol reaction of 3-(trityloxy)propanal **70** with the common thioamide **36** (1.2 equiv., applied also in the primary approach), using the 2,2,5,7,8-pentamethylchromanol **71**/mesitylcopper **37**/(*R,R*)-Ph-BPE **38b** catalytic system (6 mol% loading) in THF/DMF (1:1) solvent at  $-40^{\circ}\text{C}$ . After a 24-h reaction time, interim analysis indicated that **72** was formed at *ee* 91%. The concentrated extract of **72** that also contained the (*R,R*)-Ph-BPE-Cu complex was dissolved in dry THF and reacted with  $\text{LiAlH}_4$ , which reduced **72** to **73**, and concomitantly liberated the (*R,R*)-Ph-BPE **38b** ligand from its copper complex. After a column chromatography on a short pad of silica gel, the reaction product **73** and the ligand **38b** were easily separated, to provide 91% recovery of **38b** (after recrystallization from *i*-PrOH). The remaining secondary alcohol **73** was subjected to acidic conditions that removed the trityl protection and provided the (*R*)-5-aminopentane-1,3-diol **74** at a high 52% yield over three steps. The primary alcohol group in diol **74** was subsequently oxidized with  $\text{MnO}_2$ , and the corresponding aldehyde was coupled under Wittig conditions with the stabilized ylide **75** in refluxing toluene,



**Scheme 12** Streamlined catalytic asymmetric synthesis of the *N*-protected C-7 chiral atorvastatin lateral-chain precursor

to provide the Michael acceptor **76**. Finally, the Evans diastereoselective base-catalyzed intramolecular conjugate addition of hemiacetal-derived alkoxide (which was formed from alcohol **76** and benzaldehyde (3.5 equiv.) in the presence of *KOt*-Bu (1.2 equiv.) in THF at 0°C) was applied to provide benzylidene acetal **77** at a good 53% yield over two steps. From the overall prospective, the important features of this improved streamlined process included the strategic synthetic route design that enabled retention of nitrogen functionality in the final precursor **77** that originated from thioamide **36**. Moreover, the recovery of the expensive ligand **38b** at 91% yield also made this process commercially more attractive. All of these characteristics made this approach to **77** a particularly appealing one both from the process and the applied-chemistry perspective. This can indeed be considered as a masterpiece in process optimization.

We have recently described the first whole-cell **DERA**-catalyzed synthesis of lactols **82** from simple achiral aldehydes, such as the acetaldehyde **78** and its substituted analogs **79** (Scheme 13) [98]. The whole-cell **DERA** approach has many beneficial implications, such as the use of cheap and readily available raw materials to catalyze the multistep reactions, no need for the expensive enzyme



**Scheme 13** The first whole-cell **DERA**-catalyzed approach to a lactol-type C-6 chiral superstatin lateral-chain precursor production

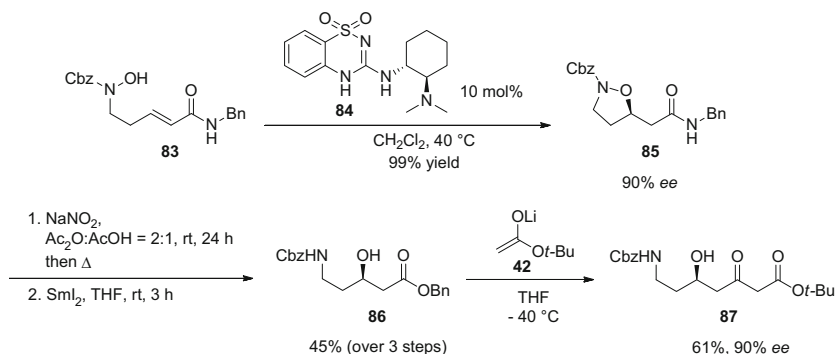
isolation and purification, and the higher stability of the enzyme. We have developed a batch-fed, high-density fermentation methodology with *E. coli* BL21 (DE3) that overexpressed the native *E. coli deoC* gene. As an added advantage, the fermentation broth can be used directly as a whole-cell **DERA** biocatalyst. The **DERA**-catalyzed sequential aldol condensation reaction system passes through the intermediates **80** and **81**, and this was investigated in detail for the acetaldehyde **78**/acetyloxy-acetaldehyde **79a** coupling partners. This provided valuable insights into the reaction dynamics. Indeed, an enhanced understanding of the enzyme activity was acquired as well as profound, although not complete, information on the formation of the reaction intermediates and the side products. This allowed an optimization of the feeding strategy of the aldehyde substrates for the improved productivities, yields, and purities.

Interestingly, no notable diffusion limitations or undesired secondary enzymatic reactions were observed that would have hindered this intracellular bioconversion. The process developed for the production of ((2*S*,4*R*)-4,6-dihydroxytetrahydro-2*H*-pyran-2-yl)methyl acetate **82** (R=OAc) had a volumetric productivity >40 g L<sup>-1</sup> h<sup>-1</sup> (up to 50 g L<sup>-1</sup> h<sup>-1</sup>) with >80% yield and >80% chromatographic purity, with titers reaching 100 g L<sup>-1</sup>. The stereoselectivity of this whole-cell **DERA** catalyst gave excellent stereochemical purities (*ee*, *de* > 99.9%), which were demonstrated on the downstream lactone intermediates **XIX** that were obtained after a chemical oxidation of lactols **82**, based on a Ca(OCl)<sub>2</sub>/NaCl/H<sub>3</sub>PO<sub>4</sub> oxidation system [98].

Ručigaj and Krajnc [99] investigated the process of the crude **DERA**-lyzate-catalyzed reaction between **78** and **79a**. Several parameters had relevant influence on the reaction outcome in terms of the ((2*S*,4*R*)-4,6-dihydroxytetrahydro-2*H*-pyran-2-yl)methyl acetate **82a** yield. Among these, the effects of the reactant **78:79a** ratio and the substrate concentrations on the inhibition of the enzyme and the reactant feeding regime were studied in detail. The process that provided the best reaction conditions was achieved by converting the reactant feeding regime from a batch reaction to a batch-fed process. The fine-tuning of this process allowed the production of the lactol **82a** at a titer of 77 g/L and at ca. 75% chemical yield.

Ručigaj and Krajnc [100] also developed an accurate and efficient kinetic model that described the **DERA**-lyzate-catalyzed reaction of acetaldehyde **78** with 2-substituted acetaldehydes **79**, to provide the corresponding lactols **82**. The proposed three-step kinetic model encompassed the formation of intermediate and main products, as well as the side products formed by the parallel undesired reactions. In addition, the loss in enzyme activity was also captured within the model. For the bisubstrate reaction examined, a random mechanism was applied. After the development of the kinetic model, a mathematical modeling successfully enabled accurate determination of the kinetic parameters by nonlinear least-squares approximation search methods, until minimal differences between the experimental and calculated data were obtained. The model developed provided the foundation for the design of optimal **DERA**-catalyzed processes, as well as the optimal reactor design.

Schallmeyer et al. [101] reported the detailed biochemical characterization of two highly engineered halohydrin dehalogenases that can transform (*S*)-4-chloro-3-

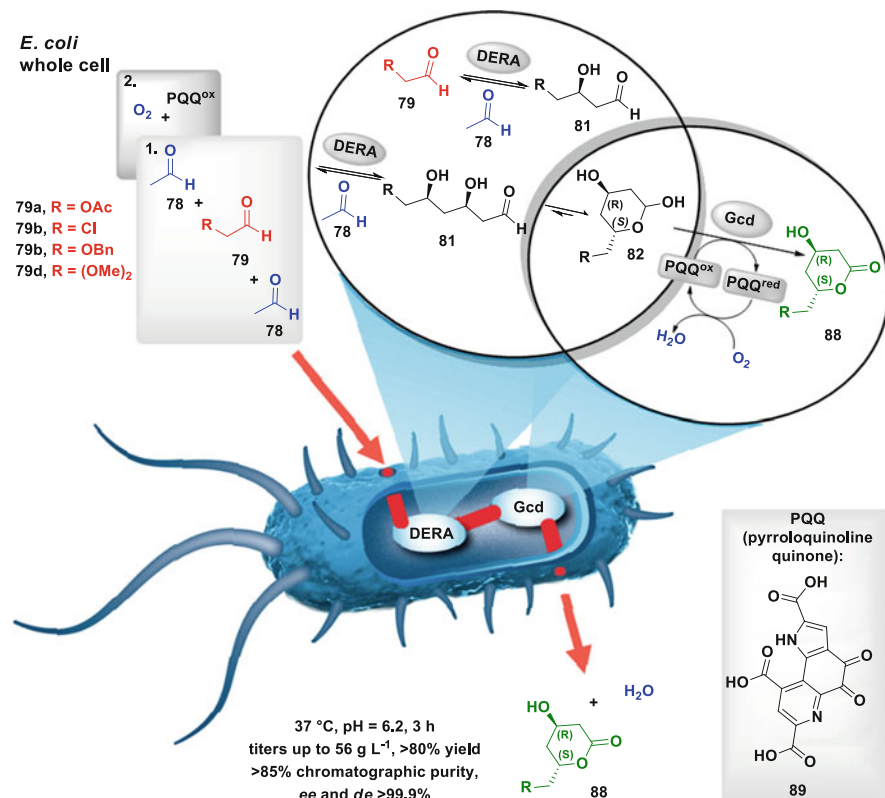


**Scheme 14** Intramolecular oxa-Michael reaction of  $\alpha,\beta$ -unsaturated amide for the construction of the C-7 amino-derivatized atorvastatin lateral-chain precursor

hydroxybutyrate **17** to (*R*)-4-cyano-3-hydroxybutyrate **19**, via (*S*)-3,4-epoxybutyrate **18**. Both of these variants of halohydrin dehalogenase were evaluated in dehalogenation and epoxide cyanolysis reactions on various substrates, and both of them outperformed the wild-type enzyme in the cyanolysis of **18** to **19**.

A fascinating construction of the C-7 amino-derivatized atorvastatin lateral-chain precursor was described recently by Kobayashi and coworkers [102]. In the initial synthetic step, they used a newly developed asymmetric intramolecular oxa-Michael reaction of an  $\alpha,\beta$ -unsaturated amide derivative for the assembly of the C-5 amino-derivatized atorvastatin lateral-chain intermediate with one chiral center. Thus, the  $\alpha,\beta$ -unsaturated amide **83** was subjected to the presence of benzothiadiazine catalyst **84** (10 mol%) in dichloromethane at ambient temperatures for 24 h. Gratifyingly, the desired isoxazolidine **85** was obtained at 99% yield and 90% enantiomeric purity. In the next step, the amide **85** was reacted with  $\text{NaNO}_2$  in  $\text{Ac}_2\text{O}/\text{AcOH}$  (2:1) solvent at ambient temperatures, to provide the *N*-nitrosoamide intermediate, which was taken up into toluene and refluxed for 3 h. This resulted in the formation of the corresponding benzyl ester intermediate that contained the isoxazolidine moiety. The subsequent treatment of the isoxazolidine moiety with samarium(II) iodide in THF at ambient temperatures resulted in the reduction (cleavage) of the isoxazolidine ring and provided the desired open-chain benzyl ester **86** at a good 45% yield over three steps. Finally, the Claisen condensation between **86** and the lithium enolate of *t*-butyl acetate **42**, which was derived in situ from *t*-BuOAc and lithium hexamethyldisilazide, provided the known atorvastatin lateral-chain precursor **87** at 61% yield and *ee* of 90% (Scheme 14) [102].

Very recently, Vajdič et al. [103] reported a landmark cascade catalytic process for a direct access to the lactone **88** precursors of the super-statin lateral chain that already contain both of the requisite stereogenic centers, with high stereochemical purity, from the simple achiral aldehydes **78** and **79** in a single-process step (Scheme 15). Indeed, Vajdič et al. [103] markedly extended recent studies on whole-cell processes for a chemoenzymatic production of lactols **82** by using



**Scheme 15** The whole-cell cascade **DERA-Gcd**-catalyzed approach to lactone-type C-6 chiral statin lateral-chain precursor production

high-density *E. coli* cultures with overexpressed **DERA** [98]. Taking into account that the compounds **82** need to be subsequently chemically oxidized to **88** in the pathway towards super-statins, a tempting step forward for this fascinating **DERA** whole-cell technology appeared to be an extension of the existing whole-cell **DERA** sequential aldol process with enzymatic regioselective oxidation via the construction of a microbial cell “factory.” As from the structural point of view lactols **82** represent artificial 6-substituted-2,4-dideoxyaldoses, enzymes that can provide regioselective mono-oxidation of similar sugars were initially investigated. Gratifyingly, several pyrroloquinoline quinone (PQQ)-dependent GDHs (PQQ-GDHs) can transform isolated **DERA**-derived lactols **82** to lactones **88**. Among the three selected and overexpressed enzymes in *E. coli*, which were the soluble periplasmic PQQ-GDH from *Acinetobacter calcoaceticus*, the soluble periplasmic PQQ-GDH from *E. coli*, and the inner-membrane-bound periplasm-facing PQQ-GDH from *E. coli* (**Gcd**), the last of these being selected as the prime candidate for the desired transformation. Based on the determination of the kinetic parameters, the membrane-bound **Gcd** (**mGDH**) was the most versatile of these systems and

operated well at the desirable pH 6.2, where **DERA** also has the desired biochemical properties, and aldol products **82** and the oxidation products **88** were chemically stable. Moreover, the *E. coli* strain BL21(DE3)pET30a-gcd that expressed **mGDH** demonstrated good activity at optimal pH towards 6-substituted-2,4-dideoxyaldoses (per gram of given biomass).

An interesting feature of the derived whole-cell oxidation catalyst is that *E. coli* itself cannot produce the essential PQQ **89** cofactor for the activity of PQQ-GDHs. Therefore, the PQQ-GDH apoenzyme must be supplemented with PQQ **89** and bivalent alkali ions (e.g.,  $Mg^{2+}$ ) to reconstitute the PQQ-GDHs into active holoenzymes. The results of the in vivo oxidation studies on the isolated **DERA**-derived lactols **82** using *E. coli* BL21 (DE3) pET30a-gcd biomass and exogenously added PQQ **89** and  $MgCl_2$  revealed that the PQQ **89** redox state can be recycled from reduced to oxidized through the use of a molecular oxygen as the cheapest oxidation source, taking an advantage of the respiratory chain as the mediator of the electron transfer to the oxygen. Furthermore, 2  $\mu M$  PQQ **89** was sufficient to achieve optimal activity of the whole-cell catalyst. Surprisingly, the *E. coli* BL21 (DE3) pET30a-gcd whole-cell catalyst showed very high oxidative activity, which had the potential to reach volumetric productivities of  $100 \text{ g L}^{-1} \text{ h}^{-1}$  for the lactol **82a** in a medium density culture, which significantly surpassed the potential of the **DERA** productivity. Gratifyingly, the in vivo conversion of **82a–d** with PQQ **89** and  $MgCl_2$ -supplemented *E. coli* BL21 (DE3) pET30a-gcd whole-cell resting cultures under aerated conditions demonstrated broad substrate acceptance and complete conversion of **82a–d** to their C1-oxidized lactone derivatives **88a–d**.

After the proof of a concept of this in vivo periplasmic oxidation of the isolated lactols **82** by whole-cell **Gcd**, a tandem enzymatic catalysis was considered as the penultimate challenge. Therefore, a sequential two-culture process was tested. The initial step consisted of a **DERA** batch-fed aldol reaction between **78** and **79a** using high-density fermentation cultures of *E. coli* BL21(DE3)pET30a-deoC, which provided a broth containing ca. 71 g/L **82a** [98]. Subsequently, PQQ **89** and  $MgCl_2$ -supplemented medium density *E. coli* BL21(DE3)pET30a-gcd cultures (ca. 21 vol% vs. primary broth volume) was added to the broth. Due to the dilution by the addition of the second culture, a mixture containing ca. 58 g/L **82a** was obtained. After incubation of the final broth with stirring and aeration at 37°C for 3 h, the lactol **82a** was fully consumed, to provide the lactone **88a** at ca. 95% yield and a titer of 55 g/L.

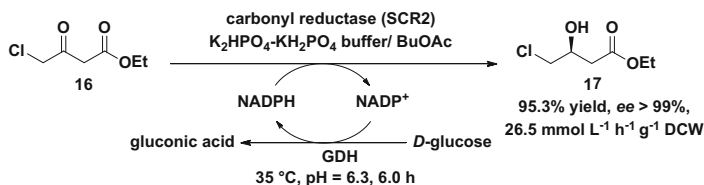
This outstanding result then left Vajdič et al. [103] with the ultimate challenge: construction of the coupled pathway of **DERA**-catalyzed intracellular aldol condensation followed by PQQ-GDH-catalyzed periplasmic oxidation within the same cells. For this purpose, co-expression of the two enzymes in the *E. coli* BL21 (DE3) host was carried out. The constructed microbial cell “factory” based on PQQ **89** and  $Mg^{2+}$ -supplemented medium density VDF fermentation culture BL21(DE3) pET30a-gcd-deoC was active and effective when fed with 360 mM **78** and 170 mM **79a**, giving the lactone **88a** at 82% yield with a marginal amount of the residual intermediates and the side products in the reaction mixture. This process was subjected to further optimization to increase its performance with respect to

substrate loads, by increasing the biomass loading through the application of high-density fermentation cultures, or through various co-expression strategies, which provided a modified and more active strain. This latter approach provided the best results, which led to the completion of the overall cascade reactions in 3 h, with the lactone **88a** at 80% yield, 85% chromatographic purity, and a titer of 56 g/L at 700 mM load of **78** and 325 mM load of **79a**. Overall, the designed enzymatic cascade provided the key statin lateral-chain precursors **88** at high stereochemical purity under mild conditions, and the simple process design resulted in a highly productive, green, and industrially scalable and inexpensive process.

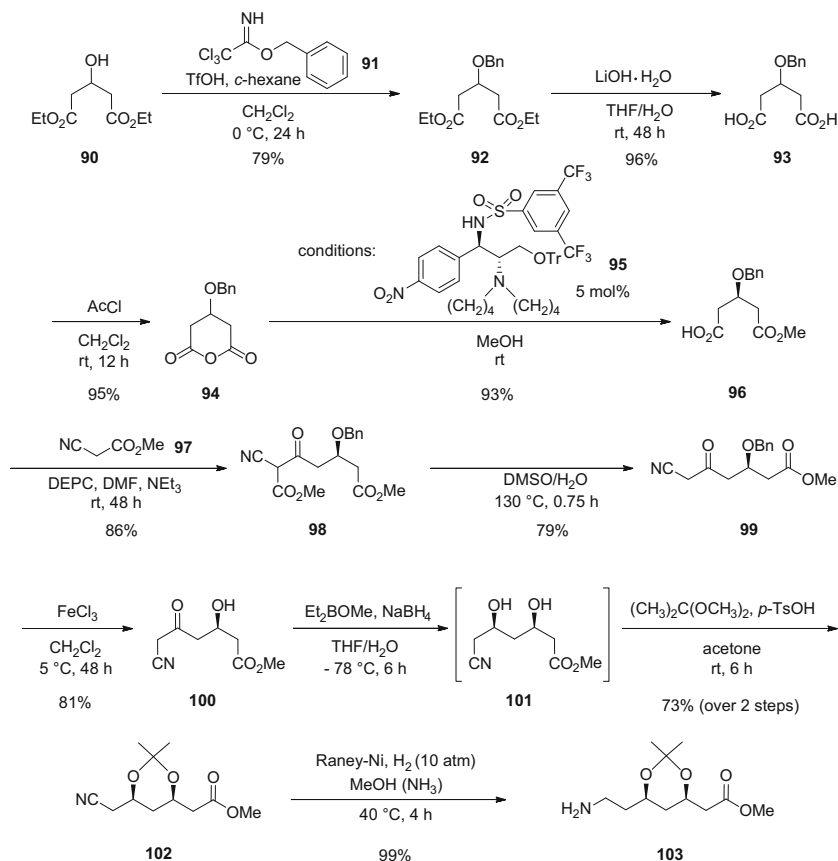
You et al. [104] reported the synthesis and expression of a new carbonyl reductase (**SCR2**) gene in *E. coli*. The prepared recombinant **SCR2** was subsequently purified, and its biochemical attributes were evaluated for the biochemical reduction of ethyl 4-chloro-3-oxobutanoate **16** to (*S*)-4-chloro-3-hydroxybutanoate **17**. A cofactor regeneration in the process was achieved via the use of **GDH**. The crude enzymes of **SCR2** and **GDH** were used as biocatalysts for the conversion of **16** to **17**. A biochemical characterization of **SCR2** was conducted through the exploration of the effects of several different parameters on the stability and activity of **SCR2**. A temperature had an important role in **SCR2** activity and stability, with the best activity observed between 20°C and 45°C and with an adequate stability at lower temperatures (<35°C). The recombinant **SCR2** best supported an environment with pH 4.0 to 6.0. The majority of metal ions had no effects on the activity of **SCR2**, except for Fe<sup>2+</sup>, Ag<sup>+</sup>, Cu<sup>+</sup>, and Cu<sup>2+</sup>, where a complete inhibition was observed. Among the solvents tested, several promoted the activity of **SCR2**. Nevertheless, BuOAc was the solvent of choice due to its low toxicity and favorable price. Next, the best process conditions with respect to yield and *ee* for the conversion of **16** to **17** were investigated. These studies demonstrated that reactions conducted at pH 6.0 to 6.5 provided >95% yield of **17**. An investigation of the optimal temperature for the bioconversion showed that the highest yield was obtained at 35°C, although the optimal activity of **SCR2** was at 45°C. As **16** and **17** are poorly soluble in pure apolar organic solvents like alkanes, BuOAc was used for the construction of the aqueous–organic solvent system, which increased the yield to >97% and *ee* to 99.5%. As **SCR2** was inhibited by the substrate, the optimal concentration range was also examined. An initial concentration of <500 mM **16** maintained a yield of **17** of >95%. To overcome the substrate inhibition issues, a batch-fed approach was also examined. Gratifyingly, the best performance was obtained in an aqueous–organic solvent system with a substrate batch-fed strategy where 1.0 M of **16** was reached via seven substrate additions, which provided 95.3% yield of **17** in 6 h. This provided the highest reported space-time yield per gram biomass (26.5 mmol L<sup>-1</sup> h<sup>-1</sup> g<sup>-1</sup><sub>dry cell weight</sub>) and turnover number of NADP<sup>+</sup> (40,000 mol/mol for NADP<sup>+</sup> to **17**) (Scheme 16).

Chen and coworkers [105] accessed the production of the C-7 amino-derivatized atorvastatin lateral-chain precursor via an organocatalytic anhydride desymmetrization and cyanide-free side-chain-elongation approach (Scheme 17).

This synthesis used a cheap chiral pool starting material with the aim to efficiently assemble the cyclic anhydride **94**. This can provide an access to the



**Scheme 16** Carbonyl reductase-catalyzed approach to lactone-type C-4-chiral statin lateral-chain precursor production



**Scheme 17** Synthesis of the C-7 amino-derivatized atorvastatin lateral-chain precursor

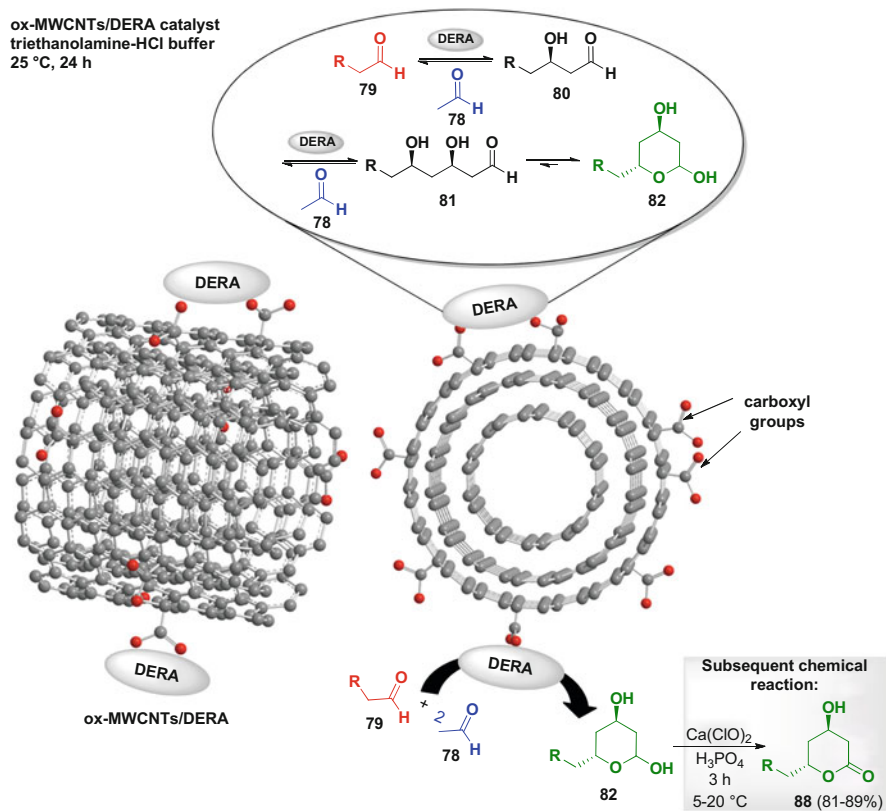
optically pure C-5 synthon of the statin lateral chain that can be further elongated to the desired C-7 analog. Thus, a conversion of diethyl 3-hydroxyglutarate **90** to its benzyl ether **92** was achieved using trichloroacetimidate **91** in the presence of catalytic amounts of trifluoromethanesulfonic acid (TfOH) in *c*-hexane/dichloromethane at 0 °C, which provided 79% yield. A treatment of **92** with LiOH

in THF/H<sub>2</sub>O at room temperature for 48 h hydrolyzed the ester moieties, and 3-(benzyloxy)-glutaric acid **93** was isolated at 96% yield. The subsequent dehydration of **93** with AcCl in dichloromethane at ambient temperatures was complete in 12 h, to provide the expected anhydride **94** at 96% yield. With the advanced intermediate **94** in hand, alcoholysis-based organocatalytic enantioselective desymmetrization was studied in detail, using in-house developed bifunctional sulfonamide catalysts. Interestingly, screening of four analogous catalysts revealed that the bifunctional sulfonamide **95** provided a high yield and good enantioselectivity in methyl *tert*-butyl ether (MTBE). Optimization of the reaction conditions defined **95** as the best-choice catalyst at 0.0125 M concentration, which provided the monoester **96** at 93% yield and *ee* 90% in 168 h at room temperature in MTBE. Then **96** had been subjected to a further transformation to reach the fully assembled C-7 side-chain precursor. This sequence started first with an insertion of the C-2 fragment via condensation of **96** with methyl cyanoacetate **97** in the presence of diethyl pyrocarbonate (DEPC) and an excess of trimethylamine in DMF at room temperature, to provide the diester **98** at 86% yield. A simple decarboxylation of **98** in wet dimethyl sulfoxide (DMSO) at 130°C gave the  $\delta$ -keto ester **99** at 79% yield, which underwent benzyl ether bond cleavage in the presence of an anhydrous FeCl<sub>3</sub> in dichloromethane at 5°C in 48 h, to provide the alcohol **100** at 81% yield. The ensuing Prasad diastereoselective 1,3-*syn* reduction of the  $\delta$ -keto moiety in **100** and an installation of the acetonide-protecting group on the 1,3-*syn*-diol **101** formed proceeded smoothly and provided **102** at 73% overall yield and dr of 95:5. Finally, the catalytic Raney-Ni hydrogenation of **102** reduced the nitrile moiety easily in methanolic ammonia at 40°C and provided the targeted 1,3-dioxane **103** at an excellent 99% yield.

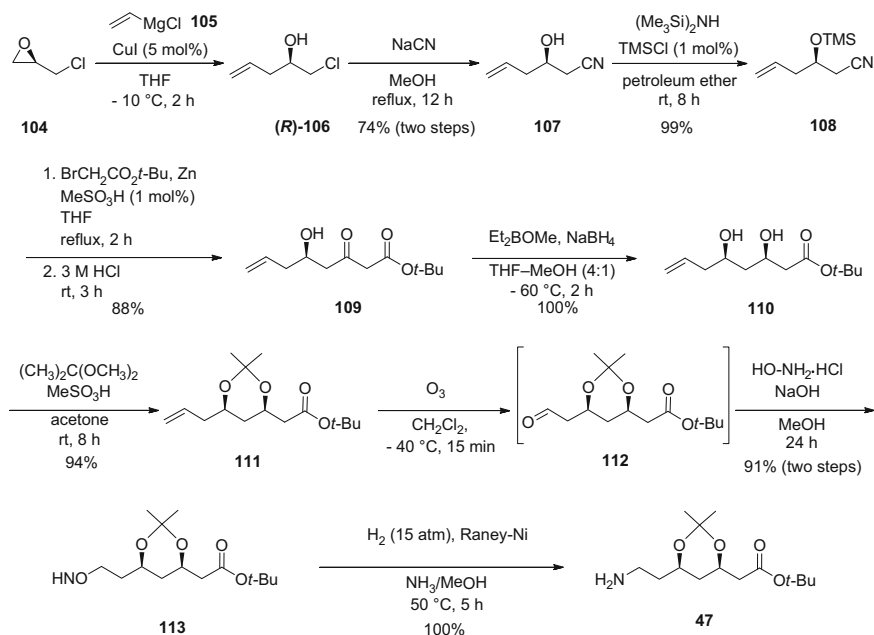
A radically different approach for the synthesis of C-6 lactone-type super-statin lateral-chain precursors using **DERA** was examined by Subrizi and coworkers [106]. Their strategy was to improve the **DERA** performance in the aldol condensation of **78** and **79** via an improvement of the activity and stability of **DERA**, and it was based on immobilization technology. Interestingly, the multiwalled carbon nanotubes (MWCNTs) were selected as the support for **DERA** immobilization. Several noncovalent conjugation methods were tested for physical adsorption of **DERA** to pristine and oxidized MWCNTs, and for some examples, polyelectrolytes or tethering agents were included. As a consequence, five different catalysts were prepared. Based on the enzyme activity measurements, carboxyl groups containing the ox-MWCNTs/**DERA** catalyst that was obtained by sonification of MWCNTs with H<sub>2</sub>SO<sub>4</sub>/HNO<sub>3</sub> (v/v, 1/3) was selected as the most promising system. Remarkably, this catalyst had higher activity than the native **DERA** when similar amounts of a free or supported **DERA** were compared. After full physical characterization using scanning electron microscopy and atomic force microscopy, the kinetic parameters of the ox-MWCNTs/**DERA** catalyst were established and compared to the native **DERA**. Also in this case, superiority of the ox-MWCNTs/**DERA** over the native **DERA** was observed, as shown by the higher  $V_{\max}$  measured for the ox-MWCNTs/**DERA**. Furthermore, a storage stability study indicated that ox-MWCNTs/**DERA** was more stable compared to the native **DERA**, and it

retained its activity almost intact after 15 days at 25°C, when native **DERA** showed only 80% of its original activity. Moreover, the **ox-MWCNTs/DERA** catalyst showed dramatically better tolerance towards inactivation by high aldehyde concentrations. Indeed, a treatment of **ox-MWCNTs/DERA** with 300 mM acetaldehyde **78** solution at 25°C for 30 min resulted in more than 80% of the initial activity, while the native **DERA** showed only ca. 20% of its original activity. All of these superior properties of the **ox-MWCNTs/DERA** catalyst were also reflected when an aldol condensation was carried out on either **78** alone or coupled **78** and **79b**. Remarkably, the yields differed notably for the lactones **88** obtained after chemical oxidation of **DERA**-derived lactols **82** with  $\text{Ca}(\text{OCl})_2/\text{H}_3\text{PO}_4$ . While the **ox-MWCNTs/DERA** catalysts provided lactones **88** at 81% to 89% yield, the native **DERA** provided the same lactones **88** at only 34% to 46% yield (Scheme 18).

A completely new approach to the formation of the atorvastatin C-7 lateral-chain precursor was recently reported by Xiong and coworkers [107], who started from the industrially accessible commodity material (*R*)-epichlorohydrin (Scheme 19).



**Scheme 18** The DERA-catalyzed cascade aldol condensation approach to the lactone-type C-6 chiral statin lateral-chain precursor using the **ox-MWCNTs/DERA** catalyst

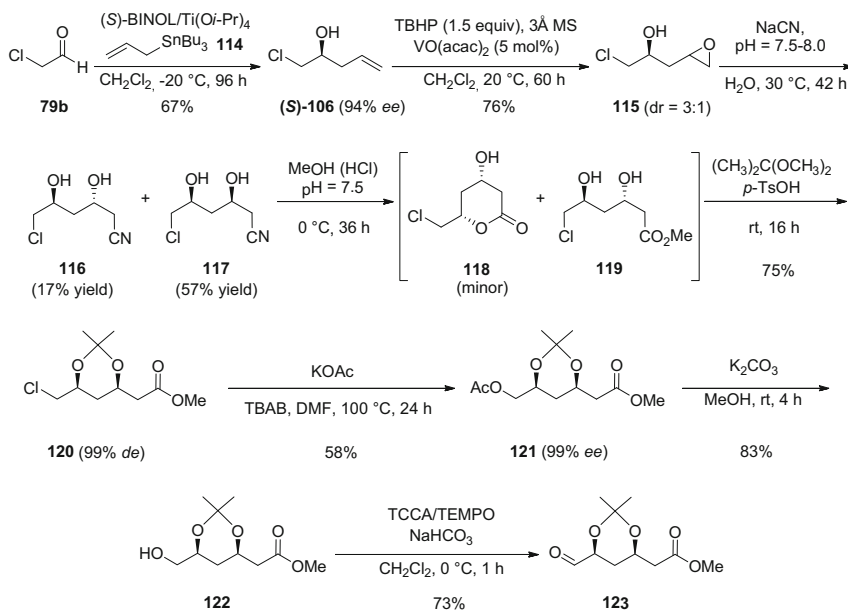


**Scheme 19** Access to the atorvastatin C-7 lateral-chain precursor via the Blaise reaction and the oxime-type C-7 intermediate

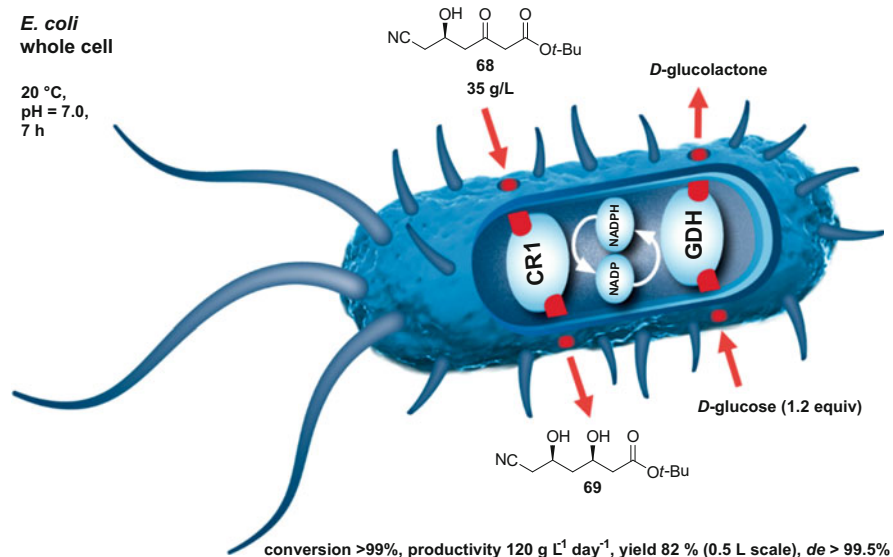
Moreover, the novelty of this route is reflected in the application of the Blaise reaction to the key step and the passage through a novel oxime-type C-7 intermediate. The proposed synthetic route started with the coupling of (*R*)-epichlorohydrin **104** and vinylmagnesium chloride **105** in the presence of CuI (5 mol%) at  $-5^\circ\text{C}$  in THF for 2 h, which provided the homoallylic alcohol (*R*)-**106**. The reaction of the compound (*R*)-**106** with NaCN in MeOH under reflux for 12 h produced the cyano derivative **107** in 74% over two steps. In the next step, the silyl ether **108** was prepared at nearly quantitative yield from **107** in petroleum ether at room temperature using hexamethyldisilazane (HMDS) and trimethylsilyl chloride (TMSCl). The key step of the synthesis was the Blaise reaction, which was carried out by the reaction of **108** with zinc *tert*-butyl bromoacetate derived in situ from Zn dust (pretreated with MeSO<sub>3</sub>H) and *tert*-butyl bromoacetate. The desired β-keto ester **109** was isolated after acidic treatment, at 88% yield. Then the ketone **109** was subjected to a stereoselective 1,3-asymmetric reduction using Et<sub>2</sub>BOMe/NaBH<sub>4</sub> in THF/MeOH (4:1) at  $-60^\circ\text{C}$ , to provide the desired *syn*-1,3-diol **110** at quantitative yield. Upon its reaction with 2,2-dimethoxypropane in acetone in the presence of *p*-MsOH, the *syn*-1,3-diol **110** provided the acetonide-protected alkene intermediate **111** at 94% yield. The oxidative cleavage reaction of the alkene **111** with ozone at low temperature provided the aldehyde **112**, which was taken up into MeOH and reacted immediately with hydroxylamine hydrochloride in the presence of NaOH for 24 h at room temperature, to give the oxime **113** at an excellent 91% yield over

two steps. A reduction of the oxime **113** with a Raney–Nickel catalyst at 15 atm H<sub>2</sub> in methanolic ammonia then provided the desired lateral chain **47** of atorvastatin at a quantitative yield and with a purity of 95% according to gas chromatography (GC) analysis, which was suitable for the assembly of atorvastatin.

Very recently, a catalytic enantioselective allylation strategy was used for the first time in the construction of the C-6 rosuva(statin) lateral-chain precursor (Scheme 20). Indeed, Chen et al. [108] started their synthetic route with Keck enantioselective allylation catalyzed by the Ti(IV)-1,1'-bi-2-naphthol (BINOL) complex in order to establish the first stereogenic center on the C-5 skeleton. Therefore, to produce the chiral homoallylic alcohol (*S*)-**106**, anhydrous chloroacetaldehyde **79b** (2 equiv.) was reacted with allyltributylstannane **114** (1 equiv.) in the presence of the (*S*)-BINOL/Ti(O*i*-Pr)<sub>4</sub> complex (ca. 20 mol% to **79b**) at –20°C for 96 h, providing 67% yield and 94% *ee* (using HPLC). Subsequently, the [VO(acac)<sub>2</sub>]/*tert*-butyl hydroperoxide-catalyzed *syn*-diastereoselective epoxidation of (*S*)-**106** at 20°C in CH<sub>2</sub>Cl<sub>2</sub> resulted in the formation of the epoxide **115** as a 3:1 inseparable mixture of epimers at 76% yield after 60 h. The resulting epoxide **115** was subjected to the reaction with aqueous NaCN at 30°C and pH 7.5 to 8.0 for 42 h, which resulted in the opening of the epoxide ring and the formation of the *syn*-1,3-diol **117** at 57% yield, along with its epimer **116**, which was isolated at 17% yield. A treatment of the pure nitrile **117** with MeOH under Pinner reaction conditions provided the ester **119**, which was contaminated with the lactone **118**. This mixture was taken directly into the next step without any purification, where it



**Scheme 20** A catalytic enantioselective allylation strategy for the C-6 statin lateral-chain precursor production



**Scheme 21** Whole-cell CR1/GDH approach to C-7 chiral atorvastatin lateral-chain precursor production

was subjected to the reaction with 2,2-dimethoxypropane in the presence *p*-TsOH in acetone, to provide the acetonide **120** (99% *de*) at a high 75% overall yield. A nucleophilic displacement of the chloride with the acetate anion in the presence of tetrabutylammonium bromide (TBAB) in DMF at 100°C provided the acetate ester **121** at a fair 57% yield and an excellent optical purity of 99% *ee*. In the penultimate step, the acetyl protection was removed with aqueous K<sub>2</sub>CO<sub>3</sub> in MeOH (room temperature, 4 h), which provided the alcohol **122** at 83% yield. Finally, **122** was oxidized to the aldehyde **123** with the trichloroisocyanuric acid (TCCA)/2,2,6,6-tetramethylpiperidinyloxy (TEMPO) couple at 0°C, at 73% yield.

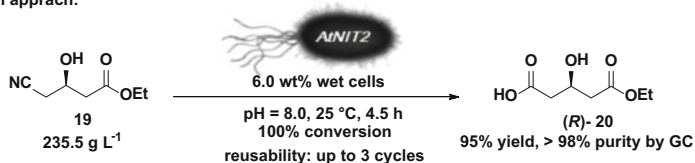
The group of Chen [109] recently reported a whole-cell catalyst for the conversion of *tert*-butyl 6-cyano-(5*R*)-hydroxy-3-oxohexanoate **68** to *tert*-butyl 6-cyano-(3*R*,5*R*)-dihydroxyhexanoate **69** (Scheme 21). The main focus of their studies was towards elimination of the shortcomings associated with the use of isolated enzymes and the necessity for expensive exogenous cofactor(s). Therefore, a recombinant *E. coli* strain that simultaneously overexpressed carbonyl reductase (CR1) from *S. cerevisiae* and GDH from *Bacillus megaterium* was constructed. This strain was more active when the vector for *gdh* was in front of *cr1*. Furthermore, it used the endogenous cofactor pool in *E. coli*, which in combination with both CR1 and GDH created a self-recycling endogenous cofactor catalytic system. Subsequent investigations of the optimal performance conditions revealed that the whole-cell catalyst performed best at neutral pH with 1.2 equiv. glucose added, with an optimal temperature range from 15°C to 25°C. Above 25°C, a large decrease in the conversion was observed. As the concentrations of the substrates

have important roles in biotransformations due to potential inhibition issues, the optimal substrate **68** concentration was also investigated; the maximum concentration of **68** had to be below 35 g/L to reach full conversion. With the desired whole-cell catalyst and optimal performance conditions in hand, a bioconversion of **68** to **69** was conducted on a 0.5-L scale at 35 g/L of substrate **68**. Here, >99% conversion was reached in 7 h without addition of exogenous cofactors, which led to a productivity of 120 g L<sup>-1</sup> d<sup>-1</sup> and which provided **69** at 82% yield and >99.5% *de*.

Very recently, Yao and coworkers [110] reported on a whole-cell biocatalytic approach for the hydrolysis of (*R*)-4-cyano-3-hydroxybutyrate **19** to (*R*)-3-hydroxyglutarate **20**, which is a well-known C-5 precursor of the chiral lateral chain of rosuvastatin. Indeed, a screening for an efficient biocatalyst that can convert industrially applicable loads (1.0 mol/L) of substrate **19** revealed that nitrilase **AtNIT2** from *Arabidopsis thaliana* was the most suitable among 14 nitrilases examined. Therefore, the whole-cell catalyst based on *E. coli* BL21 (DE3)pLysS harboring a nitrilase gene from *A. thaliana* (**AtNIT2**) was examined further for the development of an industrially viable process. With the suitable catalyst in hand, Yao and coworkers [110] investigated the optimal reaction conditions, which were obtained when the biotransformation of **19** to **20** was performed in the presence of Tris-HCl buffer at pH 8 and 25°C. Under these conditions, 6.0 wt % free whole cells completely hydrolyzed up to 1.5 mol/L (235.5 g/L) of (*R*)-**19** within 4.5 h. The possible reuse of the biocatalyst was demonstrated over three cycles, without the loss of its activity. As reuse of the free whole-cell catalyst was a challenging task, its immobilization was considered. Among several tested entrapment matrices, calcium alginate beads offered the optimal immobilization option, as shown by the highest catalyst activity and the reuse of the catalyst on this carrier. Using this immobilized catalyst, a complete conversion with up to 2.3 mol/L (361 g/L) **19** was achieved in 8 h. The reuse of the immobilized catalysts was demonstrated over 16 consecutive cycles, giving the remarkable biocatalyst productivity of 55.6 g/g wet cells and a space-time productivity of 625.5 g L<sup>-1</sup> d<sup>-1</sup> at 93% yield of **20** (Scheme 22).

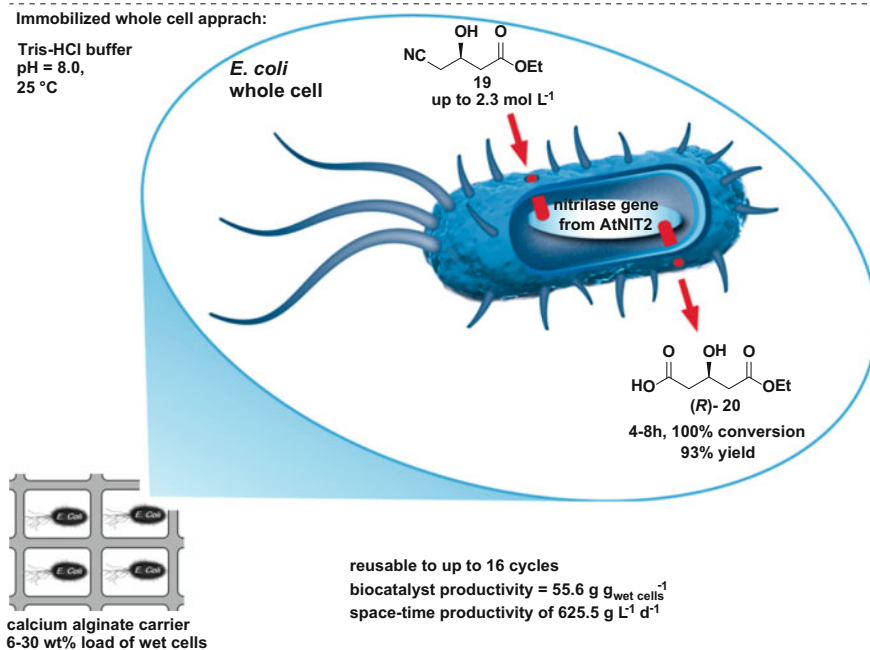
Very recently, Yao et al. [111] also presented a fascinating two-enzyme, three-chemical, one-pot approach for the synthesis of ethyl (*R*)-3-hydroxyglutarate **20** from ethyl (*S*)-4-chloro-3-hydroxybutyrate **17**, which is a well-known and cheap industrial commodity chemical. Several technologically different strategies were pursued to address the challenging direct transformation of **17** to **20** using two different enzymes: halohydrin dehalogenase and nitrilase. Yao et al. [111] again focused on the whole-cell biocatalytic approach, either through the separate expression or co-expression in the recombinant *E. coli* of genes of a mutant halohydrin dehalogenase gene from *Agrobacterium radiobacter* (**Hhe**) and a nitrilase gene from *A. thaliana* (**AtNIT2**). Here, with the biocatalyst based on *E. coli* BL21(DE3) overexpression of the **Hhe** gene (10 wt% wet cells), there was complete conversion of 1.2 mol/L of **17** to **19** in the presence of NaCN<sub>aq</sub> at pH 8–9 in 3 h. To extend the use of this finding, a whole-cell biocatalyst that simultaneously co-expressed the **Hhe** genes and encoded **AtNIT2** was constructed to achieve the biocatalytic

Free whole cell approach:



Immobilized whole cell approach:

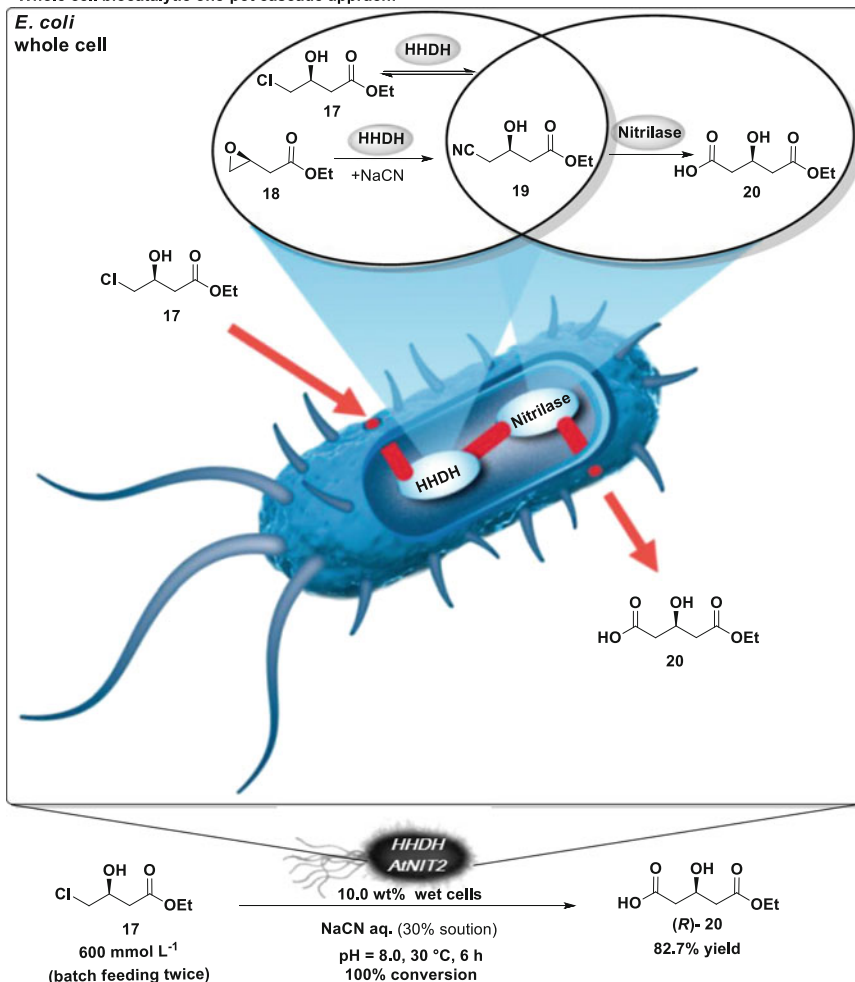
Tris-HCl buffer  
pH = 8.0,  
25 °C



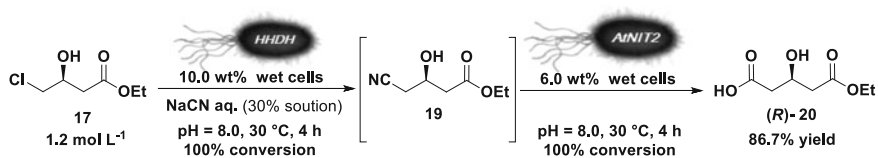
**Scheme 22** Immobilized whole-cell nitrilase approach to C-5 chiral statin lateral-chain precursor production

cascade transformation of **17** to **20**. Interestingly, although the **Hhe** within this dual biocatalyst maintained the same activity as in the cells that only expressed the **Hhe** gene, the activity of the co-expressed nitrilase was notably lower. Therefore, the key process parameters of pH, temperature, and initial substrate and CN<sup>-</sup> concentration were investigated, to determine their influence on the stability and activity of both of these enzymes when separately expressed in *E. coli*. These investigations revealed that both **Hhe** and **AtNIT2** were thermally stable up to 30°C and operated best at pH 8.0 (**Hhe**) and 9.0 (**AtNIT2**), respectively. Moreover, the inhibitory effects of CN<sup>-</sup> and **17** on **AtNIT2** were quantified. Indeed, standard activity assay measurements demonstrated that the **AtNIT2** activity was not affected by up to 200 mmol/L NaCN and 300 mmol/L **17**. Based on these data, a fine-tuning was undertaken. The inhibitory effect of NaCN was compensated for by an automatic addition of 30% NaCN solution and the control of the pH reaction broth through the reaction at pH 8. Furthermore, a batch-fed approach of **17** at the maximum

Whole cell biocatalytic one-pot cascade approach:



Whole cell biocatalytic one-pot two-step process:



**Scheme 23** Whole-cell cascade approach to lactone-type C-5 chiral statin lateral-chain precursor production

concentration of 300 mmol/L was also used to tackle the inhibitory effects of **17** on **AtNIT2**. Using these process strategies, the double batch feeding of **17** (overall 600 mmol/L) to *E. coli* co-expressing both **Hhe** and **AtNIT2** (10.0 wt% wet-cell

loading) at pH 8 and 30°C in the presence of NaCN (30% solution) provided a complete conversion of **17** to **20** in 6 h, with 82.7% yield of **20** upon isolation (Scheme 23, top). The addition of a third batch of **17** did not provide full conversion of the **19** formed to **20**.

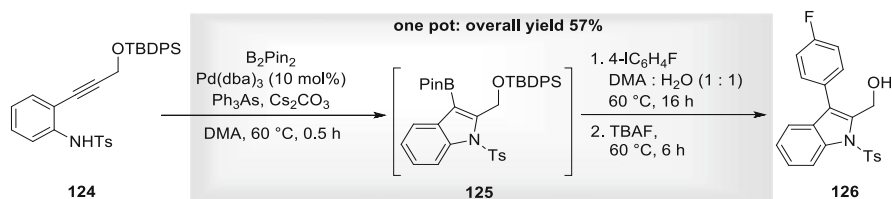
Finally, a two-step, one-pot process using the same reaction conditions as described above allowed a complete conversion of **17** to **20** at 1.2 mol/L substrate. In this case, **17** was treated with cells expressing **Hhe** for 4 h, which gave full conversion to **19**. Subsequently, cells of *E. coli* expressing **AtNIT2** were added to the mixture, which resulted in the complete conversion of **19** to **20** in 4 h and provided 86.7% isolated yield of **20** (Scheme 23; bottom).

### 3 Fluvastatin

Fluvastatin was the first fully synthetic statin on the market, and it started the era of the super-statin domination. The preparation of fluvastatin was perfected within Novartis. Therefore, there was a little room left for marginal improvements of the synthesis of fluvastatin and its building blocks. Consequently, studies in this area are scarce [10, 112].

#### 3.1 Synthesis of the Fluvastatin Indole Heterocyclic Core

An interesting methodology for the construction of the indole core of fluvastatin was described by Huang and coworkers [113] (Scheme 24). They described a Pd-catalyzed cyclization of Ts-protected *O*-alkynylanilines using B<sub>2</sub>Pin<sub>2</sub> (2 equiv.) in the presence of Cs<sub>2</sub>CO<sub>3</sub> and Ph<sub>3</sub>As, which provided a series of indole 3-boronic esters at high overall yields. This borative cyclization methodology was used in a combination with the Suzuki–Miyaura coupling for the one-pot assembly of indole derivative **126**. Therefore, when *O*-alkynylaniline **124** was reacted with B<sub>2</sub>Pin<sub>2</sub> in the presence of Pd<sub>2</sub>dba<sub>3</sub> (5 mol%) and Ph<sub>3</sub>As (10 mol%), the indole 3-boronic ester **125** was formed via a borative cyclization. Upon the addition of 4-fluoriodobenzene to the reaction mixture, it underwent a sequential Suzuki–Miyaura cross-coupling reaction. The addition of TBAF to the mixture promoted

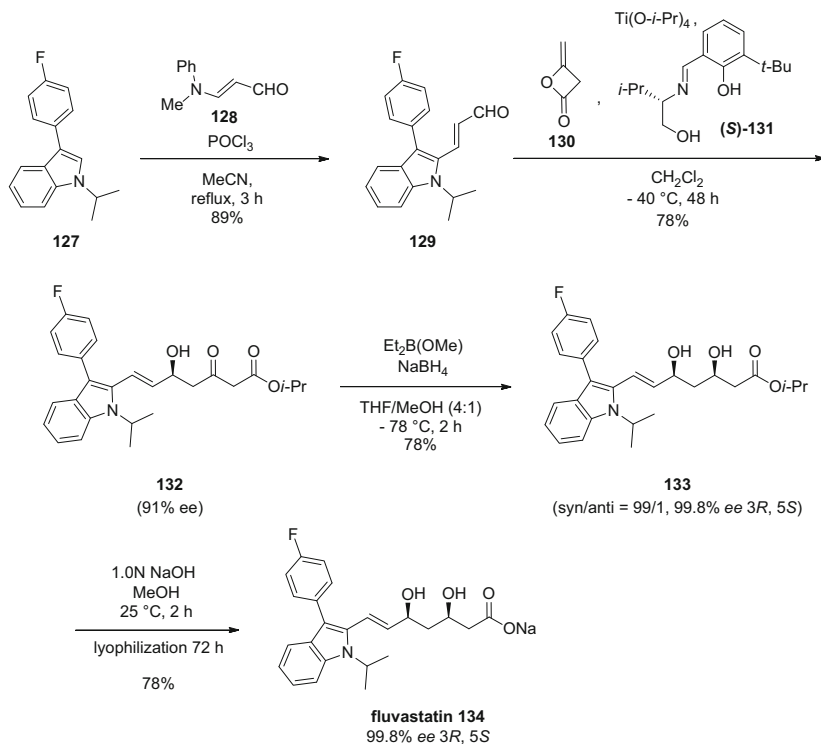


**Scheme 24** An assembly of the fluvastatin-substituted indole core using palladium catalysis

silyl ether cleavage and resulted in the formation of the substituted indole **126**, which is a convenient precursor of the fluvastatin heterocyclic core. Remarkably, the overall cyclization/cross-coupling/*O*-deprotection sequence provided the desired **126** at a high 57% yield. Although this method might not be the first choice approach for an industrial synthesis of the fluvastatin heterocyclic moiety due to the high costs of  $B_2Pin_2$  and the Pd-catalyst, it represents a well-developed combination of an advanced heterocyclic chemistry and sequential reactions within the same framework.

### 3.2 Assembly of Fluvastatin

Highly enantioselective synthesis of fluvastatin, its enantiomer, and both diastereoisomers using the asymmetric aldol reaction of C-3 aldehyde-type lateral chain containing indole moiety **129** and diketene **130** was described by Zacharia and coworkers (Scheme 25) [114]. Initially, a chiral Schiff-base ligands were prepared. Subsequently, the aldehyde-functionalized C-3 lateral-chain precursor containing indole moiety **129** was constructed in 89% yield from 3-(4-fluorophenyl)-1-



**Scheme 25** The asymmetric aldol reaction strategy towards fluvastatin

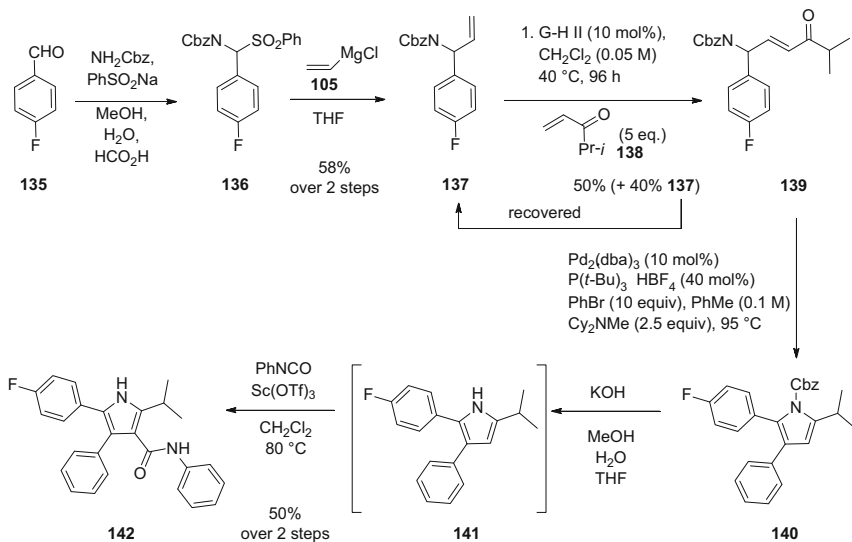
(1-methylethyl)-1*H*-indole **127** and 3-(*N*-methyl-*N*-phenyl amino)-acrolein **128** in the presence of POCl<sub>3</sub> in refluxing MeCN. Next, Ti(O-*i*-Pr)<sub>4</sub>-catalyzed asymmetric aldol condensation between aldehyde **129** and diketene **130** in the presence of a chiral Schiff-base ligands (*R*)-**131** and (*S*)-**131** was examined. When **129** was reacted with diketene **130** in the presence of 110 mol% (*S*)-**131** and Ti(O-*i*-Pr)<sub>4</sub> (100 mol%) at -40°C in CH<sub>2</sub>Cl<sub>2</sub>, the fluvastatin intermediate **132** that contained the fully assembled lateral chain and one chiral center was obtained at 78% yield and *ee* 91%. The δ-hydroxy-β-keto ester **132** was subjected to 1,3-*syn*-diastereoselective Prasad reduction with Et<sub>2</sub>B(OMe)/NaBH<sub>4</sub> in THF at -78°C, which provided the fluvastatin isopropyl ester **133** at 78% yield and high optical purity (*syn/anti* = 99/1, 99.8% *ee*). Finally, a hydrolysis of the ester moiety with NaOH in MeOH at 25°C resulted in the formation of fluvastatin sodium **134**, which was collected after lyophilization at 78% yield.

## 4 Atorvastatin

At the end of 2011, the world's bestselling drug atorvastatin lost its patent protection in the USA, which paved the way for cheaper generic versions. This interesting event brought atorvastatin from the originator market to the highly competitive generic market, where the drug and drug product manufacturing price has a key role. Therefore, an impetus for the development of highly efficient syntheses for atorvastatin should be at their peak.

### 4.1 Synthesis of the Atorvastatin Pyrrole Heterocyclic Core

An olefin cross-metathesis-based pathway to the 2,3,4,5-tetrasubstituted atorvastatin pyrrole nucleus was reported by Donohoe et al. [115] (Scheme 26). Therefore, when the 4-fluorobenzaldehyde **135** was transformed to the corresponding α-amido sulfone **136**, followed by the reaction with vinylmagnesium bromide **105**, the desired allylic amine **137** was obtained at 58% yield over two steps. The allylic amine intermediate **137** was then subjected to the cross-metathesis with the enone **138** in the presence of the Grubbs–Hoveyda second-generation catalyst, to provide the *trans*-γ-aminoenone **139** at 50% yield, along with 40% unreacted **137**, which was recovered. Interestingly, the subsequent exposure of **139** to the Heck arylation conditions with bromobenzene resulted in a ring closure, and the trisubstituted pyrrole **140** was isolated at 56% yield after a process optimization. The removal of the Cbz protection in **140** under hydrolytic conditions was achieved with KOH, giving the *N*-deprotected pyrrole **141**. The unsubstituted C4-position of the pyrrole ring in **141** was occupied by the phenylamide substituent after the Sc(OTf)<sub>3</sub>-promoted Friedel–Crafts-type acylation of **141** with phenyl isocyanate. This

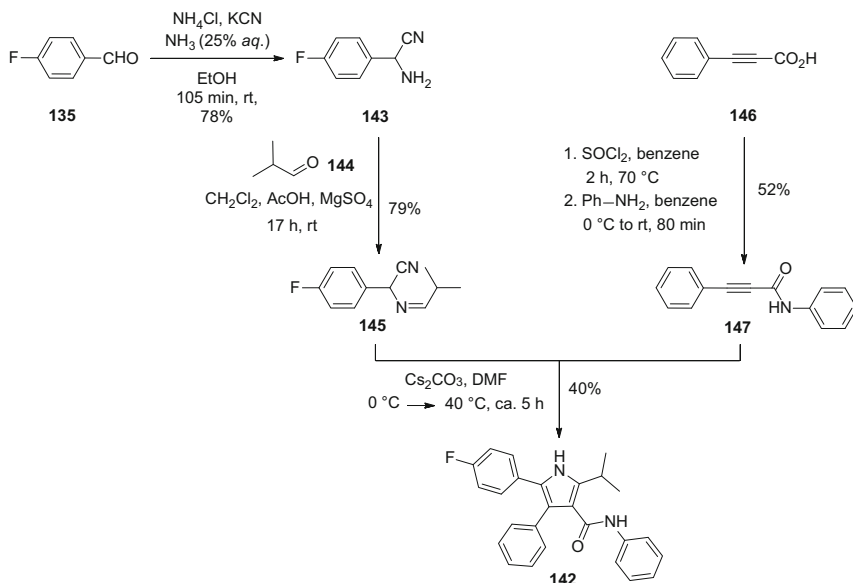


**Scheme 26** Cross-metathesis approach to the atorvastatin pyrrole nucleus

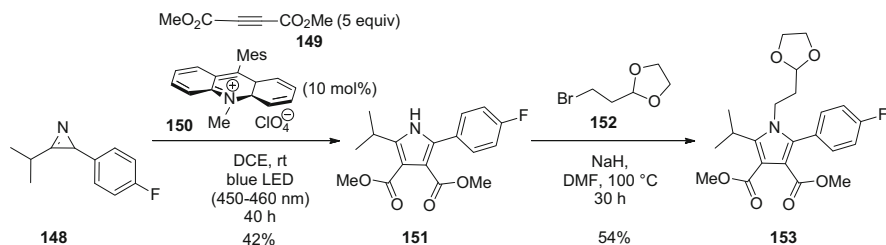
two-step sequence furnished the pyrrole nucleus of atorvastatin **142** at 50% yield over two steps.

A different approach to the pyrrole nucleus of atorvastatin **142** with no lateral-chain residues was described by Schäfer and Opatz [116] (Scheme 27). Their route was based on the  $\alpha$ -(alkylideneamino)nitrile derivative as a key precursor for the construction of the pyrrole core. In the first step, the  $\alpha$ -aminonitrile intermediate **143** was prepared at 78% yield by the Strecker reaction of the 4-fluorobenzaldehyde **135** and  $\text{NH}_4\text{Cl}/\text{KCN}$  couple. The subsequent condensation of **143** with isobutyraldehyde **144** provided the  $\alpha$ -(alkylideneamino)nitrile **145** at a high 79% yield. In a parallel synthetic sequence, 3-phenylpropionic acid **146** was converted to *N*,3-diphenylpropionamide **147** at 52% yield, via the formation of the acyl chloride intermediate and its subsequent reaction with aniline. With two key intermediates **145** and **147** in hand, the formation of the pyrrole ring was carried out with  $\text{Cs}_2\text{CO}_3$  in DMF. Unexpectedly, lower temperatures (i.e., 0–40°C) provided the best results, giving pyrrole **142** at 40% isolated yield. The main advantage of this approach is linked to the application of a convergent synthetic route design and of well-established robust chemistry from the commodity starting materials. Nevertheless, the current procedure leaves room for an improvement in terms of the yield optimization and removal of toxic solvents, such as the benzene used in the conversion of **146** to **147**.

A very interesting pyrrole ring formation method was reported by Xuan et al. [117] (Scheme 28). They developed a photocatalytic formal [3+2] cycloaddition of 2*H*-azirines with alkynes under irradiation using a visible light with the organic dye photocatalysts to construct the pyrrole ring. This method allowed the pyrrole ring formation under metal-free conditions. The developed photoredox



**Scheme 27**  $\alpha$ -(Alkylideneamino)nitrile-based route to the atorvastatin pyrrole nucleus



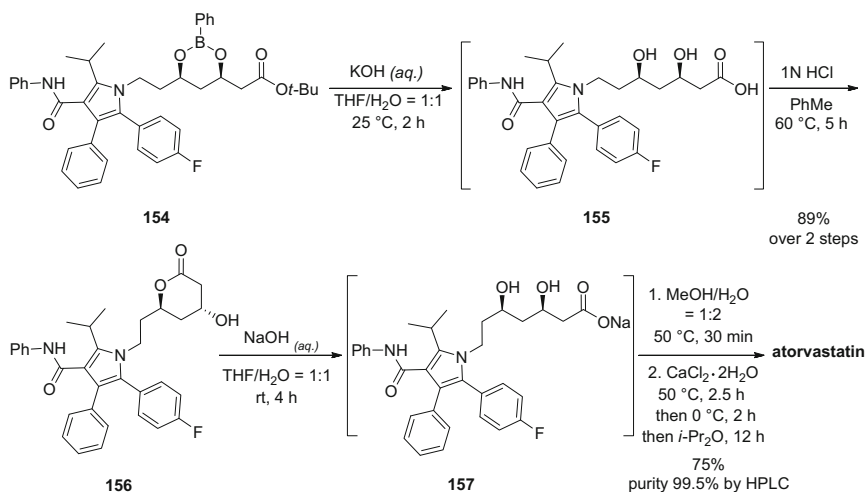
**Scheme 28** Photoredox catalytic method for the formation of a potential atorvastatin pyrrole ring precursor

catalytic method was applied to the synthesis of the potential atorvastatin heterocyclic core precursor **153**. Therefore, the 2*H*-azirine **148** was reacted with dimethyl but-2-yn-1,4-dioate **149** (5 equiv.), in the presence of mesityl-10-methylacridinium perchlorate **150** (10 mol%) and under irradiation by a blue light-emitting diode at room temperature for 40 h, which provided the pyrrole **151** at 42% yield. An alkylation of the NH group in **151** with 2-(2-bromoethyl)-1,3-dioxolane **152** in the presence of NaH in DMF at 100°C provided the pyrrole derivative **153** at 54% yield. The compound **153** can undergo mono-decarboxylation, ester hydrolysis, amide-bond formation, iodination, and the Grignard formation with a coupling to phenyl halide, to reach the well-known fully substituted pyrrole precursor of atorvastatin that already contains three atoms of the lateral chain.

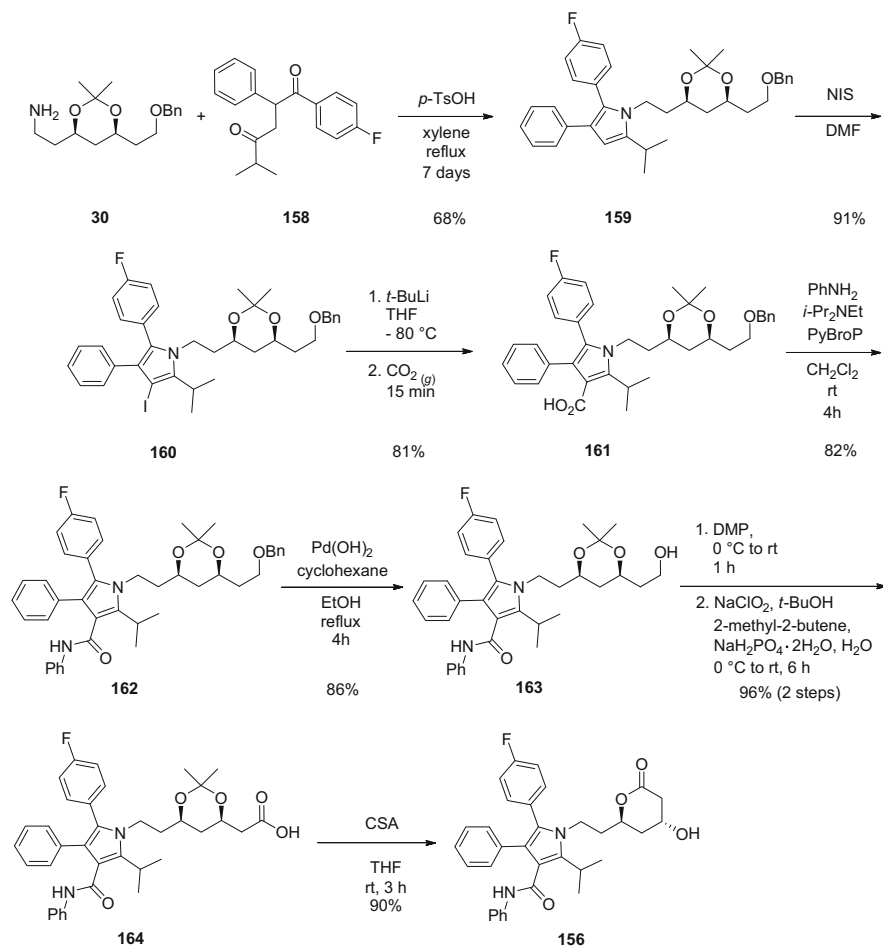
## 4.2 Assembly of Atorvastatin

Lee et al. [118] provided an efficient large-scale access to a high-purity atorvastatin from the phenyl-boronate-protected diol derivative **154** (Scheme 29). Detailed process optimization studies provided the preparation of highly pure atorvastatin in a four-step process (using two telescoping sequences) at an overall 67% yield. In the first step, the boronate ester **154** was conveniently *O*-deprotected and the *t*-Bu ester moiety was hydrolyzed with aqueous KOH, which proved to be the best base choice, in THF/H<sub>2</sub>O (1:1) at 25°C in 2 h. Upon acidification with HCl in PhMe, atorvastatin acid **155** was formed, which lactonized after 5 h of heating at 60°C, to give the atorvastatin lactone **156** at 89% yield and 98.1% HPLC purity. A subsequent lactone **156** hydrolysis with an aqueous NaOH in THF/H<sub>2</sub>O (1:1) at room temperature was completed in 4 h, to give the sodium salt of atorvastatin **157**. A cation exchange was performed in MeOH/H<sub>2</sub>O (1:2) at 50°C with an aqueous solution of CaCl<sub>2</sub>·2H<sub>2</sub>O. After cooling to 0°C, the precipitated atorvastatin was collected by filtration after 2 h. The precipitate was then slurried in *i*-Pr<sub>2</sub>O for 12 h and then filtered, to give atorvastatin at 75% yield and 99.5% chromatographic purity.

Sawant and Maier [87] also reported the synthesis of atorvastatin lactone **156** from their amino-derivatized and acetonide-protected C-7 lateral-chain precursor **30** (Scheme 30). The starting point of their synthetic approach was the condensation of **30** with 1,4-diketone **158** in the presence of *p*-TsOH (0.2 equiv.) in refluxing xylene. Although the condensation proceeded very slowly and was completed in 7 days, the 4-unsubstituted pyrrole **159** was obtained at a good 68% yield. The unoccupied 4-position of the pyrrole ring in **159** was functionalized first by an iodination with *N*-iodosuccinimide (NIS) in DMF at room temperature.

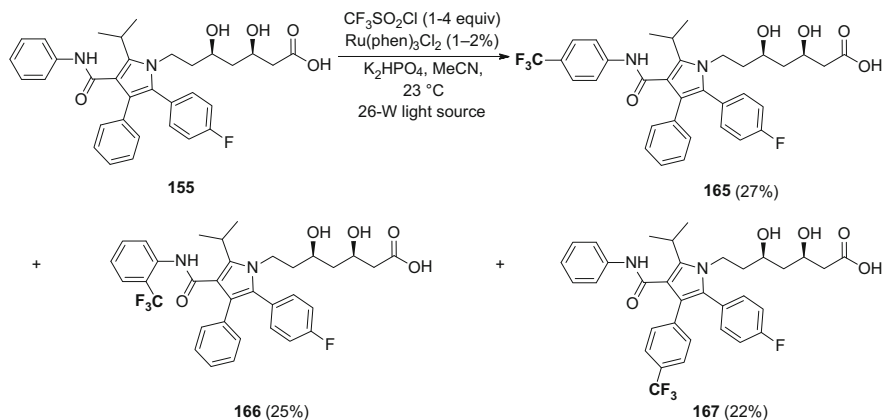


**Scheme 29** Synthesis of atorvastatin from the boronate-protected diol derivative



**Scheme 30** Stepwise synthesis of atorvastatin lactone

Interestingly, this reaction was rapid, and it provided the desired 5-iodo derivative **160** at 91% yield in 30 min. The lithiation of **160** with *t*-BuLi at  $-80^\circ\text{C}$  in THF, followed by the reaction of the organolithium intermediate with gaseous  $\text{CO}_2$ , provided the carboxylic acid derivative **161** at a high 81% yield. In the next step, the amide derivative **162** was readily produced at 82% yield via the convenient coupling of acid **161** with aniline in the presence of *N*-ethyl-diisopropyl amine and bromotripyrrolidinophosphonium hexafluorophosphate (PyBroP<sup>®</sup>) at room temperature. This provided the fully substituted atorvastatin pyrrole ring, and the remaining synthetic sequence focused on manipulation of the lateral-chain fragment, to construct the desired statin lactone moiety. Thus, the removal of the benzyl protection on the terminus of the lateral chain of **162** was achieved at a high 86% yield by hydrogenation in the presence of  $\text{Pd(OH)}_2$  and with cyclohexene as the

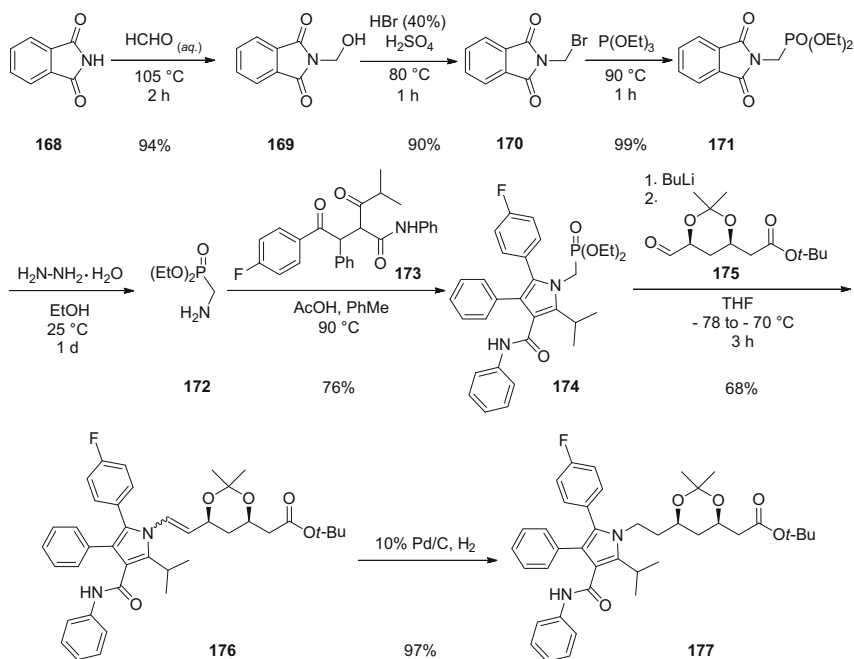


**Scheme 31** Generation of trifluoromethylated regioisomers of atorvastatin acid using photoredox catalysis

hydrogen source. The alcohol **163** that was obtained was subjected to a two-step oxidation process, where the Dess–Martin periodinane was used to convert the alcohol moiety into an aldehyde. This aldehyde was further oxidized with sodium chlorite in the presence of 2-methyl-2-butene as the chlorine trap, in *t*-BuOH at room temperature in 6 h, to provide the acid derivative **164** at 96% yield. Finally, a treatment of **164** with catalytic amounts of camphorsulfonic acid (CSA) in THF at room temperature provided the desired atorvastatin lactone **156** at 90% yield. Although some of the chemistry of this approach might not be applicable to an industrial production, and although the lengthy linear synthetic sequence might not be favorable in the same respect, the diversity of the reactions and functional groups used provides a beautiful example of synthetic creativity.

Trifluoromethylation of atorvastatin acid **155** using a photoredox catalysis was described by Nagib and MacMillan [119] (Scheme 31). When atorvastatin acid **155** was subjected to  $\text{CF}_3\text{SO}_2\text{Cl}$  and the  $\text{Ru}(\text{phen})_3\text{Cl}_2$  photocatalyst under 26-W compact fluorescent light in MeCN at  $23^\circ\text{C}$ , the three regioisomers of atorvastatin acid **165**, **166**, and **167** were isolated at 27%, 25%, and 22% yields, respectively. This approach provides an attractive option for a rapid access to trifluoromethylated analogs of bioactive molecules, and it avoids the lengthy total synthesis of each trifluoromethylated regioisomer. Therefore, the methodology presented facilitates the rapid build-up of the libraries that contain trifluoromethylated derivatives of drugs that are suitable for a rapid screening of their biological activities.

An efficient and high-yielding route towards the atorvastatin final intermediate was reported by Gao and coworkers [120] (Scheme 32). The key features of the synthetic strategy they used included cheap starting materials and the formation of the fully substituted atorvastatin core that contained the functionalized C1 moiety of the lateral chain. Therefore, phthalimide **168** was reacted with formaldehyde solution (36%) at  $105^\circ\text{C}$  for 2 h, to produce the methanol derivative **169** at 94% yield. A halogenation of the alcohol **169** using HBr in the presence of  $\text{H}_2\text{SO}_4$  at



**Scheme 32** A high-yielding synthesis of the atorvastatin final intermediate via a Horner–Wadsworth–Emmons reaction

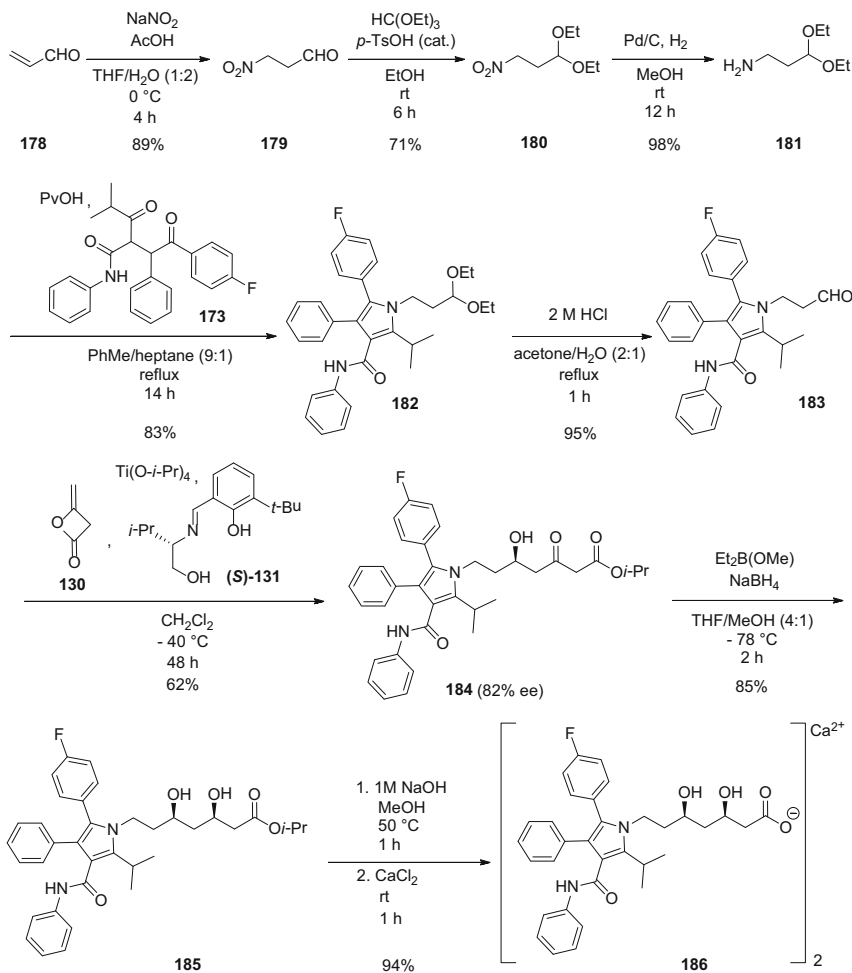
80°C provided the bromomethane derivative **170** at 90% yield. The alkylbromide **170** was taken through the Arbuzov reaction with triethylphosphite at 90°C in 1 h, to give the alkyl phosphonate **171** at nearly quantitative yield. The cleavage of the phthalimido protection in **171** was achieved with hydrazine hydrate in EtOH at 25°C in 1 day, which resulted in the formation of the diethyl (aminomethyl) phosphonate **172**. The subsequent condensation between **172** and diketone **173** was best in anhydrous toluene in the presence of AcOH, with the ratio of **173/172** set to 1.4:1. Under these conditions, the pyrrole **174** was isolated at high 76% yield. With the heterocyclic precursor **174** containing the C-1 lateral-chain unit and the installed phosphorous moiety in hand, the Horner–Wadsworth–Emmons olefination with the C-6 aldehyde-type linear lateral-chain precursor **175** was examined in detail. Optimal results were obtained when olefination was conducted with BuLi in THF, which provided the olefin **176** as a mixture of its *cis/trans* isomers in a 1/3 proportion at 68% yield. Finally, the hydrogenation of **176** proceeded smoothly in the presence of 10% Pd/C and provided the atorvastatin final intermediate **177** at nearly quantitative yield.

An assembly of atorvastatin acid **155** via the Paal–Knorr reaction of the amino-derivatized C-7 atorvastatin lateral-chain precursor **47** and 1,4-diketone **173** was described by Kawato and coworkers [90]. A telescoped reaction sequence that consisted of the condensation and deprotection reactions was designed. The

condensation was conducted with 10 mol% excess of the amine **47** in a *n*-hexane/toluene/THF (1:4:1) mixture in the presence of pivalic acid at 110°C for 30 h under argon, to produce the acetonide-protected atorvastatin acid **164**. The crude product obtained after the quench and extraction work-up was taken through the deprotection step after solvent exchange (AcOEt to THF), where it was brought into contact with 1 N HCl in MeOH at 0°C, and the mixture obtained was reacted at room temperature for 30 min. The crude product **155** obtained was primarily purified via sodium salt formation, with NaOH in THF, followed by extraction of the acid into CH<sub>2</sub>Cl<sub>2</sub>, which was obtained upon acidification of the salt with 1.0 N HCl. Finally, flash chromatographic purification provided pure atorvastatin acid **155** at 67% overall yield.

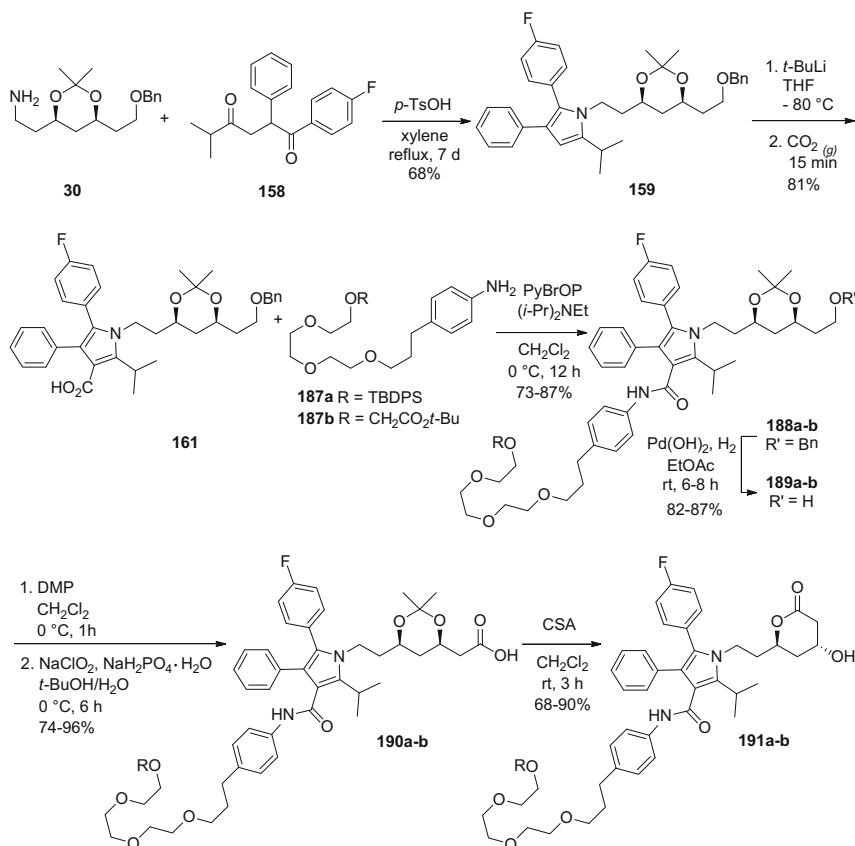
The assembly of atorvastatin via an asymmetric aldol reaction of a pyrrole precursor containing C-3 aldehyde-type lateral chain and diketene was described by Hu and coworkers [121] (Scheme 33). Initially, the C-3 amino-type lateral-chain precursor **181** was produced. Thus, nitropropanal **179** was prepared at 89% via Michael addition of sodium nitrite to acrolein **178** in THF/H<sub>2</sub>O at 0°C. Upon treatment of **179** with triethyl orthoformate in the presence of *p*-TsOH in EtOH, the diethyl acetal **180** was obtained at 71% yield; through hydrogenation (10 atm) in the presence of 10% Pd/C catalyst in MeOH, this was converted to the amine **181** at a nearly quantitative yield. The Paal–Knorr condensation between the 1,4-diketone **173** and the amine **181** was conducted in PhMe/heptane (9:1, v/v) in the presence of pivalic acid under reflux and azeotropic removal of the water formed for 14 h, which provided the pyrrole that contained the diethyl acetal-protected aldehyde-type C-3 lateral chain **182** at 83% yield.

Acid hydrolysis of the diethyl acetal group in acetone/H<sub>2</sub>O (1:1) under reflux was completed in 4 h, which provided the pyrrole-containing aldehyde-functionalized C-3 lateral chain **183** at an excellent 95% yield. This synthesis continued with a detailed study of the Ti(O-*i*-Pr)<sub>4</sub>-catalyzed asymmetric aldol condensation between **183** and diketene **130** in the presence of a variety of structurally similar chiral Schiff-base ligands. This revealed that the best results in terms of the yield and enantioselectivity were obtained with the Schiff-base ligand **131**. Indeed, when **183** was reacted with diketene **130** (5 equiv.) in the presence of 100 mol% **131** at –40°C in CH<sub>2</sub>Cl<sub>2</sub>, the atorvastatin intermediate **184** that contained the fully assembled lateral chain and one chiral center was obtained at 62% yield and 82% *ee*. The δ-hydroxy-β-keto ester **184** was subjected to the 1,3-*syn*-diastereoselective Prasad reduction with Et<sub>2</sub>B(OMe)/NaBH<sub>4</sub> in THF at –78°C, which after an addition of MeOH provided the atorvastatin isopropyl ester **185** at 85% yield. Finally, a hydrolysis of the ester moiety with NaOH in MeOH at 50°C, followed by the addition of CaCl<sub>2</sub> at room temperature, resulted in the formation of atorvastatin calcium **186** at 94% yield over two steps (Scheme 33) [121]. Although this method might not be appropriate for industrial applications due to the high load of the structurally complex ligand and the insufficient enantioselectivity, this elegant report inevitably stimulated further research in the area of asymmetric aldol chemistry for super-statin assembly.



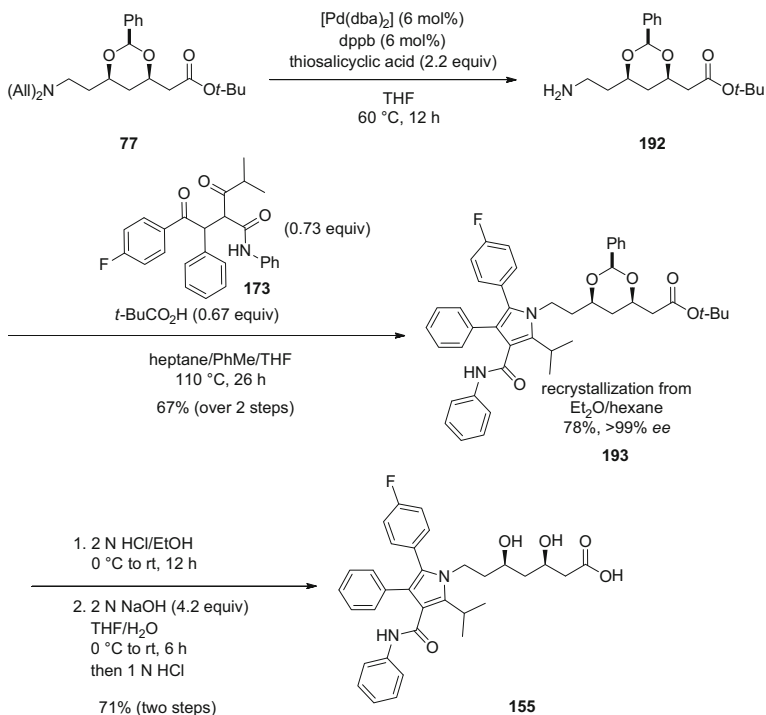
**Scheme 33** The asymmetric aldol reaction strategy for atorvastatin

Sawant and Maier [93] reported the synthesis of atorvastatin lactone analogs that contained the triethylene glycol linker moieties attached to the phenyl amide moiety of the pyrrole ring, which might have applications for an affinity-based target fishing (Scheme 34). This synthesis commenced with the Paal–Knorr condensation between the 1,4-diketone **158** and amino-derivatized C-6 precursor of the lateral statin chain **30**, which yielded the 4-unsubstituted pyrrole **159** at 68% yield after 7 days reflux in xylene. A treatment of **159** with *t*-BuLi in THF at  $-80^\circ\text{C}$  followed by the addition of gaseous  $\text{CO}_2$  provided the acid **161** at 80% yield. The PyBroP<sup>®</sup>-assisted amide-bond formation between the acid **161** and pre-prepared aniline-based triethylene glycol linkers **187a** and **187b** in the presence (*i*-Pr)NEt in  $\text{CH}_2\text{Cl}_2$  at  $0^\circ\text{C}$  provided the intermediate linker constructs **188a** and **188b** at 73%



**Scheme 34** Synthesis of atorvastatin lactone linker constructs for affinity-based target fishing

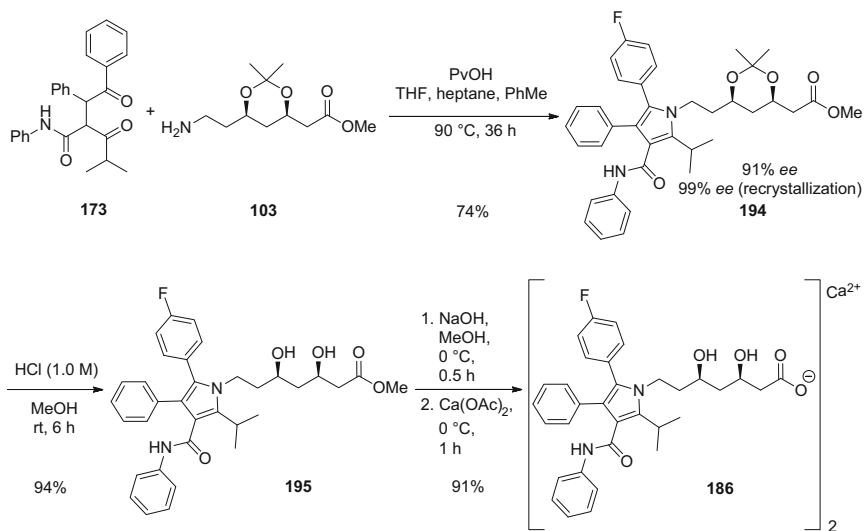
and 87% yields, respectively. The benzyl ether moiety was readily cleaved with H<sub>2</sub> in the presence of Pd(OH)<sub>2</sub> in AcOEt at room temperature, to provide the alcohol analogs **189a–b** at 82% to 87% yields, respectively. The subsequent two-step telescoped oxidation sequence of **189a–b** with the Dess–Martin periodinane provided the first of the aldehyde derivatives, which were further oxidized in turn with the Pinnick method, to the corresponding acid derivatives **190a–b** at 74% to 96% yields, respectively. Finally, the acetonide protection cleavage and the lactonization of the atorvastatin acid formed were achieved in 3 h with camphorsulfonic acid in CH<sub>2</sub>Cl<sub>2</sub> at ambient temperatures. The atorvastatin lactone linker constructs were isolated at variable yields, which ranged from 68% for *tert*-butyldiphenylsilyl-protected derivative **191a** to 90% for CH<sub>2</sub>CO<sub>2</sub>*t*-Bu analog **191b**. For both of the products **191a** and **191b**, a linker activation was readily achieved through the deprotection of the *tert*-butyldiphenylsilyl and *t*-Bu moieties and the release of the –OH and –CO<sub>2</sub>H linker groups.



**Scheme 35** Synthesis of atorvastatin acid from benzylidene-protected and amino-functionalized C-7 lateral-chain precursor

Recently, Kawato et al. [97] described an access to atorvastatin acid **155** via the benzylidene-protected *syn*-3,5-dihydroxy carboxylate ester **77** (Scheme 35). First, a telescoped reaction sequence that involved *N*-deprotection and cyclization was carried out. Thus, the allylic amine **77** was subjected to cleavage of the *N*-allyl protection through palladium catalysis in THF at  $60^\circ\text{C}$ , to provide the amine derivative **192**. This was taken directly to the Paal–Knorr condensation step, where it was reacted with the 1,4-diketone **173** in the presence of pivalic acid in a heptane/PhMe/THF mixture for 26 h at  $110^\circ\text{C}$ . The resulting benzylidene-protected *syn*-3,5-dihydroxy carboxylate ester **193** was obtained at a good 67% overall yield over two steps. An additional recrystallization of **193** from  $\text{Et}_2\text{O}$ /hexane provided it at 78% yield and *ee* > 99%. A removal of the benzylidene protection was accomplished with 2 N HCl in EtOH at  $0^\circ\text{C}$  in 12 h. The subsequent purification of the acid **155** via sodium salt formation using 2 N NaOH followed by acidification with 1 N HCl provided the atorvastatin acid **155** at 71% overall yield over two steps.

An efficient and concise assembly of atorvastatin was reported by Chen et al. [105] via the Paal–Knorr reaction between the 1,4-dicarbonyl **173** and the amino-moiety-containing C-7 lateral-chain precursor **103** (Scheme 36). Indeed, when **173** was reacted with **103** in the presence of pivalic acid at  $90^\circ\text{C}$  for 36 h in heptane/PhMe/THF (8:1:1, v/v), the acetonide-protected methyl ester of



**Scheme 36** An assembly of atorvastatin via the Paal–Knorr reaction, starting from the 1,4-diketone and the amino-moiety-containing C-7 lateral-chain precursor

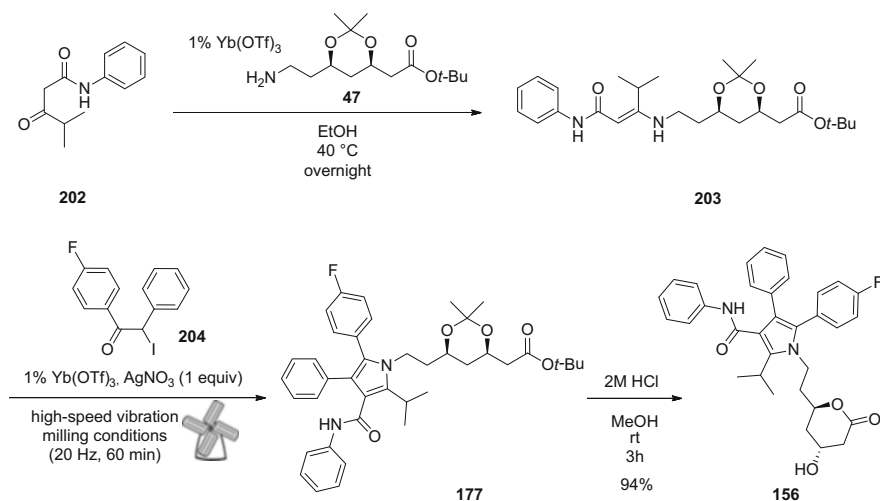
atorvastatin **194** was obtained at 74% yield and enantiomeric purity of 91%. The stereochemical purity of **194** was improved to 99% *ee* after an additional recrystallization from EtOAc/petroleum ether (1:8) at 81% recovered yield. The exposure of the 1,3-dioxalane **194** to 1.0 M HCl in MeOH at room temperature resulted in the cleavage of 1,3-dioxalane and provided the *syn*-1,3-diol **195** at an excellent 94% yield. The hydrolysis of the methyl ester **195** was conducted in MeOH with 1 M NaOH at 0°C for 30 min, which resulted in the formation of the sodium salt of atorvastatin. This was converted to atorvastatin calcium **186** upon addition of CaCl<sub>2</sub> in situ, which was isolated after 1 h stirring at 0°C at an excellent 91% yield. The stereochemical purity of atorvastatin calcium **186** obtained via this route was determined by a chiral HPLC method and was shown to be 99% *ee*.

Quite recently, Luo et al. [122] reported the very interesting synthesis of atorvastatin using asymmetric copper-catalyzed 1,6-boration of the acyclic  $\alpha,\beta,\gamma,\delta$ -unsaturated ester in the key step (Scheme 37). The synthesis started with the preparation of a suitable  $\alpha,\beta,\gamma,\delta$ -unsaturated ester precursor. For this purpose, the aldehyde **183** was reacted with the phosphorane **196**, which was prepared in parallel from the corresponding phosphonium salt and NaOH, in CH<sub>2</sub>Cl<sub>2</sub> at room temperature for 15 h, to provide the crude diene **197** as a 3:2 mixture of *E/Z* isomers. The stereochemical purity of **197** was upgraded by the I<sub>2</sub>-catalyzed isomerization in CHCl<sub>3</sub> at room temperature, which provided **197** as a 9:1 mixture of the *E/Z* isomers at >95% purity, followed by recrystallization (Et<sub>2</sub>O/hexane, 3:10), to give **197** at 60% yield (46% from the first round, 14% from the second round) as a 16:1 mixture of the *E/Z* isomers. The diene **197** (*E/Z*, 16:1) was subjected to the 1,6-boration with B<sub>2</sub>Pin<sub>2</sub> using the 0.02 mol% CuF(PPh<sub>3</sub>)<sub>3</sub>·2MeOH/Josiphos ligand **198** catalytic



$-5^{\circ}\text{C}$ , the benzylidene-protected 3,5-dihydroxy carboxylic ester **201** was obtained over four steps from **197**, at 42% yield and *ee* 87%. The additional recrystallization from hexane/*i*-PrOH provided **201** at 34% yield and *ee* > 99% with four steps from **197**. The removal of the benzylidene protection with 2.0 M HCl in MeOH/THF (1:2) at  $50^{\circ}\text{C}$  for 3 h was followed by the addition of NaOH, to give the sodium salt of atorvastatin **157** at 89% yield. Finally, the acidification of **157** with 1.0 M HCl in  $\text{CH}_2\text{Cl}_2$ /ice mixture gave atorvastatin acid **155** at 94% yield. Optionally, **197** (*E/Z*, 16:1) was further purified by recrystallization from *i*-PrOH/hexane (1:1) to a >19:1 mixture of the *E/Z* isomers. When **197** with *E/Z* > 19:1 was subjected to the borylation followed by the oxidation, **199** was obtained at 87% yield and *ee* 95%. Nevertheless, for a larger scale preparation, the use of a lower purity **199** was more convenient.

Recently, Estévez et al. [123] reported a unique mechanochemical-based approach for the assembly of atorvastatin lactone **156** (Scheme 38). In contrast to the majority of the other reports, where the Paal–Knorr reaction was used for the assembly of atorvastatin, the three-component Hantzsch reaction was used here for the construction of the penta-substituted pyrrole ring of atorvastatin. As all of the key fragments for the key Hantzsch step were either commercially available (e.g., **47**) or easily accessible via literature reports (e.g., **202**) except  $\alpha$ -haloketone **204**, the synthesis of the  $\alpha$ -haloketone **204** was developed first. Here, **204** was prepared readily from the corresponding acetophenone derivative, which was brominated to give the corresponding  $\alpha$ -bromoketone, which provided **204** upon the halogen exchange with NaI. With key fragments **47**, **202**, and **204** in hand, the Hantzsch cyclization step was studied in detail. Interestingly, initial indications suggested that  $\text{Yb}(\text{OTf})_3$  is the Lewis acid of choice and that the desired transformation should be performed sequentially. Therefore, the reaction of **47** with **202** in the presence of



**Scheme 38** A high-speed vibration milling approach to atorvastatin lactone

1 mol%  $\text{Yb}(\text{OTf})_3$  in EtOH at 40°C provided the crude enaminone **203**, which was taken directly into the next step where it was subjected to a high-speed vibration milling at 20 Hz for 1 h together with **204**, 1 mol%  $\text{Yb}(\text{OTf})_3$ , and  $\text{AgNO}_3$  (1 equiv.). Acetonide-protected atorvastatin *tert*-butyl ester **177** was then isolated at 40% yield and was readily converted to atorvastatin lactone **156** at 94% yield, using HCl in MeOH at room temperature for 3 h.

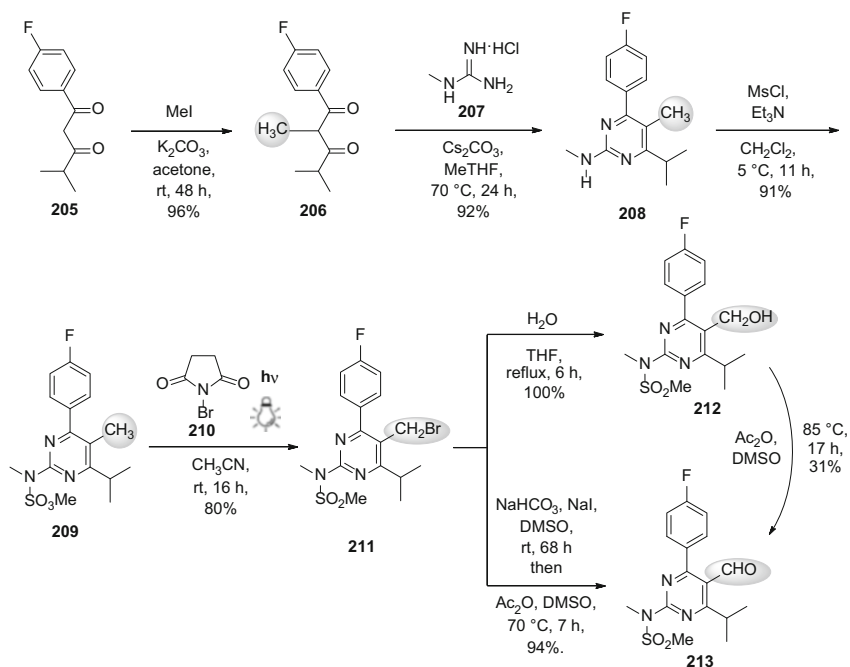
A detailed description of an improved kilogram-scale synthesis of atorvastatin calcium **186** was reported by Novozhilov and coworkers [124]. Their route started from the acetonide-protected *tert*-butyl ester of atorvastatin **177** on a 7-kg scale. Importantly, they described the key issues associated with the final steps of atorvastatin formation, which are usually neglected in typical academic reports, although they are of paramount importance in pharmaceutical process chemistry from a regulatory point of view. Therefore, **177** underwent clean deketalization with an aqueous HCl in *i*-PrOH at 60°C in 1 h, to give the corresponding *syn*-1,3-diol at 96% yield and >99% chromatographic purity. The subsequent reaction of this corresponding *syn*-1,3-diol with 1.10 to 1.15 equiv. NaOH in MeOH at 40°C resulted in its complete conversion to the sodium salt of atorvastatin **157** in 30 min. The AcOEt was a highly beneficial extraction solvent that quenched the excess NaOH and removed the majority of the impurities formed from the aqueous solution of **157**. The addition of  $\text{Ca}(\text{OAc})_2$  resulted in the formation of atorvastatin calcium **186**, which was extracted into AcOEt, followed by solvent exchange to EtOH after removal of AcOEt by evaporation. The product was collected after 3 h stirring at 20°C, which gave 79% yield of **186**, which was 99.9% pure by HPLC.

## 5 Rosuvastatin

At the moment, rosuvastatin remains one of the most important marketed superstatin family members. Since 2010, it has also gained a commercial significance, which even increased after the atorvastatin patent expired in 2011. The annual sales of rosuvastatin were over \$5 billion from 2010 to 2014. Nevertheless, the patent for rosuvastatin will expire in the USA in 2016, which will affect the position of rosuvastatin in the market. This has obviously stimulated research efforts in the area of novel rosuvastatin syntheses.

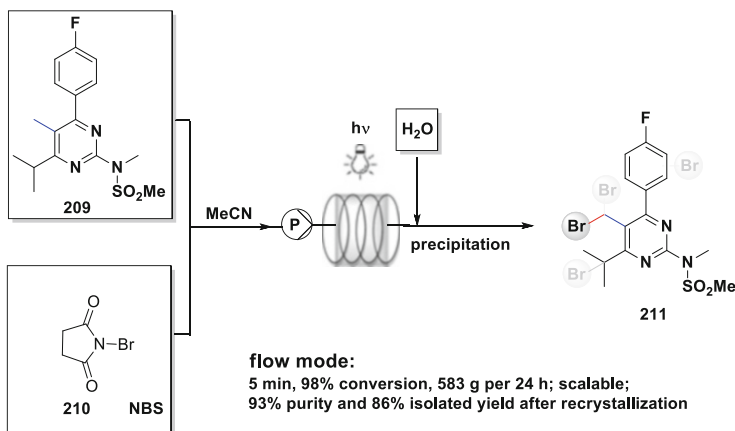
### 5.1 Synthesis of the Rosuvastatin Pyrimidine Heterocyclic Core

We have recently described a completely new synthetic approach to three functionalized pyrimidine precursors of rosuvastatin, as illustrated in Scheme 39 [125]. Our approach started with the diketone **205**, which was alkylated on the



**Scheme 39** A new concise synthesis of three functionalized pyrimidine precursors of rosuvastatin

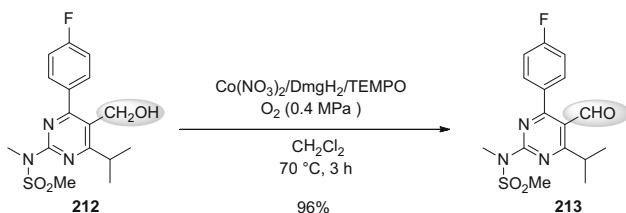
methylene group at room temperature in the presence of  $\text{K}_2\text{CO}_3$  in acetone for 48 h, to provide the  $\alpha$ -methyl  $\beta$ -diketone **206** at 96% yield. When the cyclization of **206** with *N*-methyl guanidinium hydrochloride **207** was attempted, it was discovered that the correct selection of the base and solvent was of paramount importance for the successful outcome of the reaction. The majority of bases (e.g.,  $\text{NaOH}$ ,  $\text{MeONa}$ , *t*- $\text{BuOK}$ ) and solvents (e.g.,  $\text{H}_2\text{O}$ , various alcohols, THF, DMSO) promoted substantial degrees of retro-Claisen degradation of the  $\alpha$ -methyl- $\beta$ -diketone **206** to *p*-fluoropropiophenone. Interestingly, when the  $\alpha$ -methyl  $\beta$ -diketone **206** was reacted with the *N*-methyl guanidinium hydrochloride **207** in the presence of  $\text{Cs}_2\text{CO}_3$  in MeTHF for 24 h at  $70^\circ\text{C}$ , the desired pyrimidine core **208** was isolated at 92% yield. The sulfonamide moiety was introduced into the molecule via the mesylation of the exocyclic methyl amine group with  $\text{MsCl}$  in the presence of  $\text{NEt}_3$  at  $5^\circ\text{C}$  in  $\text{CH}_2\text{Cl}_2$ , which provided the 2-*N*-methanesulfonamido-substituted pyrimidine **209** at 91% yield. The synthetic sequence from **205** to **209** was carried out on the basis that the 5-methyl moiety within **209** can undergo easy benzylic bromination. Therefore, **209** was subjected to *N*-bromosuccinimide **210** in MeCN using either a low-pressure Hg lamp ( $P$ , 4 W;  $\lambda$ , predominantly 254 nm) or a medium-pressure Hg lamp ( $P$ , 150 W;  $\lambda$ , predominantly  $>300$  nm) for 68 h or 16 h, respectively, at ambient temperatures, to provide the 5-bromomethylpyrimidine **211** at 74% to 80% yields, respectively. Although **211** already represents a key heterocyclic intermediate of rosuvastatin, which is a starting precursor for the synthesis of phosphorous-



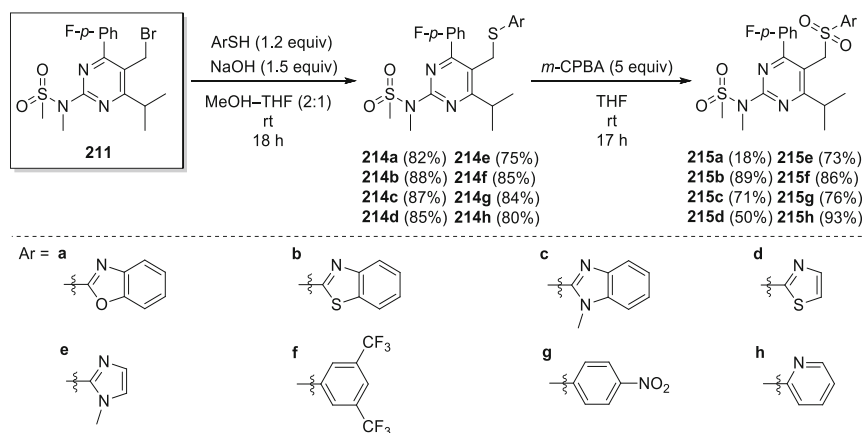
**Scheme 40** A continuous-flow photochemical bromination of the rosuvastatin pyrimidine precursor

containing coupling partners **Va–c** in the Wittig-type assemblies of rosuvastatin, its suitability for the preparation of an aldehyde-type derivative **IV** was also considered. Therefore, **211** underwent simple hydrolysis with  $\text{H}_2\text{O}$  to provide the alcohol derivative **212** quantitatively in 6 h under reflux in THF. However, after 17 h at  $85^\circ\text{C}$ , the Swern oxidation of **212** provided only 31% yield of the desired aldehyde **213**. In contrast, when the Kornblum oxidation of **211** was conducted in DMSO at room temperature for 68 h, the aldehyde **213** was obtained as the major product, along with the alcohol **212** as the main impurity. The alcohol **212** was also converted to **213** in one-pot process using Swern conditions at  $70^\circ\text{C}$  for 7 h, which provided 94% overall yield of the aldehyde **213**.

Although our initially developed photochemical bromination of **209** provided 74% to 80% yields of the desired **211** [125], the main disadvantages of this approach soon became apparent. The scale-up of the reaction indicated significantly longer reaction times and consequently the build-up of many hard-to-remove related impurities. Therefore, we carried out continuous-flow photochemical bromination of the pyrimidine **209** with the *N*-bromosuccinimide **210** (Scheme 40) [126]. Interestingly, in contrast to the batch-mode reaction, this flow approach could be scaled up. Furthermore, significant process intensification was achieved using the flow approach. Indeed, while the productivity of the batch-mode reaction was 13.6 mmol/h for **209**, the flow approach easily achieved 58.3 mmol/h conversion for **209**. Moreover, the flow-mode reaction was more chemoselective, as shown by the sum of all of the detected impurities in **211**. While the batch reaction provided a crude mixture that contained 17.6 area% of impurities, the reaction mixture obtained using the flow mode contained only 10 area% of impurities. Notably, the flow-mode reaction provided 93% pure **211** at 86% isolated yield. The remaining impurities in **211** from the flow-mode reaction appeared to be



**Scheme 41** Oxidation of hydroxymethylpyrimidine to the corresponding aldehyde derivative using molecular oxygen

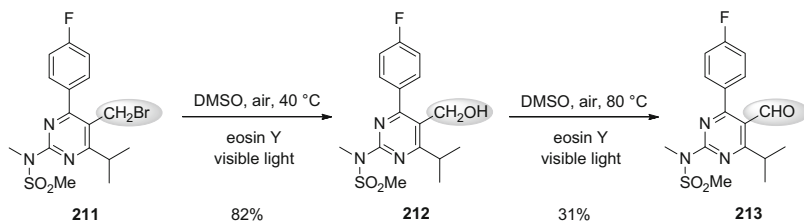


**Scheme 42** The synthesis of sulfide and sulfone heterocyclic precursors of rosuvastatin

associated with the bromination of the *p*-fluorophenyl ring, which did not cause any concern, as they were easily depleted in the subsequent synthetic steps.

Recently, Guan et al. [127] described a mild oxygen-based oxidation of the alcohol **212** to the aldehyde **213** using a three-component catalytic system based on  $\text{Co(NO}_3)_2$ , dimethylglyoxime, and TEMPO (Scheme 41). The reaction of **212** with molecular oxygen in an autoclave reactor in the presence of  $\text{Co(NO}_3)_2$ /dimethylglyoxime/TEMPO (1:4:1 mol%) at 0.4 MPa  $\text{O}_2$  pressure for 3 h at 70°C provided the desired aldehyde **213** at 96% isolated yield and a purity of 99% by HPLC analysis.

We recently reported on the preparation of a series of sulfone heterocyclic precursors (**215a–h**) of rosuvastatin that are suitable for the Julia–Kocienski olefination with chiral lateral-chain precursors (Scheme 42) [128]. In the first step, 5-bromomethylenepyrimidine **211** was reacted with a series of aromatic and heterocyclic thiols at room temperature in the presence of NaOH in MeOH/THF (2:1) as a solvent, for 18 h. The corresponding sulfides **214a–h** were obtained easily at 75% to 88% isolated yields. In the second step, an oxidation of the sulfides **214a–h** to the sulfones **215a–h** was examined in detail. Among several oxidants that were tested (e.g.,  $\text{KMnO}_4$  in AcOH/MeCN,  $\text{NaIO}_4/\text{RuCl}_3 \cdot \text{H}_2\text{O}$  in MeCN/ $\text{H}_2\text{O}$ ,



**Scheme 43** The synthesis of the formylated pyrimidine precursor of rosuvastatin

meta-chloroperoxybenzoic acid [*m*-CPBA] in THF), *m*-CPBA provided the cleanest oxidation reactions. Therefore, when the sulfides **214a–h** were reacted with *m*-CPBA in THF at room temperature for 17 h, the corresponding sulfones **215a–h** were isolated at 50% to 93% yields, except for **215a**, where only an 18% yield was achieved.

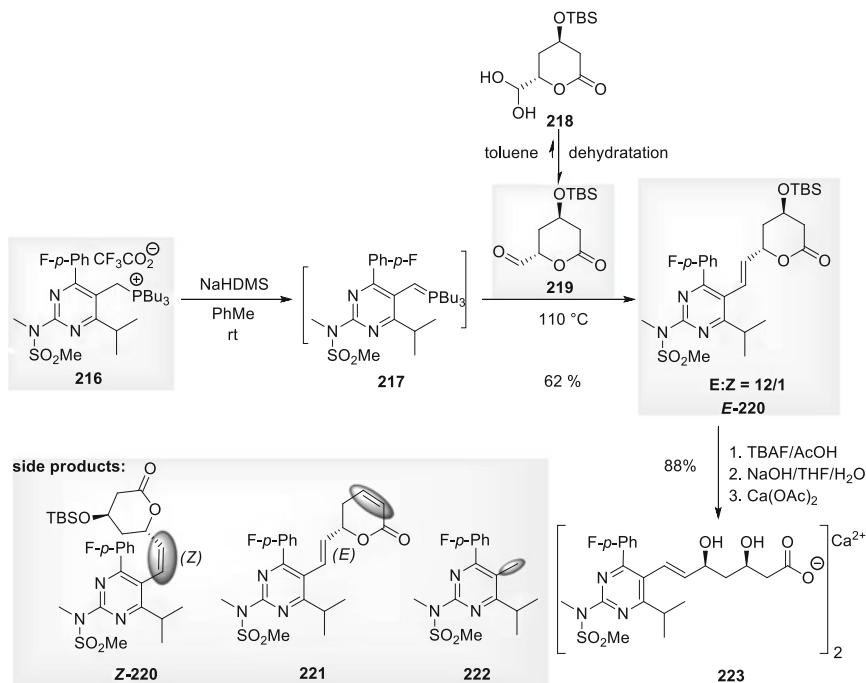
Li and colleagues [129] described an interesting eosin Y-promoted oxidation method for the conversion of arylmethyl bromides to the corresponding alcohols and aldehydes using metal-free photocatalytic conditions. The application of the established catalytic system based on DMSO/eosin Y/visible light under an air atmosphere was tested in the context of the preparation of the key rosuvastatin heterocyclic precursors **212** and **213**. Indeed, when the alkyl bromide **211** was reacted with eosin Y (5 mol%) at 40 °C in DMSO for 12 h, the alcohol derivative **212** was obtained at 82% yield. This alcohol **212** was further oxidized using the same catalytic system at 80 °C, to provide the desired aldehyde **213** at 31% yield (Scheme 43) [129].

## 5.2 Assembly of Rosuvastatin

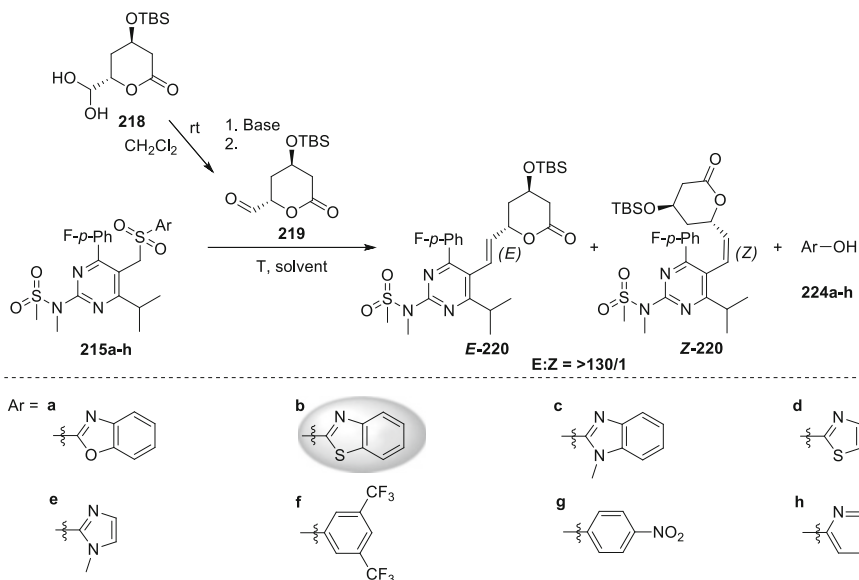
Recently, we reported the first assembly of rosuvastatin using the lactonized lateral-chain precursor **219** that contained the exocyclic formyl group functionality for the construction of C=C bond attachment of the chiral lateral chain to the heterocyclic moiety [130]. The key discovery that paved the way for the successful realization of this methodology was linked to the finding that the stable hydrated form **218** of the aldehyde **219** can be prepared and isolated easily. Unexpectedly, the hydrate **218** underwent spontaneous dehydration to the aldehyde **219** when exposed to aprotic apolar solvents [84]. Therefore, when the hydrate **218** was stirred in toluene at room temperature, the desired aldehyde **219** was formed in a few hours, along with stoichiometric amounts of water, which was removed by azeotropic distillation, to provide the dry toluene solution of the aldehyde **219**. In parallel, the ylide **217** was prepared from the corresponding phosphonium salt **216** of the pyridine heterocycle. Then, the prepared dry solution of the aldehyde **219** was added to the solution of the ylide **217**, which was warmed to 110 °C. The reactions were finished usually within 5–10 min, as shown by the decoloration of the deep orange color of the ylide.

The reaction mixture obtained after the Wittig reaction contained the desired *E*-*O*-TBS rosuvastatin lactone **E-220**, along with some unknown impurities. Additional efforts allowed us to isolate these impurities, and the full characterization showed the *Z*-*O*-TBS rosuvastatin lactone **Z-220**, the dehydro product **221**, and the 5-methylpyrimidine derivative **222**. While **Z-220** clearly originated from the unselective nature of the Wittig reaction, the origins of **221** and **222** were less obvious. Additional investigations showed that **221** was formed when the reaction mixture was exposed to a base, such as ylide **217** or NaHMDS, over a prolonged reaction time. The origin of **222** appeared to be associated with the presence of water in the reaction mixture. Therefore, a process optimization for this Wittig reaction was undertaken. The results suggested that the best conditions for this Wittig reaction were at higher temperatures (e.g., 110°C) where minimum amounts of **Z-220** (*E*/*Z*, ca. 12:1) and **221** were formed. When this Wittig reaction was performed under the optimal conditions, the desired *E*-*O*-TBS rosuvastatin lactone **E-220** was isolated at up to 62% yield. The subsequent three-step, one-pot TBS deprotection of **E-220** with TBAF, a hydrolysis of the corresponding lactone with NaOH, and an ion exchange (conversion of sodium salt to calcium salt) with Ca(OAc)<sub>2</sub> provided rosuvastatin calcium **223** at a high 88% yield (Scheme 44).

Recently, we also conducted a detailed conformational analysis of the *E*/*Z*-isomeric pairs of rosuvastatin (i.e., **E-223** and **Z-223**) and its lactonized analogs



**Scheme 44** Assembly of rosuvastatin via a Wittig reaction using the lactonized precursor of the chiral lateral chain

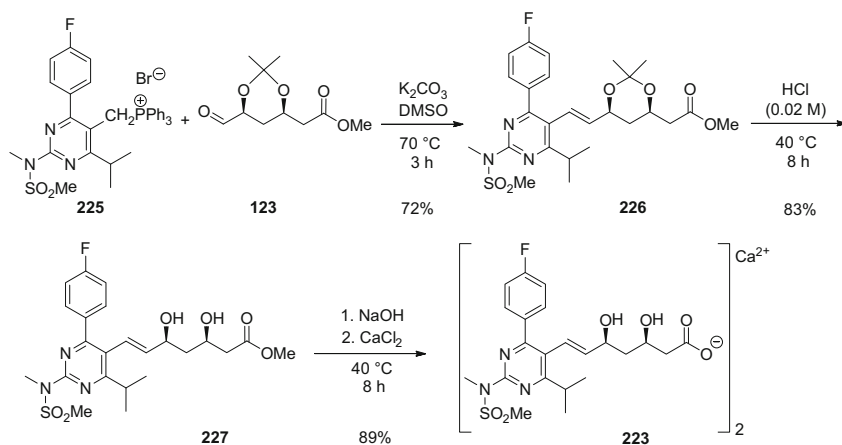


**Scheme 45** Assembly of rosuvastatin via Julia–Kocienski olefination using the lactonized precursor of the chiral lateral chain

(i.e., *E*-**220**, *Z*-**220**, and their *O*-TBS deprotected analogs) using nuclear magnetic resonance (NMR) and *ab initio* calculations [131]. This revealed that the unusual resonance line broadening that was observed exclusively in the  $^1\text{H}$  NMR spectra of the *Z*-isomeric rosuvastatin analogs at ambient temperatures is associated with dynamic exchanges between the different conformers. These exist as a pair of interconverting atropisomers. The corresponding *E*-isomeric rosuvastatin and its analogs showed only a single set of narrow resonances in the NMR spectra, which demonstrated that they exist only as a single conformer.

A study of the Julia–Kocienski olefination using the lactonized lateral-chain precursor **219** and the sulfone heterocyclic precursors of rosuvastatin **215a–h** gave some interesting results (Scheme 45) [128]. Indeed, a broad screening for the identification of the most suitable heterocyclic coupling partner revealed that the reaction proceeded best when **219** was coupled with the sulfone **215b**. Optimization of the reaction conditions demonstrated that these were met when **219** (1.2 equiv.; obtained by dehydration of **218** in  $\text{CH}_2\text{Cl}_2$ ) was reacted with **215b** (1.0 equiv.) at  $-60^\circ\text{C}$  in the presence of NaHMDS (1.3 equiv.) in THF as the solvent. In contrast to the Wittig approach where moderate stereoselectivities were observed (*E/Z*, 12:1) [130], this Julia–Kocienski olefination provided an *E*-**220**/*Z*-**220** ratio of >130:1 and a 60% HPLC yield. The preparative (1 mmol) scale reaction between **219** and **215b** provided a mixture that contained 71% *E*-**220** (according to HPLC). Finally, isolation provided a 66% yield of *E*-**220** with >97% purity.

Straightforward assembly of rosuvastatin using the dually protected open precursor of chiral lateral chain **123** was recently reported by Chen et al. [108]



**Scheme 46** Assembly of rosuvastatin via a Wittig reaction using the dually protected open precursor of the chiral lateral chain

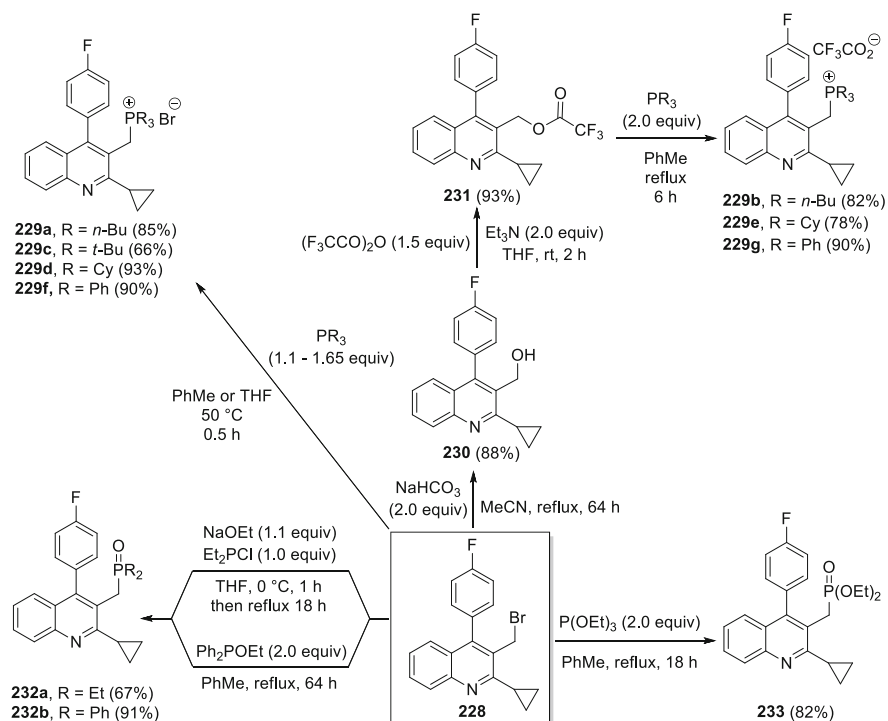
(Scheme 46). For this purpose, the phosphonium salt derivative of pyrimidine **225** was reacted with aldehyde **123** under Wittig conditions. The reaction was conducted in anhydrous DMSO at 70°C for 3 h using potassium carbonate as the base, which provided the acetonide-protected rosuvastatin methyl ester **226** at a good 72% isolated yield. The removal of the acetonide protection in **226** was achieved in 8 h using 0.02 M HCl in acetonitrile at 40°C, and the rosuvastatin methyl ester **227** was obtained at 83% yield. Finally, hydrolysis of the methyl ester moiety in **227** with NaOH in MeOH at 0°C provided rosuvastatin sodium, which was treated in situ with 0.2 M CaCl<sub>2</sub>, to obtain rosuvastatin calcium **223** at 89% yield.

## 6 Pitavastatin

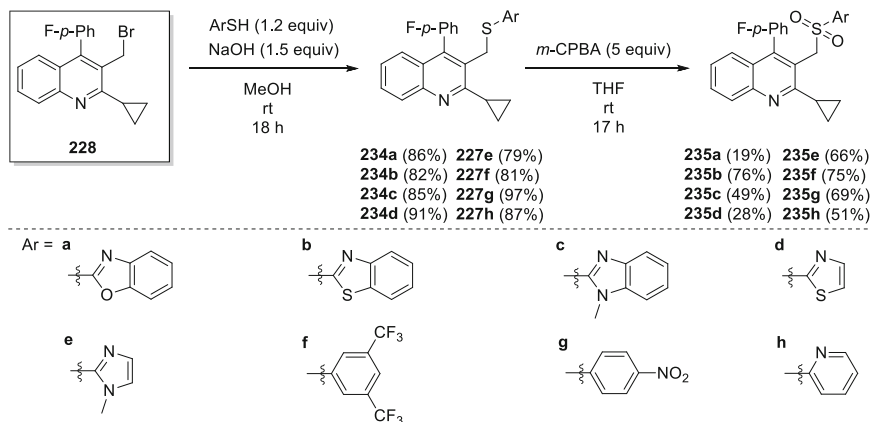
Although the chemical development of pitavastatin started more than two decades ago, this compound made it to the major markets only recently as the last of the super-statins to date. Pitavastatin was first approved in Japan in 2003, followed by an approval of the US Food and Drug Administration in 2009 and the European Medicines Agency in 2010. Besides some distinct structural features (e.g., quinoline heterocyclic core, cyclopropyl substituent), pitavastatin is little metabolized by cytochrome P450, which puts it in a unique position among the super-statins. Namely, due to its metabolism, pitavastatin is believed to be minimally involved in drug–drug interactions mediated by cytochrome P450 [132].

## 6.1 Synthesis of the Pitavastatin Quinoline Heterocyclic Core

A diverse array of phosphorous functionalized quinoline precursors that are suitable for the assembly of pitavastatin via the Wittig or Horner–Wadsworth–Emmons reactions was accessed, based on the 3-(bromomethyl)quinoline derivative **228** (Scheme 47) [133]. The alkyl bromide **228** was directly transformed to phosphonium bromide salts **229a,c,d,f** with various phosphines in toluene or THF at 50°C at 66% to 93% yields. To enable the investigation of the influence of the counterions on the stereochemical outcome of the Wittig reaction here, the preparation of the analogous trifluoroacetate salts **229b,e,g** was also pursued. In the first step, the alkyl bromide **228** was hydrolyzed with an aqueous NaHCO<sub>3</sub> in MeCN under reflux for 64 h, to provide the alkyl alcohol **230** at 88% yield. An activation of the primary alcohol moiety in **230** with trifluoromethanesulfonic anhydride (1.5 equiv.) in the presence of NEt<sub>3</sub> (2.0 equiv.) in THF at room temperature yielded the corresponding trifluoromethanesulfonate ester **231** at 93% yield. This was then subjected to reactions with various phosphines in PhMe under reflux for 6 h, which resulted in the formation of the corresponding phosphonium trifluoroacetate salts **229b,e,g**, which were isolated at 78% to 90% yields. The reaction of the alkyl



**Scheme 47** Synthesis of phosphorous-derivatized heterocyclic precursors of pitavastatin

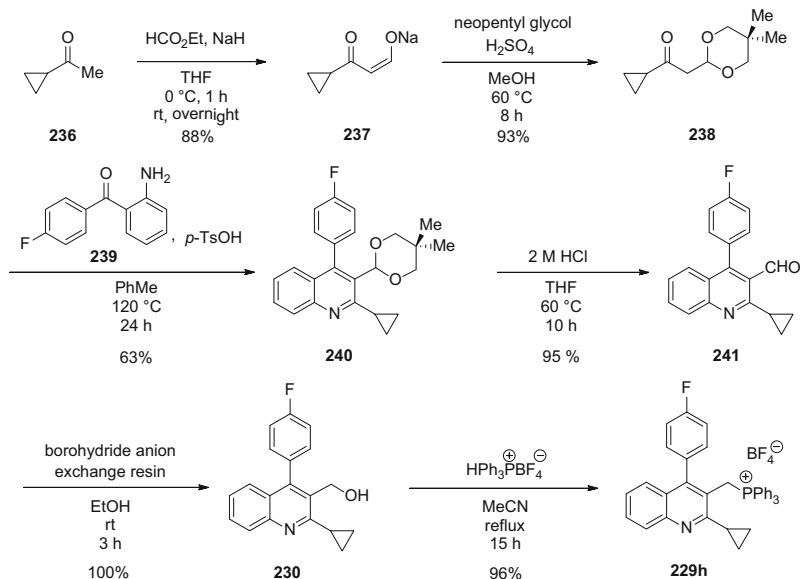


**Scheme 48** Synthesis of sulfide and sulfone heterocyclic precursors of pitavastatin

bromide **228** with in situ formed  $\text{Et}_2\text{POEt}$  (from  $\text{Et}_2\text{PCl}$  and  $\text{NaOEt}$ ) in  $\text{THF}$  under reflux for 18 h gave the phosphine oxide **232a** at 67% yield, while the analogous reaction of **228** with  $\text{Ph}_2\text{POEt}$  in  $\text{PhMe}$  under reflux for 64 h yielded the phosphine oxide **232b** at 91% yield. Finally, the phosphonate ester **233** was also made at 82% yield by the reaction of **228** with triethylphosphite in  $\text{PhMe}$  under reflux for 18 h.

A series of the sulfone-moiety-containing quinoline precursors for the assembly of pitavastatin via the Julia–Kocienski olefination was also prepared (Scheme 48) [128]. In the first step, the 3-(bromomethyl)quinoline derivative **228** was reacted with a series of aromatic and heteroaromatic thiols (1.2 equiv.) for 18 h at room temperature in  $\text{MeOH}$  using  $\text{NaOH}$  (1.5 equiv.) as the base. This provided a series of the sulfide heterocyclic derivatives **234a–h** at 79% to 97% yields. With sulfides **234a–h** in hand, the oxidation to the corresponding sulfones **235** was studied. Among several oxidants tested, including  $\text{KMnO}_4$  in  $\text{AcOH}/\text{MeCN}$ ,  $\text{NaIO}_4/\text{RuCl}_3\cdot\text{H}_2\text{O}$  in  $\text{MeCN}/\text{H}_2\text{O}$ , and  $m\text{-CPBA}$  in  $\text{THF}$ , the last of these provided the cleanest reaction and optimal results in terms of the yield. Therefore, an oxidation of **234a–h** with  $m\text{-CPBA}$  in  $\text{THF}$  at room temperature for 17 h provided the desired sulfones **235a–h** at 19% to 76% yields.

Very recently, Chen et al. [134] described the synthesis of the pitavastatin quinoline derivative **229h** that contains the triphenylphosphonium tetrafluoroborate salt moiety (Scheme 49). This synthesis started with the cyclopropyl methyl ketone **236**, which was reacted at  $0^\circ\text{C}$  with  $\text{NaH}$  in  $\text{THF}$  to provide the corresponding enolate, which was reacted with ethyl formate to provide the isolatable sodium enolate **237** at 88% yield. The reaction of **237** with 2,2-dimethyl-1,3-propanediol in  $\text{MeOH}$  in the presence of  $\text{H}_2\text{SO}_4$  for 8 h furnished the acetal **238** at 93% yield. The quinoline core **240** was assembled at 63% yield using a Friedländer reaction of ketone **238** with 2-amino-4'-fluorobenzophenone **239** in the presence of  $p\text{-TsOH}\cdot\text{H}_2\text{O}$  in toluene at  $120^\circ\text{C}$  over 24 h. Subsequently, the 1,3-dioxane moiety in **240** was deprotected using 2 M  $\text{HCl}$  in  $\text{THF}$  at  $60^\circ\text{C}$  for 10 h, to provide the quinoline-3-carbaldehyde **241** at an excellent 95% yield. The reduction of the



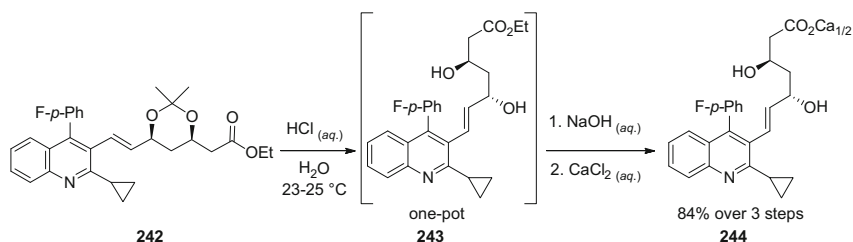
**Scheme 49** Synthesis of the quinoline core of pitavastatin and its subsequent functionalization on the 3-position

aldehyde **241** with borohydride anion exchange resin in EtOH at room temperature quantitatively provided the alcohol **230**. Finally, the reaction of the alcohol **230** with hydrogen triphenylphosphonium tetrafluoroborate under refluxing acetonitrile for 15 h provided the salt **229h** at 95% yield.

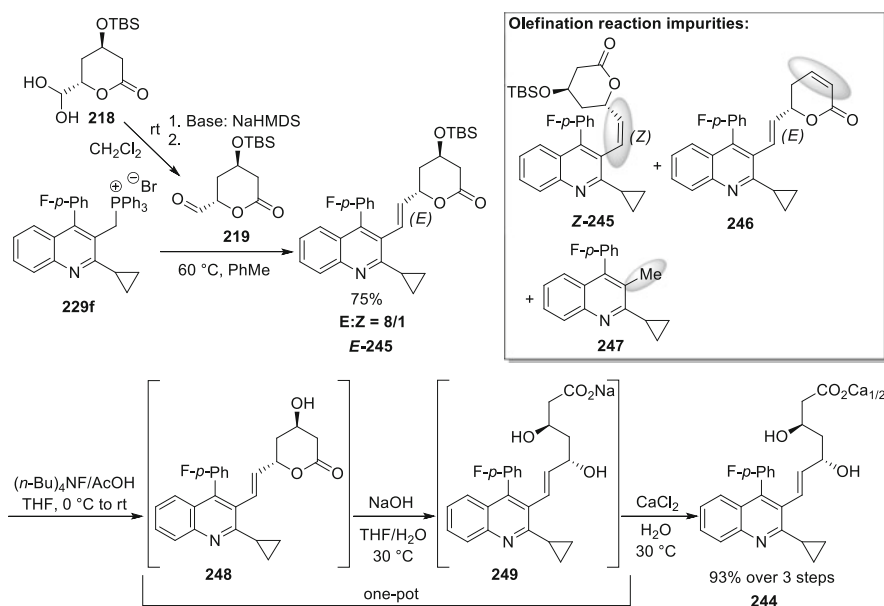
## 6.2 Assembly of Pitavastatin

Shekhawat and Sharma [135] reported a one-pot synthesis of pitavastatin calcium **244** from the acetonide-protected pitavastatin ethyl ester **242** (Scheme 50). A treatment of **242** in water with 5% aqueous HCl solution for 24 h at 23 °C to 25 °C provided the ethyl ester **243**, which was hydrolyzed with 10% aqueous NaOH solution in 3 h. The treatment of the sodium salt of pitavastatin that was formed with aqueous CaCl<sub>2</sub> solution precipitated pitavastatin calcium **244**, which was collected after 1 h stirring at ambient temperature, to provide 84% yield of **244** at 99.8 area% HPLC purity.

The assembly of pitavastatin calcium **244** was also achieved via the Wittig olefination using the lactonized lateral-chain precursor **219**, which was prepared by dehydration of the hydrate **218** in dichloromethane (Scheme 51) [133]. The screening of various phosphorous-derivatized pyrimidine precursors in the Wittig reaction with **219** showed that the triphenylphosphonium bromide salt **229f** gave the best yields. Indeed, **229f** gave the cleanest reaction, at 83% HPLC yield of

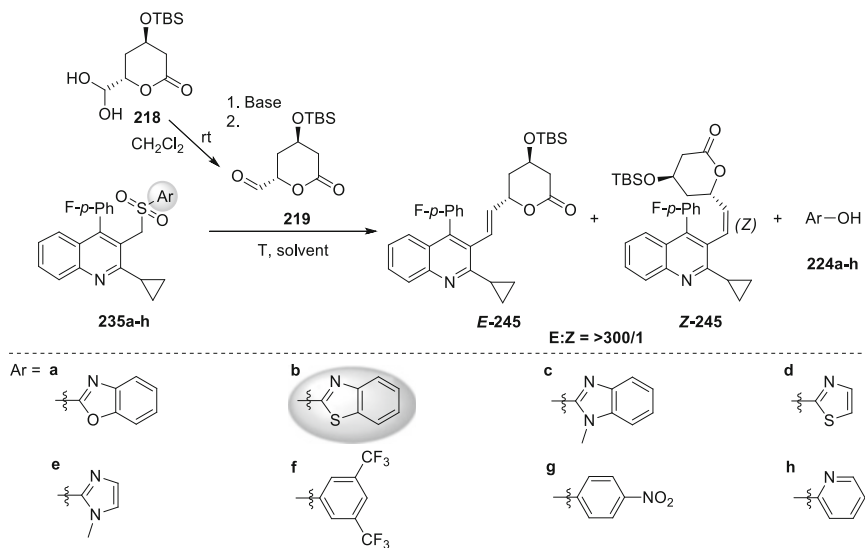


**Scheme 50** Synthesis of pitavastatin from the acetonide-protected ester precursor



**Scheme 51** Assembly of pitavastatin via a Wittig reaction using the lactonized precursor of the chiral lateral chain

**E-245**, along with 11% **Z-245** and low levels of other side products, such as the dehydro lactone derivative **246** and the 5-methylpyrimidine **247**. In contrast, the phosphine oxides **232** and the phosphonate ester **233** provided no coupling product, as they appear to be too basic and to promote the decomposition of **219**. With the lead heterocyclic coupling partner in hand, a screening for the best reaction conditions was performed by varying the type of the base, the solvent, and the temperature. This showed that the best effect on the outcome of the reaction was achieved when NaHMDS was used as the base (for the generation of the corresponding ylide from **229f**) in toluene at 60°C. With fixed optimal conditions, the preparative scale reaction enabled isolation of **E-245** at 75% yield after crystallization from an aqueous MeOH. To access pitavastatin calcium **244** in a concise

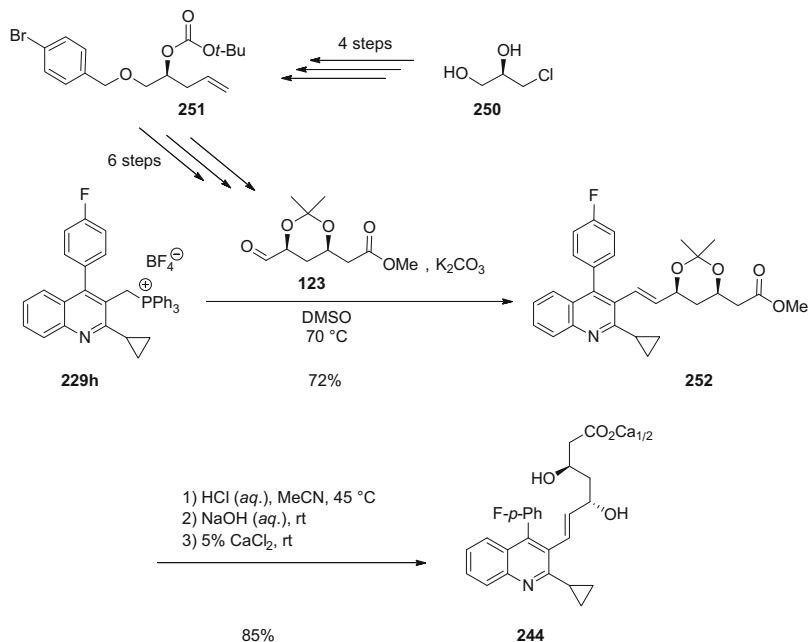


**Scheme 52** Assembly of pitavastatin via a Julia–Kocienski olefination using the lactonized precursor of the chiral lateral chain

manner, the lactone **E-245** was subjected to a three-step, one-pot reaction sequence. First, the TBS protection was removed with the *n*-Bu<sub>4</sub>F/AcOH couple in THF to provide the lactone **248**, which was hydrolyzed to pitavastatin sodium **249** with aqueous NaOH in THF/H<sub>2</sub>O, followed by cation exchange with CaCl<sub>2</sub> to furnish **244** at 93% yield over three steps.

A detailed NMR study supported by ab initio calculations of the conformations of the *Z*-isomeric pitavastatin analogs (i.e., **Z-245**, its *O*-TBS-deprotected analog, *Z*-pitavastatin) was also conducted [136]. This demonstrated that the NMR resonance line broadening that was observed at room temperature originated from the dynamic exchange between two rotamers. Moreover, this study also confirmed that for *Z*-isomeric pitavastatin analogs, the rotation across the C5′–C7 bond is crucial for the generation of a pair of atropisomers.

Recently, the Julia–Kocienski olefination was used for the assembly of pitavastatin calcium **244** using the lactonized lateral-chain precursor **219**, which was obtained by dehydration of the hydrate **218** in dichloromethane (Scheme 52) [128]. A screening of various sulfone-coupling partners **235a–h** for the olefination with **219** revealed that the cleanest reaction with the highest conversion was obtained with benzothiazole sulfone **235b**. In contrast to the analogous Wittig olefination where impurities **246** and **247** were formed in notable amounts in some cases under screening conditions [133], the only products observed in this Julia–Kocienski reaction were the desired *O*-TBS-protected pitavastatin lactone **E-245**, its geometrical isomer **Z-245**, and the corresponding arylalcohol **224a–h**



**Scheme 53** Synthesis of pitavastatin calcium via a Wittig reaction using the dually protected open precursor of the chiral lateral chain

by-product. The subsequent optimization of the Julia–Kocienski reaction conditions showed that this reaction proceeded best when **235b** reacts with **219** (1.2 equiv.) in the presence of NaHMDS (1.2 equiv.) in THF at  $-60^\circ\text{C}$ . Under these conditions, up to 71% HPLC yield of **E-245** was obtained. An excellent stereoselectivity was also obtained, with  $E/Z > 300:1$ . At the preparative scale using the optimal conditions, this gave 78% HPLC yield of **E-245** and enabled the isolation of **E-245** at 71% yield and at  $>97\%$  HPLC purity.

Chen et al. [134] described the synthesis of pitavastatin using the Wittig reaction between the triphenylphosphonium tetrafluoroborate salt **229h** and the aldehyde-type dually protected C-6 lateral-chain precursor **123** (Scheme 53). The **123** was prepared starting from (*R*)-3-chloro-1,2-propanediol **250**, via the homoallylic carbonate **251** in a total of 10 steps. The Wittig reaction of the aldehyde **123** and the ylide, which was derived from the salt **229h** with  $\text{K}_2\text{CO}_3$  base in DMSO at  $70^\circ\text{C}$ , provided the acetonide-protected pitavastatin methyl ester **252** at 72% yield. A removal of the acetonide-protecting group with HCl in MeCN at  $45^\circ\text{C}$ , followed by the hydrolysis of the ester moiety with NaOH at room temperature and the cation exchange with  $\text{CaCl}_2$ , provided pitavastatin calcium **244** at 85% yield over three steps [134].

## 7 Conclusions

Statins, and in particular the super-statins, continue to inspire and attract synthetic chemists for the development of new approaches for their efficient preparation. In this review, I have highlighted new advances in the synthesis of super-statins that have emerged in the period from 2010 to 2015, since my last review [15]. Although enormous efforts have been made towards the development of efficient synthetic methodologies for the construction of super-statins since their discovery several decades ago, the important advances that have been achieved in this area have occurred in the last few years. Indeed, enzymatic and whole-cell biocatalysis, in particular, have emerged as a promising new area of the development for the construction of the chiral statin lateral-chain precursors. These biocatalytic approaches operate with superb efficiencies and stereoselectivities, under mild reaction conditions, and in many cases in pure aqueous medium, which follows the sustainability principles, due to the minimal waste generation. Therefore, the principles of genetic engineering and synthetic biology have been applied to statin chiral side-chain assembly in cascade reactions, which has enabled efficient and easy assembly of the advanced statin chiral lateral-chain precursors from simple starting materials. Furthermore, several new and efficient organocatalytic and transition-metal-catalyzed asymmetric methodologies have appeared for the construction of the advanced intermediates of the chiral statin lateral chains. Moreover, notable advances have been realized in the area of a super-statin heterocyclic core synthesis, where several new approaches for indole, pyrrole, pyrimidine, and quinoline have been described. Last but not least, the super-statin heterocyclic cores have been successfully assembled into super-statins with chiral statin lateral-chain precursors using several new intriguing methodologies. As statins might remain the first-line treatment of hypercholesterolemia for decades to come, and as the statin market will soon become fully generic, the cost of the synthesis and formulation of the super-statins will have pivotal roles for the future commercial success of all of the market players and will bring the cost benefits to the healthcare systems worldwide. This will trigger the continuous search for the more efficient, cheaper, and sustainable synthesis of statins [137] and in particular super-statins. This has already been reflected in some reports that have appeared in the literature since this review was written [138–144].

## References

1. Endo A (1992) *J Lipid Res* 33:1569–1582
2. Endo A, Hasumi K (1993) *Nat Prod Rep* 10:541–550
3. Manzoni M, Rollini M (2002) *Appl Microbiol Biotechnol* 58:555–564
4. Endo A (2008) *Nat Med* 14:1050–1052
5. Li JJ (2009) *Triumph of the heart: the story of statins*. Oxford University Press, New York
6. Endo A (2010) *Proc Jpn Acad Ser B* 86:484–493

7. Beekman AM, Barrow RA (2014) *Aust J Chem* 67:827–843
8. Stokker GE, Hoffman WF, Alberts AW, Cragoe EJ, Deana AA, Gilfillan JL, Huff JW, Novello FC, Prugh JD, Smith RL, Willard AK (1985) *J Med Chem* 28:347–358
9. Miyachi N, Suzuki M, Ohara Y, Hiyama T (1995) *J Synth Org Chem Jpn* 53:186–196
10. Repič O, Prasad K, Lee GT (2001) *Org Process Res Dev* 5:519–527
11. Roth BD (2002) In: King FD, Oxford AW (eds) *Progress in medicinal chemistry*, vol 40. Elsevier, Amsterdam, pp 1–22
12. Li JJ, Johnson DS, Sliskovic DR, Roth BD (2004) *Contemporary drug synthesis*. Wiley, Hoboken, pp 113–124
13. Pfefferkorn JA (2007) In: Johnson DS, Li JJ (eds) *The art of drug synthesis*. Wiley, Hoboken, pp 169–182
14. Hajkova M, Kratochvila B, Radl S (2008) *Chem Listy* 102:3–14
15. Časar Z (2010) *Curr Org Chem* 14:816–845
16. Harrington PJ (2011) Lipitor<sup>®</sup> (Atorvastatin Calcium) in pharmaceutical process chemistry for synthesis: rethinking the routes to scale-up. Wiley, Hoboken
17. McPherson PAC (2012) *Mini-Rev Med Chem* 12:1250–1260
18. Wang J, Sánchez-Roselló M, Aceña JL, del Pozo C, Sorochinsky AE, Fustero S, Soloshonok VA, Liu H (2014) *Chem Rev* 114:2432–2506
19. Furberg CD, Pitt B (2001) *Curr Control Trials Cardiovasc Med* 2:205–207
20. Pfefferkorn JA (2009) *Curr Opin Invest Drugs* 10:245–252
21. Pfefferkorn JA (2011) *Expert Opin Ther Patents* 21:187–203
22. Bratton LD, Auerbach B, Choi C, Dillon L, Hanselman JC, Larsen SD, Lu G, Olsen K, Pfefferkorn JA, Robertson A, Sekerke C, Trivedi BK, Unangst PC (2007) *Bioorg Med Chem Lett* 15:5576–5589
23. Pfefferkorn JA, Song Y, Sun K-L, Miller SR, Trivedi BK, Choi C, Sorenson RJ, Bratton LD, Unangst PC, Larsen SD, Poel T-J, Cheng X-M, Lee C, Erasga N, Auerbach B, Askew V, Dillon L, Hanselman JC, Lin Z, Lu G, Robertson A, Olsen K, Mertz T, Sekerke C, Pavlovsky A, Harris MS, Bainbridge G, Caspers N, Chen H, Eberstadt M (2007) *Bioorg Med Chem Lett* 17:4538–4544
24. Larsen SD, Poel T-J, Filipinski KJ, Kohrt JT, Pfefferkorn JA, Sorenson RJ, Tait BD, Askew V, Dillon L, Hanselman JC, Lu GH, Robertson A, Sekerke C, Kowala MC, Auerbach BJ (2007) *Bioorg Med Chem Lett* 17:5567–5572
25. Cai Z, Zhou W, Sun L (2007) *Bioorg Med Chem Lett* 15:7809–7829
26. Pfefferkorn JA, Choi C, Larsen SD, Auerbach B, Hutchings R, Park W, Askew V, Dillon L, Hanselman JC, Lin Z, Lu GH, Robertson A, Sekerke C, Harris MS, Pavlovsky A, Bainbridge G, Caspers N, Kowala M, Tait BD (2008) *J Med Chem* 51:31–45
27. Park WKC, Kennedy RM, Larsen SD, Miller S, Roth BD, Song Y, Steinbaugh BA, Sun K, Tait BD, Kowala MC, Trivedi BK, Auerbach B, Askew V, Dillon L, Hanselman JC, Lin Z, Lu GH, Robertson A, Sekerke C (2008) *Bioorg Med Chem Lett* 18:1151–1156
28. Ahmad S, Madsen CS, Stein PD, Janovitz E, Huang C, Ngu K, Bisaha S, Kennedy LJ, Chen B-C, Zhao R, Sitkoff D, Monshizadegan H, Yin X, Ryan CS, Zhang R, Giancarli M, Bird E, Chang M, Chen X, Setters R, Search D, Zhuang S, Nguyen-Tran V, Cuff CA, Harrity T, Darienzo CJ, Li T, Reeves RA, Blanar MA, Barrish JC, Zahler R, Robl JA (2008) *J Med Chem* 51:2722–2733
29. Sarver RW, Bills E, Bolton G, Bratton LD, Caspers NL, Dunbar JB, Harris MS, Hutchings RH, Kennedy RM, Larsen SD, Pavlovsky A, Pfefferkorn JA, Bainbridge G (2008) *J Med Chem* 51:3804–3813
30. Hobson LA, Akiti O, Deshmukh SS, Harper S, Katipally K, Lai CJ, Livingston RC, Lo E, Miller MM, Ramakrishnan S, Shen L, Spink J, Tummala S, Wei C, Yamamoto K, Young J, Parsons RL Jr (2010) *Org Process Res Dev* 14:441–458
31. Bowles DM, Boyles DC, Choi C, Pfefferkorn JA, Schuyler S (2011) *Org Process Res Dev* 15:148–157

32. Hao Q, Cai Z, Pan J, Li Y, Xia Y, Min Y, Sheng Y, Zhou W (2011) *Chem Biol Drug Des* 78:730–733
33. Pfefferkorn JA, Litchfield J, Hutchings R, Cheng X-M, Larsen SD, Auerbach B, Bush MR, Lee C, Erasga N, Bowles DM, Boyles DC, Lu G, Sekerke C, Askew V, Hanselman JC, Dillon L, Lin Z, Robertson A, Olsen K, Boustany C, Atkinson K, Goosen TC, Sahasrabudhe V, Chupka J, Duignan DB, Feng B, Scialis R, Kimoto E, Bi Y-A, Lai Y, El-Kattan A, Bakker-Arkema R, Barclay P, Kindt E, Le V, Mandema JW, Milad M, Tait BD, Kennedy R, Trivedi BK, Kowala M (2011) *Bioorg Med Chem Lett* 21:2725–2731
34. Xiaoguang W, Xiang F, Xueyan Y, Meng N, Fanhong W (2012) *Chin J Chem* 30:2767–2773
35. Jiayi T, Naxin W, Hua X (2013) *Lett Drug Des Discovery* 10:817–822
36. Hao Q, Pan J, Li Y, Cai Z, Zhou W (2013) *Org Process Res Dev* 17:921–926
37. Chandra Sekhar BVVN, Kumar NR, Mukkanti K, Kalyan Chakravarthy A (2012) *Asian J Chem* 24:1357–1361
38. Müller M (2005) *Angew Chem Int Ed* 44:362–365
39. Liljeblad A, Kallinen A, Kanerva LT (2009) *Curr Org Synth* 6:362–379
40. Ikunaka M (2007) *Org Process Res Dev* 11:495–502
41. Andrushko N, Andrushko V, Tararov V, Korostylev A, König G, Börner A (2010) *Chirality* 22:534–541
42. Ye Q, Ouyang P, Ying H (2011) *Appl Microbiol Biotechnol* 89:513–522
43. Bornscheuer UT, Huisman GW, Kazlauskas RJ, Lutz S, Moore JC, Robins K (2012) *Nature* 485:185–194
44. Liljeblad A, Kallinen A, Kanerva LT (2013) *Adv Org Synth* 3:195–236
45. You Z-Y, Liu Z-Q, Zheng Y-G (2014) *Appl Microbiol Biotechnol* 98:11–21
46. Gupta P, Mahajan N, Taneja SC (2013) *Catal Sci Technol* 3:2462–248
47. Vasić-Rački Đ (2006) History of industrial biotransformations – dreams and realities. In: Liese A, Seelbach K, Wandrey C (eds) *Industrial Biotransformations*, 2nd edn. Weinheim, Wiley-VCH, pp 1–29
48. Liese A, Vilela Filho M (1999) *Curr Opin Biotechnol* 10:595–603
49. Schulze B, Wubbolts MG (1999) *Curr Opin Biotechnol* 10:609–615
50. Wandrey C, Liese A, Kihumbu D (2000) *Org Process Res Dev* 4:286–290
51. Zaks A (2001) *Curr Opin Chem Biol* 5:130–136
52. Koeller KM, Wong C-H (2001) *Nature* 409:232–240
53. Schmid A, Dordick JS, Hauer B, Kiener A, Wubbolts M, Witholt B (2001) *Nature* 409:258–268
54. Straathof AJJ, Panke S, Schmid A (2002) *Curr Opin Biotechnol* 13:548–556
55. Patel RN (2002) *Enzyme Microb Technol* 31:804–826
56. Bertau M (2002) *Curr Org Chem* 6:987–1014
57. Schoemaker HE, Mink D, Wubbolts MG (2003) *Science* 299:1694–1697
58. Yazbeck DR, Martinez CA, Hu S, Tao J (2004) *Tetrahedron Asymmetry* 15:2757–2763
59. Panke S, Held M, Wubbolts M (2004) *Curr Opin Biotechnol* 15:272–279
60. Panke S, Wubbolts M (2005) *Curr Opin Chem Biol* 9:188–194
61. Pollard DJ, Woodley JM (2006) *Trends Biotechnol* 25:66–73
62. Hudlicky T, Reed JW (2009) *Chem Soc Rev* 38:3117–3132
63. Tao J, Liu J, Chen Z (2010) In: Blaser H-U, Federsel H-J (eds) *Asymmetric catalysis on industrial scale: challenges, approaches and solutions*, 2nd edn. Wiley-VCH, Weinheim, pp 1–12
64. Wohlgemuth R (2010) *Curr Opin Biotechnol* 21:713–724
65. Hernáiz MJ, Alcántara AR, García JI, Sinisterra JV (2010) *Chem Eur J* 16:9422–9437
66. Zheng G-W, Xu J-H (2011) *Curr Opin Biotechnol* 22:784–792
67. Wenda S, Illner S, Mell A, Kragl U (2011) *Green Chem* 13:3007–3047
68. Muñoz Solano D, Hoyos P, Hernáiz MJ, Alcántara AR, Sánchez-Montero JM (2012) *Bioresour Technol* 115:196–207
69. Sheldon RA (2012) *Chem Soc Rev* 41:1437–1451

70. Dunn PJ (2012) *Chem Soc Rev* 41:1452–1461
71. Clouthier CM, Pelletier JN (2012) *Chem Soc Rev* 41:1585–1605
72. Ni Y, Xu J-H (2012) *Biotechnol Adv* 30:1279–1288
73. Oroz-Guinea I, García-Junceda E (2013) *Curr Opin Chem Biol* 17:236–249
74. Huisman GW, Collier SJ (2013) *Curr Opin Chem Biol* 17:284–292
75. Hoyos P, Pace V, Hernaiz MJ, Alcantara AR (2014) *Curr Green Chem* 1:155–181
76. Gijzen HJM, Wong C-H (1994) *J Am Chem Soc* 116:8422–8423
77. Gijzen HJM, Wong C-H (1995) *J Am Chem Soc* 117:7585–7591
78. Greenberg WA, Varvak A, Hanson SR, Wong K, Huang H, Chen P, Burk MJ (2004) *Proc Natl Acad Sci USA* 101:5788–5793
79. Gijzen HJM, Qiao L, Fitz W, Wong C-H (1996) *Chem Rev* 96:443–474
80. Udovič M, Tramšek M, Plantan I, Cluzeau J (2011) *PCT Pat Appl WO2011064249*
81. Liu J, Hsu C-C, Wong C-H (2004) *Tetrahedron Lett* 45:2439–2441
82. Hu S, Tao J, Xie Z (2006) *PCT Pat Appl WO06134482*
83. Časar Z (2008) *Synlett* 2036–2040
84. Časar Z, Košmrlj J (2009) *Synlett* 1144–1148
85. Ma SK, Gruber J, Davis C, Newman L, Gray D, Wang A, Grate J, Huisman GW, Sheldon RA (2010) *Green Chem* 12:81–86
86. Dong H-P, Liu Z-Q, Zheng Y-G, Shen Y-C (2010) *Appl Microbiol Biotechnol* 87:1335–1345
87. Sawant P, Maier ME (2010) *Tetrahedron* 66:9738–9744
88. Troiani V, Cluzeau J, Časar Z (2011) *Org Process Res Dev* 15:622–630
89. Wu X, Jiang J, Chen Y (2011) *ACS Catal* 1:1661–1664
90. Kawato Y, Iwata M, Yazaki R, Kumagai N, Shibasaki M (2011) *Tetrahedron* 67:6539–6546
91. Wang X, Fang X, Xiao H, Yin Y, Xia H, Wu F (2012) *J Fluorine Chem* 133:178–183
92. Fan W, Li W, Ma X, Tao X, Li X, Yao Y, Xie X, Zhang Z (2012) *Chem Commun* 48:4247–4249
93. Sawant P, Maier ME (2012) *Eur J Org Chem* 6576–6585
94. Lu M, Huang Y, White MA, Wu X, Liu N, Cheng X, Chen Y (2012) *Chem Commun* 48:11352–11354
95. You Z-Y, Liu Z-Q, Zheng Y-G, Shen Y-C (2013) *J Ind Microbiol Biotechnol* 40:29–39
96. Li X, Yajun W, Zheng C, Zhiqiang L, Yuguo Z (2013) *Chin J Bioprocess Eng* 11:29–34
97. Kawato Y, Chaudhary S, Kumagai N, Shibasaki M (2013) *Chem Eur J* 19:3802–3806
98. Ošljaj M, Cluzeau J, Orkič D, Kopitar G, Mrak P, Časar Z (2013) *PLoS One* 8, e62250
99. Ručigaj A, Krajnc M (2013) *Org Process Res Dev* 17:854–862
100. Ručigaj A, Krajnc M (2015) *Chem Eng J* 259:11–24
101. Schallmey M, Floor RJ, Hauer B, Breuer M, Jekel PA, Wijma HJ, Dijkstra BW, Janssen DB (2013) *ChemBioChem* 14:870–881
102. Kobayashi Y, Taniguchi Y, Hayama N, Inokuma T, Takemoto Y (2013) *Angew Chem Int Ed* 52:11114–11118
103. Vajdič T, Ošljaj M, Kopitar G, Mrak P (2014) *Metab Eng* 24:160–172
104. You Z-Y, Liu Z-Q, Zheng Y-G (2014) *Appl Microbiol Biotechnol* 98:1671–1680
105. Chen X, Xiong F, Chen W, He Q, Chen F (2014) *J Org Chem* 79:2723–2728
106. Subrizi F, Crucianelli M, Grossi V, Passacantando M, Botta G, Antiochia R, Saladino R (2014) *ACS Catal* 4:3059–3068
107. Xiong F-J, Li J, Chen X-F, Chen W-X, Chen F-E (2014) *Tetrahedron Asymmetry* 24:1205–1208
108. Chen X, Xiong F, Zheng C, Li J, Chen F (2014) *Tetrahedron* 70:5794–5799
109. Wu X, Gou X, Chen Y (2015) *Process Biochem* 50:104–110
110. Yao P, Li J, Yuan J, Han C, Liu X, Feng J, Wu Q, Zhu D (2015) *ChemCatChem* 7:271–275
111. Yao P, Wang L, Yuan J, Cheng L, Jia R, Xie M, Feng J, Wang M, Wu Q, Zhu D (2015) *ChemCatChem* 7:1438–1444
112. Fuenfschilling PC, Hoehn P, Mutz J-P (2007) *Org Process Res Dev* 11:13–18
113. Huang J, Macdonald SJF, Harrity JPA (2010) *Chem Commun* 46:8770–8772

114. Zacharia JT, Tanaka T, Hayashi M (2010) *J Org Chem* 75:7514–7518
115. Donohoe TJ, Race NJ, Bower JF, Callens CKA (2010) *Org Lett* 12:4094–4097
116. Schäfer I, Opatz T (2011) *Synthesis* 1691–1704
117. Xuan J, Xia X-D, Zeng T-T, Feng Z-J, Chen J-R, Lu L-Q, Xiao W-J (2014) *Angew Chem Int Ed* 53:5653–5656
118. Lee HW, Kim YM, Yoo CL, Kang SK, Ahn SK (2008) *Biomol Ther* 16:28–33
119. Nagib DA, MacMillan DWC (2011) *Nature* 480:224–228
120. Gao J, Guo YH, Wang YP, Wang XJ, Xiang WS (2011) *Chin Chem Lett* 22:1159–1162
121. Hu L, Xiong F, Chen X, Chen W, He Q, Chen F (2013) *Tetrahedron Asymmetry* 24:207–211
122. Luo Y, Roy ID, Madec AGE, Lam HW (2014) *Angew Chem Int Ed* 53:4186–4190
123. Estévez V, Villacampa M, Menéndez JC (2014) *Org Chem Front* 1:458–463
124. Novozhilov YV, Dorogov MV, Blumina MV, Smirnov AV, Krasavin M (2015) *Chem Cent J* 9:7. doi:10.1186/s13065-015-0082-7
125. Šterk D, Časar Z, Jukič M, Košmrlj J (2012) *Tetrahedron* 68:2155–2160
126. Šterk D, Jukič M, Časar Z (2013) *Org Process Res Dev* 17:145–151
127. Guan Y, Zhou G, Yang W (2014) *Heterocycl Commun* 20:11–13
128. Fabris J, Časar Z, Gazić Smilović I, Črnugelj M (2014) *Synthesis* 46:2333–2346
129. Li J, Wang H, Liu L, Sun J (2014) *RSC Adv* 4:49974–49978
130. Časar Z, Steinbücher M, Košmrlj J (2010) *J Org Chem* 75:6681–6684
131. Fabris J, Makuc D, Časar Z, Plavec J (2013) *Tetrahedron* 69:6262–6268
132. Sasaki J (2010) *Vasc Health Risk Manage* 6:997–1005
133. Fabris J, Časar Z, Gazić Smilović I (2012) *Synthesis* 44:1700–1710
134. Chen W, Xiong F, Liu Q, Xu L, Wu Y, Chen F (2015) *Tetrahedron* 71:4730–4737
135. Shekhawat KS, Sharma DK (2012) *Pharm Lett* 4:1553–1557
136. Makuc D, Fabris J, Časar Z, Plavec J (2013) *Molecules* 18:13283–13296
137. McLean KJ, Hans M, Meijrink B, van Scheppingen WB, Vollebregt A, Tee KL, van der Laan J-M, Leys D, Munro AW, van den Berg MA (2015) *Proc Natl Acad Sci USA* 112:2847–2852
138. He Y-C, Zhang D-P, Lu Y, Tao Z-C, Ding Y, Wang L-Q, Liu F (2015) *Bioengineered* 6:170–174
139. Tartaggia S, Ferrari C, Pontini M, De Lucchi O (2015) *Eur J Org Chem* 4102–4107
140. Metzner R, Hummel W, Wetterich F, König B, Gröger H (2015) *Org Process Res Dev* 19:635–638
141. Jiao X-C, Pan J, Xu G-C, Kong X-D, Chen Q, Zhang Z-J, Xu J-H (2015) *Catal Sci Technol* 5:4048–4054
142. Wang H, Li Z, Yu X, Chen X, Liu L (2015) *RSC Adv* 5:75160–75166
143. Xiong F, Wang H, Yan L, Xu L, Tao Y, Wu Y, Chen F (2015) *Org Biomol Chem* 13:9813–9819
144. Wu Y, Xiong FJ, Chen FE (2015) *Tetrahedron* 71:8487–8510

# Development of Synthetic Routes to Dolutegravir

Erwin Schreiner, Frank Richter, and Sven Nerdinger

**Abstract** Within the last decade, a new class of anti-HIV drugs, the so-called integrase inhibitors featuring a novel mode of action, became available as an additional treatment option. The design and discovery of integrase inhibitors were first focusing on targeting the catalytic site of HIV-1 integrase with a specific effect on strand transfer. This approach led to a first generation of 3'-processing and strand transfer inhibitors (INSTIs), from which raltegravir and elvitegravir have been promoted to market. These first-generation integrase inhibitors proved remarkably efficient at reducing viral load in treatment of naive patients' viral strains. However, subsequent discovery of a low genetic barrier of resistance demonstrated the pressing need for the development of second-generation INSTIs that should be active against raltegravir-resistant and elvitegravir-resistant viral strains. Very recently, dolutegravir sodium, a molecule with a significantly improved resistance profile, received approval in major markets. Dolutegravir features a tricyclic carbamoyl pyridone core comprising two chiral carbon centres. This paper will summarise several synthetic routes disclosed for the preparation of dolutegravir as well as discuss their applicability at multi-ton scale.

**Keywords** Carbamoyl pyridone • Dolutegravir • HIV-1 integrase inhibitor

## Contents

1	Introduction .....	189
2	Synthetic Routes Towards Dolutegravir .....	190
2.1	Synthetic Routes of the Originator (Shionogi, GlaxoSmithKline) .....	190
2.2	Synthetic Routes of Generic Competitors .....	198
2.3	Synthesis of (R)-3-Aminobutan-1-ol .....	202

3 Summary, Conclusions and Outlook .....	205
References .....	206

## Abbreviations

Ac	Acetyl
All	Allyl
Am	Amyl
ART	Antiretroviral therapy
Asp	Asparaginic acid
Bn	Benzyl
Bu	Butyl
<i>t</i> -Bu	<i>tert</i> -Butyl
CDI	1,1'-Carbonyldiimidazole
cDNA	Complementary DNA
cryst	Crystallisation
CSA	Camphorsulfonic acid
DBU	1,8-Diazabicyclo [5.4.0]undec-7-ene
DIEA	<i>N,N</i> -Diisopropylethylamine
DME	Dimethoxyethane
DMF	Dimethylformamide
DMSO	Dimethyl sulfoxide
dppp	1,3-Bis(diphenylphosphino)propane
DuanPhos	2,2'-Di- <i>tert</i> -butyl-2,3,2',3'-tetrahydro-1 <i>H</i> ,1' <i>H</i> -(1,1') biisophosphindolyl
EDC	1-Ethyl-3-(3-dimethylaminopropyl)carbodiimide
<i>ee</i>	Enantiomeric excess
Et	Ethyl
Glu	Glutamic acid
HATU	1-[Bis(dimethylamino)methylene]-1 <i>H</i> -1,2,3-triazolo[4,5- <i>b</i> ] pyridinium 3-oxid hexafluorophosphate
HIV	Human immunodeficiency virus
HOBt	1-Hydroxybenzotriazol
INSTI	Integrase strand transfer inhibitor
IP	Intellectual property
LAH	Lithium aluminium hydride
LiHMDS	Lithium hexamethyldisilazide lithium bis(trimethylsilyl)amide
<i>m</i> -CPBA	<i>m</i> -Chloroperoxybenzoic acid
Me	Methyl
MW	Microwave irradiation
Ms	Methanesulfonyl (mesyl)
NBS	<i>N</i> -Bromosuccinimide
NMO	<i>N</i> -Methylmorpholine <i>N</i> -oxide

NMP	<i>N</i> -Methylpyrrolidone
NNRTI	Non-nucleosidic reverse transcriptase inhibitor
NRTI	Nucleoside/nucleotide reverse transcriptase inhibitor
Ph	Phenyl
Pro	Proline
<i>i</i> -Pr	Isopropyl
rt	Room temperature
Raney-Ni	Raney nickel
TangPhos	1,1'-Di- <i>tert</i> -butyl-(2,2')-diphospholane
TBME	<i>tert</i> -Butyl methyl ether
TFA	Trifluoroacetyl
THF	Tetrahydrofuran
Ts	4-Toluenesulfonyl (tosyl)
Xantphos	4,5-Bis(diphenylphosphino)-9,9-dimethylxanthene

## 1 Introduction

Significant advances in the management of human immunodeficiency virus type-1 (HIV-1) infection during the past two decades have resulted in a dramatic reduction of HIV-1-caused morbidity and HIV-1-caused mortality [1]. However, effective antiretroviral therapy (ART) requires life-long and daily administration of multiple antiretroviral drugs as part of a combination treatment regimen. Recommended are combinations consisting of at least three ART drugs. Very often, those comprise two nucleoside/nucleotide reverse transcriptase inhibitors (NRTIs) plus a third agent selected from a non-nucleosidic reverse transcriptase inhibitor (NNRTI), a ritonavir-boosted HIV protease inhibitor or integrase inhibitor. All integrase inhibitors, developed so far, bind to the active catalytic site of the virus enzyme in complex with viral DNA, blocking the strand transfer in the cDNA integration process. For this reason, they are usually termed integrase strand transfer inhibitors (INSTIs). The title molecule, dolutegravir (**1**) (Fig. 1), is a second-generation INSTI featuring enhanced mutation resistance compared to those reaching the market before [2–4].

As observed for all INSTIs, pharmacophores in **1** comprise (1) a triad of coplanar heteroatoms (highlighted in red), which chelates two magnesium ions in the active site of the HIV reverse transcriptase [5–7], and (2) a mono- or bis-fluorinated phenyl ring connected via a flexible linker facilitating a hydrophobic interaction in a pocket vacated by adenosine base 17 [8, 9]. Key features of the binding of **1** to its target are summarised in Fig. 2.

Furthermore, a hydrophobic interaction of the tricyclic core with the side chain of proline 145 is of importance for the correct positioning of the drug molecule in the binding site.

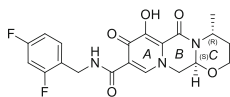


**Fig. 1** Chemical structure of dolutegravir (**1**)

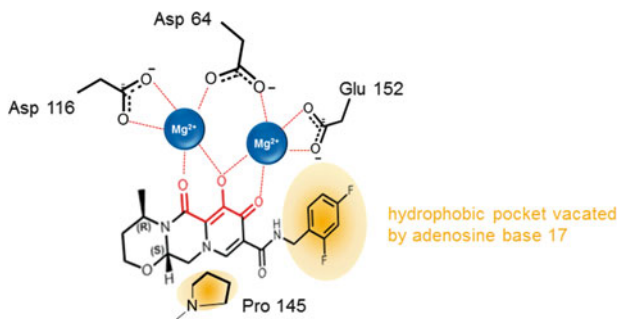


**Fig. 2** Schematic visualisation of key interactions of dolutegravir (**1**) with HIV integrase

## 2 Synthetic Routes Towards Dolutegravir

Identification of a robust, safe and economical efficient route for a highly functionalised tricyclic molecule as **1** is an attractive challenge for synthetic development chemists. Although the drug received its first approval in the USA by Food and Drug Administration just in the middle of 2013, marketed volume for **1** between March 2014 and March 2015 was already about one ton (Source: Thomson Reuters). Far higher amounts of the API needed are expected for the future.

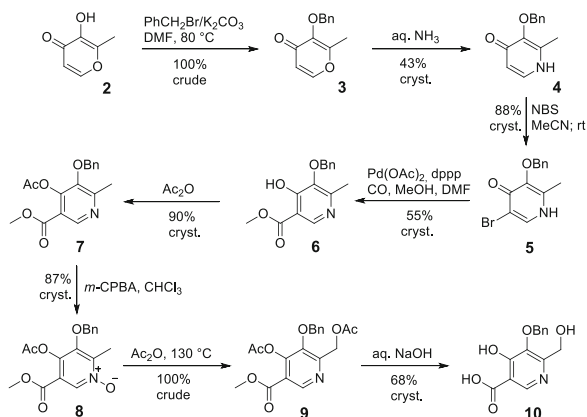
In this article, we will differentiate between two players on the scene, the so-called originator(s) and their generic competitors.

### 2.1 Synthetic Routes of the Originator (Shionogi, GlaxoSmithKline)

Originator(s), inventor or licensee, is the first one preparing and usually also dealing with industrial production of an individual drug substance. Consequently, it is their privilege to freely select among many potential routes and to protect IP for processes and intermediates involved, if they can proof novelty, inventive step and industrial applicability.

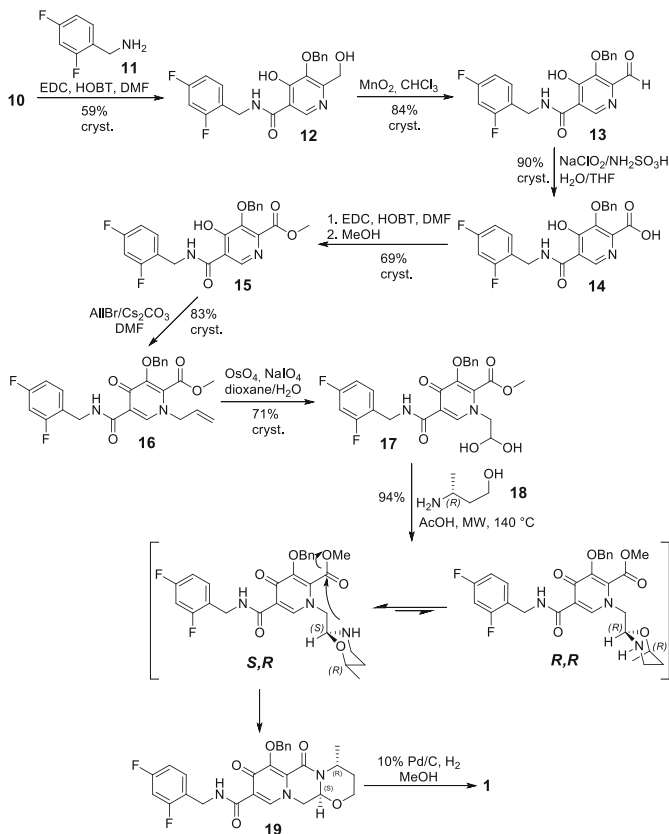
The concept for INSTIs comprising polycyclic cores had been disclosed already in 2001 by Shionogi scientists [10]; however, no tricyclic compounds had been disclosed nor methods for producing them were presented. Five years later, in 2006, the group disclosed dolutegravir **1** among numerous examples of bicyclic and tricyclic integrase inhibitors in another patent application [11].

**Scheme 1** Synthesis of A-ring building block **10** according to [11]



They start their synthesis from maltol, 3-hydroxy-2-methyl-4*H*-pyran-4-one, (**2**) which is transformed into the crystalline *O*-benzylated 2-methylpyridin-4(*1H*)-one (**4**) in a two-step process via alkylation providing **3** and subsequent treatment with aqueous ammonia in 43% overall yield. Regioselective introduction of bromine at the 5-position followed by Pd-catalysed carbonylation in methanol and *O*-acetylation yield crystalline **7** in 44% via intermediates **5** and **6**. Oxidation of the pyridine nitrogen to the N-oxide (**8**) with *m*-CPBA followed by *O*-acetylation of the N-oxide, subsequent rearrangement at 130°C and final alkaline acetate ester saponification provides the crystalline A-ring building block **10** in 11% total yield starting from **2** (see Scheme 1).

Next, the hydrophobic side chain is introduced by coupling of **10** with (2,4-difluorophenyl)methanamine (**11**) in the presence of EDC/HOBT yielding crystalline **12** (59%). Selective sequential oxidation of the benzylic hydroxyl group with manganese dioxide to the aldehyde (**13**) followed by treatment with bleach gives the crystalline acid derivative (**14**) in 76% yield. EDC/HOBT-mediated esterification with methanol delivers crystalline methyl ester **15**, which by *N*-allylation with the system allyl bromide/Cs<sub>2</sub>CO<sub>3</sub> and subsequent osmium tetroxide-catalysed oxidative cleavage of the double bond affords the aldehyde derivative (**17**) in its hydrated crystalline form in 41% from **14**. Reaction of **17** with (*R*)-3-aminobutan-1-ol (**18**) results first in the formation of the intermediate cyclic *N,O*-acetals with *R,R* and *S,R* stereochemistry. The *S,R*-isomer featuring the two alkyl side chains in equatorial position should be thermodynamically favoured and, therefore, predominately exist in the reaction mixture. Subsequent lactam formation by nucleophilic attack of the ester carbonyl by the amine provides the final tricyclic *O*-protected intermediate (**19**). Finally, hydrogenolytic cleavage of the benzyl ether liberates the target molecule **1** (Scheme 2). However, in [11] the final two steps are described only for the five-membered analogue of **1**, but not for the title compound itself. Later, this synthetic approach has also been described in a comprehensive publication about the discovery of dolutegravir (**1**) [7].

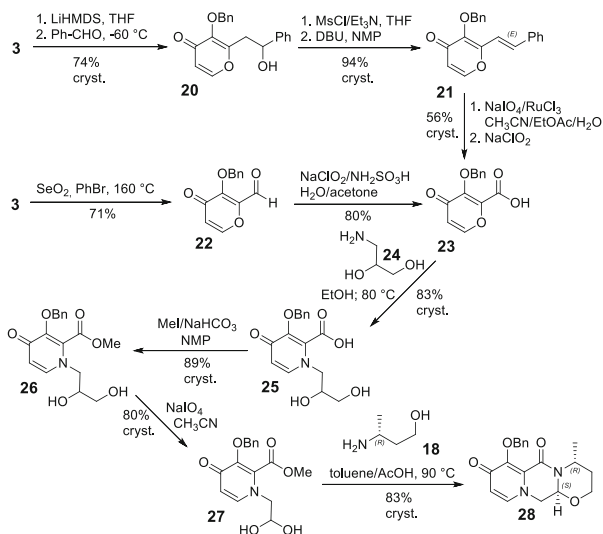


**Scheme 2** Assembly of tricyclic core and deprotection providing **1** according to [11]

Overall, the route comprises 16 steps and provides an estimated total yield of 2%. A positive feature of this so-called base patent route is that most intermediates could be isolated in crystalline form. However, *m*-CPBA and osmium tetroxide are not suitable for an industrial setup due to safety and toxicity issues, respectively. Furthermore,  $\text{Cs}_2\text{CO}_3$  is a serious cost driver, which requires replacement by a cheaper base without compromising yield. Finally, costs arising from catalyst load required at industrial scale in combination with bulk prices for metal and ligand might limit applicability of the palladium-catalysed carbonylation process.

A collaborative effort of Shionogi and GlaxoSmithKline chemists resulted in an alternative route disclosed in a 2010 patent application [12]. The sequence starts from 3-(benzyloxy)-2-methyl-4*H*-pyran-4-one (**3**) which upon deprotonation of the methyl group with LiHMDS at  $-60^\circ\text{C}$  reacts with benzaldehyde providing the crystalline racemic aldol addition product (**20**) in 74% yield. Mesylation of the hydroxyl group followed by base-triggered elimination using DBU furnishes stereoselectively the crystalline (*E*)-isomer of olefin (**21**) in 94% yield. Selective oxidative cleavage of the exocyclic double bond with  $\text{RuCl}_3/\text{NaIO}_4$  followed by a

**Scheme 3** Assembly of tricyclic core **27** described in example **1** of [12]



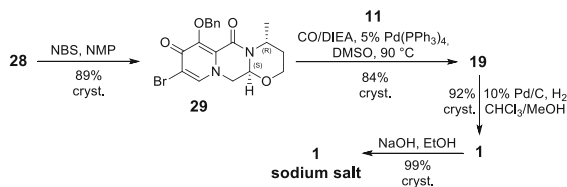
bleach oxidation of the intermediate aldehyde (**22**) furnishes crystalline 3-(benzyloxy)-4-oxo-4*H*-pyran-2-carboxylic acid (**23**) in 38% overall yield from **3**. This route represents a circumvention of a two-step sequence involving a SeO<sub>2</sub>-mediated oxidation at 160 °C reported in the literature in 2004 [13].

Reaction of pyrone **23** with 3-aminopropane-1,2-diol (**24**) produces the corresponding *N*-substituted dihydropyridine analogue (**25**), which upon transformation into the methyl ester (**26**) is subject of periodate oxidation at room temperature to form the crystalline aldehyde derivate (**27**) in its hydrated form (80%). The yield of the process was improved to 90% by running the reaction at between 14 and 17 °C. In the next step, condensation of **27** with (*R*)-3-aminobutan-1-ol (**18**) provides the crystalline tricyclic intermediate (**28**) in an efficient one-pot process in 83% yield (Scheme 3).

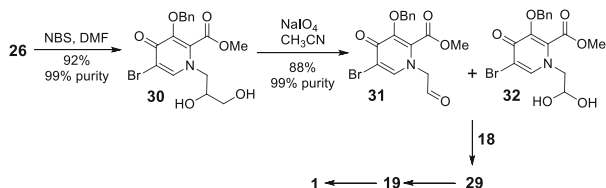
To introduce the carboxamide residue, **28** is first regioselectively transformed by treatment with NBS into the 9-bromo analogue (**29**), which is used as the substrate for a Pd-catalysed aminocarbonylation in the presence of **11**. This conversion delivers the final crystalline *O*-protected intermediate (**19**) in 84% isolated yield. Again, final hydrogenolytic deprotection of the hydroxyl group gives crystalline **1** in 92% isolated yield. The sodium salt of **1** is conveniently obtained from sodium hydroxide in ethanol in almost quantitative yield (Scheme 4).

All together, the route, described for a 500 g scale, comprises 12 linear steps and provides an estimated total yield of about 13%. Compared with the first route from 2006, the number of steps was reduced from 16 to 12 and total yield increased by a factor of 6. As in the base patent route, most intermediates are isolated in crystalline form. Another positive aspect is the engagement of the carbonylation at a very late stage of the synthesis potentially reducing the volume. Although the aldol condensation step could be optimised up to a stage which produces 97% yield of the desired product [14], running this reaction at multi-ton scale remains a challenge.

**Scheme 4** Final steps towards **1** described in example **1** of [12]



**Scheme 5** Route towards **1** described in example C of [12]

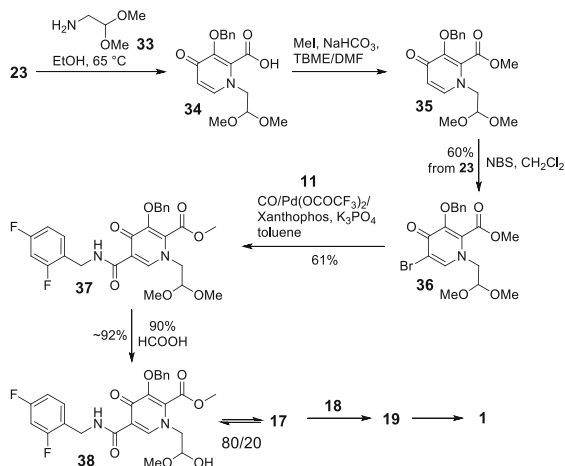


Furthermore,  $\text{NaIO}_4$  and  $\text{RuCl}_3$ , for which substitution might be difficult, will function as cost drivers.

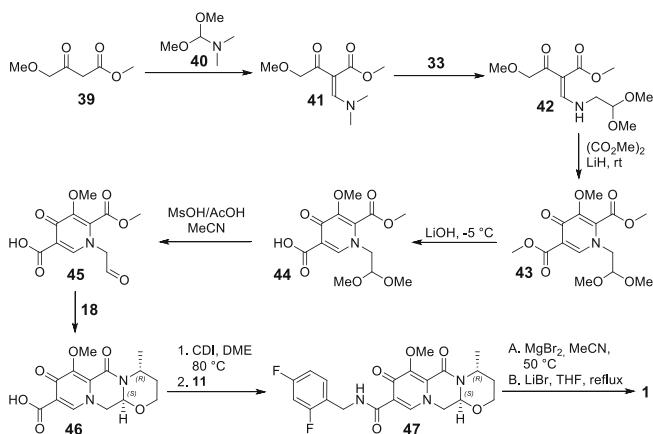
For kilogram-scale production, they disclosed a variation of the route described above wherein the bromine is already introduced into **26** providing the dihydropyridine derivative (**30**) which is then the subject of the sodium periodate cleavage (see Scheme 5). The mixture of aldehyde (**31**) and its hydrate (**32**) obtained is directly used for the condensation reaction with **18**. This process further improves the overall yield of **1** to about 18% starting from **2**.

Another version of this approach avoids the relatively costly periodate cleavage by using 2,2-dimethoxyethanamine (**33**) instead of **24** for the reaction with the pyrone derivative (**23**). No yield for **34** obtained is reported. Next, the carboxyl group is alkylated with methyl iodide and  $\text{NaHCO}_3$  as base to obtain the methyl ester (**35**). Bromination with NBS in dichloromethane yields 60% of **36**. Aminocarbonylation with **11** in the presence of  $\text{K}_3\text{PO}_4$  and 8 mol% of the catalyst  $(\text{Pd}(\text{TFA})_2/\text{Xantphos})$  in toluene at  $100^\circ\text{C}$  provides **37** in 61% yield. Cleavage of the dimethyl ketal is managed by treatment with 90% formic acid at  $40^\circ\text{C}$  resulting in a mixture of the aldehyde **17** in equilibration with the methyl hemiacetal **38** in 92% yield which is then used for the condensation with **18** (Scheme 6).

In a 2011 patent application, GSK chemists switched the starting material from maltol (**2**) to methyl 4-(methoxy)-3-oxobutanoate (**39**) [15], a strategy outlined by McCombie [16] and applied already by Shionogi scientists for other antiviral 3-hydroxy-pyridone-type inhibitors [17]. First, **39** is treated with 1,1-dimethoxy-*N,N*-dimethylmethanamine (**40**) forming the enaminone (**41**) which subsequently is treated with **33** to obtain intermediate **42**. Condensation with dimethyl oxalate in the presence of lithium methanolate at  $40^\circ\text{C}$  provides first the dimethylester (**43**), which immediately is regioselectively saponified to **44** by addition of  $\text{LiOH}$  at  $5^\circ\text{C}$ . Liberating the free aldehyde by acidic cleavage of the ketal with  $\text{MsOH}/\text{AcOH}$  in acetonitrile and condensation with **18** provides the tricyclic acid (**46**). Then, CDI-mediated coupling with **11** furnishes 7-*O*-protected dolutegravir (**47**). Finally, the methyl ether is cleaved with  $\text{MgBr}_2$  in acetonitrile at  $50^\circ\text{C}$ . The sequence



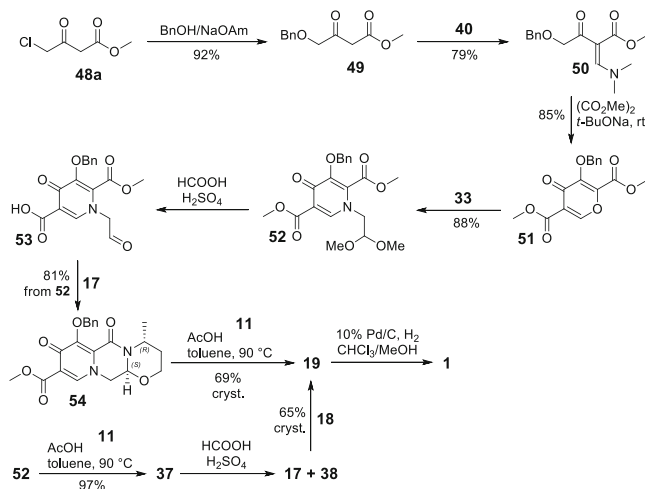
**Scheme 6** Alternative route towards **1** described in example 2 of [12]



**Scheme 7** Enaminone route disclosed by GSK chemists towards dolutegravir (**1**) in [15]

comprises just nine steps, however, no statements regarding yield and physical form of intermediates were made (see Scheme 7).

In a later application, Shionogi chemists disclose a similar route selecting a benzyl ether for protection of the 7-hydroxyl group [18], which had successfully been used already in the base patent [11]. In the first step, nucleophilic substitution of the chlorine of methyl 4-chloro-3-oxobutanoate (**48a**) by phenylmethoxide generated from benzyl alcohol and sodium amylate group provides **49** in 92% yield. Formation of the corresponding enaminone (**50**) followed by condensation with dimethyl oxalate gives crystalline dimethyl 3-(benzyloxy)-4-oxo-4H-pyran-2,5-dicarboxylate (**51**) in 85% yield. Reaction of **51** with 2,2-dimethoxyethanamine



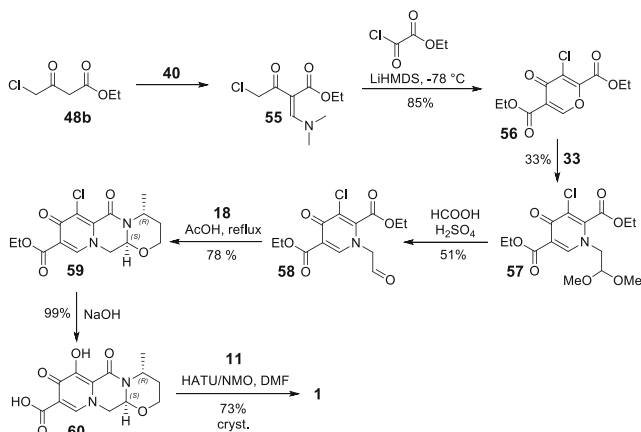
**Scheme 8** Variation 1 of enaminone route towards dolutegravir (**1**) disclosed in [18]

(**33**) provides in 88% the pyridine analogue (**52**) as an oil, which can be crystallised from ethyl acetate. Acidic cleavage of the ketal followed by assembling of the B and C ring by condensation of the intermediate aldehyde (**53**) with **17** affords **54** in 81% yield from **52**. Heating the methyl ester **52** in toluene in the presence of acetic acid and (2,4-difluorophenyl)methanamine (**11**) provides 69% of the final intermediate (**19**) as yellow crystals. Finally, hydrogenolytic cleavage of the benzyl ether liberates **1**. Altogether, this route comprises eight steps and provides dolutegravir (**1**) in a reported overall yield of 26% (Scheme 8).

In another example, the amide bond is formed first by treatment of **52** with **11** in the presence of acetic acid furnishing **37** in 97% yield. Then acidic cleavage of the dimethyl ketal provides a mixture of the aldehyde **17** and the hemihydrate **38** which by reaction with **18** delivers 65% of crystalline **19** (Scheme 8). Again, this route comprises eight steps and produces dolutegravir (**1**) in a slightly improved overall yield of 34%.

The same route featuring ethyl ester groups decorating the A ring is reported to provide a total yield of just 6% due to low yields in the third and fourth step.

Another sequence following the same fundamental strategy is depicted in Scheme 9. For this, ethyl 4-chloro-3-oxobutanoate (**48b**) is transformed into the enaminone (**55**), which upon deprotonation with LHMDS in THF at  $-78^{\circ}\text{C}$  is reacted with ethyl 2-chloro-2-oxoacetate providing pyrone (**56**) in 85% yield. Transformation of **56** into the pyridone derivative (**57**) by treatment with **33** suffers from poor yield (33%) and would need further optimisation. Acidic cleavage of the ketal and subsequent assembly of the B and C ring by condensation of the intermediate aldehyde (**58**) with **18** affords just 40% of **59** from **57** due to a low yield in the first step. Simultaneous saponification of the ethyl ester and hydrolytic replacement of the chlorine atom by treatment with aqueous sodium hydroxide



**Scheme 9** Variation 2 of enaminone route towards dolutegravir (**1**) disclosed in [18]

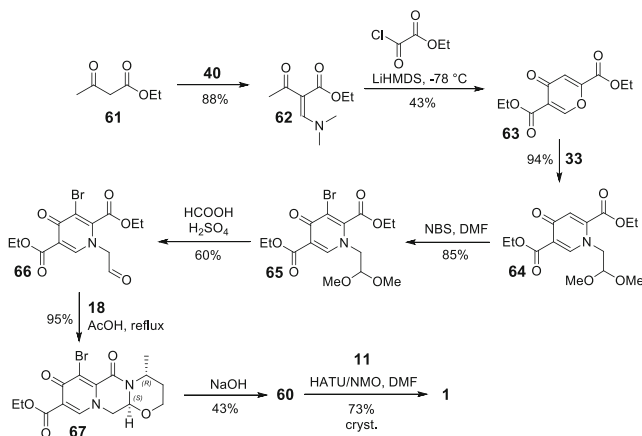
afford the tricyclic acid **60** in almost quantitative yield. Finally, coupling with **11** in the presence of HATU and NMO in DMF provides **1** in 73% yield.

This sequence is described just in the milligram scale; purification is generally achieved by chromatography on silica gel. Therefore, its potential as a commercial route is difficult to assess.

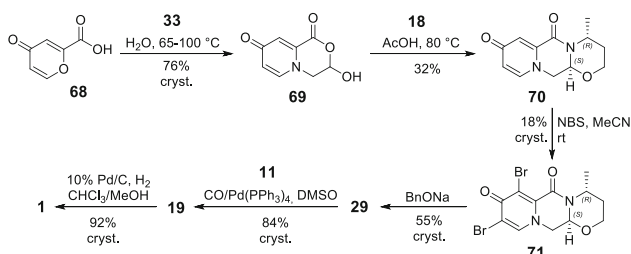
Another variation presented is late introduction of the halogen atom (Scheme 10). Starting from ethyl 3-oxobutanoate (**61**) is again transformed into the enaminone (**62**). The corresponding anion obtained by deprotonation with LHMDS in THF at  $-78^{\circ}\text{C}$  is reacted with ethyl 2-chloro-2-oxoacetate furnishing pyrone (**63**) in 43% yield. Treatment of **63** with **33** provides the pyridone derivative (**64**) in excellent yield (94%). Again, acidic cleavage of the ketal delivering the free ketone (**66**) followed by assembling of the B and C ring by condensation with **18** affords 57% of **67** from **65** due to a moderate yield in the first step. Simultaneous saponification of the ethyl ester and hydrolytic replacement of the bromine atom by treatment with aqueous sodium hydroxide afford the tricyclic acid **60** in only 43% yield. Again, final coupling with amine **11** in the presence of HATU and NMO in DMF provides **1** in 73% yield.

Finally, Sumino et al. [18] discloses a route with a strategy different from those depicted in Schemes 8, 9 and 10. The starting material 4-oxo-4*H*-pyran-2-carboxylic acid (**68**), also called comanic acid, can be accessed from glucuronic acid in two convenient steps [19, 20] in greater than 90% yield (Scheme 11).

Condensation of **68** with **33** in water provides crystalline bicyclic intermediate (**69**) in 76% yield. Then, the C ring is established by reaction of **69** with **18** in acetic acid at  $80^{\circ}\text{C}$ , furnishing **70** in only 32% yield. The next step, wherein **70** is treated with NBS in acetonitrile to obtain the 7,9-bisbrominated derivative (**71**), is also suffering from a low 18% yield. Regioselective replacement of the bromine atom in the 7-position by benzyl alcohol provides crystalline **29** in 55% yield. As described



**Scheme 10** Variation 3 of enaminone route towards dolutegravir (**1**) disclosed in [18]



**Scheme 11** Alternative strategy via A,B-bicyclic intermediate disclosed in [18]

in [18], introduction of the side chain by aminocarbonylation in the presence of **11** followed by hydrogenolytic cleavage of the benzyl ether affords **1**.

The highlight of this route is certainly the low number of six steps. Further positive aspects of this route are the fact that the starting material comanic acid (**63**) can be vertically integrated back to glucose and that all intermediates are isolated as crystalline solids. However, low yields in the C ring forming condensation and bromination reactions result in an estimated overall yield of just 2%.

## 2.2 Synthetic Routes of Generic Competitors

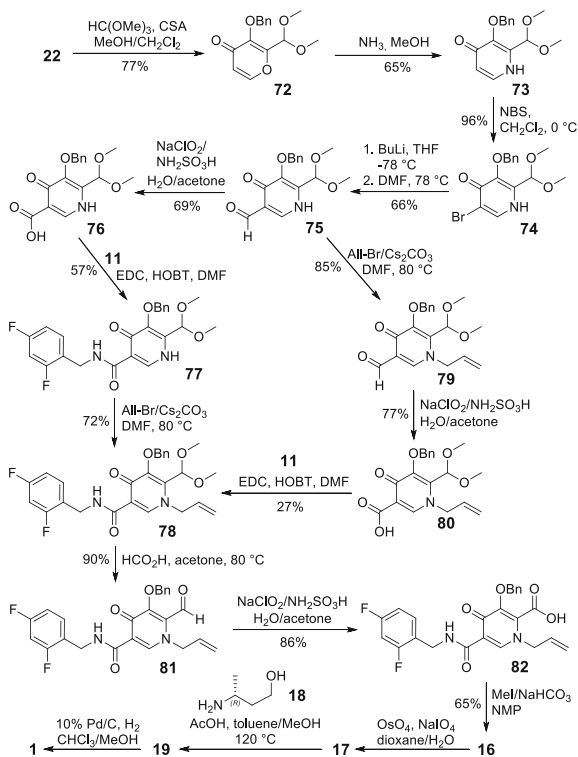
Originator(s), inventor or licensee, is the first one preparing and usually also dealing with industrial production of an individual drug substance. Therefore, they can freely decide on their production route. However, for generic competitors, the situation is different. They start later when most of the disclosures of the originator have already been published. Therefore, they generally adopt

two strategies, a smart design around the most attractive sequence, what is called the benchmark synthesis, or the development of an entirely new synthetic route.

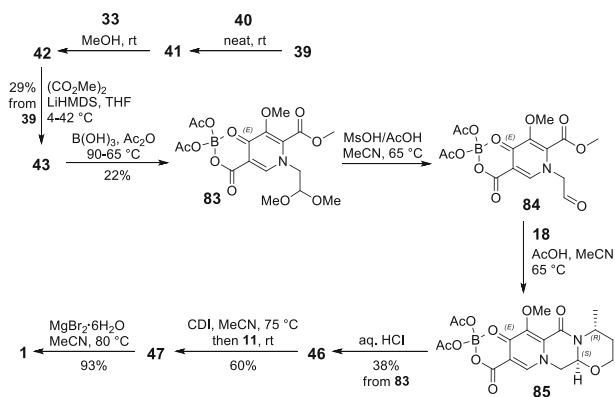
Early in 2015, Hetero Drugs was the first generic drug company reporting a novel synthetic route towards dolutegravir **1** in a patent application [21]. Their synthetic approach shows some common features with that one outlined in the base patent [11]; see Schemes 1 and 2. Their synthesis starts from 3-(benzyloxy)-4-oxo-4*H*-pyran-2-carbaldehyde (**22**) which is first transformed into its dimethyl ketal derivative (**72**) by treatment with trimethyl orthoformate in the presence of CSA (77%). Reaction of the protected pyrone (**72**) with ammonia in methanol provides pyrimidone (**73**) in 65% yield. Next, regioselective bromination of the 5-position is achieved by treatment with NBS providing **74** in almost quantitative yield. Then, bromine–lithium exchange with *n*-butyl lithium in THF at  $-78^{\circ}\text{C}$  followed by addition of DMF as the electrophile affords aldehyde (**75**) in 66% yield. Oxidation of aldehyde (**75**) with bleach in the presence of aminosulfonic acid furnishes acid derivative (**76**) followed by coupling with amine **11** in the presence of EDC and HOBt producing **77** completes assembly of the side chain. Selective allylation of the pyrimidine nitrogen with allyl bromide in the presence of caesium carbonate in DMF provides **78** in 28% yield from **75**. In an alternative sequence towards **78**, allylation of **75** under similar conditions to those described above provides **79**. Then, **79** is subjected to bleach oxidation affording **80**, followed by amide bond formation producing **78** in 16% overall yield from **75**. Next, acidic cleavage of the dimethyl ketal protecting group by treatment with formic acid in acetone gives **81** in 90% yield, followed by oxidation affording the free-acid derivative (**82**). Alkylation of **82** with methyl iodide in NMP using solid sodium bicarbonate as base provides the methyl ester derivative (**17**) in 65% yield. Then, as described in [11], condensation of **17** with (*R*)-3-aminobutan-1-ol (**18**) results in simultaneous formation of the B and C ring of the final tricyclic *O*-protected intermediate (**19**) which by hydrogenolytic cleavage of the benzyl ether is transformed into **1** (Scheme 12).

Altogether, the route comprises 13 consecutive steps and provides an estimated overall yield of about 2%. Chemical steps for the preparation of **22** have further to be considered. No information on solid states of intermediates is disclosed. Metalation chemistry at  $-78^{\circ}\text{C}$  might be a cost issue at the multi-ton scale. Caesium carbonate and sodium periodate have to be considered as additional cost drivers. Engagement of osmium tetroxide is a well-known serious safety concern.

Another synthetic approach has been disclosed in a patent application by Mylan Pharmaceuticals scientists (Scheme 13) [22]. Similarly, as described in [15], their approach starts from methyl 4-methoxy-3-oxobutanoate (**39**), which is transformed into enaminone (**41**). Subsequent transamination with **33** and condensation with dimethyl oxalate in the presence of LiHMDS provide synthon (**43**) in 29% yield from **39**. Reaction of **43** with a mixed anhydride generated from heating boric acid with 4 equiv. of acetic anhydride delivered the intermediate (**83**) featuring a cyclic anhydride structure which functions as a quite unusual protecting group for the carboxylic acid. Next, acidic cleavage of the dimethyl ketal protecting group with methane sulphonic acid in acetic acid provides the aldehyde derivative (**84**), which was subsequently treated with amine (**18**) in the presence of acetic acid to form the

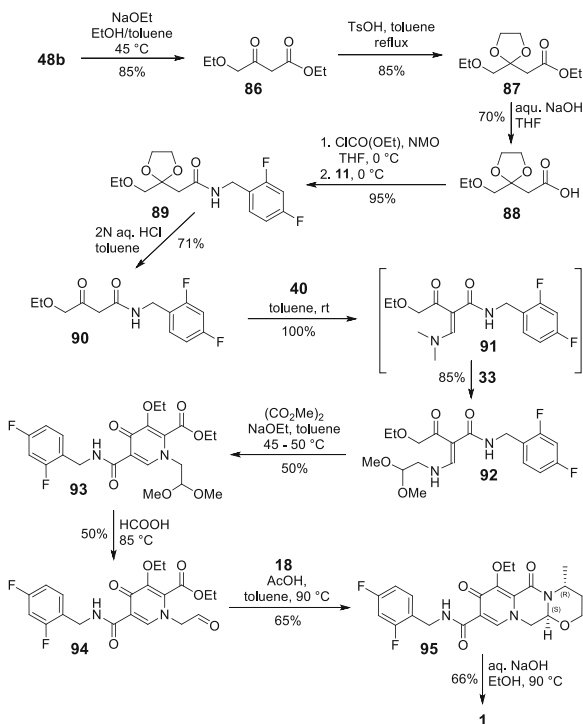


Scheme 12 Hetero Drugs Ltd. route towards dolutegravir (1) disclosed in [21]



Scheme 13 Mylan Pharmaceuticals route towards dolutegravir (1) disclosed in [22]

**Scheme 14** Laurus Labs route towards dolutegravir (**1**) disclosed in [23, 24]



tricyclic intermediate (**85**). Treatment with hydrochloric acid in the course of the work-up directly provides **46** in 38% yield from **83**. Next, CDI-mediated coupling with amine (**11**) gives 7-*O*-protected dolutegravir (**47**). Finally, the methyl ether is again cleaved with  $\text{MgBr}_2$  in acetonitrile at 80°C.

The sequence comprises just 9 steps; however, low yields in the formation of **43**, **83** and **46** from **83** resulting in an estimated overall yield of about 1.5% suggest that significant improvement of yields of those reaction steps are required. No statements regarding yield and physical form of intermediates are made.

In two similar patent applications [23, 24], development chemists from Laurus Labs report a novel route towards dolutegravir (**1**) (Scheme 14). Starting from ethyl 4-chloro-3-oxobutanoate (**48b**), nucleophilic substitution of the chloride by ethoxide provides the ethoxy derivative (**86**) in 85% isolated yield.

Protection of the ketone by dioxolane formation is achieved by treatment with ethylene glycol in the presence of *p*-toluenesulfonic acid producing **87** in 85% yield. Alkaline cleavage of the ethyl ester provides acid (**88**) in 70% yield. For performing the sequence from **48b** to **88** in telescope mode, the authors report an isolated overall yield of 70%. Next, coupling with (2,4-difluorophenyl) methanamine (**11**) via a mixed anhydride obtained from treatment with ethyl chloroformate in the presence of NMO provides the protected amide (**89**) in 95% yield. Treatment with aqueous hydrochloric acid in toluene results in liberation of the ketone (**90**; 71%), which by treatment with 1,1-dimethoxy-*N,N*-dimethylmethanamine (**40**) is quantitatively transformed into intermediate (**91**), which by

subsequent transamination reaction with 2,2-dimethoxyethanamine (**33**) affords enamionone (**92**) in 85% yield from **90**. Formation of the A ring is achieved by condensation with oxalic acid diesters in the presence of sodium ethoxide in toluene at 50°C delivering pyridone (**93**). Reported yields for the ethyl and methyl ester are 50% and 75%, respectively. Liberation of the aldehyde (**94**) from the dimethyl ketal (**93**) is performed by heating with formic acid at 90°C. Reaction of (**94**) with (*R*)-3-aminobutan-1-ol (**18**) in the presence of acetic acid in toluene at 90°C provides the *O*-protected dolutegravir derivative (**95**) in moderate 33% yield from **93**. Finally, alkaline hydrolysis of the enol ether of **95** provides **1** in 66% yield and 88% HPLC purity.

The sequence comprises 11 steps and provides an overall yield of about 4%. Only for early non-solid intermediates, statements regarding physical form are made.

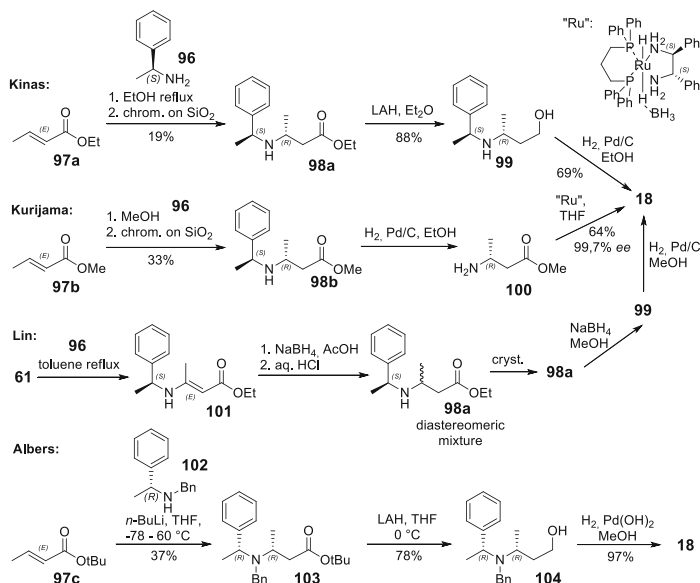
### 2.3 Synthesis of (*R*)-3-Aminobutan-1-ol

One building block required for all synthetic routes leading to dolutegravir is (*R*)-3-aminobutan-1-ol (**18**). This synthon has to be introduced as its pure (*R*)-enantiomer, which can be accessed by chiral synthesis or a racemic approach following resolution of the enantiomers.

Early approaches are using (*S*)-1-phenylethanamine (**96**) for introducing chirality. Kinast et al. and Kurijama et al. report [25–27] reaction of **96** with (*E*)-ethyl or (*E*)-methyl but-2-enoate (**97a,b**). Chromatographic resolution of the diastereomeric mixture of the Michael addition products yield the desired (*S,R*)-isomer of the  $\beta$ -amino acid derivatives (**98a**) or (**98b**) in 19% and 33% yield, respectively (Scheme 15). Reduction of the ester to the alcohol and hydrogenolytic cleavage of the benzylic C–N bond provides **18** via intermediates **98a,b-100** in good yield and high enantiomeric purity. Alternatively, Lin et al. (Scheme 15) first produced the isomeric mixture containing **98a** by condensation of **96** with ethyl 3-oxobutanoate (**61**) resulting in the formation of enamine (**101**) followed by reduction using sodium borohydride in presence of acetic acid [28, 29]. At this stage these scientists achieved isolation of the pure (*S,R*)-isomer (**98a**) by selective crystallisation from the mixture. Again, reduction of the ester to the alcohol (**99**) and hydrogenolytic cleavage of the benzylic C–N bond provides **18** in good yield and high enantiomeric purity.

A further variation to access **18** via a Michael addition has been reported by Albers et al. [30]. They at –78°C stereoselectively add the lithium salt of (*R*)-*N*-benzyl-1-phenylethanamine (**102**) to (*E*)-*tert*-butyl but-2-enoate (**97c**) producing **103** in 37% yield. Again, a sequence of ester reduction affording the protected alcohol (**104**) followed by hydrogenolytic cleavage delivers **18** in 76% yield and high enantiomeric purity from **103**.

A different approach reported by Besse et al. [31] comprises enantioselective reduction of the ketone of **61** with baker's yeast followed by reduction of the ester, selective protection of the primary hydroxyl group protection and introduction of



**Scheme 15** Early chiral synthesis for (R)-3-aminobutan-1-ol involving Michael addition

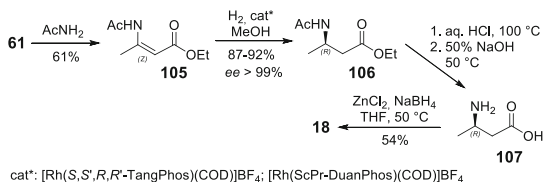
the nitrogen by a Mitsunobu reaction under inversion of the configuration. Furthermore, Achmatowicz et al. [32] transformed L-alanine into **18** applying a five-step sequence comprising homologisation of the acid via the corresponding diazo ketone and subsequent silver-mediated Arndt–Eistert reaction followed by ester reduction and final N-deprotection.

Since the discovery of dolutegravir (**1**), processes for the preparation of **18** have been consequently designed for cost-efficient and safe production at ton scale in an industrial plant. Chinese chemists in a patent application [33] disclose a route taking advantage of the highly enantioselective hydrogenation of 2-(acylamino)-acrylates by chiral rhodium catalysts [34]. Starting from **61** they first generate (Z)-ethyl 3-acetamidobut-2-enoate (**105**) in 61% yield by reaction with acetamide. Then hydrogenation in the presence of complexes of rhodium with (*S,S',R,R'*)-TangPhos and ScRp-DuanPhos gives the amino acid ester **106** in 87–92% yield and 99.2–99.4% *ee*. Hydrolysis of the amide and ester bonds provides the crude amino acid (**107**), which is reduced to **18** with zinc borohydride in THF in 54% yield and 99.3% *ee* from **106** (Scheme 16).

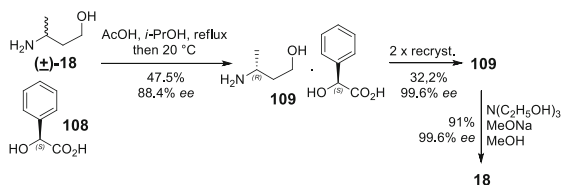
Two other recent processes disclosed in the patent literature by chemists from BASF and Aurobindo Pharma afford **18** by resolution of the racemic amino alcohol by crystallisation of salts with (*S*)-mandelic acid [35] and (*S,S*)-tartaric acid [36], which are cheap resolution agents.

The BASF process starts with dissolution of racemic mixture of **18** and its enantiomer and (*S*)-mandelic (**108**) acid in a refluxing *i*-PrOH/H<sub>2</sub>O and acetic acid. Subsequent cooling to room temperature causes crystallisation of the corresponding salt **109** in 88.4% optical purity. Two recrystallisations from *i*-PrOH/H<sub>2</sub>O provide

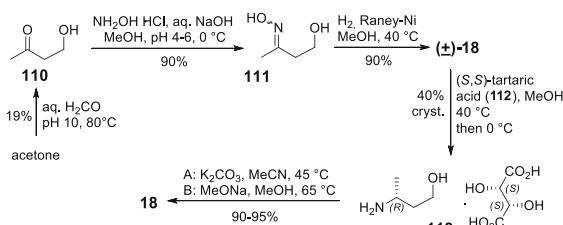
**Scheme 16** Asymmetric hydrogenation process for the preparation of **18** according to [33]



**Scheme 17** BASF resolution process for the preparation of **18** according to [35]



**Scheme 18** Aurobindo Pharma process for the preparation of **18** according to [36]



the final material in 99.6% *ee* and a chemical yield of 32%. Liberation of **18** is achieved by treatment with sodium methanolate in the presence of triethanolamine in methanol without any loss of optical purity and 91% yield (Scheme 17).

Successful resolution of *O*-benzyl- and *O*-*tert*-butyl- protected derivatives of **18** disclosed in additional examples indicates a broad scope of the methodology.

Besides a protocol for chiral resolution of **18**, Aurobindo Pharma scientists developed a route towards the racemic starting material as well. Their process starts from acetone, which by reaction with aqueous formaldehyde at 80 °C provides 4-hydroxybutan-2-one (**110**) in 19% yield. A similar process had been disclosed by Ogura et al. in a Japanese patent application providing **110** with 74% selectivity at 57% conversion [37]. Next, **110** is transformed into the corresponding oxime (**111**) in 90% yield. Finally, hydrogenation in the presence of Raney nickel provides the racemic amino alcohol (90%). Resolution is performed by adding (*S,S*)-tartaric acid (**112**), the non-natural enantiomer, to methanolic solution of racemic **18** at 40 °C. Cooling to 5 °C causes selective crystallisation of (*R*)-3-aminobutan-1-ol (2*S,3S*)-2,3-dihydroxysuccinate (**113**). Treatment of **113** with potassium carbonate in acetonitrile or with sodium methoxide in methanol provides **18** in 95% or 90% yield, respectively. No information on enantiomeric purity of **18** obtained is reported (Scheme 18).

The same group recently reported an alternative two-step sequence towards racemic 3-aminobutan-1-ol **18** starting from ethyl 3-oxobutanoate (**61**) via oxime formation following simultaneous lithium aluminium hydride-mediated reduction of the oxime and the ester functionality [38].

### 3 Summary, Conclusions and Outlook

In summary, 10 synthetic sequences towards dolutegravir **1**, seven from originators (Shionogi, GlaxoSmithKline) and three from generic companies (Hetero Drugs, Mylan Pharmaceuticals, Laurus Labs), have been reviewed. In order to get an overview on their fundamental strategies, they were clustered by the sequence of ring fission (A, B, C) and assembly of the 3-(2,4-difluorobenzyl)-carboxamide side chain (S). Based on the assumption that BC ring formation occurs in a sequential manner as proposed in [7], 13 hypothetical pathways exist. However, so far only four of them, represented as clusters 1–4, have been chosen for realisation (Fig. 3).

Out of 13 routes, 12 take advantage of the A→AC→ABC strategy, represented by clusters 1–3 mostly differing by the stage at which the side chain is assembled.

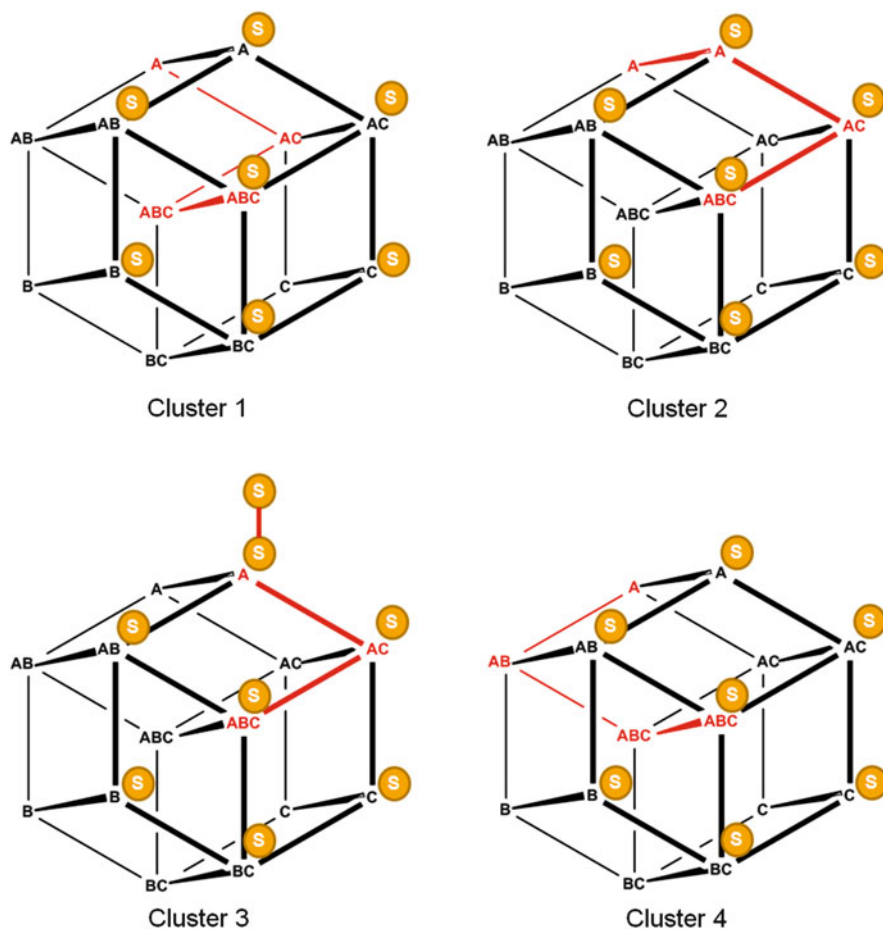


**Fig. 3** Overview on realised synthetic strategies towards dolutegravir **1** summarised in clusters 1–4

This is due to the fact that all these routes apply basically the same protocol, namely, condensation of an A ring building block featuring an aldehyde and an ester group with the chiral aminoalcohol (**18**) to form the tricyclic scaffold. The striking advantage of this process is the good control of the stereochemistry at the *N,O*-acetal carbon atom by the chirality of **18**. In one case, represented by cluster 3, the synthesis starts with a building block comprising the side chain, which is then transformed into the A–S intermediate. Only one route, depicted on Scheme 11, follows the A→AB→ABC strategy and therefore can be clearly distinguished from all others.

Synthetic approaches based on early assembly of the B, C or BC rings have not been realised yet. The decision to preferentially introduce the only chiral and originally costly starting material at a rather late stage might have contributed to this selection. However, the development of industrial applicable processes for (*R*)-3-aminobutan-1-ol induced by the discovery of dolutegravir based on catalytic asymmetric hydrogenation or chiral resolution of the racemic alcohol via diastereomeric salts make this starting material a commodity now and might trigger exploration of previously unattractive assembly strategies for the title compound in the future.

## References

1. Bor J, Herbst AJ, Newell ML, Bärnighausen T (2013) Increases in adult life expectancy in rural South Africa: valuing the scale-up of HIV treatment. *Science* 339:961–965
2. Fantauzzi A, Mezzaroma I (2014) Dolutegravir: clinical efficacy and role in HIV therapy. *Ther Adv Chronic Dis* 5:164–177
3. Gandhi M, Gandhi RT (2014) Single-pill combination regimens for treatment of HIV-1 infection. *N Engl J Med* 371:248–259
4. Geretti AM, Tsakiroglou M (2014) HIV: new drugs, new guidelines. *Infect Dis* 27:545–553
5. Johns BA, Svolto AC (2008) Advances in two-metal chelation inhibitors of HIV integrase. *Expert Opin Ther Pat* 18:1225–1237
6. Kawasuji T, Fuji M, Yoshinaga T, Sato A, Fujiwara T, Kiyama R (2006) A platform for designing HIV integrase inhibitors. Part 2: a two-metal binding model as a potential mechanism of HIV integrase inhibitors. *Bioorg Med Chem* 14:8420–8429
7. Johns BA, Kawasuji T, Weatherhead JG, Taishi T, Temelkoff DP, Yoshida H, Akiyama T, Taoda Y, Murai H, Kiyama R, Fuji M, Tanimoto N, Jeffrey J, Foster SA, Yoshinaga T, Seki T, Kobayashi M, Sato A, Johnson MN, Garvey EP, Fujiwara T (2013) Carbamoyl pyridone HIV-1 integrase inhibitors 3. A diastereomeric approach to chiral nonracemic tricyclic ring systems and the discovery of dolutegravir (S/GSK1349572) and (S/GSK1265744). *J Med Chem* 56:5901–5916
8. Xue W, Jin X, Ning L, Wang M, Liu H, Yao X (2013) Exploring the molecular mechanism of cross-resistance to HIV-1 integrase strand transfer inhibitors by molecular dynamics simulation and residue interaction network analysis. *J Chem Inf Model* 53:210–222
9. Hare S, Smith SJ, Metifiot M, Jaxa-Chamiec A, Pommier Y, Hughes SH, Cherepanov P (2011) Structural and functional analyses of the second-generation integrase strand transfer inhibitor dolutegravir (S/GSK1349572). *Mol Pharmacol* 80:565–572
10. Kiyama R, Kawasuji T (2001) Inhibitor for enzyme having two divalent metal ions as active centers. WO 2001/095,905, 20.12.2001. 140 pp

11. Yoshida H, Kawasuji T, Taoda Y (2006) Bicyclic carbamoylpyridone derivative having HIV integrase inhibitory activity. WO 2006/088,173, 24 Aug 2006, 138 pp
12. Yoshida H, Taoda Y, Johns B, Kawasuji T, Nagamatsu D (2006) Synthesis of carbamoylpyridone HIV integrase inhibitors and intermediates. WO 2010/068,253, 17 June 2010, 59 pp
13. Pace P, Nizi E, Pacini B, Pesci S, Matassa V, De Francesco R, Altamura S, Summa V (2004) The monoethyl ester of meconic acid is an active site inhibitor of HCV NS5B RNA-dependent RNA polymerase. *Bioorg Med Chem Lett* 14:3257–3261
14. Fukui Y, Oda S, Suzuki H, Hakogi T, Yamada D, Takagi Y, Aoyama Y, Kitamura H, Ogawa M, Kikuchi J (2012) Process optimization of Aldol-type reaction by process understanding using in situ IR. *Org Process Res Dev* 16:1783–1786
15. Wang H, Goodman SV, Mann D, Kowalski M (2011) Process for preparing carbamoylpyridone derivatives and intermediates. WO 2011/119,566, 29 Sept 2011, 21 pp
16. McCombie SW, Metz WA, Nazareno D, Shankar BB, Tagat J (1991) Generation and in situ acylation of enamionone anions: a convenient synthesis of 3-carbomethoxy-4(1H)-pyridinones and -4-pyrone and related compounds. *J Org Chem* 56:4963–4967
17. Sumino Y, Okamoto K, Masui M, Aklyama T (2010) Method of producing pyrone and pyridone derivatives. WO 2010/110,409, 30 Sept 2010, 145 pp
18. Sumino Y, Masui M, Yamada D, Ikarashi F, Okamoto K (2012) Method of producing compounds having HIV integrase inhibitory activity. WO 2012/018,065, 09 Feb 2012, 132 pp
19. Tajima K (1986) Anomer-specificity in the degradation reaction of D-glucopyranic acid tetraacetate leading to comanic acid in the acetic anhydride-base system. *Tetrahedron Lett* 27:6095–6098
20. Tietze LF, Schuster HJ, Schmuck K, Schubert I, Alves F (2008) Duocarmycin-based prodrugs for cancer prodrug monotherapy. *Bioorg Med Chem* 16:6312–6318
21. Parthasaradhi Reddy B, Muralidhara Reddy D, Narsingam M, Vamsi Krishna B (2015) Process for the preparation of intermediates of dolutegravir. WO 2015/001,572, 08 Jan 2015, 31 pp
22. Dandala R, Vellanki SRP, Nadella MM, Balusu PK (2015) Process for the preparation of dolutegravir and intermediates thereof. WO 2015/019,310, 12 Feb 2015, 22 pp
23. Chava S, Gorantla SRA, Dammalapati VLN, Kotala MB, Aduri R (2015) Novel process for the preparation of dolutegravir and pharmaceutically acceptable salts thereof. WO 2015/110,897, 30 July 2015, 77 pp
24. Chava S, Gorantla SRA, Dammalapati VLN, Kotala MB (2015) Novel process for the preparation of dolutegravir and pharmaceutically acceptable salts thereof. WO 2015/111,080, 30 July 2015, 78 pp
25. Kinas R, Pankiewicz K, Stec WJ (1977) Synthesis and absolute configuration of the optically active forms of 2-[Bis(2-chloroethyl)amino]-4-methyltetrahydro-2H-1,2,3-oxazaphosphorine 2-oxide (4-methylcyclophosphamide). *J Org Chem* 42:1650–1652
26. Kuriyama W, Ino Y, Ogata O, Sayo N, Saito T (2010) A homogeneous catalyst for reduction of optically active esters to the corresponding chiral alcohols without loss of optical purities. *Adv Synth Catal* 352:92–96
27. Ino Y, Kuriyama W, Ogata O, Matsumoto T (2010) An Efficient synthesis of chiral alcohols via catalytic hydrogenation of esters. *Top Catal* 53:1019–1024
28. Lin J, Lin Z, Que L (2009) Process for preparation of chiral 3-amino-1-butanol. CN 101,417,954, 20 Apr 2009, 15 pp
29. Furukawa M, Okawara T, Noguchi Y, Terawaki Y (1979) Asymmetric syntheses of  $\beta$ -amino acids by the reduction of enamines. *Chem Pharm Bull* 27:2223–2226
30. Albers R, Ayala L, Clareen SS, Delgado Mederos MM, Hilgraf R, Hedge S, Hughes K, Kois A, Plantevin-Krenitsky V, McCarrick M, Nadolny L, Palanki M, Sahasrabudhe K, Sapienza J, Satoh Y, Sloss M, Sudbeck E, Wright J (2006) Preparation of haloaryl substituted aminopyrines for use as a prodrug in the treatment of cancers, cardiovascular or renal diseases. WO 2006/076,595, 20 July 2006, 194 pp

31. Besse P, Ciblat S, Canet JL, Troin Y, Veschambre H (1999) Stereoselective chemoenzymatic synthesis of both enantiomers of protected 4-amino-2-pentanone. *Tetrahedron Asymmetry* 10: 2213–2224
32. Achmatowicz M, Szumna A, Zielinski T, Jurczak J (2005) Structure-driven design and synthesis of chiral dioxocyclam derivatives. *Tetrahedron* 61:9031–9041
33. Wu S, Tian C, Hu S, Bai J, Li T, Wu L, Li W (2015) Process for preparation of optically active 3-aminobutanol. CN 104,370,755 A, 25 Feb 2015, 18 pp
34. Tang W, Zhang X (2002) Highly efficient synthesis of chiral  $\beta$ -amino acid derivatives via asymmetric hydrogenation. *Org Lett* 4:4159–4161
35. Ditrich K, Bartsch M, Winsel H (2010) Preparation of (R) and (S)-3-amino-1-butanol. WO 2010/081,865, 22 July 2010, 26 pp
36. Budidet SR, Dussa N, Kaki GR, Yatcherla SR, Sanapureddy JMR, Danda SR, Katuroju S, Meenakshisunderam S (2014) Intermediates and process for the preparation of dolutegravir. WO 2014/128,545, 24 Aug 2014, 34 pp
37. Ogura T, Maeda T, Nagao M, Takesawa T, Ishizaki T (2004) Preparation of hydroxy ketones from ketones and paraformaldehyde. JP 2004/210,650 A, 29 July 2004, 14 pp
38. Yatcherla SR, Islam A, Nageswar D, Hari BB (2015) A simple and convenient route for the synthesis of (R)-3-aminobutanol, an intermediate for the synthesis of Dolutegravir. *Heterocycl Lett* 5:241–244

# Story of Eribulin Mesylate: Development of the Longest Drug Synthesis

Armin Bauer

**Abstract** Eribulin mesylate (Halaven™), approved in 2010 as an anticancer agent, represents a simplified analogue of the marine natural product halichondrin B, which was isolated in 1986 from the sea sponge *Halichondria okadai*. The story of the discovery, development, and launch of this drug impressively demonstrates how far the limits of total synthesis of natural products have been pushed today on an industrial scale since it can be considered the most complex synthetic drug today.

**Keywords** Anticancer drugs • Breast cancer • Catalytic asymmetric Nozaki–Hiyama–Kishi reaction • Eribulin • Fragment coupling • Halaven • *Halichondria okadai* • Halichondrin • Homohalichondrin • Macrolide • Marine natural products • Norhalichondrin • Nozaki–Hiyama–Kishi reaction • Polyether • Process development • Scale-up • Structure-activity relationships • Total synthesis • Transition-metal-mediated coupling reactions

## Contents

1	Introduction .....	212
2	Isolation and Biological Activities of the Halichondrins .....	213
3	Total Synthesis of the Halichondrins .....	215
4	Discovery and Process Development of Eribulin .....	218
4.1	Discovery of Eribulin .....	218
4.2	Process Development of Eribulin: From Milligram Scale to Commercial Manufacture .....	221
5	Recent Progress Toward the Synthesis of the Halichondrins and Eribulin .....	234
5.1	Kishi's Syntheses of Halichondrin and Eribulin Building Blocks .....	235

---

A. Bauer (✉)

Sanofi-Aventis Deutschland GmbH, R&D LGCR/Chemistry, Industriepark Höchst G878,  
65926 Frankfurt am Main, Germany  
e-mail: [Armin.Bauer@sanofi.com](mailto:Armin.Bauer@sanofi.com)

5.2	Kishi's Total Synthesis of Halichondrin C .....	242
5.3	Kishi's Total Synthesis of Halichondrin A .....	247
5.4	Kishi's Approach to a Unified Synthesis of the Halichondrins .....	248
5.5	Recent Contributions from Eisai .....	251
5.6	Recent Contributions from Other Groups .....	259
6	Clinical Development of Eribulin .....	265
7	Conclusion and Outlook .....	266
	References .....	267

## Abbreviations

(DHQ) <sub>2</sub> AQN	Hydroquinine anthraquinone-1,4-diyl diether
(DHQ) <sub>2</sub> PYR	Hydroquinine 2,5-diphenyl-4,6-pyrimidinediyl diether
9-BBN	9-Borabicyclo[3.3.1]nonane
Ac	Acetyl
AD	Asymmetric dihydroxylation
API	Active pharmaceutical ingredient
aq	Aqueous
Ar	Aryl
asymm.	Asymmetric
BHT	Butylated hydroxytoluene, 2,6-di- <i>tert</i> -butyl-4-methylphenol
B-I-9-BBN	B-iodo-9-borabicyclo[3.3.1]nonane
BINOL	1,1'-Bi-2-naphthol
Bn	Benzyl
Boc	<i>tert</i> -Butoxycarbonyl
Bz	Benzoyl
cat.	Catalyst, catalytic
CoPc	Cobalt phthalocyanine
Cp	Cyclopentadienyl
CSA	Camphorsulfonic acid
Cy	Cyclohexyl
DBU	1,8-Diazabicyclo[5.4.0]undec-7-ene
DDQ	2,3-Dichloro-5,6-dicyano-1,4-benzoquinone
de	Diastereomer excess
DEAD	Diethyl azodicarboxylate
DEP	2,9-Diethyl-1,10-phenanthroline
DIAD	Diisopropyl azodicarboxylate
DIBAL-H	Diisobutylaluminum hydride
DIEA	<i>N,N</i> -Diisopropylethylamine
DLD-1	Human colorectal adenocarcinoma cancer cell line isolated by D. L. Dexter
DMAP	4-(Dimethylamino)pyridine
DMDO	Dimethyldioxirane
DME	1,2-Dimethoxyethane

DMF	Dimethylformamide
DMP	2,9-Dimethyl-1,10-phenanthroline
DMPU	1,3-Dimethyl-3,4,5,6-tetrahydro-2(1 <i>H</i> )-pyrimidinone
DMSO	Dimethyl sulfoxide
dr	Diastereomer ratio
DTBMP	2,6-Di- <i>tert</i> -butyl-4-methylpyridine
ee	Enantiomeric excess
equiv.	Equivalent(s)
Et	Ethyl
EtCN	Propionitrile
g	Gram
GMP	Good manufacturing practice
HWE	Horner–Wadsworth–Emmons (reaction)
hν	Light
im	Imidazole
<i>i</i> -Pr	Isopropyl
kg	Kilogram
KHMDS	Potassium hexamethyldisilazide, potassium bis(trimethylsilyl)amide
LAH	Lithium aluminum hydride
LDA	Lithium diisopropylamide
LiHMDS	Lithium hexamethyldisilazide, lithium bis(trimethylsilyl)amide
LOX	Metastatic human melanoma cell line
MDR	Multidrug resistant
Me	Methyl
Me <sub>2</sub> CO	Acetone
MeCN	Acetonitrile
Mes	Mesityl, 2,4,6-trimethylphenyl (not methanesulfonyl)
mL	Milliliter
MMeTr	Monomethoxy trityl
MNBA	2-Methyl-6-nitrobenzoic anhydride (Shiina's reagent)
mol	Mole(s)
MOM	Methoxymethyl
Ms	Methanesulfonyl (mesyl)
MTBE	Methyl <i>tert</i> -butyl ether
NaHMDS	Sodium hexamethyldisilazide, sodium bis(trimethylsilyl)amide
<i>n</i> -Bu	<i>n</i> -Butyl
NCI	United States National Cancer Institute
NCS	<i>N</i> -Chlorosuccinimide
ng	Nanogram
NHK	Nozaki–Hiyama–Kishi (reaction)
NiCl <sub>2</sub> ·DEP	Nickel(II)-chloride 2,9-diethyl-1,10-phenanthroline complex
NiCl <sub>2</sub> ·DMP	Nickel(II)-chloride 2,9-dimethyl-1,10-phenanthroline complex
NIS	<i>N</i> -Iodosuccinimide

NMM	<i>N</i> -Methylmorpholine
NMO	<i>N</i> -Methylmorpholine <i>N</i> -oxide
NMP	<i>N</i> -Methyl-2-pyrrolidone
P-gp	P-Glycoprotein
Ph	Phenyl
PhH	Benzene
PhMe	Toluene
PMB	4-Methoxybenzyl
PMP	4-Methoxyphenyl
PNB	4-Nitrobenzoyl
PNBCl	4-Nitrobenzoyl chloride
PNBOH	4-Nitrobenzoic acid
PPTS	Pyridinium <i>p</i> -toluenesulfonate
<i>p</i> -TsOH	4-Toluenesulfonic acid
Pv	Pivaloyl
py	Pyridine
Raney Ni	Raney nickel
RCM	Ring-closing metathesis
rt	Room temperature
SAR	Structure-activity relationship(s)
Sia	1,2-Dimethylpropyl
SMB	Simulated moving bed
S <sub>N</sub>	Nucleophilic substitution
TBAF	Tetra- <i>n</i> -butylammonium fluoride
TBDPS	<i>tert</i> -Butyldiphenylsilyl
TBS	<i>tert</i> -Butyldimethylsilyl
<i>t</i> -Bu	<i>tert</i> -Butyl
TEMPO	(2,2,6,6-Tetramethylpiperidin-1-yl)oxyl
TES	Triethylsilyl
Tf	Trifluoromethanesulfonyl (triflyl)
TFA	Trifluoroacetic acid
THF	Tetrahydrofuran
TMEDA	<i>N,N,N',N'</i> -Tetramethyl-1,2-ethylenediamine
TMS	Trimethylsilyl
TPAP	Tetra- <i>n</i> -propylammonium perruthenate
Ts	Tosyl, 4-toluenesulfonyl

## 1 Introduction

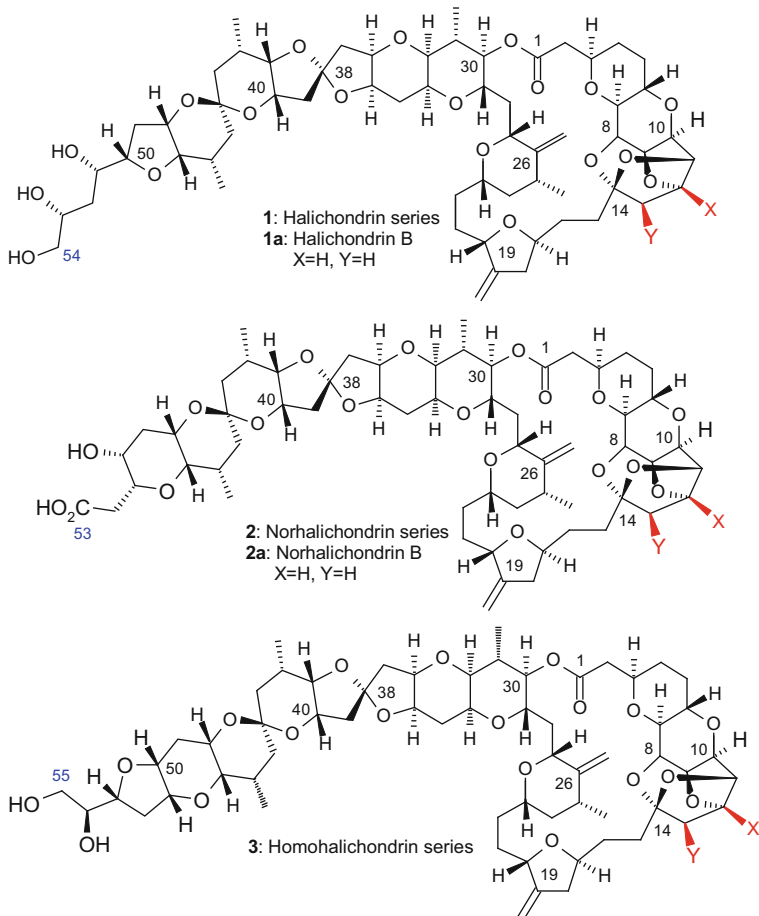
Halichondrin B is a large polyether macrolide, which was identified as the most potent of closely related congeners of *Halichondria okadai* metabolites displaying antiproliferative effects on a panel of cancer cell lines (including the NCI-60 panel). Studies toward the mode of action revealed an interaction of the compound with

tubulin. As a result, the assembly of microtubules is suppressed, which leads ultimately to cell cycle arrest in the G2-M phase and apoptosis. The medium-to-large-scale supply of sufficient quantities of drug substance in GMP quality turned out to be the crucial hurdle for clinical studies. Although initial attempts to provide material from aquacultures of a related sponge delivered a sub-gram batch of halichondrin B after considerable efforts, it soon became obvious that the sourcing issue could only be addressed by total synthesis, which was accomplished for halichondrin B in 1992 by the Kishi group. Despite the high convergency of this modular approach (and of others elaborated subsequently), a cost-effective process still remained an ambitious goal. However, systematic profiling of simpler analogues produced by Eisai chemists and scientists from the Kishi group led to the identification of the minimum pharmacophore. Further functional group exploration and optimization of the biological profile and pharmacokinetic properties led to the discovery of eribulin, which is structurally considerably less complex than halichondrin B but is yet of high complexity with its 19 stereogenic centers.

## 2 Isolation and Biological Activities of the Halichondrins

The halichondrin family of natural products is characterized by several structurally related, highly complex polyether macrolides which feature an unusual 2,6,9-trioxatricyclo[3.3.2.0]decane ring system. Since the reported isolation of the first representative, norhalichondrin A, in 1985 by Uemura and coworkers from the Pacific sponge *Halichondria okadai* [1], there has been considerable interest in this compound class from biologists, chemists, and pharmacologists due to their unique structural features and outstanding antitumor properties. After norhalichondrin A had been isolated from *Halichondria okadai* (this organism was earlier shown to produce also the phosphatase inhibitor okadaic acid) [2] in a yield of 50 ppb (from wet animals) by a bioassay-guided strategy monitoring, the activity of extracts and fractions against B-16 melanoma cells and growth inhibition potency of the pure natural product on this cell line was determined at an  $IC_{50}$  of 5 ng/mL. Subsequently, further 600 kg of *Halichondria okadai* were harvested. From this campaign, seven further members of the halichondrin family were isolated (cf. Fig. 1) [3].

The halichondrins are subgrouped into the A–C series or the norhalichondrin–halichondrin–homohalichondrin series, depending on the length of the carbon backbone or the oxidation state at C12 and C13 of the C8–C14 polycycle, respectively. With the exception of halichondrin A, all the members of the subgroups are known [4]. Halichondrins originally isolated from *Halichondria okadai* and further congeners were subsequently discovered in unrelated sponges like *Phakellia carteri* [5], *Lissodendoryx* sp. [6–8], and *Axinella* spp. [9]. The isolation, structure elucidation, and biological activities of the halichondrins have been comprehensively reviewed along with synthetic efforts toward this compound class [10].



	Halichondrin	Norhalichondrin	Homohalichondrin
A series (X=OH, Y=OH)	unknown	known	known
B series (X=H, Y=H)	known	known	known
C series (X=OH, Y=H)	known	known	known

**Fig. 1** Subseries of the halichondrins

With an  $IC_{50}$  of 0.0093 ng/mL in the B-16 melanoma cell cytotoxicity assay *in vitro*, halichondrin B turned out to be the most potent of these closely related compounds. In-depth profiling revealed that **1a** displays growth inhibition on a panel of various cancer cell lines (including the NCI 60-cell line panel) at nanomolar concentrations [9, 11], and the activity observed in these cytotoxicity assays translates into considerably increased survival times in mice models of melanoma and leukemia [3].

In further studies, **1a** has been shown to interact with tubulin to create nonproductive tubulin aggregates, resulting in the suppression of microtubule assembly without disruption of the existing tubulin architecture. This interaction led to arrest in the G<sub>2</sub>-M phase of the cell cycle and subsequently to apoptosis. Further investigations revealed that **1a** bound to the vinblastine site of tubulin in a noncompetitive fashion and had no effect on colchicine binding [11–14]. This unprecedented mechanism of action strongly contributes to the therapeutic value of the halichondrin family of antimicrotubule agents: activity is still displayed on cancer cells resistant to other antimicrotubule agents like the taxanes [15].

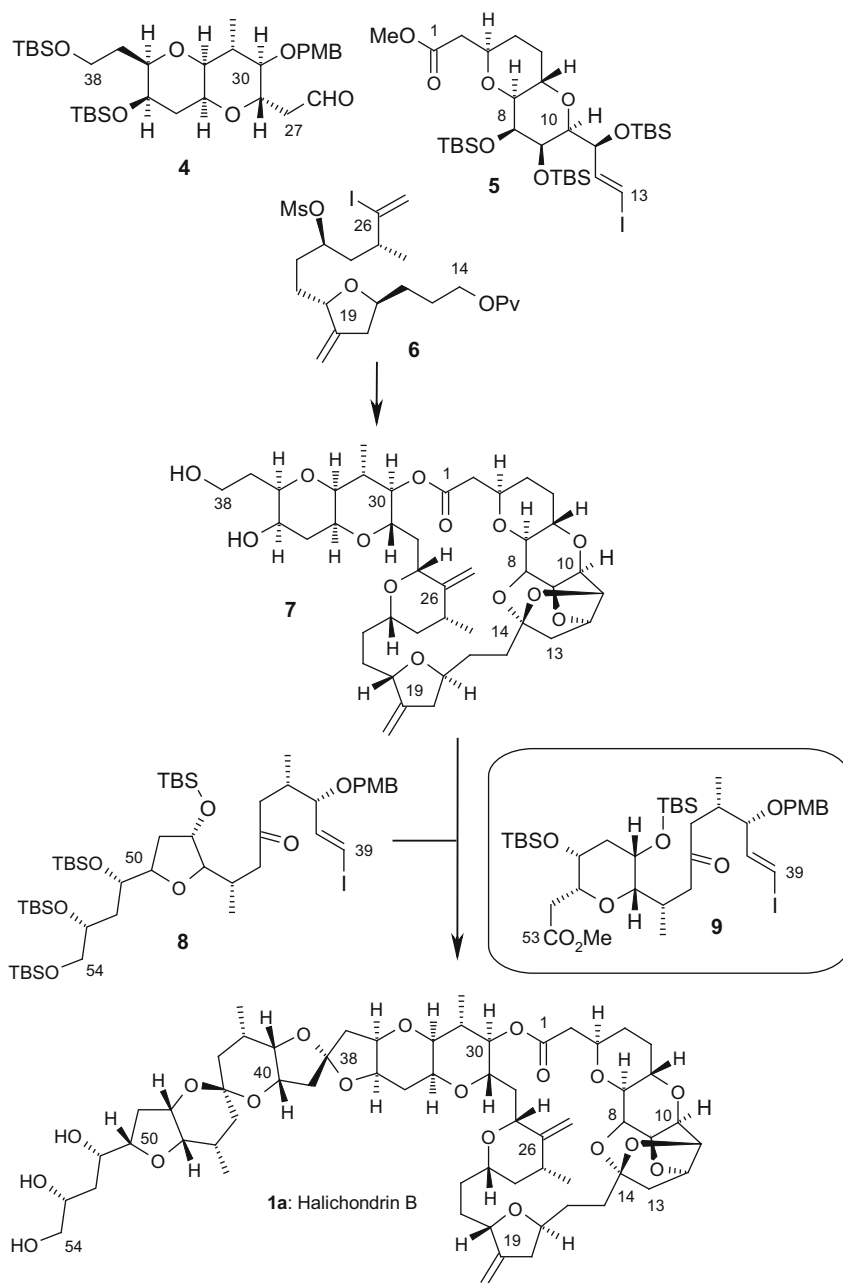
Triggered by its remarkable antitumor activities and the unique mechanism of action, halichondrin B was suggested for preclinical trials by the US National Cancer Institute (NCI). Compound supply was faced as the major hurdle for any development efforts since the beginning. The initial amount to start development activities was calculated to be around 10 g of halichondrin B **1a**, and the future commercial demand of drug substance was estimated to be 1–5 kg/year [16]. Due to the rare abundance of organisms producing **1a** and the extremely low yield of isolated compound, collection from the wild was soon ruled out. The supply issue for the start of preclinical studies was partially solved by aquaculture of *Lissodendoryx*, which led to the provision of 310 mg of **1a** from 1 t of sponge [17]. Nevertheless, it became soon obvious that the only viable alternative would be total synthesis.

### 3 Total Synthesis of the Halichondrins

Since the first reports on the isolation of members of the halichondrin family, several laboratories reported synthetic studies toward the halichondrins, with a particular focus on the most active congener **1a**. As a result of a groundbreaking effort of the Kishi group at Harvard, the first successful syntheses of both halichondrin B **1a** and norhalichondrin B **2a** were reported in 1992 [18]. Further synthetic approaches to subunits of halichondrins [10, 19] were reported and subsequently, a total synthesis of norhalichondrin B was reported by Philips and coworkers in 2009 [20]. More recently, total syntheses of halichondrin C (in 2012) [21] and the “missing member” of the class, halichondrin A (in 2014), were disclosed by the Kishi group [22] (cf. also Sects. 5.2 and 5.3).

Kishi’s approach toward the total synthesis of halichondrin B was highly convergent connecting together four subunits corresponding to the C27–C38 **4**, C14–C26 **6**, C1–C13 **5**, and C39–C54 **8** fragments (cf. Scheme 1 and Fig. 2). The synthesis turned out to be extremely flexible, allowing modifications to be made independently in each module. Thus, with the “right-half” fragment **7** in hands, norhalichondrin B could be prepared conveniently employing the C39–C53 building block **9** in the place of the C39–C54 intermediate **8** used for halichondrin B.

The strategy implemented in this syntheses impressively demonstrates the power of the Ni/Cr Nozaki–Hiyama–Kishi (NHK) reaction [22] which served to construct five carbon–carbon bonds, most of them representing key couplings for the subunits



**Scheme 1** Kishi's convergent total syntheses of halichondrin B and norhalichondrin B

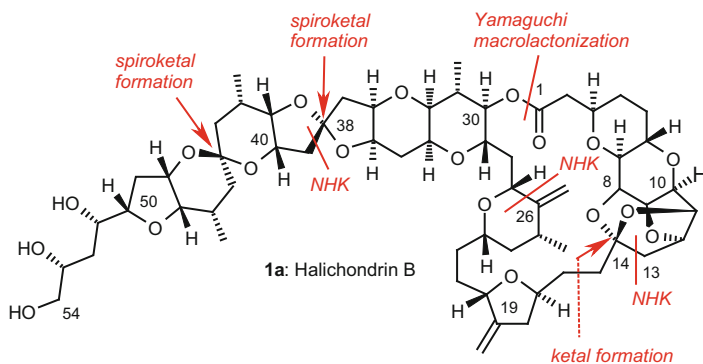
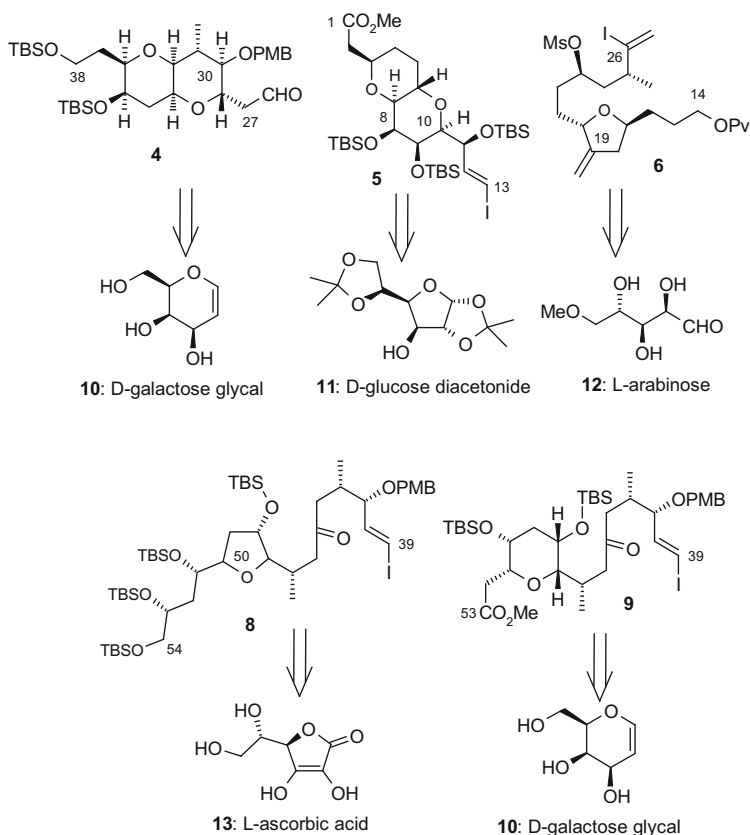


**Fig. 2** Kishi's retrosynthetic analysis of the halichondrin B series: key disconnections



**Scheme 2** Chiral pool-based building blocks for key intermediates

in good to excellent yields. As shown in Scheme 2, another important aspect of the strategy was the use of readily available carbohydrate-based starting materials.

## 4 Discovery and Process Development of Eribulin

### 4.1 Discovery of Eribulin

The highly convergent and modular synthesis approach was further improved [10] and used by the Kishi group and medicinal chemists at Eisai in order to produce simpler analogues and to identify the minimum pharmacophore of **1**. The testing of intermediates from the halichondrin's total synthesis efforts both at Eisai and the NCI revealed that growth inhibitory activity on DLD-1 cells could be traced back to the right-half macrolactone fragment **7** while none of the left-half fragments were found to display any activity on the panel of cell lines tested. These observations showed that structural simplifications of halichondrin could be performed without dramatic loss of the growth inhibitory activity *in vitro* and the material supply problem associated with this compound class seemed to be manageable by a fully synthetic approach. During lead optimization, medicinal chemists at Eisai first aimed at identifying the pharmacophore and then embarked on modifications of the structure guided by an increase of synthetic feasibility. As a first objective, an *in vivo* proof of concept in a tumor model was envisaged and a 100 mg batch of **7** based on Kishi's route could be provided in order to conduct this study.

However, in striking contrast to the natural product **1**, the intermediate **7** was devoid of activity in human tumor xenograft models. Based on the hypothesis that the right-half intermediate **7** only induced a reversible mitotic block under the dosing schemes of the *in vivo* experiments, several regions of the polyether moiety were systematically modified, and the resulting analogues were tested in a sophisticated flow cytometric assay using U937 human histiocytic lymphoma cells in order to characterize their ability to induce a complete mitotic block after drug washout [23]. The optimization program started with the working hypothesis that the array of functional groups of the C35–C38 region should represent more closely that of halichondrin B. Several analogues of **7** were therefore evaluated (cf. Fig. 3). Though they displayed a similar antiproliferative activity compared to the lead compound **7**, only analogue **14** induced an acceptable level of irreversible mitotic block and exhibited a good antitumor activity in the LOX human melanoma xenograft model [24].

In the following optimization cycle, functional groups were deleted or modified in order to obtain further simplified, more accessible structures without affecting activity. As no clear directions for modifications in the C1–C13 region could be deduced, simplifications of the C14–C26 fragment were envisaged subsequently. Whereas deletion of both olefin functions at C19 and C26 (as exemplified in compounds **20** and **21**) was tolerated, the removal of the methyl substituent at C25 in compound **22** led nearly to a loss of activity (cf. Fig. 4). As these

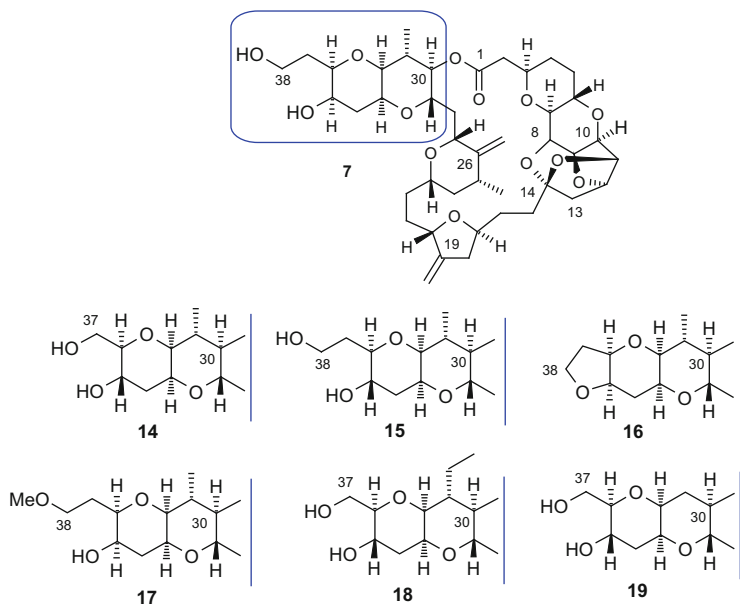


**Fig. 3** Selected halichondrin B analogues modified in the C30–C38 region

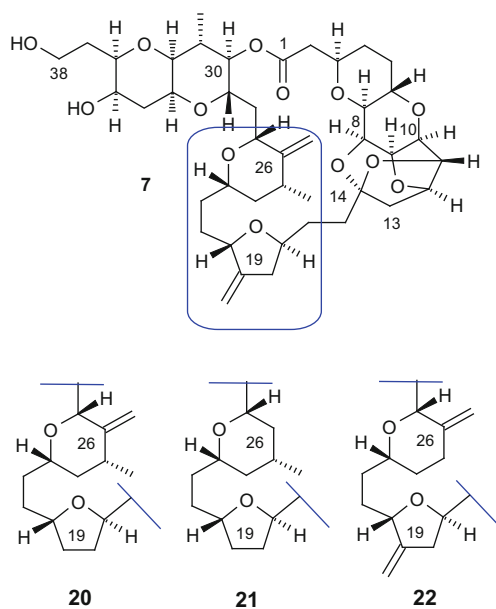


**Fig. 4** Structure-activity relationships in the C19–C26 region

modifications within the macrocycle only resulted in analogues with comparable or reduced activity, it was hypothesized that the macrolactone core of the halichondrins represents the minimum pharmacophore for antiproliferative activity. As a consequence, no further variations of the core structure (C1–C26) were envisaged and modifications were focused on the C27–C38 pyrano-pyran ring system.

Along these lines, it was discovered that simple tetrahydrofuran or tetrahydropyran fragments could replace the western-fused pyran moiety. More than 20 compounds were evaluated in this series. From the tetrahydropyran subseries, compound **23** displayed an acceptable level of irreversible mitotic block in the U937 cell line assay; however, no effect could be observed in vivo in the LOX melanoma mouse xenograft model which could be traced back to the finding that **23** was not stable in the presence of mouse serum. Further optimization focused on the tetrahydrofuran subseries, which turned out to deliver more active (cell growth inhibition on DLD-1 cells) and more irreversible (U937 assay) analogues such as **24** (cf. Fig. 5), but as in the case of the tetrahydropyrans and in contrast to the fused octahydropyrano[3,2*b*]pyran analogues (cf. Fig. 4), no improvement with regard to stability in mouse serum could be obtained [25].

Several possible explanations for these findings were discussed, and since the action of nonspecific mouse serum esterases on the C1 lactone bond was considered most likely, further optimization efforts aimed at the introduction of hydrolytically more stable bioisosteres of the C1 ester function. Along these lines, ether and amide functionalities were realized but these modifications led to less potent derivatives compared to the corresponding lactones. Finally, further functional group exploration and the replacement of the ester linkage in the macrolactone ring by a ketone led to the identification of the advanced lead compound **25** (ER-076349, NSC707390) [26] which was extensively profiled in vivo. Compound **25** displayed marked activities against four human xenografts (MDA-MB-435 breast cancer, COLO 205 colon cancer, LOX melanoma, and NIH:OVCA-3 ovarian cancer) with no evidence of severe side effects [27]. A variety of functional group modifications at C34 and C35 were explored and had little impact on the in vitro activity of the compounds as expected from SAR data hitherto accumulated. However, amine **26**, which was obtained from **25** by treatment with TsCl followed by NH<sub>3</sub>,

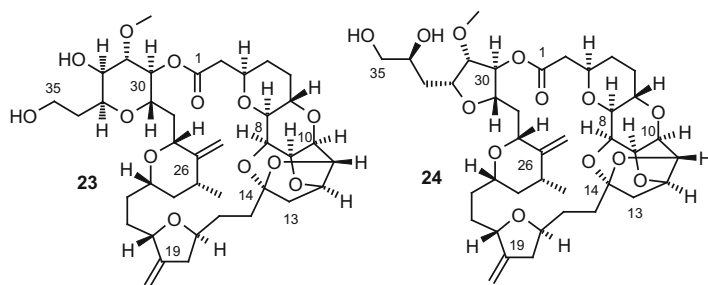
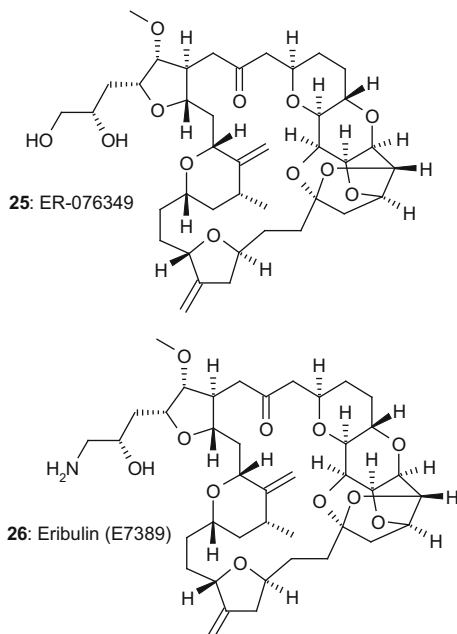


**Fig. 5** Tetrahydropyran and tetrahydrofuran macrolactone analogues

**Fig. 6** Structure of ER-076349 and eribulin

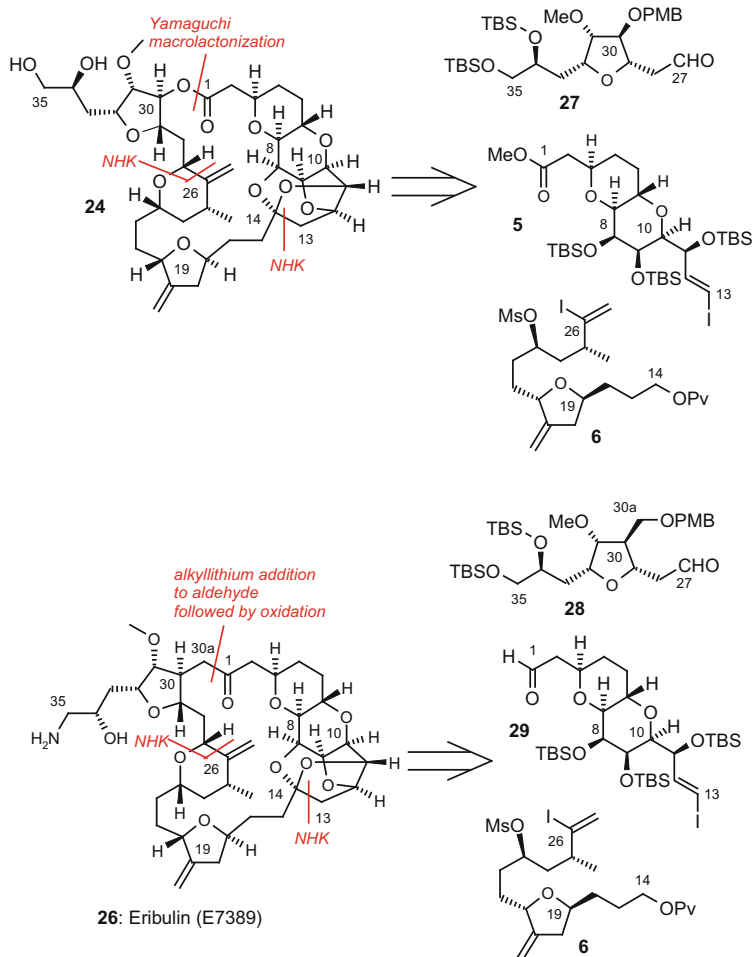


displayed a remarkable activity in the U937 human histiocytic lymphoma cells reversibility assay: it was the first compound that exhibited a reversibility ratio of one and was thus able to maintain a complete mitotic block even after a washout period of 10 h. Compound **26** (Eribulin, E7389, previously ER-086526) demonstrated remarkable efficacy (0.05–1 mg/kg) in a variety of human tumor xenograft models [27]. Due to its convincing biological profile, **26** was selected for preclinical development at Eisai [26] (Fig. 6).

## 4.2 Process Development of Eribulin: From Milligram Scale to Commercial Manufacture

### 4.2.1 First-Generation Synthesis of Eribulin

Although the molecular architecture of eribulin **26** is significantly simpler than that of halichondrin B **1a**, the compound still contains 19 stereogenic centers and can be regarded as the structurally most complex drug substance on the market which is prepared by total synthesis to date. During preclinical development, the major obstacles which had to be overcome in the context of this unprecedented complex structure were cost of goods and synthetic feasibility. As outlined below continuous scientific contributions from the Kishi group and considerable efforts from Eisai's chemical development teams finally led to a cost-effective, scalable synthesis of **17**



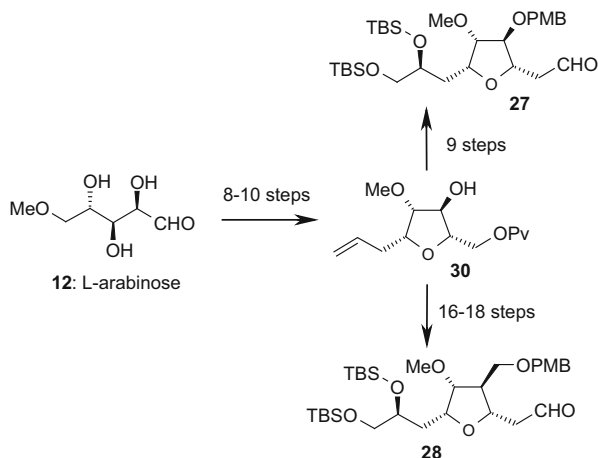
**Scheme 3** Retrosynthetic analysis of macrolactone and macrocyclic ketone analogues of halichondrin B

in 62 steps [16, 28, 29] which opened the way for the first clinical phase I trials in collaboration with the NCI.

Since the discovery of eribulin was preceded by the exploration of structure-activity relationships around simplified macrolactone analogues such as **24** (cf. Fig. 5), the very first synthesis of eribulin **26** and its direct precursor **25** was based on building blocks for synthetic routes toward the establishment of a key ester bond between C1 and C30 which were turned into intermediates with which a ketone moiety could be constructed.

The C1–C26 framework of the macrolactone analogues is identical to that of halichondrin B. Therefore the C1–C13 **5** and C14–C26 **6** subunits from the halichondrin B total synthesis could be directly employed for the synthesis of

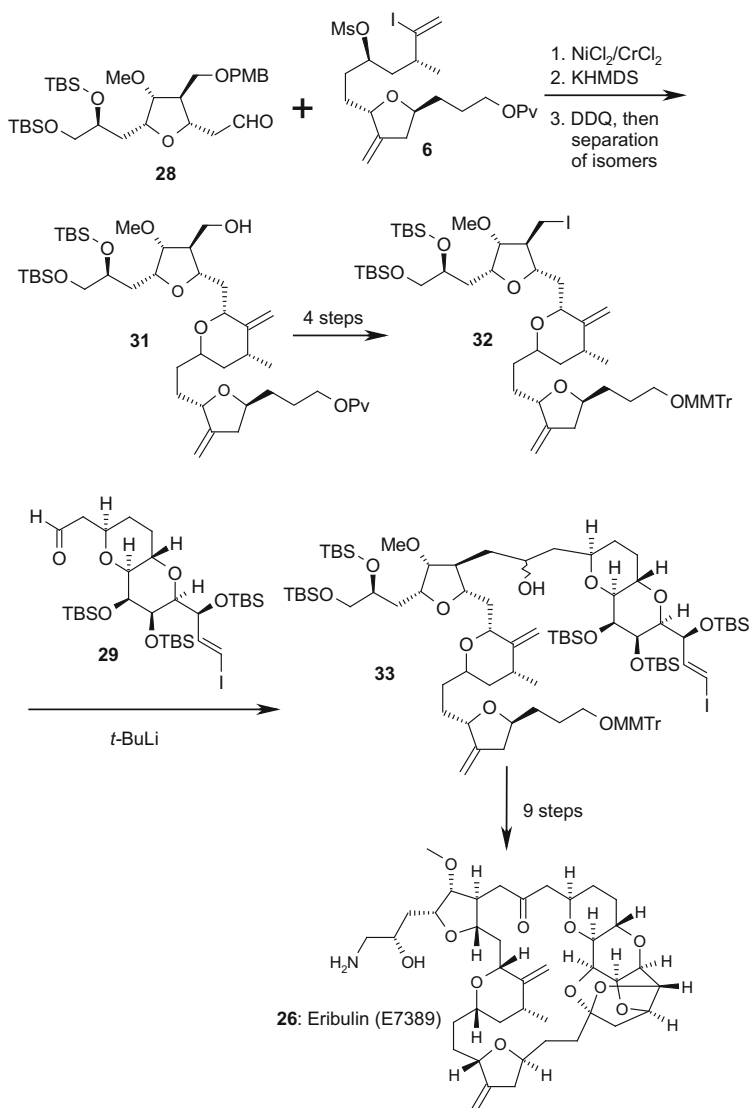
**Scheme 4** Syntheses of C27–C35 fragments from L-arabinose



macrolactone analogues, while for the C27–C35 fragment, **27** new approaches had to be elaborated. To this end, two synthesis routes starting from L-arabinose were developed yielding key intermediate **30** in 8–10 steps (Schemes 3 and 4) [25, 30, 31]. One of the key sequences in the synthesis of eribulin is the bond formation between C1 and C30a followed by the establishment of the C1 keto function (Scheme 3). In the first published, milligram scale synthesis of eribulin, an addition of an alkyl lithium species (generated from an alkyl iodide) to an aldehyde followed by oxidation of the addition product – a secondary alcohol – was envisaged to achieve this sequence (Scheme 4) [30, 31]. The required aldehyde **29** could be obtained in a straightforward manner by DIBAL-H reduction of ester **5**, which was obtained in 12 steps by an improved synthesis starting from L-mannono- $\gamma$ -lactone on a multigram scale [32].

In contrast, the original C1–C13 building block **5** synthesis started from D-glucose diacetonide **11** and required 30 steps [18, 33, 34]. Several transformations turned out to be roadblocks in attempts to scale up this route. In the course of the first synthesis of the C<sub>1</sub>-homologated building block **28**, the common intermediate **30** from the L-arabinose route to **27** was used (cf. Scheme 4).

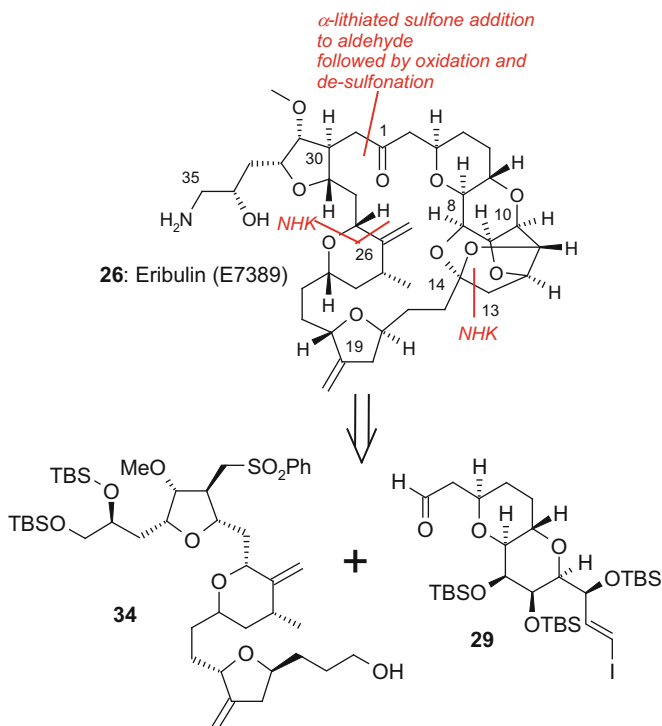
Coupling of **28** with the C14–C26 building block **6** under Nozaki–Hiyama–Kishi conditions followed by formation of the tetrahydropyran ring under basic conditions (Williamson ether cyclization) delivered intermediate **31** which was transformed into the iodide **32** in a six-step sequence. Iodide **32** was transformed to the corresponding organolithium species employing a halogen–metal exchange reaction with *t*-BuLi, which was subsequently coupled with aldehyde **29**. The resulting alcohol **33** was then converted into eribulin **26** in nine steps along the routes established in the total synthesis of halichondrin B employing another Nozaki–Hiyama–Kishi reaction for the key ring-closing step to the macrocycle [31] thereby delivering the first 0.6 mg batch of eribulin **26**, which was used for analytical characterization and first in vitro biological profiling [35] (cf. Scheme 5).



**Scheme 5** First-generation synthesis of eribulin

#### 4.2.2 Second-Generation Synthesis of Eribulin

Although the initial route provided sufficient amounts of material for the basic profiling of the compound, this approach was not considered as a reliable path forward since during the scale-up to the gram scale, the key coupling reaction between iodide **32** and aldehyde **29** delivered only unsatisfactory yields of **33**. Due to increased needs of eribulin for preclinical toxicology studies, the search for

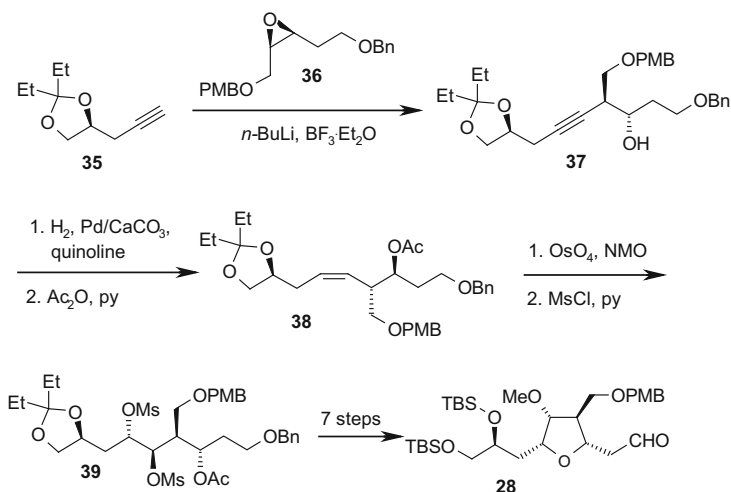


**Scheme 6** Second-generation synthesis of eribulin

alternative methods of assembling the fragments was pursued with high priority in parallel to the development of improved routes toward the tetrahydrofuran building block **28** and related intermediates for different coupling strategies. As a result of these studies, the reaction of an  $\alpha$ -lithiated sulfone **34** with an aldehyde **29** was found to be a viable alternative to the initial halogen–metal exchange-based methodology for the connection of the C1–C13 and the C14–C35 subunits (cf. Scheme 6) [26, 35].

While the synthesis of C27–C35 tetrahydrofuran building blocks like **28** based on *L*-arabinose met the needs for a high flexibility to provide quickly several analogues during SAR studies en route to **26**, a shorter and more robust route was developed in the course of the second-generation eribulin synthesis.

As outlined in Scheme 7, an improved synthesis of the C27–C35 fragment **28** started from commercially available (*2S*)-butane-1,2,4-triol (from reduction of (*S*)-malic acid [36]) which was transformed into alkyne **35** in four steps. Epoxide **36** (obtained from 1-butyn-4-ol in five steps) was regioselectively opened with the acetylide derived from **35**. Lindlar reduction of the coupling product **37** followed by acetylation delivered the *cis*-olefin **38**, which was dihydroxylated followed by mesylation to yield **39**. Compound **39** was subsequently transformed in a few steps to building block **28** [26].

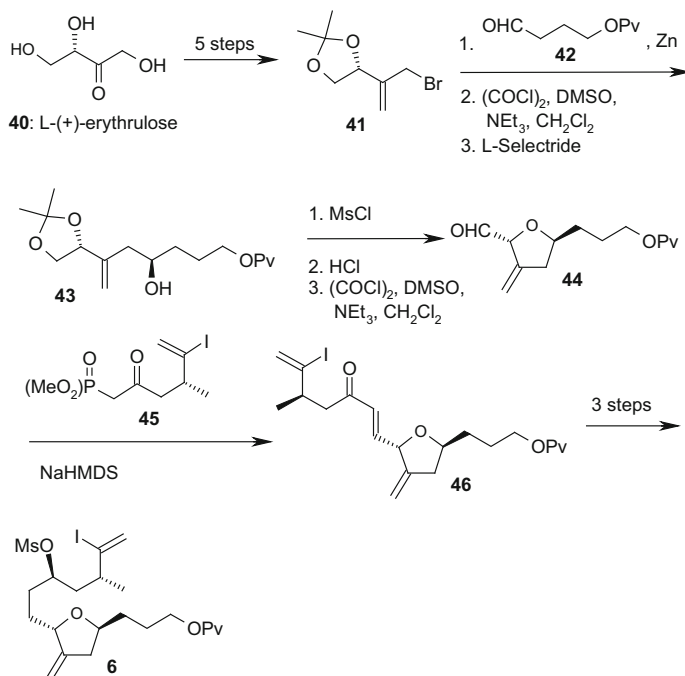


**Scheme 7** Second-generation synthesis of the C27–C35 fragment

A practical synthesis of the vinyl iodide intermediate **6** started from commercially available L-(+)-erythrulose which was transformed into allyl bromide **41** in a straightforward manner. A mixture of secondary alcohols was obtained by coupling of **41** with **42** (prepared from 1,4-butanediol in three steps) in the presence of zinc. Oxidation under Swern conditions followed by stereoselective reduction with L-Selectride provided **43** as a major product which was converted to the C14–C21 aldehyde building block **44** in three steps. Coupling of **44** with ketophosphonate **45** (prepared by a modification of the original Kishi synthesis [35]) afforded the enone **46**, which was proceeded to **26** according to the first halichondrin B synthesis [18, 34] (cf. Scheme 8).

Nozaki–Hiyama–Kishi conditions as applied in the original halichondrin B synthesis [18] were used to couple vinyl iodide **6** and aldehyde **28** in order to furnish a 3:1 mixture of C27-isomers in favor of the desired product, the PMB-protected precursor of intermediate **31**. Separation of the isomers at this stage was not practical, but could be achieved by flash chromatography after removal of the PMB group yielding intermediate **31** in 59% yield which was transformed in four steps into phenyl sulfone **34** required for the coupling with C1–C13 intermediate **29** [26]. The synthesis of intermediate **34** comprised 59 synthetic steps in total with the longest linear sequence of 26 steps from readily available commercial starting materials. Although a number of issues such as the need for several chromatographic separations were associated with this route, 65 g of the phenyl sulfone **34** could be prepared [35].

Coupling of **34** with the aldehyde **29** provided a mixture of alcohols which was oxidized with Dess–Martin periodinane to ketone **47**. The sulfone group was then removed with  $\text{SmI}_2$ . This reaction sequence could be scaled up to the multigram level. The following macrocyclic ring closure under Nozaki–Hiyama–Kishi

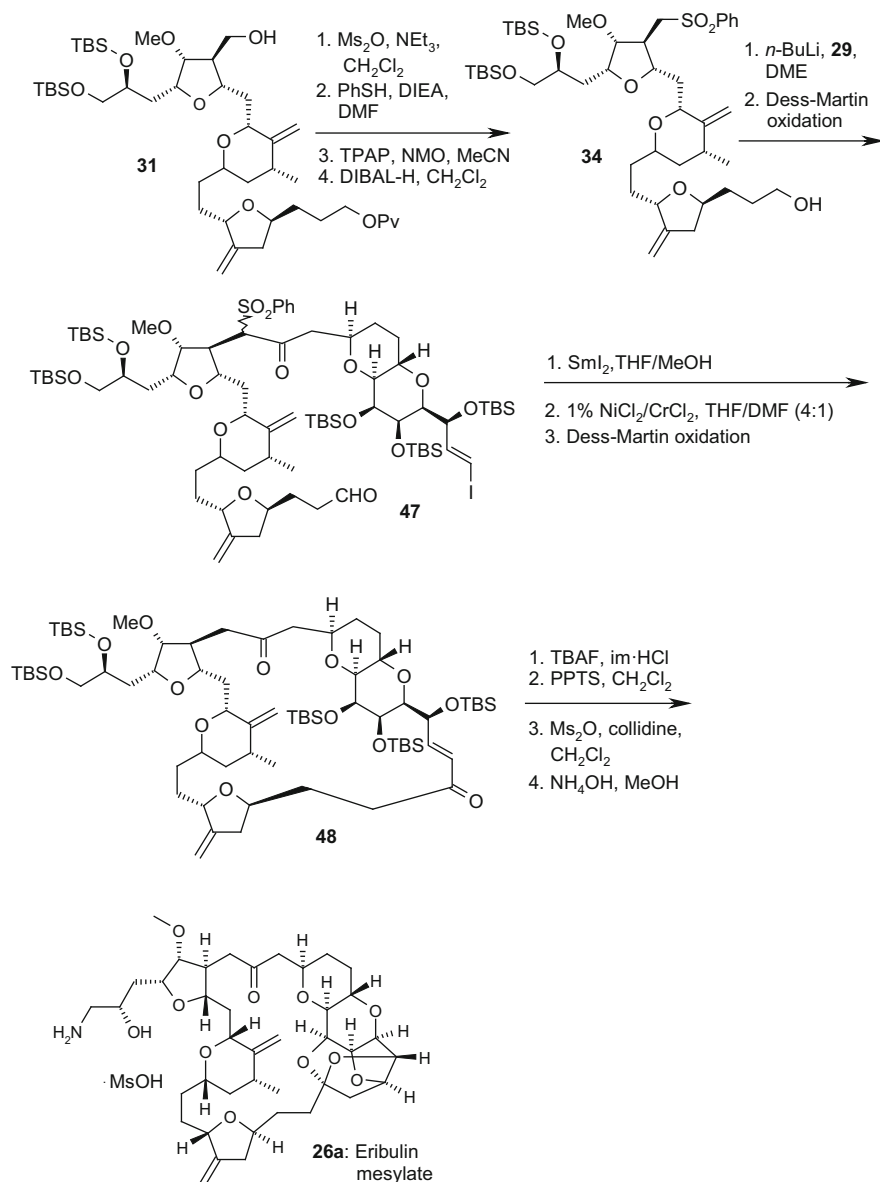


**Scheme 8** Synthesis of the C14–C26 key intermediate

conditions proceeded smoothly with 95% yield. The resulting allylic alcohols were oxidized to the corresponding enone **48**, followed by removal of the silyl protecting groups and Michael addition in buffered TBAF solution. Subsequently, the “cage” structure was established using PPTS yielding diol **25** (ER-076349) in 69% overall yield which was converted to eribulin mesylate **26a** by mesylation followed by ammonolysis. After column chromatography, filtration, and precipitation from hexanes, 8.9 g of eribulin mesylate was obtained as a white solid (17% overall yield from sulfone **34**; cf. Scheme 9). This was the first multigram total synthesis of eribulin that opened the way for first clinical phase I trials in collaboration with the NCI [35].

### 4.2.3 Process-Scale Synthesis of Eribulin

Though the first multigram-scale synthesis provided substantial quantities of material in order to support significantly the preclinical development, the route still required major improvements from process development research toward an industrial-scale manufacture. In particular, the number of chromatographic purifications steps had to be reduced, and several chemo-, regio-, and stereoselective transformations had to be mastered. Moreover, the macrocyclization under high-dilution conditions presented a number of challenges.



**Scheme 9** Final steps in the first gram-scale synthesis of eribulin

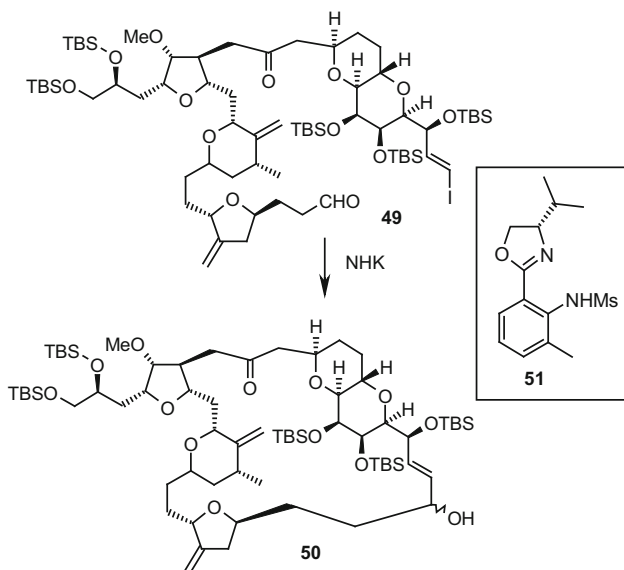
The coupling of sulfone **34** with aldehyde **29** was originally carried out with an excess of *n*-BuLi (2.7 equiv. vs. the theoretically required 2 equiv.) in DME. However, incomplete conversion and low reproducibility were observed. Therefore, this key transformation had to be optimized, and solvents, reaction temperature, and base stoichiometry were investigated. Deuterium-labeling studies

revealed that at  $-40^{\circ}\text{C}$  the deprotonation of **34** (at the  $\alpha$ -position of the sulfone) was incomplete. Complete deprotonation could be achieved with 2.0 equiv. of *n*-BuLi at  $0^{\circ}\text{C}$ . Although the following reaction of the dianion generated at  $0^{\circ}\text{C}$  with aldehyde **29** carried out at low temperature led to an improved product quality, unreacted sulfone **34** was still present after completion of the reaction. Competitive enolization [37] of the aldehyde **29** during reaction was ruled out by another labeling experiment: when C2-deuterated aldehyde **29** was incubated with the sulfone dianion under reaction conditions, no deuterium transfer was observed. Based on the hypothesis that coordinating solvents might affect the nucleophilicity of the dianion generated from **34**, other solvent combinations were investigated. In the optimized procedure, a solution of **34** in a minimal amount of THF was deprotonated with 2.0 equiv. of *n*-BuLi at  $0^{\circ}\text{C}$ , and the resulting dianion solution was reacted with a solution of **29** in hexane at  $<-65^{\circ}\text{C}$ . After quenching with ammonium chloride solution and chromatographic purification, 86% of the desired addition product (along with 8% of the recovered sulfone **34**) was obtained, which was converted to **47** with Dess–Martin periodinane. The addition of catalytic amounts of water to the oxidation reaction [38] turned out to be essential in order to obtain high yields in a reproducible manner.

The scale-up of the macrocyclic ring closure reaction from **49** (obtained by  $\text{SmI}_2$ -mediated desulfonylation of **47**) to **50** under Nozaki–Hiyama–Kishi (NHK) conditions represented another major challenge. The original procedure required super-stoichiometric amounts of  $\text{NiCl}_2/\text{CrCl}_2$  (1% w/w) reagent, high-dilution conditions, THF/DMF (4:1) as the solvent and several days of reaction time [39].

It was postulated that the addition of the aldehyde function of **49** to a highly reactive species generated from the vinyl iodide could simulate high-dilution conditions, if the formation of the macrocycle proceeded in an efficient manner. Despite the fact that no stereoselectivity in the reaction was required since the generated alcohol **50** would be oxidized to **48** subsequently, a ligand-accelerated, asymmetric Ni(II)/Cr(II) coupling protocol developed by the Kishi group [40] was adopted to provide a first, stoichiometric process using the ligand **51** in MeCN/THF in the presence of  $\text{NEt}_3$  leading to a considerable reduction of volume and increased reaction rates [41]. Further development based on the catalytic Kishi protocol for the asymmetric Ni(II)/Cr(II) coupling [42] led to an improved process, which can be carried out on kilogram scale: a solution of **49** in MeCN/THF is added to a mixture of  $\text{NiCl}_2$  and the preformed complex of **51** and  $\text{CrCl}_2$  in MeCN. Compound **50** is obtained in 78% yield as a mixture of diastereomers after a nonaqueous work-up (Scheme 10).

The oxidation of **50** leads to ketone **48**, which is further elaborated to the diol **25** (ER-076349) by removal of the TBS protecting groups with buffered TBAF solution at  $0^{\circ}\text{C}$  followed by treatment with PPTS. The transformation of the diol **25** into eribulin on a production scale is accomplished by the transformation into the C35 primary tosylate, which upon treatment with alcoholic ammonia forms first an epoxide intermediate (that can be crystallized [43]) which further reacts to eribulin **26**. A solution of the free base thus obtained in MeCN is treated with aqueous ammonium mesylate, which yields after solvent exchange, precipitation, and drying



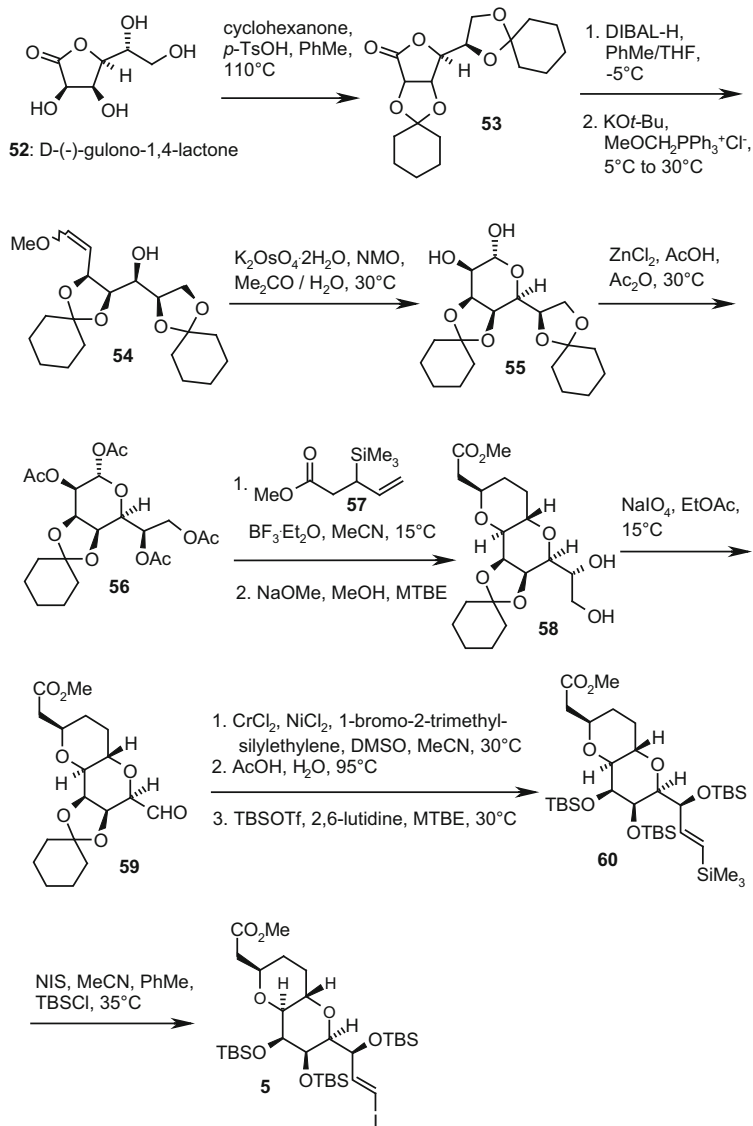
**Scheme 10** Key macrocyclic ring closure under Nozaki–Hiyama–Kishi conditions

the active pharmaceutical ingredient (API), eribulin mesylate **26a** as an amorphous solid ready for formulation [44].

Recently, further late-stage process improvements have been disclosed [45–47]. Furthermore, a novel Cr(II)-mediated desulfonation method for intermediate **47** was developed, which employed the addition of Mn and a bipyridyl-type ligand. These conditions effectively replaced the original SmI<sub>2</sub>-based protocol [48].

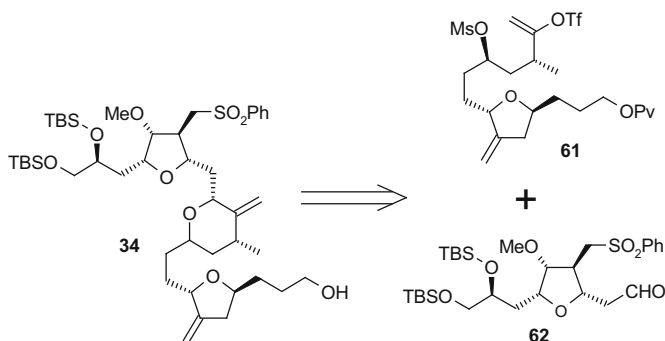
During the process development at Eisai, considerable improvements in the synthesis of the key building blocks **29** (C1–C13) and **34** (C14–C35) have been accomplished in order to meet the requirements of a sustainable supply and high quality standards for the API production. Since the large supply of D-mannonolactone, which served as a starting material for **29** in the gram-scale route toward **26**, became an issue, alternatives had to be considered. Since one of the stereogenic centers of D-mannonolactone (corresponding to C11 in the halichondrin/eribulin numbering) is destroyed during the transformations toward **29**, the sugar epimeric with regard to this center, D-gulonolactone, readily available in bulk quantities, was chosen as the starting material for the process route.

D-Gulonolactone **52** was converted to the known bis-lactone **53**, which was obtained in pure form after crystallization. Compound **53** was reduced to the corresponding lactol with DIBAL-H, which was transformed to intermediate **54** via Wittig reaction. Scale-up of this reaction was achieved by inverse addition of the lactol to the preformed methoxymethylene ylid at 0°C. The use of maleic anhydride as a triphenyl phosphine scavenger in the work-up and triphenylphosphine oxide precipitation with MTBE/heptane yielded **54** as a product of sufficient quality that could be used directly for the next step without further



**Scheme 11** Process-scale synthesis of the C1–C13 building block from D-(-)-gulono-1,4-lactone

purification. Stereoselective osmylation provided **55** as a ca. 3:1 mixture of crystalline  $\alpha$ -hydroxy lactols. Due to the lability of the ancillary cyclohexylidene group, a protocol of an one-pot cyclohexylidene mono-deprotection/acetate protection yielding **56** was developed. Compound **56** was then C-glycosylated with **11** analogously as reported for the D-mannonolactone series [32]. The product was treated with sodium methoxide undergoing global deacylation, olefin conjugation, and



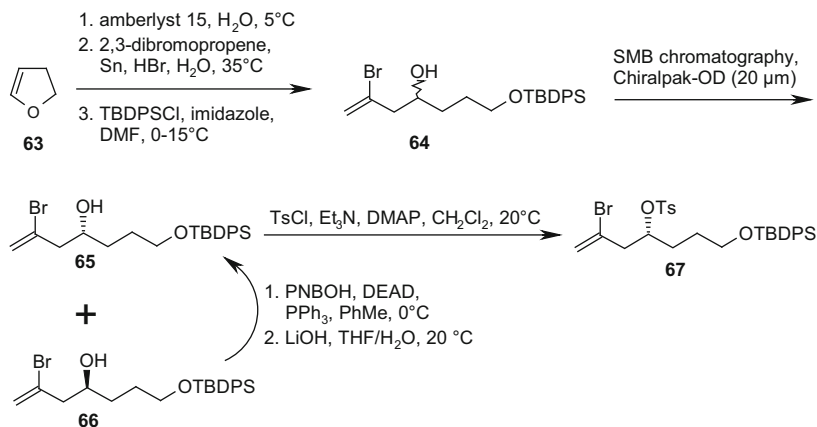
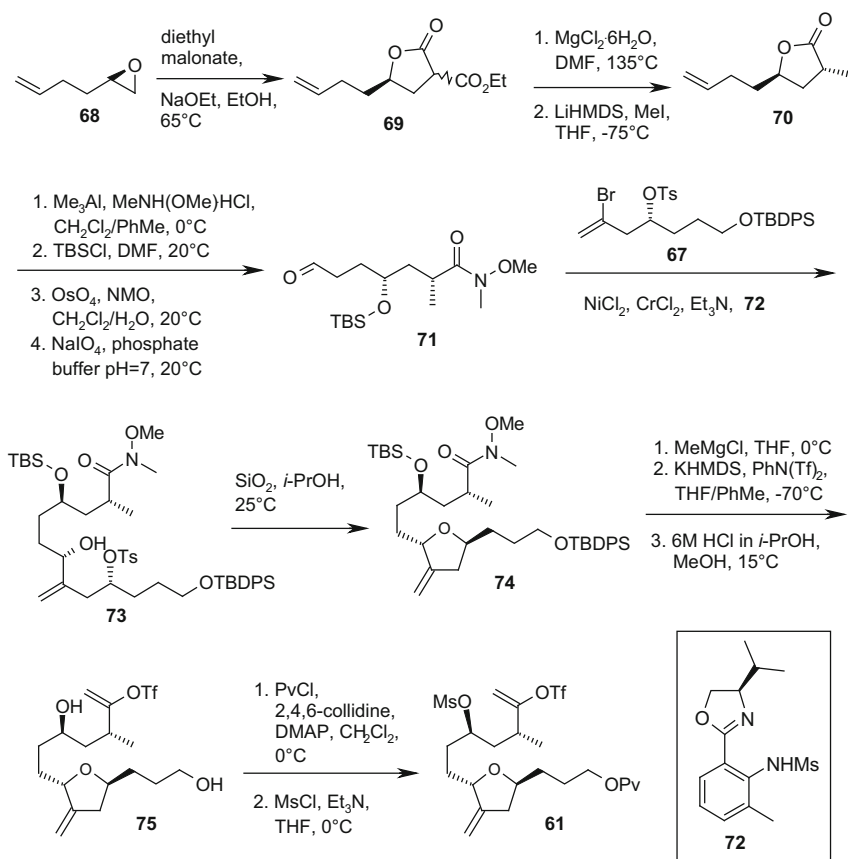
**Scheme 12** Key intermediates for the process-scale synthesis of the C14–C35 building block

oxy-Michael addition and thus providing **58** as a crystalline intermediate, which was converted to aldehyde **59** after reaction with sodium periodate. Ni(II)/Cr(II)-mediated coupling of the aldehyde **59** with 1-bromo-2-trimethylsilylethylene followed by removal of the cyclohexylidene protecting group and silylation of the resulting triol furnished crystalline tris-silyl ether **60**, which was converted to key building block **5** with NIS in the presence of catalytic amounts of TBSCl [49] (cf. Scheme 11).

The strategy for the production-scale route toward the C14–C35 subunit **34** was based on building blocks **61** (C14–C26) and **62** (C27–C35) closely related to the key intermediates **6** and **28**, respectively, employed in the first- and second-generation syntheses (cf. Scheme 12).

In the C14–C19 fragment synthesis, the 2,3-dihydrofuran **63** was used, which was converted to the alcohol **64** (racemic mixture) by an acid-catalyzed hydration, a tin-mediated addition of 2,3-dibromopropene, and a selective silylation of the primary hydroxy function. Both enantiomers, **65** and **66**, were separated by chiral simulated moving bed (SMB) chromatography [50] to >98% *ee*. The (*S*)-isomer **66** was converted into the desired (*R*)-isomer **65** by Mitsunobu inversion followed by hydrolysis. C14–C19 fragment **67** was subsequently obtained after tosylation of the free hydroxy group of **65** with >99% *ee* after chromatographic purification and crystallization (cf. Scheme 13).

The C20–C26 fragment was synthesized from (2*R*)-2-but-3-enyloxirane **68**, which was obtained from the corresponding racemic oxirane with >99% *ee* by Jacobsen hydrolytic kinetic resolution [51]. Reaction with diethyl malonate provided lactone **69**, which was decarboxylated and subsequently diastereoselectively alkylated to yield **70** as the major isomer (*dr* = 6:1) with the desired C25 configuration. In a four-step sequence, lactone **70** was then further elaborated to aldehyde **71** which was coupled to the C14–C19 fragment **67** under carefully controlled asymmetric Ni(II)/Cr(II)-mediated coupling conditions [40, 42, 52] employing the chiral ligand **72**. The coupling product **73** was subjected to silica-mediated cyclization providing **74** as a mixture of diastereomers (C20 *dr* = 8:1 and C25 *dr* = 6:1) after chromatography. A Grignard reaction was used for the transformation of the


**Scheme 13** Synthesis of the C14–C19 fragment

**Scheme 14** Synthesis of the C20–C26 fragment and conversion to the C14–C26 building block

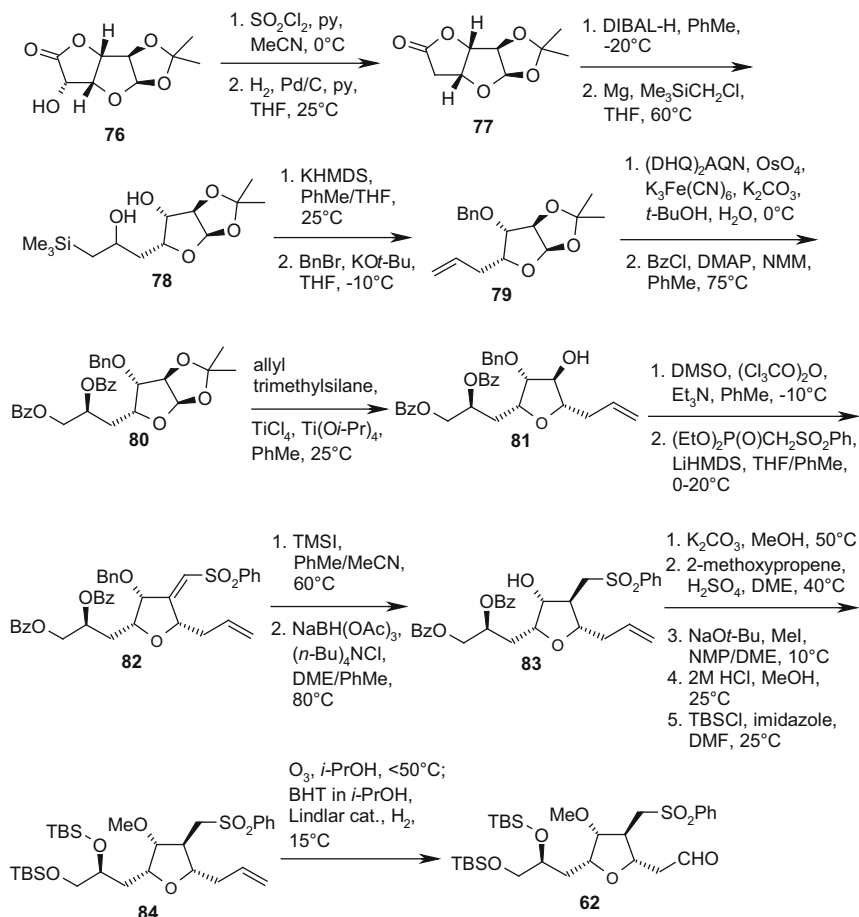
Weinreb amide to a methyl ketone, which was converted to the corresponding vinyl triflate. Diol **75** was obtained after desilylation and chromatography as a mixture of C20 and C25 diastereomers. Key intermediate **61** was finally obtained after selective pivaloyl protection of the primary hydroxy group and mesylation of the secondary hydroxy function (cf. Scheme 14).

In contrast to the second-generation synthesis of the C27–C35 fragment which relied upon the malic acid-derived building block **35** and Sharpless asymmetric dihydroxylation to construct three stereocenters of intermediate **28** (cf. Scheme 7), the process-scale synthesis was based again on a carbohydrate, D-glucurono-3,6-lactone, and was adapted from a procedure developed for an acetonide analogue of **62** developed in the Kishi group [53]. During the development for an industrial-scale manufacture, several critical steps had to be mastered. D-Glucurono-3,6-lactone acetonide **76** was obtained from the reaction of D-glucurono-3,6-lactone with acetone under acidic conditions. Deoxygenation of **76** was performed by treatment with sulfuryl chloride followed by catalytic hydrogenation. The resulting crystalline lactone **77** was converted to  $\beta$ -hydroxysilane **78** by DIBAL-H reduction and subsequent addition of trimethylsilylmagnesium chloride. Basic elimination and benzylation yielded olefin **79**, which was subjected to Sharpless asymmetric dihydroxylation providing, after dibenzoylation, intermediate **80** as a mixture of diastereomers ( $dr = 3:1$ ) in favor of the desired isomer at C34. C-glycosylation with allyl trimethylsilane yielded alcohol **81**, which was recrystallized in order to remove the undesired C34 epimer. Transformation of the secondary alcohol to the corresponding ketone by a modified Moffat oxidation followed by a Horner–Wadsworth–Emmons reaction gave the sulfone **82**. The C31 benzyl ether was selectively cleaved with trimethylsilyl iodide to set the stage for a hydroxy-directed conjugate reduction to **83**, which was subsequently converted to the olefin **84** in a five-step sequence. The crystalline key building block **62** (C27–C35) was finally obtained after ozonolysis and reductive work-up (cf. Scheme 15).

Asymmetric Ni(II)/Cr(II)-mediated coupling of key building blocks **61** and **62** in the presence of (*S*)-ligand **51** provided intermediate **85** with a  $dr = 20:1$  at the newly established C27 chiral center. The C23–C27 pyran ring was closed under carefully controlled conditions with KHMDS at low temperature, and, finally, the C14–C35 building block **34** was obtained after removal of the pivaloyl protecting group with DIBAL-H (cf. Scheme 16) [54].

## 5 Recent Progress Toward the Synthesis of the Halichondrins and Eribulin

Due to the outstanding structural features and biological activities of the halichondrins and the emerging therapeutic potential of eribulin, several academic and industry groups have intensively contributed to both total syntheses and alternative building block approaches. The total syntheses of halichondrin B and

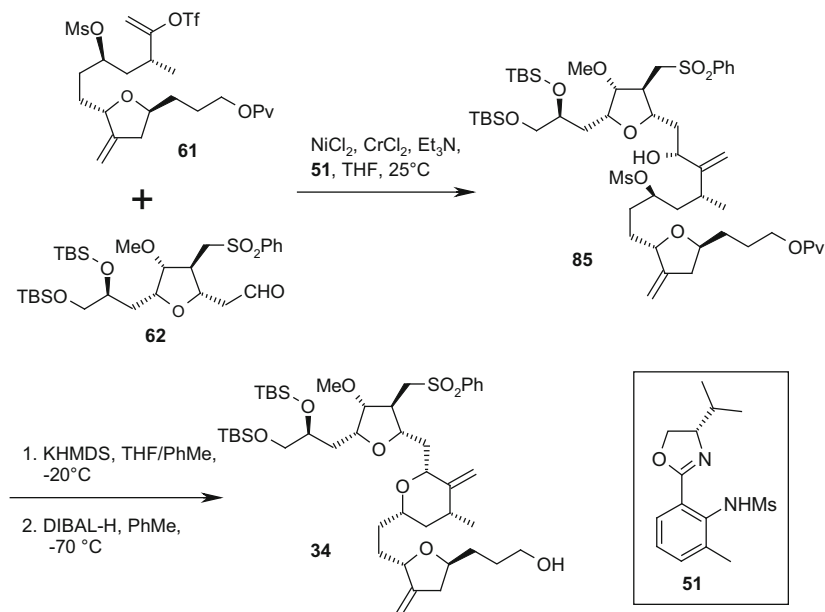


**Scheme 15** Process-scale synthesis of the C27–C35 building block from D-glucurono-3,6-lactone

norhalichondrin B and subsequent improvements by the Kishi group have been extensively reviewed as well as the total synthesis of norhalichondrin B by Philips and coworkers along with contributions from the groups of Horita and Yonemitsu and Salomon and Burke until 2008 [10]. Therefore only progress thereafter will be touched upon in the following section.

### 5.1 Kishi's Syntheses of Halichondrin and Eribulin Building Blocks

The original D-glucurono-3,6-lactone route to the C27–C35 fragment was also further elaborated by the Kishi group. Following the initial route [53], intermediate

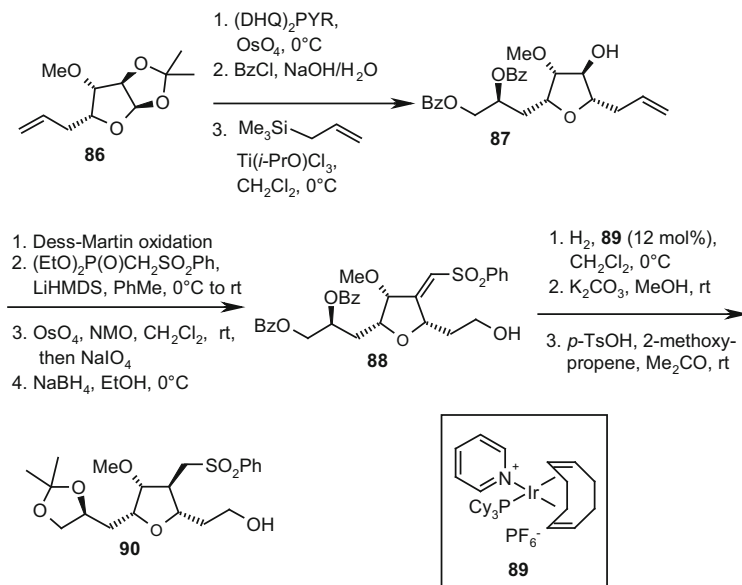


**Scheme 16** Final steps of the C14–C35 building block synthesis

**86** (closely related to **79**) was obtained from 1,2-*O*-isopropylidene- $\alpha$ -D-5-deoxyglucuro-6,3-lactone **77** in a similar fashion as outlined in Scheme 15 by methylation of the secondary alcohol instead of benzylation. Catalytic asymmetric dihydroxylation was used to install the C34 alcohol in a diastereoselective fashion ( $dr = 3:1$ ). The mixture of diastereomers was further elaborated to a mixture of  $\alpha$ -C-allylated products. The desired product **87** displayed excellent crystallinity and could be separated from the oily, undesired minor C34-diastereomer by simple crystallization. Transformation of the secondary alcohol to the corresponding ketone by Dess–Martin oxidation followed by Horner–Wadsworth–Emmons reaction gave the corresponding  $\alpha,\beta$ -unsaturated sulfone as a 30:1 *Z/E* mixture. Conversion of the terminal olefin in two steps furnished alcohol **88**, which was subjected to hydrogenation [55] in the presence of the Crabtree catalyst **89** [56]. The reduction of the double bond proceeded with a >100:1 diastereoselectivity, and the C27–C35 building block **90** was obtained after switching of the protecting groups from bis-benzoyl to the corresponding acetonide (cf. Scheme 17) [57].

Cr-mediated couplings have been exploited extensively by the Kishi group. A “toolbox” of effective ligands for catalytic asymmetric Cr-mediated coupling reactions has been developed (examples shown in Fig. 7) [58, 59] and systematically applied to the various C–C bond-forming reactions in syntheses of eribulin and halichondrin and their building blocks.

Based on this catalyst toolbox, in particular, several alternative approaches to C14–C35 building blocks (and C14–C38 in the halichondrin series, respectively)



**Scheme 17** Kishi's improved synthesis of a C27–C35 building block

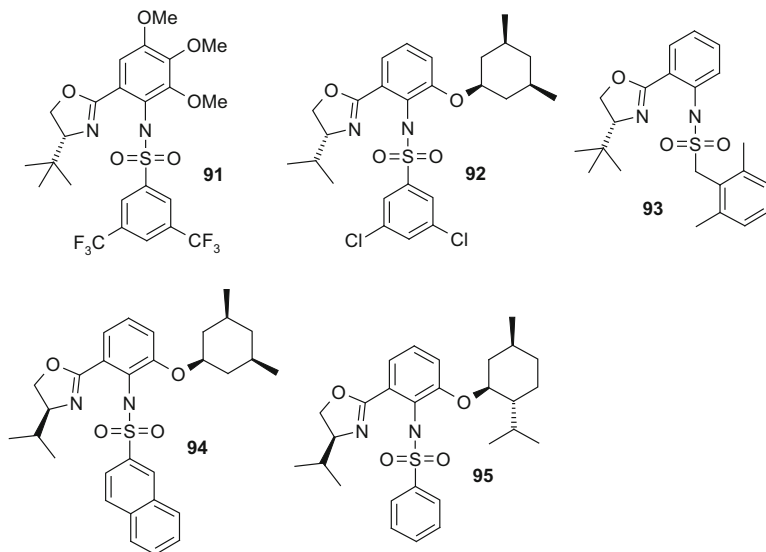


**Fig. 7** Ligands for catalytic asymmetric Cr-mediated coupling reactions developed by the Kishi group

have been elaborated. A first series followed the original strategy of assembling C14–C26 (with the preformed C17–C20 tetrahydrofuran ring) and C27–C35 fragments in a convergent fashion.

One route to the C14–C26 fragment started from aldehyde **97**, which was converted to alcohol **98** by catalytic asymmetric Cr-mediated propargylation with propargyl bromide **96**. In an optimized protocol, **98** was obtained in 78% yield and 90% *ee* with 10 mol% of CrBr<sub>3</sub> and (*R*)-catalyst **91**. Since after extensive catalyst and condition screening the *ee* could not be improved above 90%, a method in order to enrich the optical purity of **98** by selective hydrolysis of the acetate of (*S*)-**98** with *Amano lipase PS-800* was established. Optically pure **98** was then transformed into the vinyl iodide **99** by S<sub>N</sub>2 reaction of the alcohol followed by iodoboration [60]. Catalytic asymmetric coupling of **99** with aldehyde **100** was performed with ≤10 mol% of the Cr complex of (*R*)-catalyst **92** and 3 mol% of NiCl<sub>2</sub>·2,9-dimethyl-1,10-phenanthroline (NiCl<sub>2</sub>·DMP) and furnished the cyclization precursor **101** in 90% yield with a *dr* = 22:1. Cyclization was achieved by treatment with KH and 18-crown-6 and deprotection followed by Swern oxidation yielded aldehyde **102** [61].

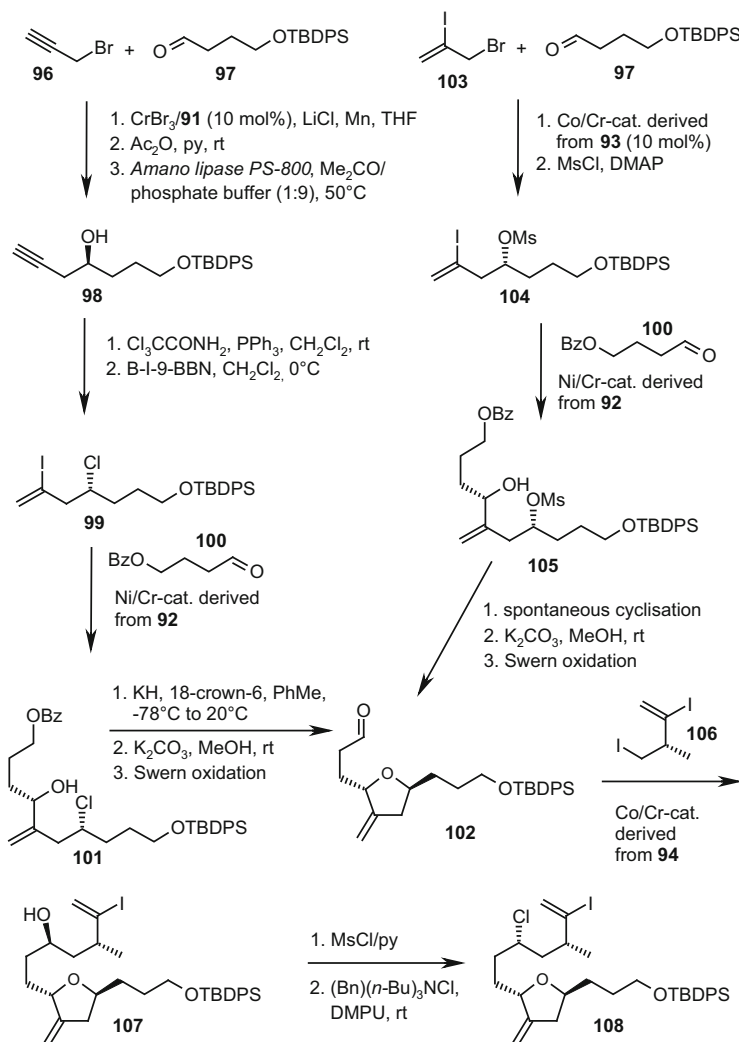
An alternative route toward **102** commenced with an asymmetric 2-haloallylation of aldehyde **97** using 10 mol% of the Cr complex of (*S*)-catalyst **93** and 0.2 mol% of cobalt phthalocyanine (CoPc) which delivered an alcohol in 85% yield and 93% *ee* [62] that was converted to the mesylate **104** [61]. Ni/Cr-mediated coupling with aldehyde **100** (as outlined above for **99** using a catalyst loading of 20 mol%) furnished **105** in 90% yield with a *dr* = 22:1 that slowly cyclized spontaneously to the corresponding tetrahydropyran, which was converted to aldehyde **102** as above.

The C14–C26 intermediate **107** was then obtained by a Co/Cr-mediated coupling with the diiodide **106** [53] in 82% yield with a *dr* = 22:1 using the Cr-catalyst derived from (*S*)-**94** and catalytic amounts of CoPc. The coupling product **107** was further elaborated to chloride **108** in two steps (cf. Scheme 18) [61].

Catalytic asymmetric Ni/Cr coupling of **108** with the C27–C35 eribulin building block **90** [53, 57] in the presence of (*S*)-ligand **95** furnished cyclization precursor **109** in 91% yield with a *dr* > 55:1. Formation of the tetrahydropyran ring of key intermediate **110** was best achieved with 3 equiv. of AgBF<sub>4</sub> and 2,6-di-*tert*-butyl-4-methylpyridine (DTBMP) in *tert*-butyl acetate (cf. Scheme 19) [61].

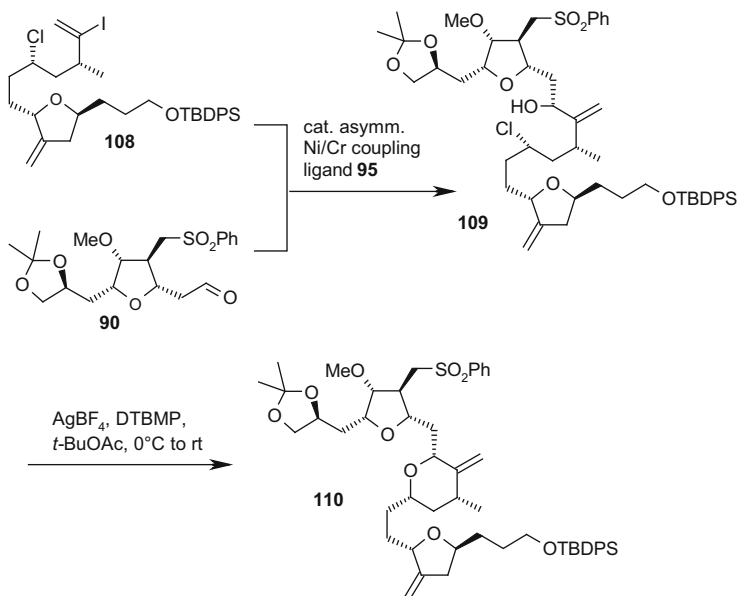
An oxy-Michael addition was proposed as an alternative for the C23–C27 pyran ring formation: unsaturated ester **111** (*E/Z* = 1.4:1 mixture) was coupled to **90** in the presence of (*S*)-ligand **95** yielding the cyclization precursor **112** in 87% yield with a *dr* > 50:1 (at the newly established C27 stereogenic center). Ring closure of **112** by base-induced oxy-Michael reaction proceeded smoothly to yield the cyclization product **113** which was subjected to a two-step Barton decarboxylation process after saponification of the methyl ester furnishing the C14–C35 building block **114** (cf. Scheme 20) [63].

In a second series, the C27–C35 building block **90** was first extended to a C20–C35 fragment in which the tetrahydropyran ring was formed by reductive cyclization. This fragment was then coupled to the C14–C19 segment **99** followed by late-



**Scheme 18** Kishi's syntheses of a C14–C26 fragment employing Cr-mediated asymmetric couplings

stage closure of the C17–C20 tetrahydrofuran ring to construct the C14–C35 key building block. Ni/Cr-mediated coupling of **90** and vinyl iodide **115** (1.5 equiv.) in the presence of (*S*)-ligand **95** yielded 92% of intermediate **116** with a *dr* ≈ 50:1. Treatment with a mixture of trimethylsilyl triflate (2 equiv.) and triethylsilane (10 equiv.) in CH<sub>2</sub>Cl<sub>2</sub> induced cleavage of the ketal and formation of the oxonium ion intermediate **117**, which was reduced in situ to the corresponding tetrahydropyran. Concomitant cleavage of the TBDPS protecting group furnished alcohol **118**, which was oxidized to the aldehyde **119**. Ni/Cr-mediated coupling

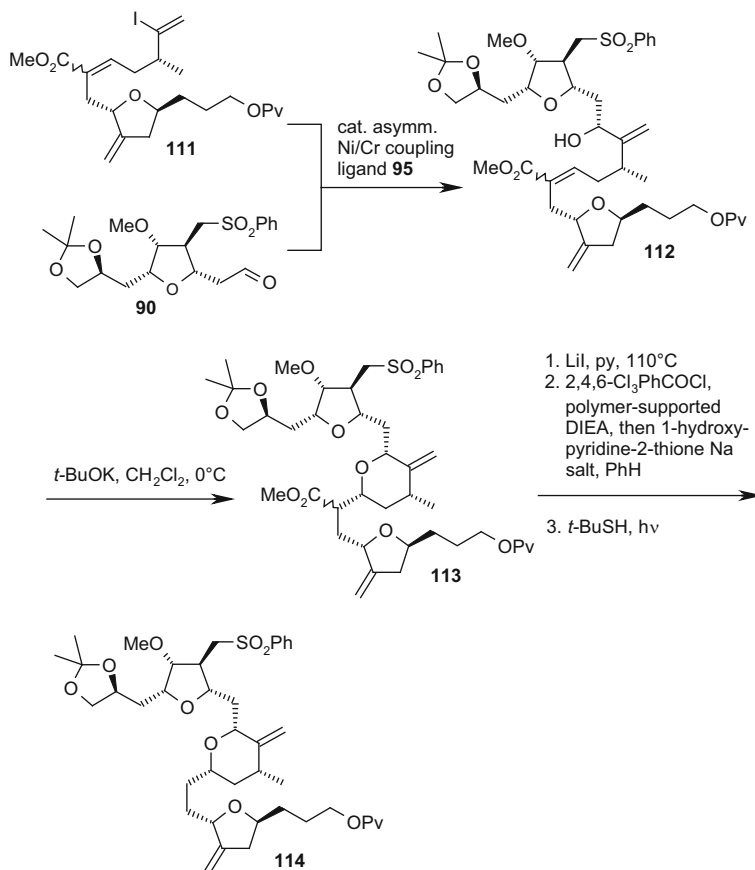


**Scheme 19** C14–C35 building block synthesis: tetrahydropyran ring formation by nucleophilic substitution

with vinyl iodide **99** in the presence of (*R*)-catalyst **92** furnished 85% of **120** with a  $dr \approx 32:1$ . Base-induced cyclization with KH in toluene in the presence of 18-crown-6 finally afforded cleanly the C14–C35 building block **121** (cf. Scheme 21) [63].

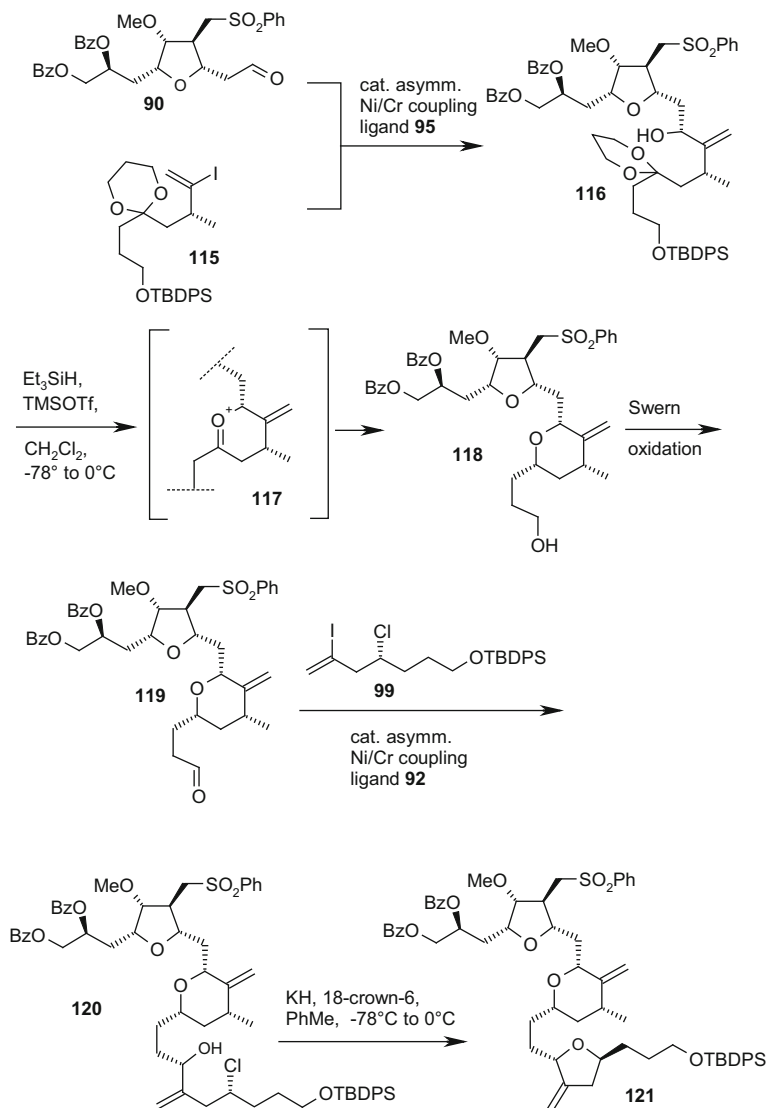
The synthetic strategies toward the eribulin C14–C35 key building blocks **110**, **114**, and **121** outlined in Schemes 19, 20, and 21 were also analogously applied in order to construct the corresponding halichondrin C14–C38 building blocks by replacing the eribulin C27–C35 fragments by halichondrin C27–C38 intermediates such as **4** (cf. Scheme 1) [61, 63]. A scalable, highly stereoselective synthesis of the C20–C26 fragment was developed starting from epoxide **122** that was obtained by Jacobsen kinetic resolution [51]. The epoxide was opened with the lithium acetylide of TES-protected propargyl alcohol **123** to yield alcohol **124**, which was subjected to Trost ruthenium-catalyzed hydrosilylation [64, 65]. Alcohol **125** was obtained after selective removal of the TES group. The C5 methyl group was introduced by a highly selective ( $dr \approx 150:1$ )  $\text{S}_{\text{N}}2'$  reaction with  $\text{LiCu}(\text{Me})(\text{CN})$  of the mesylate obtained from **125**. Selective conversion of the vinyl silane function into the corresponding vinyl iodide was achieved with iodine monochloride. Removal of the TBS group then furnished the C20–C26 fragment **127** with a  $dr > 200:1$  and  $ee > 99\%$  (cf. Scheme 22) [66].

The addition of an  $\alpha$ -lithiated sulfone to an aldehyde represents one of the key transformations in the advanced synthetic routes toward eribulin (cf. S6 and 9). During the ongoing work in the halichondrin and eribulin field, the Kishi group



**Scheme 20** C14–C35 building block synthesis: tetrahydropyran ring formation by oxy-Michael addition

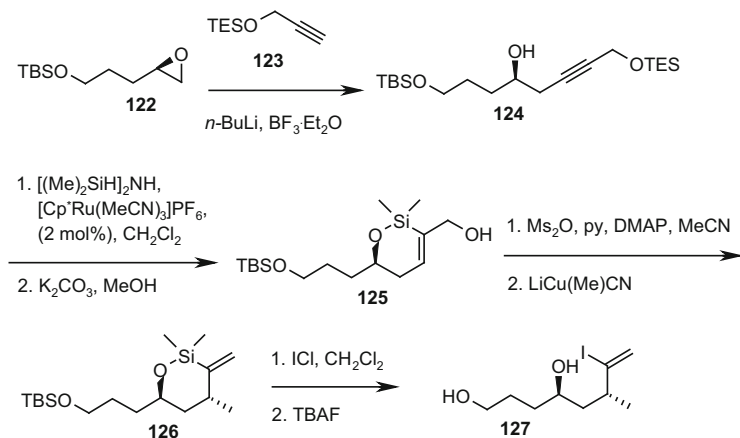
became interested in the transformation of an arylsulfonyl group ( $\text{RCH}_2\text{SO}_2\text{Ph}$ ) to a primary alcohol. Inspired from earlier work of Uguen [67], a method development based on the  $\alpha$ -deprotonation of sulfones  $\text{RCH}_2\text{SO}_2\text{Ph}$  with different bases and subsequent reaction with a variety of borane reagents followed by treatment with alkaline  $\text{H}_2\text{O}_2$  was performed. For primary substrates such as **128**, disiamylborane turned out to be the best suitable reagent, and a better conversion was observed for substrates bearing electron-withdrawing groups on the phenyl ring. In the eribulin series, 100% conversion (89% isolated yield) of the *m*-fluorophenyl sulfone **128** to alcohol **129** was observed, whereas with the corresponding phenyl sulfone, only ~94% conversion and 76% isolated yield of **129** were achieved (cf. Scheme 23) [68].



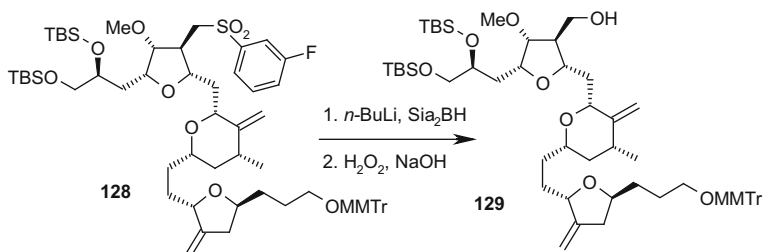
**Scheme 21** C14–C35 building block synthesis: reductive cyclization route

## 5.2 Kishi's Total Synthesis of Halichondrin C

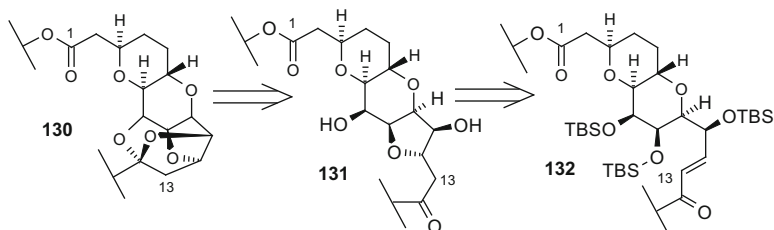
In the classification of the halichondrins, the hydroxylation pattern at C12 and C13 of the polycyclic C8–C14 subunit defines the A, B, and C series (cf. Fig. 1). In the original approach toward halichondrin B [18], the construction of this caged C8–C14 polycycle (**130**) relied upon an oxy-Michael addition of an alcohol (C9) to the C12–C14 enone followed by ketalization (cf. Scheme 24).



**Scheme 22** Hydrosilylation route to a C20–C26 fragment



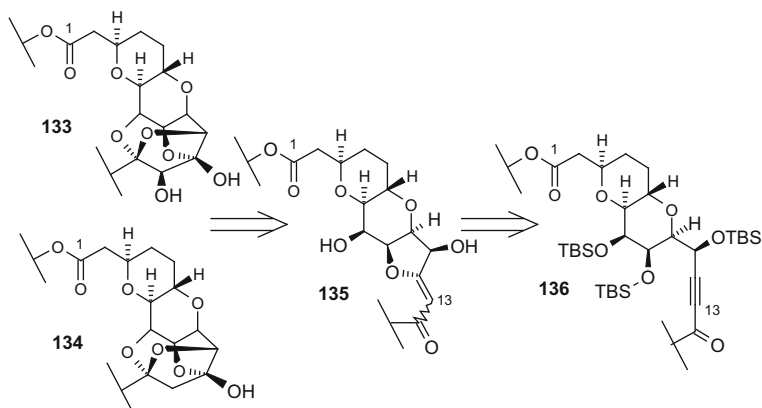
**Scheme 23** C14–C35 building block: transformation of an aryl sulfone to a primary alcohol



**Scheme 24** Retrosynthetic analysis of the C8–C14 polycyclic structure of the halichondrin B series

Analogously, it was planned to construct the C8–C14 structure of halichondrins A (**133**) and C (**134**) from an ynone precursor **136**, which should pave the way for the introduction of the additional hydroxy functions at C12 and C13, respectively (cf. Scheme 25).

The feasibility of this approach was investigated in model studies with ynone **137** which was prepared from a C1–C11 fragment [69]. Ynone **137** was treated with



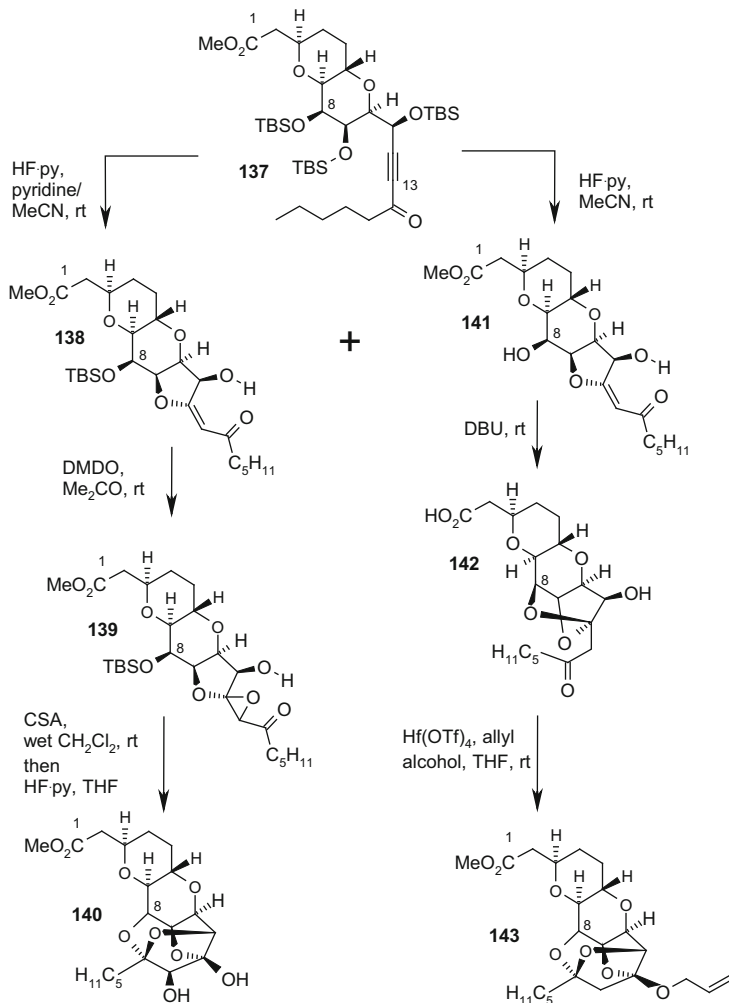
**Scheme 25** Retrosynthetic analysis of the C8–C14 polycyclic structure of the halichondrin A and C series

HF/pyridine in acetonitrile to yield a mixture of 40% of **138** (as a 4:1 *Z/E* mixture) and 30% of the ketal **142** resulting from oxy-Michael addition of the C8–OH to the enone in **141**. The yield of **142** could be increased to 90% by DBU treatment of the crude product obtained by the reaction of **137** with HF/pyridine. The conversion of the ketal **142** to the C8–C14 polycyclic structure **143** was achieved with a Lewis acid in the presence of an alcohol. As a result of a screening of different Lewis acids, Hf(OTf)<sub>4</sub> turned out to be the most effective, and allyl alcohol was chosen since the thereby formed allyl ether could be removed under mild, palladium-catalyzed conditions in the highly complex framework of the targeted halichondrin C.

Selective transformation of **137** to **138** (as a 11:1 *Z/E* mixture) leaving the C8–OH group blocked was achieved with HF/pyridine in acetonitrile with an excess of pyridine. The chromatographically purified *E* isomer was epoxidized to **139** with DMDO furnishing **140** upon treatment with acid (*dr* > 30:1 in favor of the desired C13 stereoisomer), which represents the C8–C14 polycyclic unit of the halichondrin A series (cf. Scheme 26) [4].

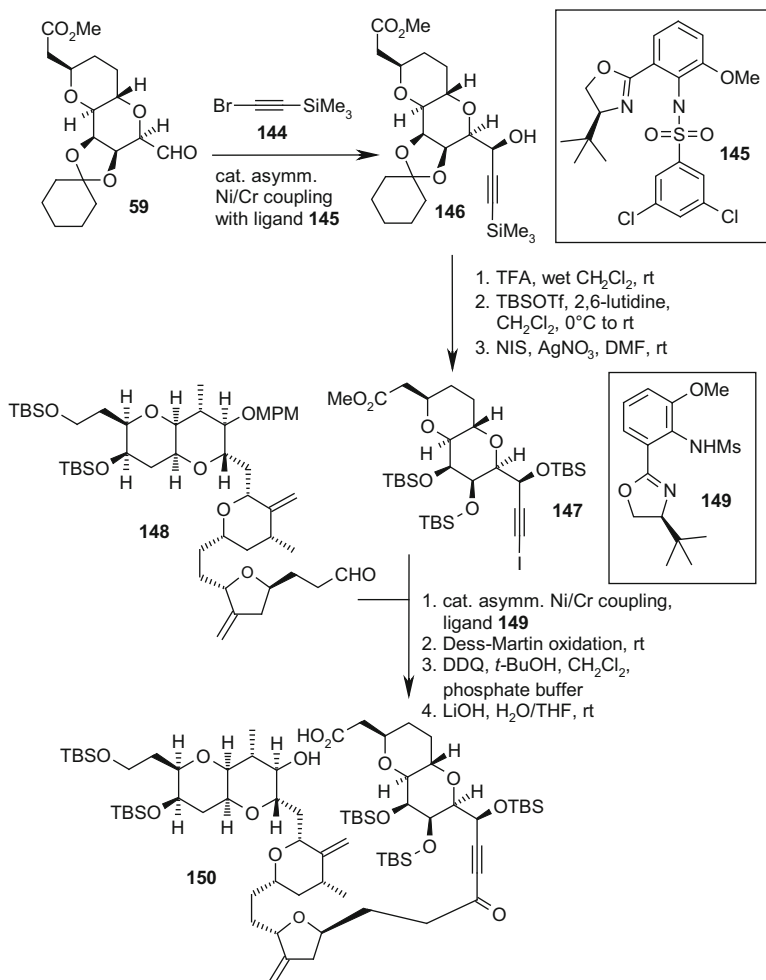
Based on these results, a total synthesis of halichondrin C was envisaged that closely followed the synthetic strategy employed in the synthesis of halichondrin B, which relies upon the C–C bond forming between C13 and C14 by Ni/Cr-mediated coupling of C1–C13 and C14–C38 building blocks, respectively, followed by macrolactonization between the C30–OH and the C1 carboxylic acid to construct the right-half macrocycle (cf. Scheme 1).

While previously used C14–C38 and C39–C54 building blocks could be directly incorporated into the synthesis, the iodoalkyne C1–C13 fragment **147** was prepared starting from aldehyde **59**. Catalytic asymmetric Ni/Cr coupling with **144** in the presence of catalyst **145** furnished the trimethylsilylalkyne **146** with high diastereoselectivity. Conversion to the iodoalkyne **147** was performed in a three-step sequence. Ni/Cr-mediated coupling with the C14–C38 fragment **148** was



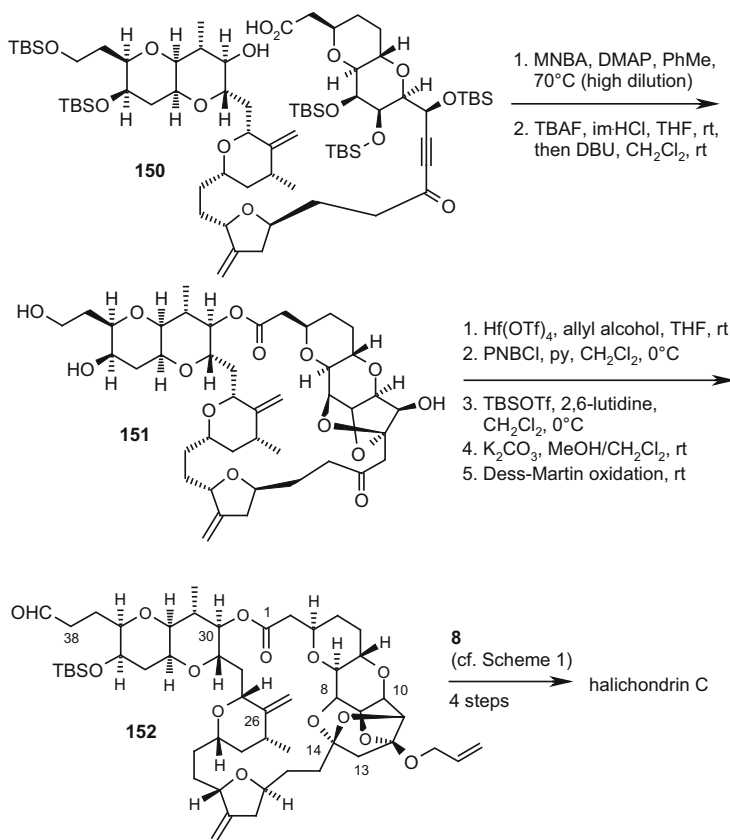
**Scheme 26** Model studies for the construction of the halichondrin A and C C8–C14 polycyclic structures

performed in the presence of ligand **149**. Although a chiral ligand was not necessary in this step since the resulting mixture of alcohols was subsequently oxidized to the corresponding ketone, the coupling turned out to be more effective in the presence of chiral sulfonamide ligands. Selective deprotection of the functional groups at C1 and C30 furnished seco acid **150**, which was converted to the corresponding macrolactone with MNBA (Shiina's reagent) [70]. Treatment with buffered TBAF solution followed by DBU yielded ketal **151**, which delivered the right-half (C1–C38) fragment **152** of halichondrin B upon treatment with Hf(OTf)<sub>4</sub> and allyl alcohol followed by functional group transformations at C35 and C38. Again,



**Scheme 27** Synthesis of the right-half (C1–C38) building block of halichondrin C

a Ni/Cr-mediated reaction (in this case stoichiometric) served to couple aldehyde **152** to the C39–C54 building block **8** (cf. Scheme 1) and the resulting product was transformed to halichondrin C (cf. Fig. 1) in three further steps comprising a selective, Pd-catalyzed removal of the allyl protecting group at the C12 hydroxy function (cf. Schemes 27 and 28) [4].



**Scheme 28** Synthesis of the right-half (C1–C38) building block of halichondrin C (continued)

### 5.3 Kishi's Total Synthesis of Halichondrin A

For the approach toward halichondrin A, the “missing member” of the halichondrin family that had not been isolated from natural sources, a different strategy for the assembly of the C1–C38 right half was envisaged that relied upon alternative disconnections and building block strategies as outlined in Sect 5.1. It was characterized by a higher degree of convergence than the previous routes and had the potential to be extended to a unified approach to the halichondrin B and C series, too.

Along these lines, the bond formation between C19 and C20 followed by closure of the C17–C20 tetrahydropyran ring was envisaged as the key step. Based on this strategy and the results from the model studies (cf. Scheme 26), the concisely functionalized C1–C19 building block **155** was synthesized by Ni/Cr-mediated coupling of iodoalkyne **147** with aldehyde **153** in the presence of ligand **154** followed by Dess–Martin oxidation of the resulting mixture of propargyl alcohols.

Selective TBS deprotection followed by DMDO oxidation, acid treatment, and ketalization with *p*-anisaldehyde dimethyl acetal provided intermediate **156**. Initial attempts to approach a building block with the fully established C8–C14 polycyclic structure by an identical sequence with the C19-iodo analogue of aldehyde **153** were hampered by a side reaction in the DMDO step leading to oxidation of the C19-iodo function to an iodoso intermediate, which eliminated to form a terminal alkyne.

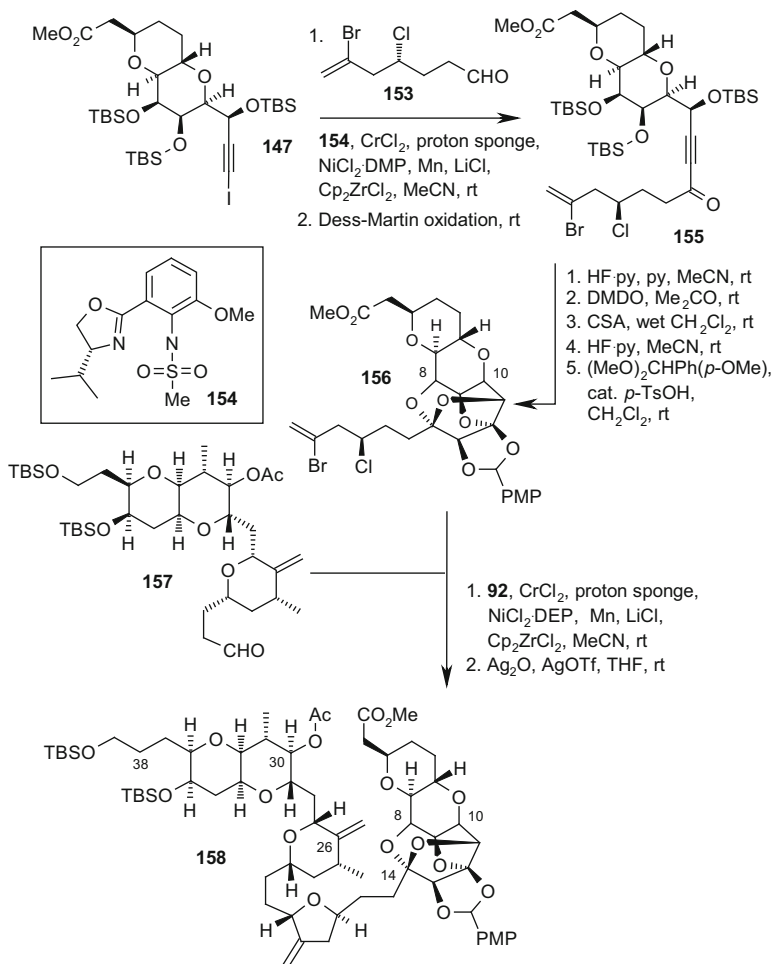
The C20–C38 fragment **157** was synthesized in the same fashion as the eribulin C20–C35 building block **119** as outlined in Sect. 5.1 (cf. Scheme 21) using a halichondrin C27–C38 aldehyde intermediate analogously to **4** (cf. Scheme 1) in place of aldehyde **90** [63]. Ni/Cr-mediated coupling of **156** and **157** was performed with the Cr-catalyst obtained from (*R*)-ligand **92** (cf. Fig. 7). 40 mol% of the Cr reagent was required due to the bromo-olefin **155** being less reactive than the corresponding iodo-olefin. Subsequently, treatment of the cyclization product with AgOTf/Ag<sub>2</sub>O furnished intermediate **158** with a *dr* = 20:1. The right-half **159** of halichondrin A was obtained by saponification of both methyl ester (C1) and acetate (C30) of **158**, macrolactonization under Shiina conditions [70, 71], and selective deprotection of the primary C38-OH function.

The completion of the synthesis was performed in an analogous fashion to the halichondrin B total synthesis [18]. After oxidation of **159** to the corresponding C38 aldehyde with Dess–Martin periodinane, Ni/Cr-mediated coupling with the C39–C54 fragment **8** was performed in the presence of the Cr-catalyst derived from ligand **149**. The resulting coupling product was converted to halichondrin A in a four-step sequence comprising deprotection of TBS, PMB, and the anisylidene group at C12/C13 and formation of the [5,5]- and [6,6]-spiroketals at C38 and C44, respectively (cf. Schemes 29 and 30) [21].

#### 5.4 *Kishi's Approach to a Unified Synthesis of the Halichondrins*

In an extension of the key C19–C20 bond formation strategy developed for halichondrin A to halichondrin B, a practically identical C20–C38 building block (such as **157**, cf. Scheme 29) could be directly used, while a new synthesis of the C1–C19 intermediate had to be elaborated.

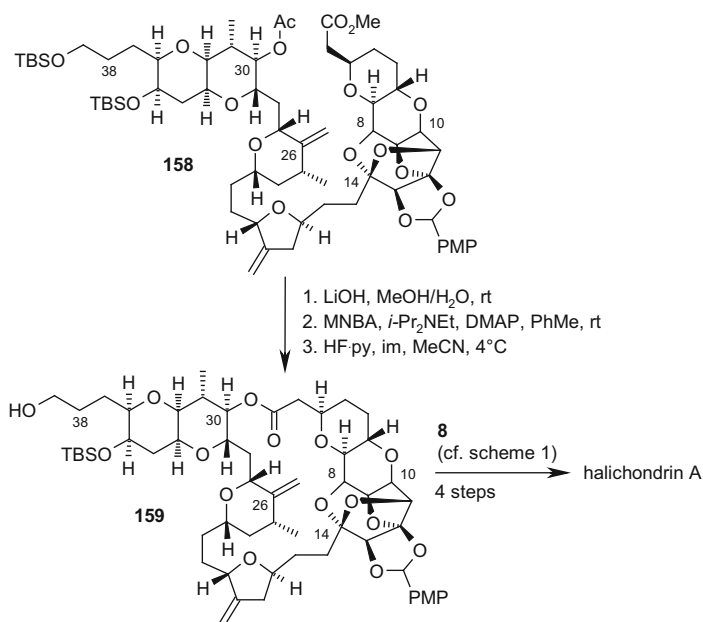
As a first approach, addition of a vinylogous acyl anion generated from a highly functionalized  $\beta$ -haloenone corresponding to a C12–C19 fragment to the C1–C11 aldehyde **59** was envisaged. An extensive method development had to be performed in order to achieve a selective activation of the  $\beta$ -haloenone versus the vinyl iodide and the chloride as well as an effective coupling of the vinylogous acyl anion. As a result, the  $\beta$ -bromoeneone **160** turned out to be more reactive than the respective  $\beta$ -iodo- and  $\beta$ -chloroenones, and a low loading of an optimized Ni-phenanthroline cocatalyst was critical for selective coupling over the vinyl iodide. In an optimized



**Scheme 29** Synthesis of the right-half (C1–C38) building block of halichondrin A

protocol, **160** was coupled to aldehyde **59** in the presence of 10 mol% Cr-catalyst derived from (*S*)-ligand **161** and 0.05 mol% of the soluble Ni-catalyst **162** to provide **163** in 87% yield. As the resulting coupling product, a  $\gamma$ -hydroxy enone, was prone to furan formation under the conditions of the cyclohexylidene group removal, the hydroxy function was temporarily protected as a *p*-nitrobenzoate. Treatment with TFA followed by aqueous Na<sub>2</sub>CO<sub>3</sub> then furnished a mixture of oxy-Michael products **164** (epimers at C12).

It had been shown earlier [72] that the  $\beta$ -isomer (*S*-configuration at C12) of these types of products could be converted to the desired caged polycyclic structure of the halichondrins with PPTS whereas the  $\alpha$ -isomer (*R*-configuration at C12) could be recycled via equilibration under basic conditions. Thus, an ion-exchange resin-based device based on a polymer-bound guanidine and polymer-bound PPTS

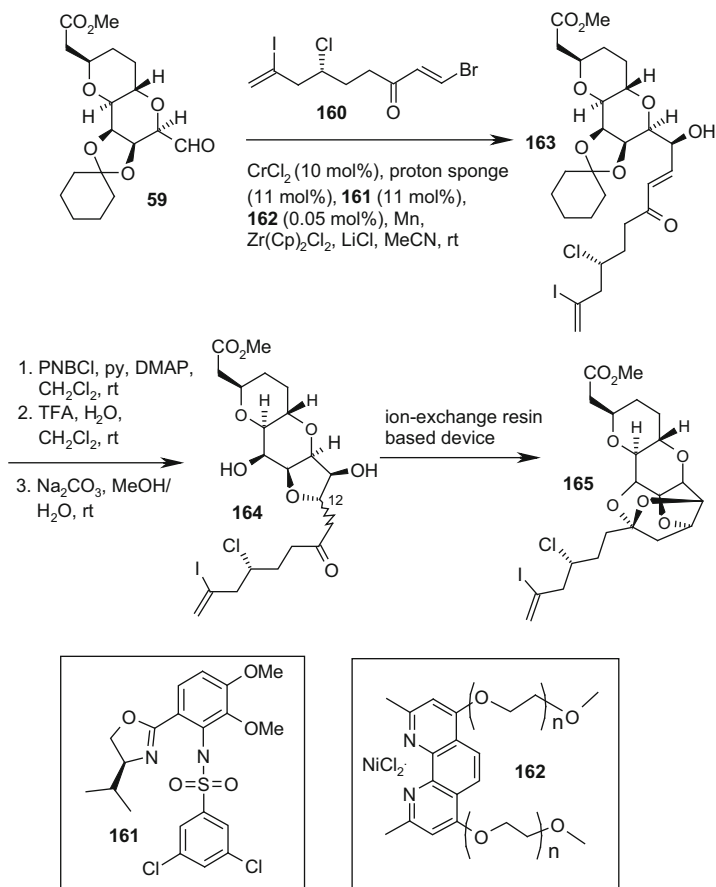


**Scheme 30** Synthesis of the right-half (C1–C38) building block of halichondrin A (continued)

[72, 73] was used to transform **164** into the desired C1–C19 intermediate **165** (cf. Scheme 31) [74].

A unified synthesis of the C1–C19 building blocks of halichondrins A, B, and C was elaborated based on the intermediates **167** and **168** (cf. Scheme 32). Ni/Cr-mediated coupling of **168** with C1–C11 building block **166** followed by acidic ketal cleavage furnished intermediate **171** nearly identical to **155** (the only difference being a free C11-OH) which was converted to halichondrin A intermediate **156** as outlined above (cf. Scheme 29).

The coupling product of **166** and **167** delivered vinyl iodide **170** after TFA treatment, which was further elaborated into halichondrin B and C intermediates, respectively. While conversion to the halichondrin C intermediate **173** could be performed smoothly in two steps along the protocols developed for the model systems (cf. Scheme 26), the required adjustment from ynone to enone oxidation state in the halichondrin B series required considerable optimization. Attempts to develop synthetically useful direct reduction conditions from ynone to enone were met with limited success. However, a practical route was established by reducing enone **174** (formed by oxy-Michael addition of C9-OH to the ynone after deprotection with HF/py in pyridine as an *E/Z* mixture) with Me<sub>4</sub>NBH(OAc)<sub>3</sub> yielding, after TBAF treatment, **164** as a ~1:1 mixture of  $\alpha$ - and  $\beta$ -diastereomers at C12. Compound **164** was transformed into the desired C1–C19 intermediate **165** by an ion-exchange resin-based device as outlined above for the  $\beta$ -haloenone approach (cf. Schemes 31 and 33) [75].



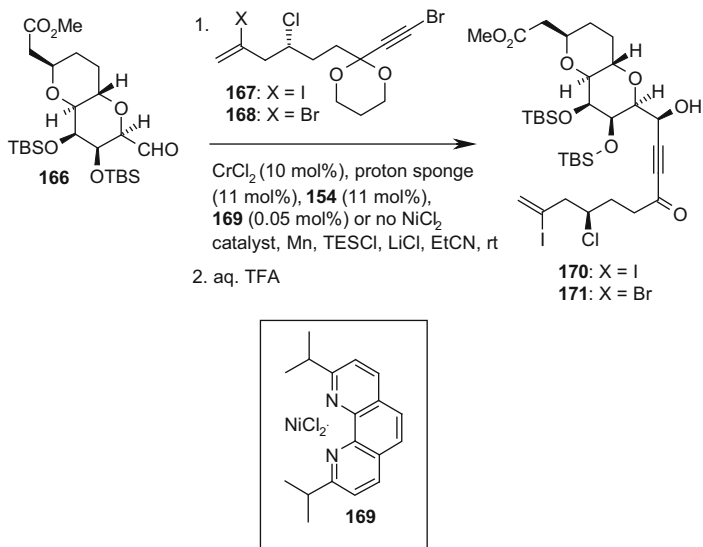
**Scheme 31** Synthesis of a C1–C19 building block of halichondrin B

## 5.5 Recent Contributions from Eisai

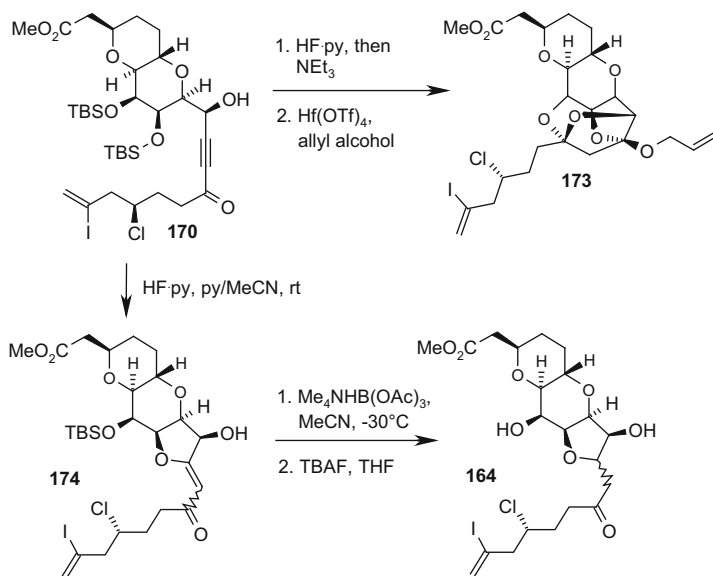
### 5.5.1 Alternative Syntheses of Eribulin Building Blocks

The manufacturing process of the C1–C13 and C27–C35 building blocks of eribulin was characterized by crystallization-based routes, which could be realized due to efficient stereocontrol originating from cyclic carbohydrate templates. On the other hand, the C14–C26 building block represented a challenge since several noncontiguous acyclic stereocenters had to be effectively controlled. Therefore, in an alternative approach toward the C14–C26 subunit, a rigid bicyclic template was used to establish the stereogenic centers at C17, C21, and C23 that would lead to highly crystalline intermediates.

As a readily available starting material serving as a source for all stereocenters of the C14–C26 building block, D-quinic acid **175** was chosen, which was converted to



**Scheme 32** Synthesis of a C1–C19 building block of halichondrin C



**Scheme 33** Transformation of the common C1–C19 intermediate to halichondrin B and C building blocks

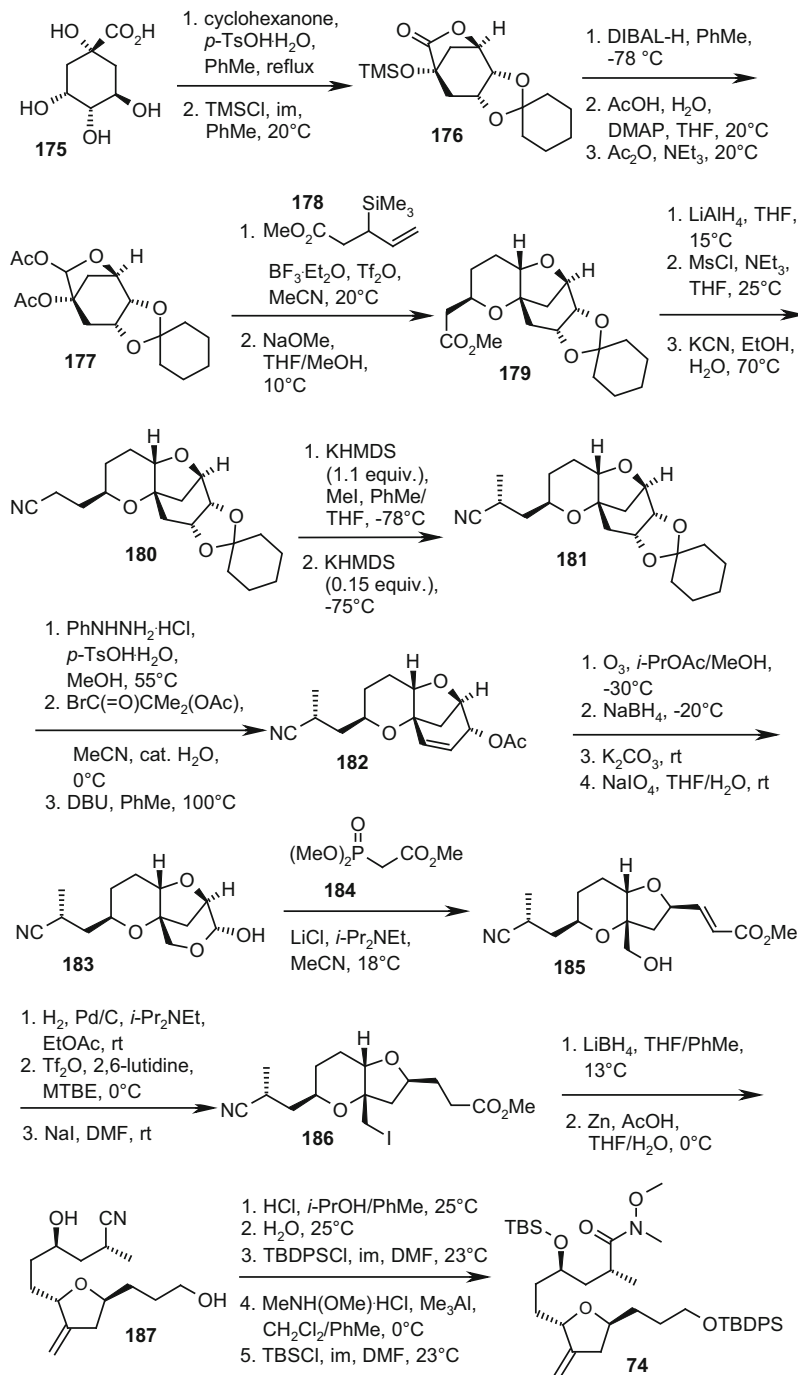
intermediate **176** by lactonization. DIBAL-H reduction and acetylation furnished the crystalline bis-acetate **177**. The fused tetrahydropyran **179** was obtained after Lewis acid mediated C-glycosylation with allyl silane **178** and treatment of the

adduct with sodium methoxide thereby establishing the stereogenic centers at C20 (as a single isomer) and at C23 ( $dr = 9:1$ ). LAH reduction of the methyl ester, mesylation of the resulting alcohol, and nucleophilic substitution with cyanide gave nitrile **180** which was crystallized to enhance the diastereomeric purity with regard to C23 to  $>100:1$ . The C25 stereocenter was established by methylation of the nitrile with KHMDS and methyl iodide yielding **181** as a 2:1 mixture of diastereomers in favor of the desired epimer. The selectivity could be enhanced to  $>4:1$  by treatment of this mixture with a catalytic amount of KHMDS, and a product with a  $dr \approx 20:1$ – $30:1$  was finally obtained after crystallization. The yield could be further enhanced by re-equilibration of the mother liquors.

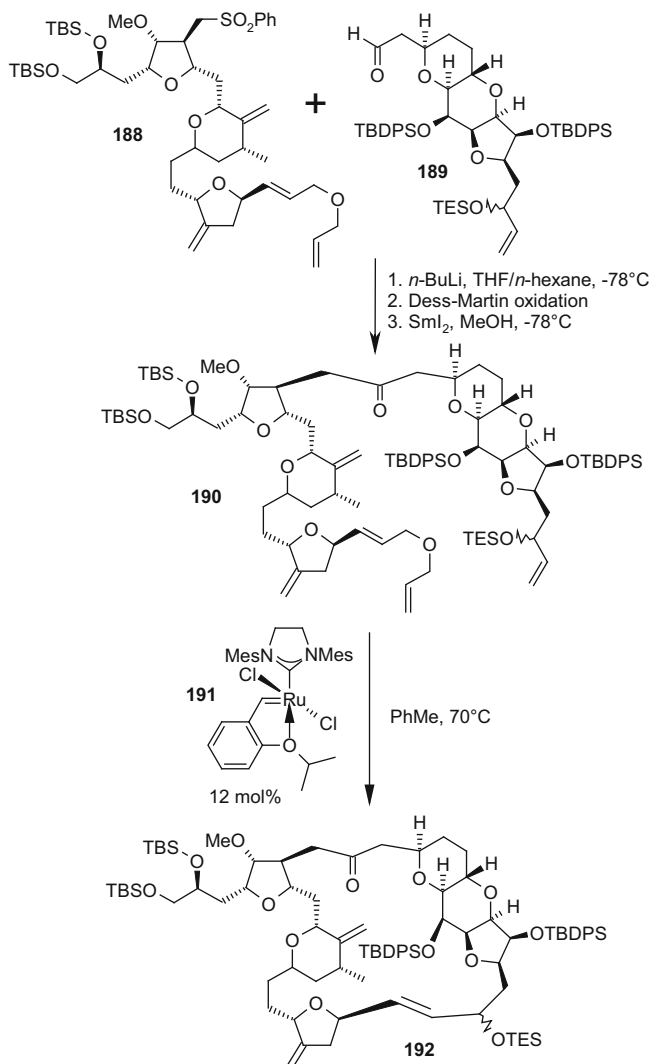
Hydrolysis of the ketal of **181** furnished a diol, which was selectively transformed into a bromoacetate. Subsequent dehydrobromination furnished crystalline allylic acetate **182**, which was converted to the crystalline lactol **183** by ozonolysis followed by reductive quenching, deacetylation, and periodate cleavage in a single-pot protocol. Compound **183** was subjected to a Horner–Wadsworth–Emmons (HWE) reaction with phosphonate **184** under Masamune–Roush conditions [76] to give the  $\alpha,\beta$ -unsaturated ester **185**, which was elaborated to iodoester **186** by catalytic hydrogenation and transformation of the alcohol to the corresponding iodide via the triflate. All stereogenic centers in the crystallized iodoester **186** displayed a  $dr > 1000:1$ . The ester function of **186** was reduced to the corresponding primary alcohol, and treatment with Zn induced a Vasella fragmentation [77] to establish the *exo*-methylene group at C19 and the free hydroxy function at C23. Diol **187** thus obtained was converted to the previously described [54] Weinreb intermediate **74** in a five-step sequence (cf. Schemes 14 and 34). Although the quinic acid-based route is less convergent than the previously elaborated route (27 steps vs. 20 steps and a longest linear sequence of 13 steps), it delivers the C14–C26 fragment in 2% overall yield vs. 1%. Furthermore, a 78% improvement with regard to raw material cost and 80% waste reduction could be achieved mainly due to the fact that the new route did not require chromatographic purification associated with the need of high volumes of solvents [78–80].

In the original process-scale synthesis of eribulin, the key macrocyclization relied upon a Nozaki–Hiyama–Kishi coupling between C13 and C14. Besides different approaches for NHK cyclizations (which partly rely upon the strategies developed by the Kishi group as outlined above in Sects. 5.1, 5.2, and 5.3), experimental details of alternative methods for the macrocyclization of intermediates in the synthesis of eribulin have been disclosed recently by Eisai scientists in the patent literature [81]. In one approach, macrocyclization between C15 and C16 is realized by ring-closing metathesis (RCM). Suitable precursors were prepared by the assembly of C1–C15 and C16–C35 fragments by addition of the lithiated phenyl sulfone **188** to aldehyde **189** – a route closely associated with the previously reported process-scale strategy. RCM with the resulting cyclization precursor **190** was performed in the presence of the second-generation Hoveyda–Grubbs catalyst **191** [82] to afford the macrocyclic intermediate **192** (cf. Scheme 35).

An alternative approach relied upon the elaboration of a substrate to replace the phenyl sulfone chemistry by a ring-closing metathesis between C3 and C4. The key

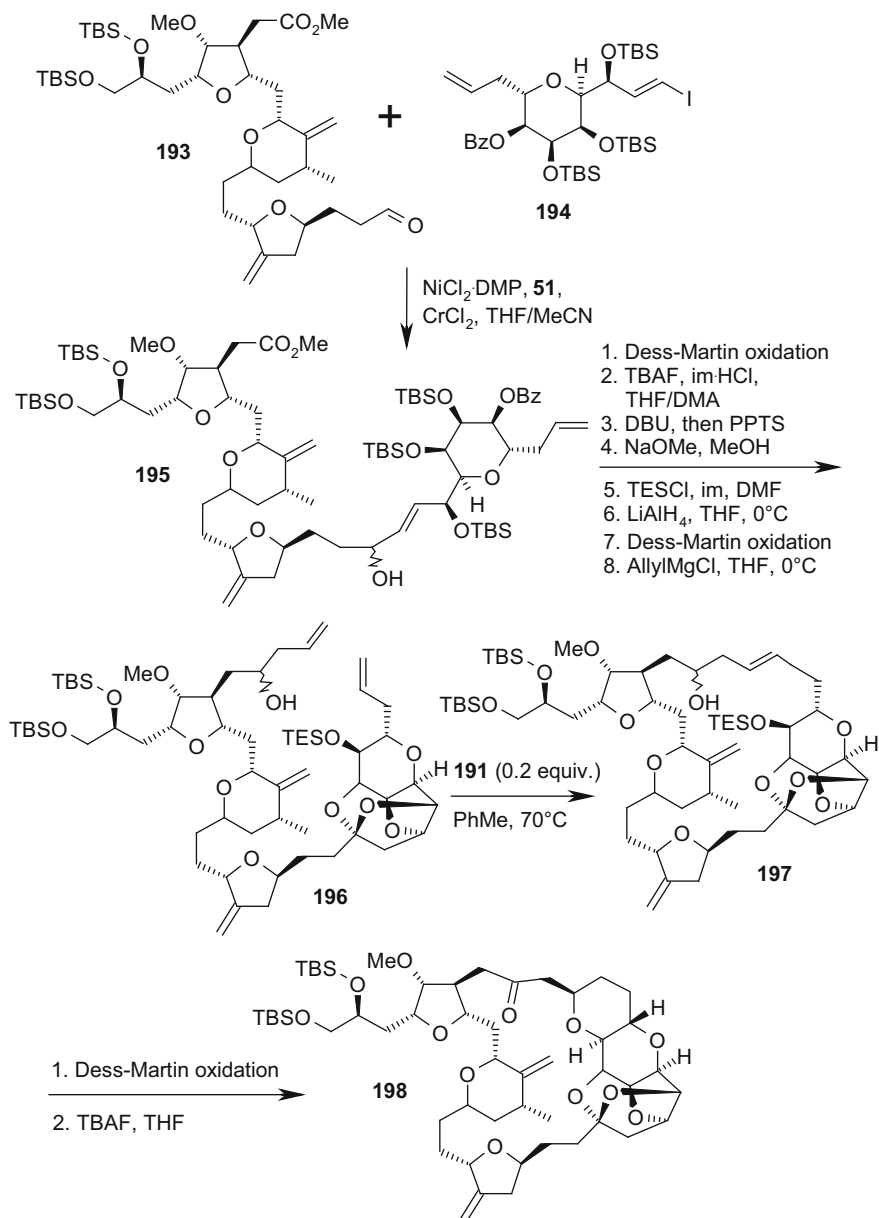


**Scheme 34** Synthesis of eribulin C14–C26 building blocks from D-quinic acid



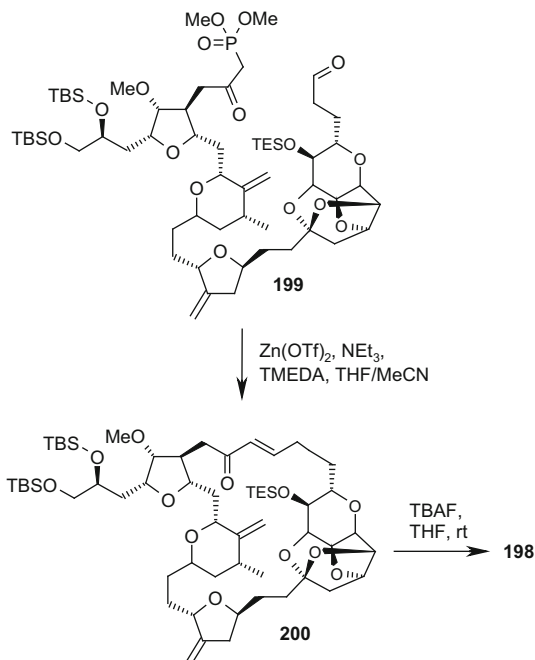
**Scheme 35** Synthesis of the eribulin macrocycle by olefin ring-closing metathesis between C15 and C16

step for the assembly of fragments is again represented by a Nozaki–Hiyama–Kishi coupling between C13 and C14 which was performed with the coupling partners **193** and **194** in a stoichiometric fashion in the presence of the Cr complex formed with ligand **51** (cf. Scheme 16) and a catalytic amount of NiCl<sub>2</sub>-DMP. The coupling product **195** was converted into the cyclization precursor **196** in an eight-step sequence thereby introducing the required terminal olefin at C3 and establishing the polycyclic C8–C14 moiety. Again, the second-generation Hoveyda–Grubbs catalyst **191** [82] was employed for the macrocyclization to **197**, and the C3–C7



**Scheme 36** Synthesis of the eribulin macrocycle by olefin ring-closing metathesis between C3 and C4

**Scheme 37** Synthesis of the eribulin macrocycle by Horner–Wadsworth–Emmons reaction between C2 and C3



tetrahydropyran ring of **198** was established after oxidation of the C1–OH group and selective deprotection of the C7–OH function (cf. Scheme 36).

Yet another macrocyclization was realized between C2 and C3 by a mild zinc-promoted Horner–Wadsworth–Emmons (HWE) reaction [83, 84]. The cyclization precursor **199** was obtained in a few steps from **195**. Subsequently, the C3–C7 tetrahydropyran ring was established by an oxy-Michael addition of the free C7–OH obtained after TBAF deprotection to the C1–C3 enone function resulting from the HWE product **200** (cf. Scheme 37).

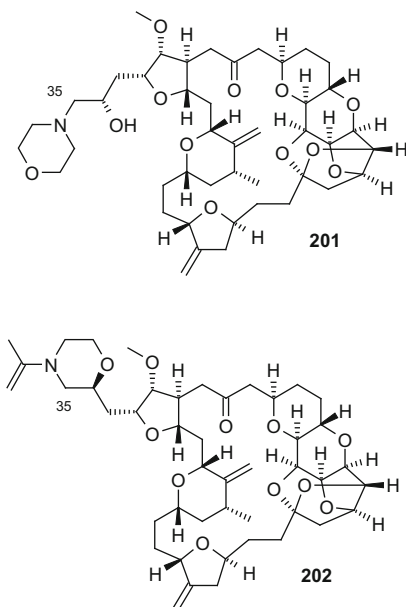
### 5.5.2 Approaches Toward Second-Generation Eribulins

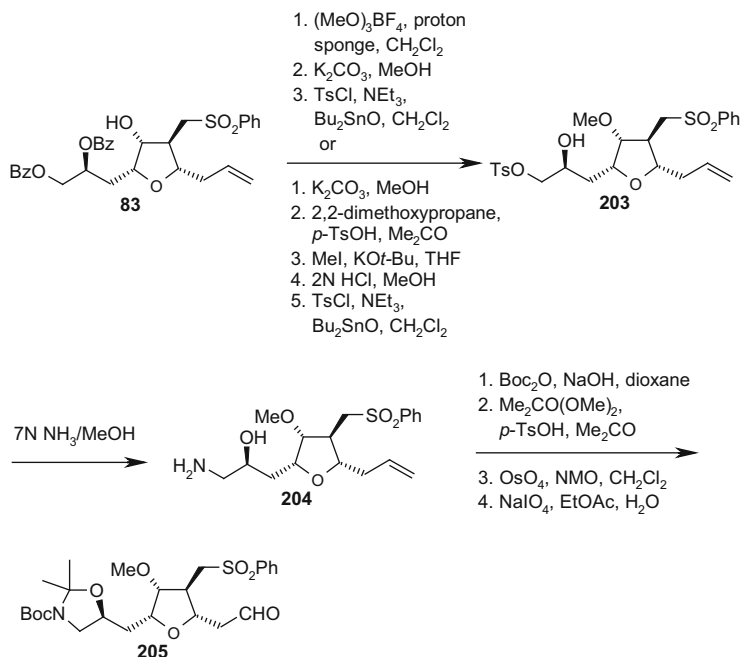
In routine clinical settings, many anticancer drugs including eribulin are administered by the intravenous route. However, in certain circumstances an orally available compound may be beneficial. Ongoing medicinal chemistry efforts at Eisai have therefore focused on improving the oral bioavailability and activity against multidrug resistant (MDR) tumors. Limited oral absorption, low brain penetration, and resistance are mainly caused by P-glycoprotein (P-gp)-mediated drug efflux [85–87]. Eribulin was shown to be a substrate for P-gp. Therefore, decreasing the efflux mediated by P-gp was identified as the main objective for optimization toward improved, second-generation drugs based on the eribulin scaffold.

Structure-activity relationships established during discovery and development of eribulin revealed that important parameters such as potency, P-gp susceptibility, and physicochemical properties could be significantly modified by variations of the C32–C35 side-chain moiety. Based on the consideration that compounds displaying primary amine functions are often P-gp substrates, a series of compounds was synthesized by replacing the basic C35 substituent by neutral C32 side chains (starting from diol **25**, cf. Fig. 6). These modifications led to compounds with extremely low P-gp susceptibilities that displayed low- to sub-nM antiproliferative activities against both resistant and susceptible cancer cell lines *in vitro*. However, only in some cases activity in *in vivo* mouse xenograft tumor models could be observed [88].

In the course of further studies, analogues that still contained an amino group, albeit with reduced basicity at the nitrogen, were also synthesized. As in the “neutral” series, compounds with low P-gp susceptibility could be identified. Furthermore, some of the compounds such as the morpholino analogue **201** (cf. Fig. 8) showed *in vivo* efficacy in mouse xenograft MDR tumor models both after intravenous and oral administration [89, 90]. It was also demonstrated for the related compound **202** that derivatives with attenuated basicity have a significant higher blood-brain barrier than eribulin and are active in an orthotopic murine model of human glioblastoma [91, 92].

**Fig. 8** Eribulin analogues displaying low P-gp susceptibility





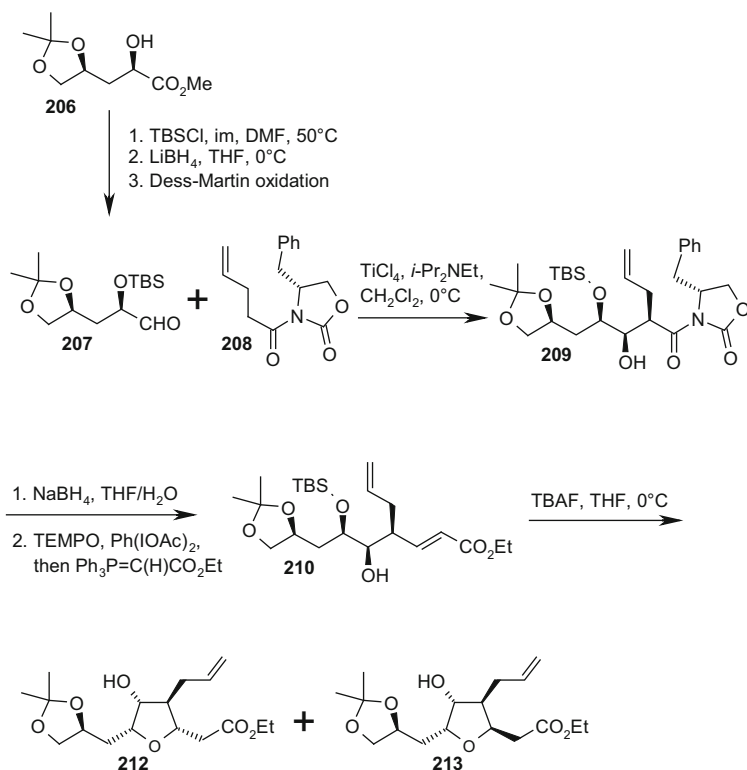
**Scheme 38** C27–C35 building block for the early introduction of the C35 amino group

## 5.6 Recent Contributions from Other Groups

Several other groups have also contributed to the synthesis of intermediates and building blocks for eribulin. While in the original Eisai route the introduction of the amino group at C35 is performed as one of the last steps in the synthesis, scientists at Alphora have pursued a strategy of an early introduction of the amino group to a C27–C35 building block.

The synthesis commences with advanced intermediate **81** and follows essentially the previously described [54] route to phenyl sulfone **83** (cf. Scheme 15) which was converted to tosylate **203** by methylation of the C31-OH, deprotection of the side-chain hydroxy groups, and selective primary mono-tosylation. Nucleophilic substitution with ammonia furnished amine **204**. Transformation to the C27–C35 building block **205** was achieved by Boc protection and ketalization (cf. Scheme 38). Alternatively, the sequence was also performed analogously with the corresponding *p*-tolyl sulfone in the place of the phenyl sulfone [93].

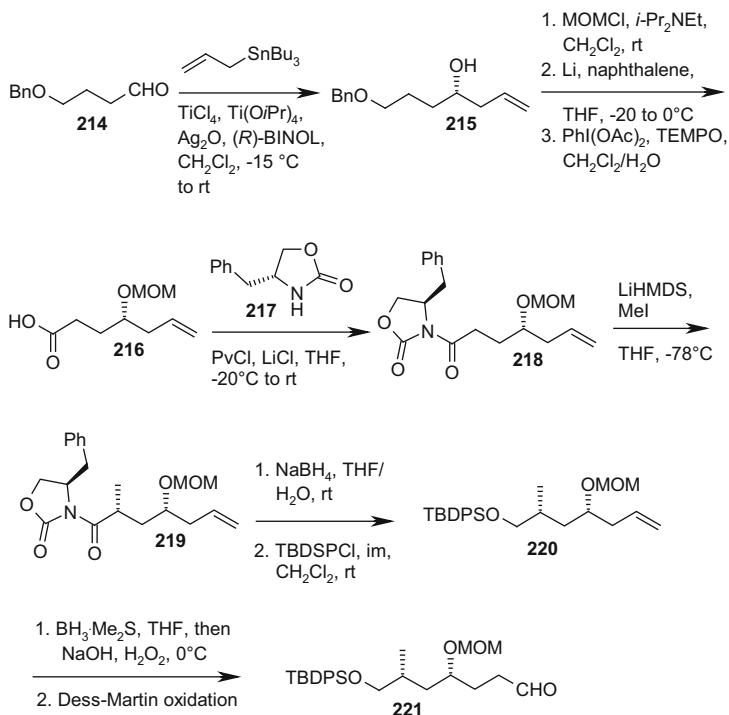
In the context of establishing a toolbox with different types of natural product-inspired macrocycles, a team at Dr. Reddy's Institute of Life Science has developed a synthesis of a C27–C35 eribulin fragment based on an asymmetric *syn*-aldol and an intramolecular oxy-Michael reaction. Introduction of the correct stereochemistry at the C32 and C34 center, respectively, relied upon D-xylose which was converted to ester **206** following a known procedure [94]. TBS protection and reduction of the



**Scheme 39** C27–C35 building block synthesis based on an asymmetric *syn*-aldol and an intramolecular oxy-Michael reaction

ester function followed by Dess–Martin oxidation afforded aldehyde **207**. Titanium-mediated Evans aldol reaction with **208** furnished exclusively the *syn*-product **209** as a single diastereomer. Reductive removal of the auxiliary and subsequent oxidation of the resulting alcohol yielded an aldehyde, which was subjected to a Wittig reaction giving the two-carbon homologated ester **210**. Removal of the silyl protecting group liberated an alcohol that spontaneously underwent oxy-Michael cyclization to a separable mixture of *cis* and *trans* diastereomers, **212** and **213**, with a 1.2:1 (*cis:trans*) ratio slightly in favor of the correct stereochemistry of the corresponding eribulin moiety (cf. Scheme 39) [95].

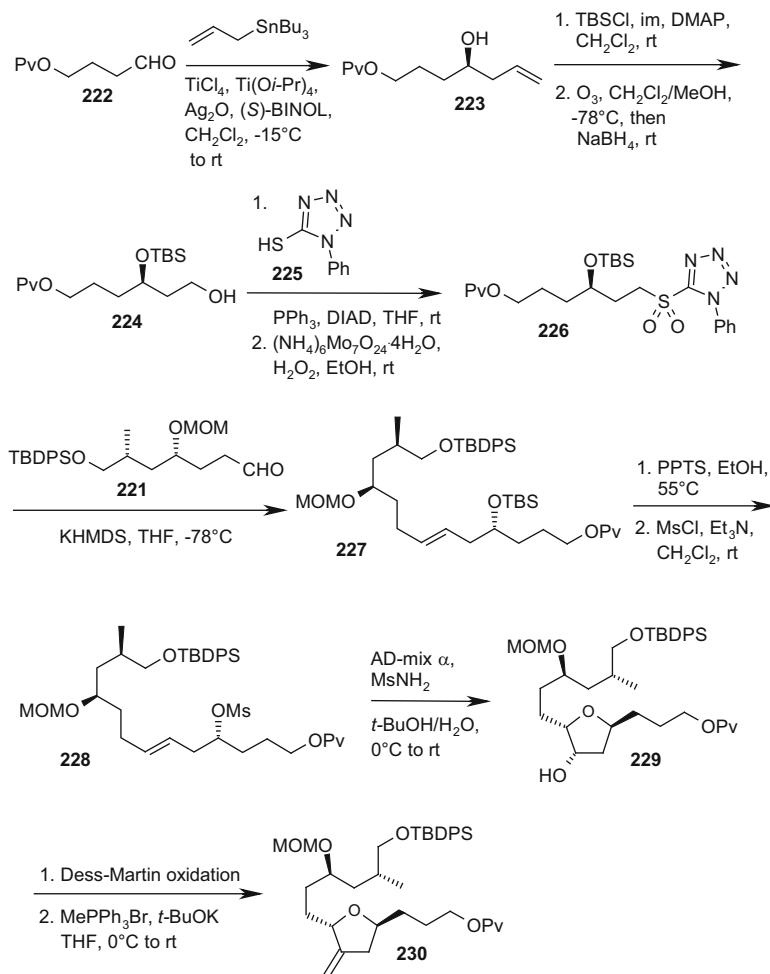
Major contributions in the halichondrin and eribulin field have also been published by a group of the Indian Institute of Chemical Technology. Besides the synthesis of the C45–C53 tetrahydropyran domain of norhalichondrins, the C14–C22 tetrahydrofuran moiety of the halichondrins [96], and the left-half C38–C54 spiroketal fragment of halichondrin B [97], new routes to eribulin building blocks have been elaborated that match well with the original Eisai strategy of assembling key C1–C13, C14–C26, and C27–C35 subunits.



**Scheme 40** Synthesis of a C20–C26 aldehyde employing Maruoka allylation and Evans alkylation

A convergent synthesis of a C14–C26 subunit was described that used a Julia–Kociński olefination as the key step for the connection of a C14–C19 sulfone and a C20–C26 aldehyde fragment. The synthesis started with a Maruoka allylation [98] of aldehyde **214** (obtained from 1,4-butanediol) by using the titanium complex from allyl tri-*n*-butylstannane and (*R*)-BINOL to afford the homoallyl alcohol **215** with 96% *ee*, which was converted to acid **216** in a three-step sequence. Coupling of the Evans auxiliary **217** via the mixed anhydride gave imide **218** that was diastereoselectively methylated to afford a mixture of diastereomers in favor of **219** (85% *de*). Pure **219**, which was obtained after chromatographic separation of the diastereomers, was converted to intermediate **220** by NaBH<sub>4</sub> reduction and TBDPS protection of the resulting alcohol. Hydroboration of the terminal olefin followed by Dess–Martin oxidation finally furnished the C20–C26 aldehyde **221** (cf. Scheme 40).

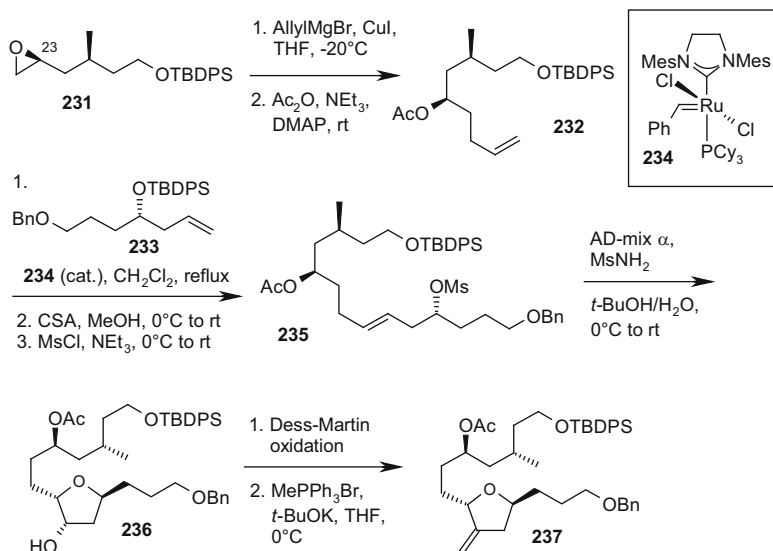
The synthesis of the C14–C19 sulfone started again with a Maruoka allylation, in this case employing (*S*)-BINOL to afford homoallyl alcohol **223** in 70% yield and 95% *ee* from aldehyde **222**. TBS protection followed by ozonolysis of the terminal olefin and reductive work-up furnished alcohol **224**, which had been converted to the sulfone **226** by reaction with thiol **225** under Mitsunobu conditions followed by



**Scheme 41** Synthesis of the C14–C19 sulfone and completion of the C14–C26 fragment

ammonium molybdate oxidation of the resulting sulfide. Coupling of the sulfone **226** with aldehyde **221** under Julia–Kocienski conditions yielded exclusively *E*-olefin **227**, which was transformed into mesylate **228** in two steps. The tetrahydrofuran ring of **229** was formed by a tandem Sharpless asymmetric dihydroxylation/*S<sub>N</sub>2* cyclization sequence. Finally, oxidation of the free secondary alcohol followed by Wittig methylenation afforded the C14–C26 building block **230** (cf. Scheme 41) [99].

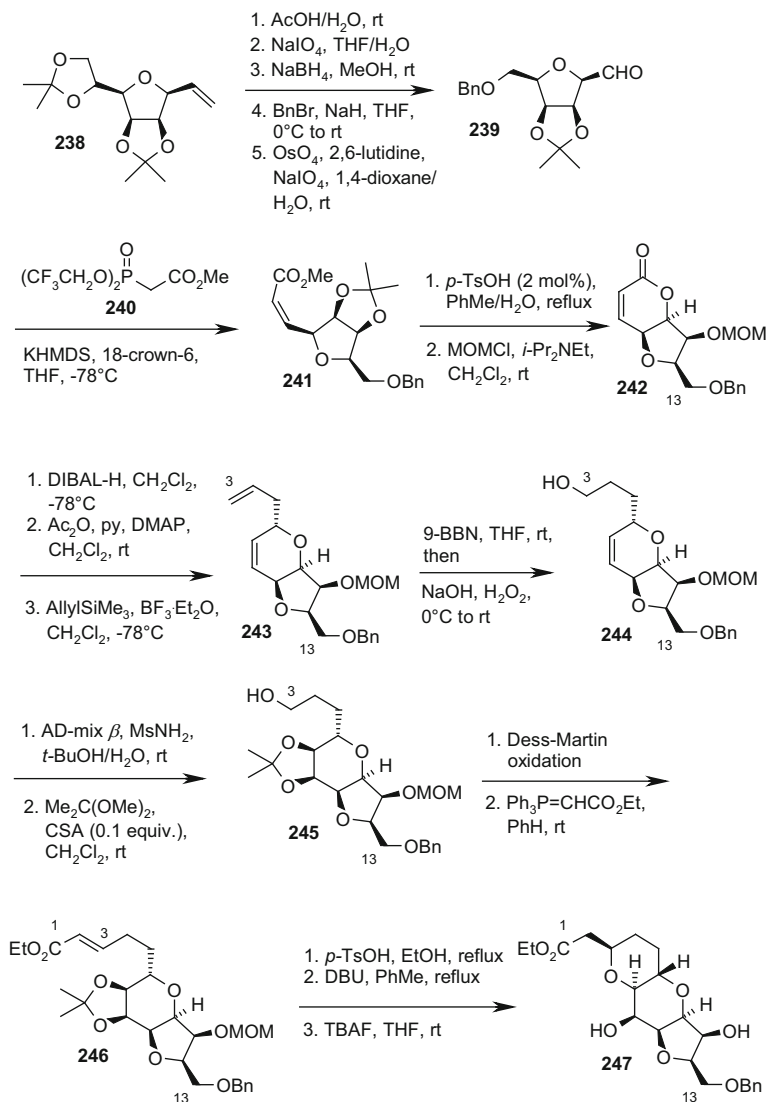
Another straightforward synthesis of the C14–C26 subunit was disclosed that used readily available (*R*)-(+)-citronellol as the starting material which was converted to epoxide **231** in a previously reported three-step sequence comprising an organocatalytic reaction to introduce the stereogenic center at C23



**Scheme 42** Synthesis of a C14–C26 fragment via cross-metathesis

[100, 101]. Regioselective opening of the epoxide with allylmagnesium bromide was achieved under Cu catalysis. The terminal olefin **232** was obtained after protection of the free hydroxy group generated by the ring opening. Cross-metathesis with olefin **233** (obtained by TBDPS protection of **215**, cf. Scheme 40) in the presence of Grubbs II catalyst **234** [102] followed by transformation of the TBS ether into a mesylate furnished intermediate **235**, which was subjected to Sharpless asymmetric dihydroxylation/ $\text{S}_{\text{N}}2$  cyclization conditions as outlined above. Again, oxidation of the free secondary alcohol of **236** followed by Wittig methylenation afforded the C14–C26 fragment **237** (cf. Scheme 42) [103].

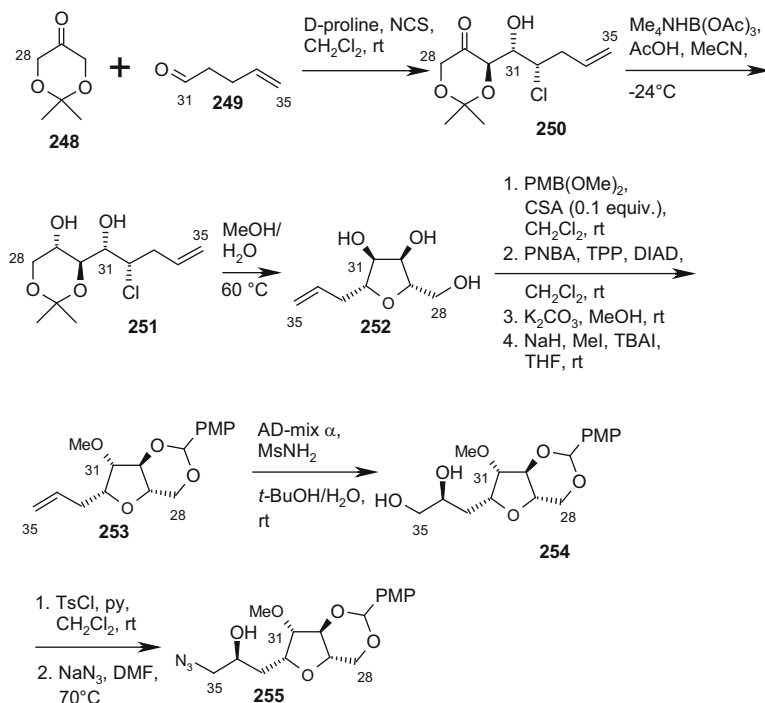
A C1–C13 building block synthesis started with bis-acetonide **238** that was obtained from D-mannose by a known three-step process [104]. Compound **238** was converted to aldehyde **239** in a five-step sequence comprising selective hydrolysis of the primary acetonide, oxidative cleavage of the resulting diol, and reduction of the aldehyde, protecting of the thereby formed primary alcohol as a benzyl ether and finally dihydroxylation and oxidative cleavage of the terminal olefin. Aldehyde **239** was subjected to the Still–Gennari variant of the HWE reaction [105] using phosphonate **240** to afford the unsaturated *Z*-ester **241**. Deprotection of the remaining acetonide triggered lactonization, resulting in bicycle **242** after MOM protection of the free alcohol resulting from cyclization. DIBAL-H reduction furnished the corresponding lactol, which, after acetylation, was reacted with allyltrimethylsilane in the presence of  $\text{BF}_3 \cdot \text{Et}_2\text{O}$  to furnish **243** as a single isomer. Hydroboration yielded alcohol **244**, which was subsequently converted to **245** by Sharpless asymmetric dihydroxylation with AD-mix  $\beta$  and protection of the resulting diol as the acetonide. Oxidation of the primary hydroxy group to the



**Scheme 43** Synthesis of a C1–C13 building block from D-mannose

corresponding aldehyde set the stage for a two-carbon elongation to **246** by a Wittig reaction. The C3–C7 tetrahydropyran ring of the target C1–C13 building block **247** was finally installed by an oxy-Michael reaction after deprotection of the acetonide. The *dr* was improved from 2:1 to 10:1, when the cyclization product was equilibrated with TBAF (cf. Scheme 43) [106].

An asymmetric organocatalytic process represents the key step in a recently published approach to a C28–C35 subunit of eribulin. This key reaction for the



**Scheme 44** Organocatalytic approach to a C28–C35 building block

assembly of a C28–C30 and a C31–C35 fragment consists of a tandem  $\alpha$ -chlorination/aldol reaction [107] of dihydroxyacetone derivative **248** and aldehyde **249** in the presence of D-proline and NCS to afford chlorohydrin **250** with a  $dr = 5:1$  and 91%  $ee$  in 62% yield. Upon cleavage of the acetonide protection, allylfuranose **252** was obtained. The 1,3-diol function was protected as the *p*-methoxybenzylidene acetal, and the configuration of the C31 stereogenic center was adjusted to the one corresponding to the correct eribulin stereochemistry by Mitsunobu inversion. Methylation of the inverted C31-OH function then provided **253**. The C34–C35 diol function of **254** was installed by Sharpless asymmetric dihydroxylation with AD-mix  $\alpha$ , and selective tosylation of the primary alcohol followed by treatment with azide afforded the C28–C35 building block **255** (cf. Scheme 44) [108].

## 6 Clinical Development of Eribulin

The clinical development of eribulin mesylate started with two phase 1 studies [109, 110] in patients with advanced solid malignancies that had either progressed following standard therapy or for which no standard therapy existed. The maximum

tolerated dose, toxicity profile, preliminary anticancer activity, and pharmacokinetics of a 1-h infusion of eribulin mesylate in a weekly or 3-weekly schedule were determined. Eribulin mesylate displayed a manageable toxicity profile in both schedules at up to 2 mg/m<sup>2</sup>, with further dose escalation limited by neutropenia and fatigue. In two large phase 2 trials, eribulin was then studied in heavily pretreated patients with metastatic breast cancer with a further modified administration schedule [111, 112].

These studies confirmed that eribulin has antitumoral activity in extensively pretreated patients with locally advanced breast cancer or metastatic breast cancer previously treated with at least an anthracycline, a taxane, and capecitabine. Importantly, eribulin demonstrated a manageable tolerability profile with a notably low incidence of chemotherapy-induced peripheral neuropathy. On the basis of the activity and manageable tolerability profile observed in phase 2 testing, two randomized phase 3 studies in patients with locally advanced breast cancer or metastatic breast cancer were initiated. The positive outcome of one of these phase 3 studies [113] in patients previously treated with established drugs in a setting where most treatment schemes failed finally led to the approval of eribulin mesylate as Halaven™ in 2010 in the USA and 2011 in Europe [114].

## 7 Conclusion and Outlook

As outlined during this review, multiple challenges had to be mastered from the discovery of the halichondrins to the development and commercial manufacture of eribulin mesylate. The development of eribulin mesylate was greatly facilitated by a partnership between academic and industry scientists. Two of the main issues on the path from a lead structure to a viable drug have been successfully addressed:

- Systematic evaluation of intermediates from the total synthesis approaches of the halichondrins led to the discovery of structurally less complex analogues with improved pharmacodynamic and pharmacokinetic properties.
- The ability to establish a manufacturing process at this level of complexity for the large-scale supply of the drug substance, which indicates that the total synthesis of natural product targets can be achieved to deliver sufficient material for human health care impact by contemporary methodology of modern synthetic chemistry.

The success story of eribulin represents an outstanding example of how a natural product continues to stimulate various fields of research. After its approval numerous clinical studies have been and are still being conducted in order to assess the therapeutic value of this agent as a monotherapy or in combination therapies for breast cancer [115–117]. Further studies have been carried out on the mechanism of action of eribulin [118, 119], and – as outlined in this review – various alternative routes and improvements for the synthesis of key building blocks for the preparation of eribulin and the halichondrins have been elaborated. Since the most common adverse effects associated with eribulin are asthenia, fatigue, neutropenia, alopecia,

nausea, and peripheral neuropathy, there is a continuous search for second-generation analogues with a more favorable side-effect profile [88–92]. Moreover, due to its complexity and need for better and more efficient processes, eribulin synthesis is continuing to attract scientist's attention as evidenced in reports, which appeared published after this review was composed [120].

## References

1. Uemura D, Takahashi K, Yamamoto T (1985) *J Am Chem Soc* 107:4796–4798
2. Tachibana K, Scheuer PJ, Tsukitani Y, Kikuchi H, Van Engen D, Clardy J, Gopichand Y, Schmitz FJ (1981) *J Am Chem Soc* 103:2469–2471
3. Hirata Y, Uemura D (1986) *Pure Appl Chem* 58:701–710
4. Yamamoto A, Ueda A, Brémond P, Tiseni PS, Kishi Y (2012) *J Am Chem Soc* 134:893–896
5. Pettit GR, Tan R, Gao F, Williams MD, Doubek DL, Boyd MR, Schmidt JM, Chapuis J-C, Hamel E, Bai R, Hooper JNA, Tackett LP (1993) *J Org Chem* 58:2538–2543
6. Litaudon M, Hart JB, Blunt JW, Lake RJ, Munro MHG (1994) *Tetrahedron Lett* 35:9435–9438
7. Litaudon M, Hickford SJH, Lill RE, Lake RJ, Blunt JW, Munro MHG (1997) *J Org Chem* 62:1868–1871
8. Hickford SJH, Blunt JW, Munro MHG (2009) *Bioorg Med Chem* 17:2199–2203
9. Pettit GR, Herald CL, Boyd MR, Leed JE, Dufresne C, Doubek DL, Schmidt JM, Cerny RL, Hooper JNA, Rützler KC (1991) *J Med Chem* 34:3339–3340
10. Jackson KL, Henderson JA, Philips AJ (2009) *Chem Rev* 209:3044–3079
11. Bai R, Paull KD, Herald CL, Malspeis L, Pettit GR, Hamel E (1991) *J Biol Chem* 266:15882–15889
12. Ludueña RF, Roach MC, Prasad V, Pettit GR (1993) *Biochem Pharmacol* 45:421–427
13. Dabydeen D, Burnett JC, Bai R, Verdier-Pinard P, Hickford SJH, Pettit GR, Blunt JW, Munro MHG, Gussio R, Hamel E (2006) *Mol Pharmacol* 70:1866–1875
14. Jordan MA, Kamath K, Manna T, Okouneva T, Miller HP, Davis C, Littlefield BA, Wilson L (2005) *Mol Cancer Ther* 4:1086–1095
15. Overmoyer B (2008) *Clin Breast Cancer* 8:S61–S70
16. Yu MJ, Zheng W, Seletsky BM, Littlefield BA, Kishi Y (2011) *Annu Rep Med Chem* 46:227–241
17. Munro MHG, Blunt JW, Dumdei EJ, Hickford SJH, Lill RE, Li S, Battershill CN, Duckworth AR (1999) *J Biotechnol* 70:15–25
18. Aicher TD, Buszek KR, Fang FG, Forsyth CJ, Jung SH, Kishi Y, Matelich MC, Scola PM, Spero DM, Yoon SK (1992) *J Am Chem Soc* 114:3162–3164
19. Yu MJ, Kishi Y, Littlefield BA (2012) Discovery of E7389, a fully synthetic macrocyclic ketone analog of halichondrin B. In: Cragg GM, Kingston DGI, Newman DJ (eds) *Anticancer agents from natural products*, 2nd edn. CRC Press, Boca Raton, pp 317–345
20. Jackson KL, Henderson JA, Motoyoshi H, Philips AJ (2009) *Angew Chem Int Ed* 48:2346–2350
21. Ueda A, Yamamoto A, Kato D, Kishi Y (2014) *J Am Chem Soc* 136:5171–5176
22. Hargarden GC, Guiry PJ (2007) *Adv Synth Catal* 349:2407–2424
23. Towle MJ, Salvato KA, Wels BF, Aalfs KK, Zheng W, Seletsky BM, Zhu X, Lewis BM, Kishi Y, Yu MJ, Littlefield BA (2011) *Cancer Res* 71:496–505
24. Wang Y, Habgood GJ, Christ WJ, Kishi Y, Littlefield BA, Yu MJ (2000) *Bioorg Med Chem Lett* 10:1029–1032

25. Seletsky BM, Wang Y, Hawkins LD, Palme MH, Habgood GJ, DiPietro LV, Towle MJ, Salvato KA, Wels BF, Aalfs KK, Kishi Y, Littlefield BA, Yu MJ (2004) *Bioorg Med Chem Lett* 14:5547–5550
26. Zheng W, Seletsky BM, Palme MH, Lydon PJ, Singer LA, Chase CE, Lemelin CE, Shen Y, Davis H, Tremblay L, Towle MJ, Salvato KA, Wels BF, Aalfs KK, Kishi Y, Littlefield BA, Yu MJ (2004) *Bioorg Med Chem Lett* 14:5551–5554
27. Towle MJ, Salvato KA, Budrow J, Wels BF, Kuznetsov G, Aalfs KK, Welsh S, Zheng W, Seletsky BM, Palme MH, Habgood GJ, Singer LA, DiPietro LV, Wang Y, Chen JJ, Quincy DA, Davis A, Yoshimatsu K, Kishi Y, Yu MJ, Littlefield BA (2001) *Cancer Res* 61:1013–1021
28. Wang Y (2007) *Drugs Future* 32:681–698
29. Ledford H (2010) *Nature* 468:608–609
30. Littlefield BA, Palme M, Seletsky BM, Towle MJ, Yu MJ (1999) Macrocylic analogs and methods of their use and preparation. PCT Int Appl WO 99/65894, 23 Dec 1999
31. Littlefield BA, Palme MH, Seletsky BM, Towle MJ, Yu MJ, Zheng W (2001) Macrocylic analogs and methods of their use and preparation. US Patent 6,214,865, 10 April 2001
32. Stamos DP, Kishi Y (1996) *Tetrahedron Lett* 37:8643–8646
33. Aicher TD, Kishi Y (1987) *Tetrahedron Lett* 28:3463–3466
34. Kishi Y, Fang FG, Forsyth CJ, Scola PM, Yoon SK (1995) Synthesis of halichondrin B and norhalichondrin B. US Patent 5,436,238, 25 July 1995
35. Yu MJ, Zheng W, Seletsky BM (2013) *Nat Prod Rep* 30:1158–1164
36. Smith AB, Chen SSS, Nelson FC, Reichert JM, Salvatore BA (1995) *J Am Chem Soc* 117:12013–12014
37. Magnus PD (1977) *Tetrahedron* 33:2019–2045
38. Meyer SD, Schreiber SL (1994) *J Org Chem* 59:7549–7552
39. Littlefield BA, Palme MH, Seletsky BM, Towle MJ, Yu MJ, Zheng W (2002) Intermediate compounds for preparing macrocyclic analogs. US Patent 6,365,759, 2 April 2002
40. Wan ZK, Choi H, Kang FA, Nakajima K, Demeke D, Kishi Y (2002) *Org Lett* 25:4431–4434
41. Austad B, Chase CE, Fang FG (2005) Intermediates for the preparation of halichondrin B. PCT Int Appl WO 2005/118565, 15 Dec 2005
42. Choi H, Nakajima K, Demeke D, Kang FA, Jun HS, Wan ZK, Kishi Y (2002) *Org Lett* 25:4435–4438
43. Hu Y (2009) Halichondrin B analogs. PCT Int Appl WO 2009/124237, 8 Oct 2009
44. Austad BC, Calkins TL, Chase CE, Fang FG, Horstmann TE, Hu Y, Lewis BM, Niu X, Noland TA, Orr JD, Schnaderbeck MJ, Zhang H, Asakawa N, Asai N, Chiba H, Hasebe T, Hoshino Y, Ishizuka H, Kajima T, Kayano A, Komatsu Y, Kubota M, Kuroda H, Miyazawa M, Tagami K, Watanabe T (2013) *Synlett* 24:333–337
45. Chiba H, Fukuyama T, Takigawa T, Komatsu Y (2012) Microreactor process for halichondrin B analog synthesis. PCT Int Appl WO 2012/147900, 1 Nov 2012
46. Hu Y, Zhang H, Chiba H, Komatsu Y (2015) Methods useful in the synthesis of halichondrin B analogs. PCT Int Appl WO 2015/085193, 11 June 2015
47. Fukuyama T, Chiba H, Kuroda H, Takigawa T, Kayano A, Tagami K (2016) *Org Process Res Dev* 20:503–509
48. Inanga K, Fukuyama T, Kubota M, Komatsu Y, Chiba H, Kayano A, Tagami K (2015) *Org Lett* 17:3158–3161
49. Chase CE, Fang F, Lewis BM, Wilkie GD, Schnaderbeck MJ, Zhu X (2013) *Synlett* 24:323–326
50. Rajendran A, Paredes G, Mazzotti M (2009) *J Chromatogr A* 1216:709–738
51. Tokunaga M, Larrow JF, Kakiuchi F, Jacobsen EN (1997) *Science* 277:936–938
52. Kurosu M, Lin MH, Kishi Y (2004) *J Am Chem Soc* 126:12248–12249
53. Choi H, Demeke D, Kang FA, Kishi Y, Nakajima K, Nowak P, Wan ZK, Xie C (2003) *Pure Appl Chem* 75:1–17

54. Austad BC, Benayoud F, Calkins TL, Campagna S, Chase CE, Choi H, Christ W, Costanzo R, Cutter J, Endo A, Fang FG, Hu Y, Lewis BM, Lewis MD, McKenna S, Noland TA, Orr JD, Pesant M, Schnaderbeck MJ, Wilkie GD, Abe T, Asai N, Asai Y, Kayano A, Kimoto Y, Komatsu Y, Kubota M, Kuroda H, Mizuno M, Nakamura T, Omae T, Ozeki N, Suzuki T, Takigawa T, Watanabe T, Yoshizawa K (2013) *Synlett* 24:327–332
55. Stork G, Kahne DE (1983) *J Am Chem Soc* 105:1072–1073
56. Crabtree RH, Felkin H, Fellebeen-Khan T, Morris GE (1979) *J Organomet Chem* 168:183–195
57. Yang YR, Kim DS, Kishi Y (2009) *Org Lett* 11:4516–4519
58. Guo H, Dong CG, Kim DS, Urabe D, Wang J, Kim JT, Liu X, Sasaki T, Kishi Y (2009) *J Am Chem Soc* 131:15387–15393
59. Liu X, Henderson JA, Sasaki T, Kishi Y (2009) *J Am Chem Soc* 131:16678–16680
60. Liu S, Kim JT, Dong CG, Kishi Y (2009) *Org Lett* 11:4520–4523
61. Kim DS, Dong CG, Kim JT, Guo H, Huang J, Tiseni PS, Kishi Y (2009) *J Am Chem Soc* 131:15636–15641
62. Zhang Z, Huang J, Kishi Y (2008) *Org Lett* 10:3073–3076
63. Dong CG, Henderson JA, Kaburagi Y, Sasaki T, Kim DS, Kim JT, Urabe D, Guo H, Kishi Y (2009) *J Am Chem Soc* 131:15642–15646
64. Trost BM, Ball ZT (2003) *J Am Chem Soc* 125:30–31
65. Trost BM, Ball ZT, Laemmerhold KM (2005) *J Am Chem Soc* 127:10028–10038
66. Shan M, Kishi Y (2012) *Org Lett* 14:660–663
67. Uguen D (1981) *Bull Chim Soc Fr* II:99–102
68. Liu L, Henderson JA, Yamamoto A, Brémond P, Kishi Y (2012) *Org Lett* 14:2262–2265
69. Duan JJW, Kishi Y (1993) *Tetrahedron Lett* 34:7541–7544
70. Shiina I, Katoh T, Nagai S, Hashizume M (2009) *Chem Rec* 9:305–320
71. Shiina I, Kubota M, Ibuka R (2002) *Tetrahedron Lett* 43:7535–7539
72. Namba K, Yun H-S, Kishi Y (2004) *J Am Chem Soc* 126:7770–7771
73. Kaburagi Y, Kishi Y (2007) *Org Lett* 9:723–726
74. Yan W, Li J, Kishi Y (2015) *J Am Chem Soc* 137:6219–6225
75. Li J, Yan W, Kishi Y (2015) *J Am Chem Soc* 137:6226–6231
76. Blanchette MA, Choy W, Davis JT, Essenfeld AP, Masamune S, Roush WR, Sakai T (1984) *Tetrahedron Lett* 25:2183–2186
77. Bernet B, Vasella A (1979) *Helv Chim Acta* 62:1990–2016
78. Belanger F, Chase CE, Endo A, Fang FG, Li J, Mathieu SR, Wilcoxon AZ, Zhang H (2015) *Angew Chem Int Ed* 54:5108–5111
79. Liu KKC, Sakya SM, O'Donnell CJ, Flick AC, Ding HX (2012) *Bioorg Med Chem* 20:1155–1174
80. Chase C, Endo A, Fang FG, Li J (2009) Intermediates and methods for the synthesis of halichondrin B analogs. PCT Int Appl WO 2009/046308, 9 April 2009
81. Kim D-S, Choi H-W, Chase CE, Lee J (2015) Macrocyclization reactions and intermediates useful in the synthesis of analogs of halichondrin B. PCT Int Appl WO 2015/066729, 7 May 2015
82. Garber SB, Kingsbury JS, Gray BL, Hoveyda AH (2000) *J Am Chem Soc* 122:8168–8179
83. Schauer DJ, Helquist P (2006) *Synthesis* 3654–3660
84. Pirrung MC, Biswas G, Ibarra-Rivera TR (2010) *Org Lett* 12:2402–2405
85. Lin JH, Yamazaki M (2003) *Drug Metab Rev* 35:417–454
86. Goda K, Bacsó Z, Szabo G (2009) *Curr Cancer Drug Targets* 9:281–297
87. Chan LMS, Lowes S, Hirst BH (2004) *Eur J Pharm Sci* 21:25–51
88. Narayan S, Carlson EM, Cheng H, Du H, Hu Y, Jiang Y, Lewis BM, Seletsky BM, Tendyke K, Zhang H, Zheng W, Littlefield BA, Towle MJ, Yu MJ (2011) *Bioorg Med Chem Lett* 21:1630–1633

89. Narayan S, Carlson EM, Cheng H, Condon K, Du H, Eckley S, Hu Y, Jiang Y, Kumar V, Lewis BM, Saxton P, Schuck E, Seletsky BM, Tendyke K, Zhang H, Zheng W, Littlefield BA, Towle MJ, Yu MJ (2011) *Bioorg Med Chem Lett* 21:1634–1638
90. Yu MJ, Zheng W, Tendyke K (2012) *Bioorg Med Chem Lett* 22:7363–7366
91. Narayan S, Carlson EM, Cheng H, Condon K, Du H, Eckley S, Hu Y, Jiang Y, Kumar V, Lewis BM, Saxton P, Schuck E, Seletsky BM, Tendyke K, Zhang H, Zheng W, Littlefield BA, Towle MJ, Yu MJ (2011) *Bioorg Med Chem Lett* 21:1639–1643
92. Dasari B, Jimmidi R, Arya P (2015) *Eur J Med Chem* 94:497–508
93. Rudolph A, Alberico D, Jordan R, Pan M, Souza FES, Gorin B (2013) *Tetrahedron Lett* 54:7059–7061
94. Okabe M, Sun RC, Zenchoff GB (1991) *J Org Chem* 56:4392–4397
95. Jimmidi R, Gudru SKR, Arya P (2015) *Org Lett* 17:468–471
96. Sabitha G, Chandrasekhar G, Yadav JS, Rachineni K, Jagadeesh B (2012) *RSC Adv* 2:10157–10159
97. Yadav JS, Reddy CN, Sabitha G (2012) *Tetrahedron Lett* 53:2504–2507
98. Hanawa H, Hahimoto T, Maruoka K (2003) *J Am Chem Soc* 125:1708–1709
99. Murthy AS, Mahipal B, Chandrasekhar S (2012) *Eur J Org Chem* 6959–6966
100. Chandrasekhar S, Yaragorla SR, Sreelakshmi L, Reddy CR (2008) *Tetrahedron* 64:5174–5183
101. Hodgson DM, Salik S (2012) *Org Lett* 14:4402–4405
102. Scholl M, Ding S, Lee CW, Grubbs HR (1999) *Org Lett* 1:953–956
103. Lavanya N, Kiranmai N, Mainkar PS, Chandrasekhar S (2015) *Tetrahedron Lett* 56:4283–4285
104. Liu J, Liu Y, Zhang X, Zhang C, Gao Y, Wang L, Du Y (2012) *J Org Chem* 77:9718–9723
105. Still WC, Gennari C (1983) *Tetrahedron Lett* 24:4405–4408
106. Murthy AS, Chandrasekhar S (2015) *Tetrahedron Lett* 56:4280–4282
107. Bergeron-Brlek M, Teoh T, Britton R (2013) *Org Lett* 15:3554–3557
108. Chavan LN, Chegondi R, Chandrasekhar S (2015) *Tetrahedron Lett* 56:4286–4288
109. Goel S, Mita AC, Mita M, Rowinsky EK, Chu QS, Wong N, Desjardins C, Fang F, Jansen M, Shuster DE, Mani S, Takimoto CH (2009) *Clin Cancer Res* 15:4207–4212
110. Tan AR, Rubin EH, Walton DC, Shuster DE, Wong NY, Fang F, Ashworth S, Rosen LS (2009) *Clin Cancer Res* 15:4213–4219
111. Vahdat L, Pruitt B, Fabian CJ, Rivera RR, Smith DA, Tan-Chiu E, Wright J, Tan AR, DaCosta NA, Chuang E, Smith J, O’Shaughnessy J, Shuster DE, Meneses NL, Chandrawansa K, Fang F, Cole PE, Ashworth S, Blum JL (2009) *J Clin Oncol* 27:2954–2961
112. Cortes J, Vahdat L, Blum JL, Twelves C, Campone M, Roché H, Bachelot T, Awada A, Pardaens R, Goncalves A, Shuster DE, Wanders J, Fang F, Gurnani R, Richmond E, Cole PE, Ashworth S, Allison MA (2010) *J Clin Oncol* 28:3922–3928
113. Cortes J, O’Shaughnessy J, Loesch D, Blum JL, Vahdat LT, Petrakova K, Chollet P, Manikasd A, Diéras V, Delozier T, Vladimirov V, Cardoso F, Koh H, Bougnoux P, Dutcuc CE, Seegobin S, Mir D, Meneses N, Wanders J, Twelves C (2011) *Lancet* 377:914–923
114. Aftimos P, Awada A (2011) *Adv Ther* 28:973–985
115. Gaducci A, Guerrieri ME (2015) *Expert Opin Pharmacother* 16:335–346
116. Thara E, Gitlitz BJ (2014) *Future Oncol* 10:1913–1924
117. Koczywas M, Frankel PH, Synold TW, Lenz H-J, Mortimer JE, El-Khoueiry AB, Gandara DR, Cristea MC, Chung VM, Lim D, Reckamp KL, Lau DH, Doyle LA, Ruel C, Carroll MI, Newman EM (2014) *Br J Cancer* 111:2268–2274
118. O’Rourke B, Yang C-PH, Sharp D, Horwitz SB (2014) *Cell Cycle* 13:3218–3221
119. Yoshida T, Ozawa Y, Kimura T, Sato Y, Kuznetsov G, Xu S, Uesugi M, Agoulnik S, Taylor N, Funahashi Y, Matsui J (2014) *Br J Cancer* 110:1497–1505
120. Fukuyama T, Chiba H, Takigawa T, Komatsu Y, Kayano A, Tagami K (2016) *Org Process Res Dev* 20:100–104

# Index

## A

Active pharmaceutical ingredient (API), 3, 8  
Aminobutanol, 202  
1-Aminocyclopropanecarboxylic acid (ACCA), 96  
Aminonon-8-enoic acid, 100  
Amino-2-vinylcyclopropanecarboxylic acid, 96  
5-Aminothiazolo[4,5-*d*]pyrimidine-2,7-(3*H*,6*H*)-dione, 7  
5-Aminothiazolo[4,5-*d*]pyrimidine-2(3*H*)-thione, 12  
5-Amino-3-(tri-*O*-benzoyl- $\beta$ -*D*-ribofuranosyl)-3*H*-thiazolo[4,5-*d*]pyrimidin-2,7-dione, 7  
Anticancer drugs, 209, 257  
Antiretroviral therapy (ART), 189  
Aryl glycosides, 34  
Arylalanes, 46  
Asymmetric synthesis, 113  
Atherosclerosis, 117  
Atorvastatin, 113, 118, 127, 153–167

## B

3-(Benzyloxy)-4-oxo-4*H*-pyran-2-carbaldehyde, 199  
BILN 2061, 89, 94, 95  
Bis-silyl acetamide (BSA), 15  
Breast cancer, 209, 220, 266  
5-Bromopyrimidine-2,4-diamine, 11  
Butyl 6-cyano-(5*R*)-hydroxy-3-oxohexanoate, 134

## C

Canagliflozin, 29, 31, 39, 43  
Cancer, 54, 212, 220, 257, 266  
Carbamoyl pyridone, 187  
Cardiovascular diseases, 117, 119  
Catalysis, 23, 76, 113, 127, 163, 263  
Cerivastatin, 120  
Cholesterol, 117, 120  
Citronellol, 262  
Comanic acid, 197  
Compactin, 117  
Coronamic acid, 98  
Coronary heart disease, 117–120  
Coupling reactions, transition-metal-mediated, 209  
Cytidine, functionalization, 59, 65

## D

Dapagliflozin, 29, 31, 35, 43  
2-Deoxyribose-5-phosphate aldolase (DERA), 134  
Diabetes, type 2, 29, 31, 42  
2,6-Diaminopyrimidin-4(3*H*)-one, 8  
Diarylzinc, 43  
Diketoreductase, 127  
Direct-acting antivirals (DAAs), 56  
Dolutegravir, 187

## E

Empagliflozin, 31, 37  
Eribulin, 209, 218, 266  
Ertugliflozin, 29, 31, 39  
Ethyl 4-chloro-3-oxobutanoate, 196

Ethyl glycinate, 96

Ezetimib, 120

## F

Fluorination, 51, 58, 74, 85, 122

Fluvastatin, 113, 118, 151

Fragment coupling, 209

## G

Glioblastoma, 258

Gluconolactones, 33

Glucose dehydrogenase, 128

Glycine imines, 96

Glycosylation, 1  
carbon, 29, 42

## H

Halaven, 209

*Halichondria okadai*, 209, 213

Halichondrin, 209, 212

Hepatitis C virus, 51, 89

Heterocycles, 1, 113

HIV-1 integrase inhibitor, 187

reverse transcriptase, 189

Homohalichondrin, 209, 214

Horner–Wadsworth–Emmons (HWE) reaction,  
253, 257

Hoveyda–Grubbs catalyst, 255

4-Hydroxy-7-methoxyquinolines, 98

3-Hydroxy-3-methylglutaryl-coenzyme A  
(HMG-CoA) reductase, 117

Hypercholesterolemia, 117, 181

## I

Indoles, 113

Integrase inhibitors, 187, 190

Integrase strand transfer inhibitors (INSTIs),  
187, 189

Interferons, 2, 54, 58, 91

Ipragliflozin, 29, 31

Isatoribine, 2

## L

Lipase, immobilized, 1, 21

Liver cirrhosis, 55, 89

Lovastatin, 117

Low-density lipoprotein cholesterol  
(LDL-C), 117

Luseogliflozin, 29, 31, 35

## M

Macrocyclic peptides, 89

Macrolides, 209

Marine natural products, 209

Melanoma, 213, 214, 220

Methyl 4-methoxy-3-oxobutanoate, 194, 199

Methyl *tert*-butyl ether (MTBE) 143

Mevastatin, 117

ML-236B, 117

MWCNTs, 143

Myalgia, 120

## N

Non-nucleosidic reverse transcriptase inhibitor  
(NNRTI), 189

Norhalichondrin, 209, 213

Nozaki–Hiyama–Kishi reaction, 209, 255

NS3/NS4A protease inhibitors, 89

Nucleoside/nucleotide reverse transcriptase  
inhibitors (NRTIs), 189

Nucleosides, 64  
synthesis, 51

## O

Okadaic acid, 213

Omura–Sharma–Swern oxidation, 60, 65

## P

Paritaprevir, 92

Peptides, macrocyclic, 89

Peptidomimetic inhibitors, 92

*Phakellia carteri*, 213

Phosphoramidates, synthesis, 51

Pitavastatin, 118, 120, 174

Polyether, 209

Potassium xanthogenate, 12

Pravastatin, 118

Process development, 209

Pyrimidine-2,4-diamine, 9, 11

Pyrimidines, 113

Pyrroles, 113, 120, 153, 181

Pyrrolidine, 106

Pyrroloquinoline quinone, 139

## Q

Quinolines, 98, 113, 120, 175, 181

## R

Reproducibility, 5

Reverse transcriptase, 189

Rhabdomyolysis, 118  
Ribavirin, 55, 57  
Ribofuranose, 7, 18, 67  
Ring-closing metathesis (RCM), 101  
RNA-dependent RNA polymerase (RdRp)  
  inhibitors, 56  
Robustness, 5  
Rosuvastatin, 118, 120, 167  
Ruthenacyclopentene, 106

**S**

Scale-up, 209  
Simeprevir, 92  
Simvastatin, 118, 120  
Sodium-coupled glucose cotransporter  
  2 (SGLT-2) inhibitors, 29, 31  
Sofosbuvir, 51  
Sotagliflozin, 29, 31, 40  
Statins, 113  
Structure-activity relationships, 209

Subtilisin, 98  
Super-statins, 113, 118  
  hepatoselective, 119

**T**

Tetra-*O*-acetyl- $\beta$ -D-ribofuranose, 2  
Thiazolidine-2,4-dione, 9  
Thiazolo[4,5-*d*]pyrimidine nucleoside, 2  
Tofogliflozin, 29

**V**

Vinylcyclopropanes, 105  
Viruses, 51, 89, 189  
  HCV, 51, 54, 89, 91  
  HIV, 187, 189

**X**

Xanthogenate, 12